

UNIVERSIDAD DE GRANADA

Facultad de Ciencias

Departamento de Mineralogía y Petrología



**Pigment-binder interaction under urban atmosphere:
novel approaches to unravel chemical-physical
degradation in model paintings**

Programa de Doctorado: Ciencias de la Tierra

TESIS DOCTORAL

Juan Agustín Herrera Rubia

Granada, 2018



Departamento de Mineralogía y Petrología
Facultad de Ciencias
UNIVERSIDAD DE GRANADA



**Pigment-binder interaction under urban atmosphere: novel
approaches to unravel chemical-physical degradation in model
paintings**

Programa de Doctorado: Ciencias de la Tierra

Memoria presentada por Juan Agustín Herrera Rubia, Licenciado en Química, para optar
al grado de Doctor por la Universidad de Granada.

Granada, 21 de febrero de 2018

VºBº de las directoras

Fdo. Carolina Cardell Fernández

Fdo. Natalia África Navas Iglesias

Fdo. Juan Agustín Herrera Rubia

Editor: Universidad de Granada. Tesis Doctorales
Autor: Juan Agustín Herrera Rubia
ISBN: 978-84-9163-945-9
URI: <http://hdl.handle.net/10481/52551>

El doctorando

The doctoral candidate

Juan Agustín Herrera Rubia

y las directoras de la tesis

and the thesis supervisors

Carolina Cardell Fernández

Natalia África Navas Iglesias

Garantizamos, al firmar esta tesis doctoral, que el trabajo ha sido realizado por el doctorando bajo la dirección de las directoras de la tesis y hasta donde nuestro conocimiento alcanza, en la realización del trabajo, se han respetado los derechos de otros autores a ser citados, cuando se han utilizado sus resultados o publicaciones.

Guarantee, by signing this doctoral thesis, that the work has been done by the doctoral candidate under the direction of the thesis supervisor/s and, as far as our knowledge reaches, in the performance of the work, the rights of other authors to be cited (when their results or publications have been used) have been respected.

En Granada, a 02 de abril de 2018.

Fdo. Carolina Cardell Fernández
Supervisor

Fdo. Natalia África Navas
Iglesias
Supervisor

Fdo. Juan Agustín Herrera
Rubia
Doctoral candidate

A mis padres y hermana

Agradecimientos

He tenido mucha suerte a lo largo de mi carrera científica, me he encontrado a tanta gente buena que es muy complicado comenzar estos agradecimientos. Sin embargo, es imposible no comenzar agradeciendo a las personas que apostaron por mí y me dieron la oportunidad de comenzar mi carrera como investigador, como no, me refiero a mis directoras de Tesis Doctoral: la Dra. Carolina Cardell Fernández y la Dra. Natalia África Navas Iglesias. Para mí han sido un ejemplo de trabajo, constancia, calidad científica y, lo que es más importante, calidad humana. Agradezco de corazón todo lo que he aprendido con vosotras a nivel científico y humano, que no ha sido poco. Espero que siempre me recordéis por los buenos momentos vividos, como cuando os tuve que agarrar de la mano en el vuelo para el congreso de Catania debido a mi miedo a volar jeje. Nunca os olvidaré y espero que estéis siempre presentes en mi vida.

Puesto que no quiero olvidar a nadie, agradezco al departamento de Mineralogía y Petrología que me ha acogido como a uno más, en especial a los integrantes del grupo de investigación RMN-179, gracias por vuestra ayuda. Tampoco puedo olvidarme de mi segunda casa, me refiero al departamento de Química Analítica, en especial al grupo de investigación FQM-118, donde siempre me han recibido con los brazos abiertos. Por supuesto, también hago extensible mi agradecimiento al centro de instrumentación científica de la Universidad de Granada donde me conoce casi todo el mundo y donde me han aguantado tantas horas.

No puedo continuar con los agradecimientos sin hablar de los personajes que habitan el despacho número 29 (Pendejolandia) donde he estado estos últimos años. Es complicado hablar de mis amigos, así que lo haré por orden cronológico a como los conocí y espero que ninguno se sienta más o menos querido, es decir que no me guardéis pelusilla. Tengo que comenzar con mi *abuelica* (Nazaret), más buena niña imposible, te agradezco todo lo que has hecho por mí y todo que me has aguantado, espero que este verano nos vayamos otra temporada de vacaciones playeras a Rota con Montxo. *Ayyy mi Lejandro* (Alejandro

Burgos), que puedo decir de tremendo personaje XD; inteligente y trabajador como nadie, ojalá hubiéramos realizado más cosas de investigación juntos. Citando al *Dr. Lejandro et al 2018*, "...no sin mi Fuu", *Fosfato Fu (Fu₃PO₄)*, *Fufania*, y un largo etc, trabajadora incansable y mejor persona, gracias Estefanía por tu ayuda y por estar siempre ahí. Espero que nos vayamos este verano otra temporada de vacaciones pero, a poder ser, que no tengamos que coger el avión jejeje. *Ma che palle* Fulvio, te voy a echar mucho de menos cuando te vayas en junio, espero que nos sigamos viendo y que vengas de visita frecuentemente con Fede. Compañero de piso P de pelusilla (Luis), tremendo personaje adquirido en la última temporada y mejor compañero de piso. Ante mi futuro incierto, no sé si seguiremos juntos en el despacho y/o piso, pero si no fuera así, seguro que seguiremos en contacto porque no me gustaría perder tu amistad. Mi Mari Tere, más graciosa imposible, lástima que no hayamos podido investigar mucho juntos porque me pillaste en la etapa de escritura de la Tesis. Te has hecho querer en muy poco tiempo y eso dice mucho de ti como persona. Por último, recibimos todos el milagro de la Blanca Paloma (Cristina), la palomilla de las arenas y dunas, eres única y excepcional, eres lo mejor que le ha pasado al despacho, nos has hecho cambiar a todos para mejor. Quiero agradecer también a la Zalamera (Marta) y el muchachillo de Priego (Javier), gracias por vuestra compañía y por los buenos momentos vividos, espero que hayáis aprendido un poco de mí. Por último, no puedo olvidar y dejar de agradecer la ayuda de mis antiguos compañeros del departamento de Química Analítica: Inma, José y Antonio (El largo).

Como no acordarme de mi estancia en la Universidad de Milán con el Dr. Roberto Todeschini y Dr. Davide Ballabio, donde estuve tan a gusto y me sentí como uno más desde el primer día. Muchísimas gracias por aceptarme y aprender tanto en tan poco tiempo. También agradezco a la Universidad de Vigo, especialmente a la Dra. Teresa Rivas y al Dr. Santiago Pozo por la ayuda prestada a lo largo de estos cuatro años.

Agradezco profundamente la ayuda y estabilidad emocional que he dado mi novia Macarena "*mi morenasa*" "*mi Maka*", sin su comprensión y cariño me hubiera sido imposible terminar este largo camino. A pesar de que actualmente atraviesa un momento

muy duro en su vida, sigue siempre ayudándome, apoyándome y no perdiendo nunca los papeles. Deseo de corazón que vengan tiempos mejores para los dos y, por fin, podamos estar juntos, *te quiero*.

Por último y no menos importante agradezco a mis padres y hermana, los pilares básicos en mi vida. Sin ellos nada de esto sería posible. En especial mi madre Marisa, la persona más importante en mi vida, trabajadora incansable y la mejor persona, sus tantos sacrificios por mí la hacen una madre insuperable. Aunque no lo suelo decir a menudo quiero que sepáis que os quiero.

Esta Tesis Doctoral ha sido financiada por los proyectos de investigación españoles AERIMPACT (CGL2012-30729) y EXPOAIR (P12-FQM-1889). Además, agradezco al Ministerio de Economía, Industria y Competitividad de España por el contrato predoctoral (ref.BES-2013- 065507) como formación profesional investigador (FPI) asociado al Proyecto AERIMPACT.

Índice

<i>Acronyms and Abbreviations</i>	<i>i</i>
<i>Summary</i>	<i>v</i>
<i>General objective</i>	<i>ix</i>
<i>Specific objectives</i>	<i>xi</i>
<i>Structure of the Doctoral Thesis</i>	<i>xiii</i>
Resumen	<i>xvii</i>
Objetivo general.....	<i>xxiii</i>
Estructura de la Tesis Doctoral	<i>xxvii</i>

Introducción	1
I. Patrimonio pictórico	1
II. Deterioro de pinturas históricas por atmosferas urbanas	3
III. Mecanismos de alteración físico-química de pinturas históricas	8
IV. Caracterización de pinturas históricas	23
Referencias	32

Parte experimental

Capítulo 1. Materiales y métodos

1.1. Materiales.....	47
1.1.1. Pigmentos históricos inorgánicos.....	47
1.1.2. Aglutinantes proteicos	50
1.1.2.1. Dosímetros pictóricos: elaboración.....	50
1.2. Metodología.....	54
1.2.1. Instrumentos de laboratorio	54
1.2.1.1. Balanza.....	54

1.2.1.2. Ultrasonicador.....	54
1.2.1.3 Centrifugadora.....	55
1.2.1.4. Agitador	55
1.2.1.5 Evaporizador o concentrador.....	56
1.2.2. Caracterización composicional de los dosímetros pictóricos.....	57
1.2.2.1. Difracción de Rayos X (XRD).....	57
2.2.2.2. Microscopía electrónica de barrido (FESEM)	57
1.2.2.3. Espectroscopía micro-Raman (RMS).....	59
1.2.2.4. Espectroscopia infrarroja con transformada de Fourier (FTIR) con reflectancia total atenuada (ATR).....	59
1.2.2.5. Espectrometría de masas asistida por láser con detector de tiempo de vuelo (MALDI-TOF-MS).....	60
1.2.2.6. Termogravimetría (TGA)	60
1.2.3. Determinación de propiedades físicas y superficiales	61
1.2.3.1. Granulómetro.....	61
1.2.3.2. Espectrofotómetro	61
1.2.3.3. Estereomicroscopio o Lupa binocular	62
1.3. Ensayos de envejecimiento de dosímetros pictóricos.....	64
1.3.1. Envejecimiento natural por exposición a la atmosfera urbana de Granada capital.....	64
1.3.2. Ensayos de envejecimiento acelerado	65
1.4 Tratamiento estadístico de datos	66
1.4.1 Quimiometría.....	66
1.4.2 Tecnicas ómicas.....	67
Referencias	69

Resultado y discusión : caracterización de la interacción pigmento-aglutinante bajo atmosfera contaminada

Capítulo 2: An evaluation of the impact of urban air pollution on paint dosimeters by tracking changes in the lipid MALDI-TOF mass spectra profile

Hipótesis de partida	77
Objetivo de la investigación.....	78
Abstract	79
2.1. Introduction	80
2.2. Materials and Methods.....	83
2.2.1. Chemicals and reagents.....	83
2.2.2. Paint dosimeters	83
2.2.3. Natural ageing test	84
2.2.4. Lipid extraction procedure	84
2.2.5. MALDI-TOF-MS and data analysis	85
2.3. Results and discussion	86
2.3.1. Optimization of the lipid extraction procedure.....	86
2.3.2. Optimization of the MALDI-TOF-MS procedure.....	87
2.3.3. Characterization of the blank paint dosimeters.....	88
2.3.4. Outdoor aged paint dosimeters characterization.....	93
2.3.5. White lead-based paint dosimeter as an exceptional case.....	96
2.4. Conclusions	98
References	101

Capítulo 3: Principal Component Analysis to interpret changes in chromatic parameters on paint dosimeters exposed long-term to urban air

Hipótesis de partida	109
Objetivos de la investigación	110

Abstract	111
3.1. Introduction	112
3.2. Materials and methods	114
3.2.1. <i>Painting materials</i>	114
3.2.2. <i>Paint dosimeters</i>	117
3.2.3. <i>Natural air pollution aging test</i>	117
3.2.4. <i>Color measurements</i>	119
3.2.5. <i>Principal component analysis (PCA)</i>	119
3.3. Results and discussion	120
3.3.1. <i>Malachite</i>	126
3.3.2. <i>Azurite</i>	129
3.3.3. <i>Lapis lazuli</i>	133
3.4. Conclusions	134
References	136

Capítulo 4: Pigment-size effect on the physico-chemical behavior of azurite-tempera dosimeters under natural and accelerated photo aging

Hipótesis de partida	142
Objetivos de la investigación	144
Abstract	146
4.1. Introduction	147
4.2. Materials and Methods	148
4.2.2. Paint dosimeters preparation	151
4.2.3. <i>UV-accelerated aging test</i>	151
4.2.4. <i>Outdoor sunlight exposure test</i>	152
4.2.5. <i>Analytical techniques</i>	153
4.3. Results and discussion	155
4.3.1. <i>Stereomicroscope study of paint dosimeters</i>	155
4.3.2. <i>Particle size analysis of powder pigments</i>	158

4.3.3. Thermogravimetric analysis of pigments and dosimeters	159
4.3.4. XRD of pigments and dosimeters	160
4.3.5. SEM-EDX of paint dosimeters.....	161
4.3.6. Chromatic features of paint dosimeters	165
4.3.7. Raman analysis	167
4.4. Conclusions	174
References	175

Capítulo 5: Effect of proteinaceous binder on pollution-induced sulfation of lime-based tempera paints

Hipótesis de partida	184
Objetivos de la investigación	185
5.1. Introduction.....	187
5.2. Materials and Methods.....	188
5.2.1. Pigments and binders.....	188
5.2.2. Preparation of paint dosimeters	189
5.2.3. Outdoor exposure test.....	190
5.2.4 Accelerated SO ₂ -aging test.....	192
5.2.5. Analytical techniques	193
5.3. Results and Discussion	194
5.3.1. XRD analysis of pigments and dosimeters before and after accelerated SO ₂ -aging test and outdoor exposure.....	194
5.3.2. Optical microscope study of blank and outdoor exposed dosimeters	199
5.3.3. Color measurements of blank and outdoor-exposed dosimeters	202
5.3.4. FESEM analysis of pigments and paint dosimeters before and after long-term outdoor exposure and accelerated SO ₂ -aging test.....	204
5.4. Raman analysis.....	211
5.5. Conclusions.....	212

<i>References</i>	214
<i>I. General conclusions</i>	222
<i>II. Specific conclusions</i>	224
III. Conclusiones generales	232
IV. Conclusiones específicas.....	234
<i>Appendix I</i>	244
<i>Appendix II</i>	258
<i>Appendix III</i>	264

Acronyms and Abbreviations

ΔE = Total Color difference

A-CHCA = α -cyano-4-hydroxycinnamic acid

ATR = Attenuated Total Reflection

AZ = Azurite ($\text{Cu}_3(\text{CO}_3)_2(\text{OH})_2$)

BD = Bligh-Dyer

BSG = Bianco di San Giovanni

C = Coarse

C^* = Chroma or Saturation of color

Ca = Calcite (CaCO_3)

CCD = Charge Coupled Device

Cer = Ceramide

CIN = Cinnabar (HgS)

DG = Diglycerides

DHA = Docosahexaenoic acid

DHB = 2,5-dihydroxybenzoic acid

DRIFTS = Diffuse Reflectance Infrared Fourier Transform Spectroscopy

E or EY = Egg Yolk

EC: Extra Coarse

EDX = Energy Dispersive X-Ray analysis

EDS = Energy Dispersive Spectroscopy

EF = Extra Fine

FESEM = Field Emission Scanning Electron Microscopy

FORS = Fiber Optics Reflectance Spectroscopy

FTIR = Fourier-Transform Infrared Spectroscopy

G = Gypsum ($\text{CaSO}_4 \cdot 2\text{H}_2\text{O}$)

GC = Gas Chromatography

GC-MS = Gas Chromatography Mass Spectrometry

Gly = Glycine

h^* = Hue

HE = Hematite (Fe_2O_3)

HPLC = High-Pressure Liquid Chromatography

L^* = Lightness or luminosity of color

LAP = Lapis lazuli ($\text{Na}_{8-10}\text{Al}_6\text{Si}_6\text{O}_{24}\text{S}_{2-4}$)

M = Medium

MAL: Malachite ($\text{Cu}_2\text{CO}_3(\text{OH})_2$)

MALDI-TOF = Matrix assisted Laser Desorption Ionisation Time of Flight

MIN = Minium (Pb_3O_4)
MP = Michael Price
MS = Mass Spectrometry
Pc(s) = Principal Componen(s)
PCA = Principal Component Analysis
PM = Particulate Matter
PMF = Peptide Mass Fingerprinting
RG or G= Rabbit Glue
RH or HR = Relative Humidity
RS = Raman Spectroscopy
RMS = Raman Micro-Spectroscopy
SA = Sinapinic acid
SCE = Specular Component Excluded
SCI = Specular Component Included
SEM = Scanning Electron Microscopy
ST = Standard
T = Temperature
TAG or TG = Triacylglycerol or Triglycerides
PL = Phospholipids
PC = Phosphatidylcholine
PE= Phosphatidylethanolamine
LPC = Lisophosphatidylcholine
SM = Sphingomyelin
LPE = lysophosphatidylethanolamine
PI = Phosphatidylinositol
TFA = Trifluoroacetic acid
TGA = Thermogravimetric Analysis or Thermal Gravimetric Analysis
Tr = Trace
UV = Ultraviolet radiation
Vis= Visible
VP = Variable Pressure
WHO = World Health Organization
WL = White Lead or Lead White
XRD = X-Ray Diffraction

Summary

In this doctoral thesis we evaluated the impact of the urban atmospheric aerosol on the physicochemical decay of paint dosimeters (model paint samples) exposed long-term (up to 40 months) to the elements in (semi-) open pilot monuments in the city of Granada, exploring in depth the pigment-binder interaction processes that take place at the interface between the paint and the exposure atmosphere and are responsible for the changes in paint color caused by a variety of atmospheric pollution scenarios. These results have been compared with those obtained in accelerated aging tests in the laboratory in which the paint dosimeters were exposed to SO₂ and UV radiation. In addition, for the first time in this kind of research we analyzed the effect of pigment grain size and the quantity of paint binder in the decay processes affecting paints used in artworks.

In order to achieve the objectives proposed in this thesis, we made a detailed study of the paint dosimeters at different scales (nano- to macroscale), applying a series of complementary analytical techniques that are widely used in research on historic paintings (e.g. SEM-EDX, FTIR-ATR, XRD, RS, spectrophotometry, etc.). We also presented the design of new analysis protocols with enormous potential in research into artists' paints. These include the updating of the lipidomic analytical techniques used in the analysis of the interaction between the lipid binder and the pigment. We also applied chemometric techniques (PCA) to spectrophotometry data from model paint samples exposed to the elements, so as to improve our understanding of the color changes they undergo and assess the decay tendencies produced by exposure to different atmospheric pollution scenarios.

In the first piece of research in this Doctoral Thesis, we used MALDI-TOF-MS to characterize the lipids in the model paint samples made by mixing egg yolk with one of the following pigments: calcite, gypsum, lead white, hematite, minium, cinnabar, azurite, lapis lazuli and malachite. We then analyzed the same paint dosimeters after they had been exposed to the elements for six months in different (semi-) open monuments in the city of Granada.

By comparing the mass spectra for the fresh and decayed paint samples, we were able to evaluate the impact of urban pollution on the lipids in the egg yolk binder used in the paints, paying special attention to the interaction between the binder and the pigment. In order to make this evaluation using MALDI-TOF-MS we optimized the method for extracting the lipids from the paint samples. The results revealed that in the mass spectra for the lipids, certain masses are repeated in all the paint dosimeters (except for the one containing lead white), and they can therefore be used as indicators of the presence of egg yolk in the binder. This also suggests that beta oxidation is the mechanism responsible for the decomposition of the lipids in all the aged paint samples (except for those made with lead white pigment).

In the second piece of research presented here we conducted color measurements using a portable spectrophotometer over a period of 18 months in paint dosimeters exposed to the elements in 7 pilot monuments in the city of Granada. The dosimeters we analyzed were made with egg yolk or rabbit glue mixed with azurite (with different grain sizes), lapis lazuli or malachite (binary mixtures). With the color data obtained we tested a multivariate approach for the discrete chromatic parameters in a pioneering study that combined spectrophotometric data and principal component analysis (PCA) to detect anti-aesthetic changes in the color of the model paints exposed to different urban atmospheres, in this case in the city of Granada (Spain). Our results reveal that the specific chromatic parameters that cause the changes in color for each kind of paint dosimeter can be evaluated by assessing the influence of the nature of the binder and the pigment and of the grain size of the pigment. This new approach is capable of differentiating between paint samples according to their composition, so enabling a better understanding of their aging process.

In the third piece of research that makes up this doctoral thesis, we applied a multi-analytical approach which combined spectroscopic and surface techniques to characterize and compare model paint dosimeters made with rabbit glue and azurite with different grain sizes and their corresponding, naturally aged (by exposure to the elements) and artificially

aged (by UV radiation in the laboratory) dosimeters. In these paint samples we analyzed the role played by pigment grain size in pigment-binder interaction. The results demonstrated its importance in paint decay processes. The research also provided new data about the probable formation of protein-copper complexes (organometallic compounds) that change the physicochemical properties of the paints, so altering their behavior when subjected to aging. The accelerated aging tests revealed that the dosimeters containing the finest grain azurite suffered the greatest structural changes in the binder. The grain size of the azurite also affected the formation of cracks in the paint, which are more abundant the larger the pigment grain size, as there is a higher proportion of binder in the paint.

The last piece of research evaluates the effect of SO₂ on paint dosimeters made by mixing a protein binder (egg yolk or rabbit glue) with calcite, or with calcite and portlandite. In these samples the particle size of the mineral phases also varied. As in the previous study, we characterized and compared the control paint dosimeters with others aged by long-term exposure to the elements in the urban atmosphere of the city of Granada, and a third group aged in an accelerated aging test with SO₂ in the laboratory. This comparative study enabled us to find out more about the sulfation process in artist's paints made with calcite, a question that has so far never been addressed in the literature.

The results of the artificial aging tests in the laboratory revealed that the binder delays the sulfation process (formation of a gypsum crust) in the paints made with calcite and in those made with calcite and portlandite. Those made only with calcite were less affected by this problem. There were no clear signs of sulfation on the naturally aged paint samples from pilot monuments in the city of Granada which were exposed to the elements for 40 months.

General objective

The general objective of this Doctoral Thesis is to find out more about the processes of chemical and physical deterioration that take place in artists' paints made with tempera due to exposure to urban atmospheric pollution. The research focuses above all on the interaction between the pigment and the binder and for the first time analyses the effect of pigment grain size and the amount of binder on decay in these paints. With this general objective in mind, we prepared various paint dosimeters (model samples of paint made according to historical recipes) which were then subjected to natural aging tests (exposure to the elements in (semi-) open pilot monuments in the city of Granada) and artificial aging in the laboratory. This general objective is made up of the following more specific objectives.

Specific objectives

1. An in-depth study at different scales (nano- to macroscale) of the interaction between paint materials (mineral pigments and protein binders, e.g. rabbit glue and egg yolk) when exposed to the urban atmospheric aerosol. In order to achieve this specific objective a wide range of complementary analytical techniques were applied to the paint dosimeters and compared with the results of natural aging tests (exposure to the air in the city of Granada), and accelerated aging tests (exposure to SO₂ and UV radiation).
2. Assessment of the influence of the grain size and the mineralogical composition of the pigment on the pigment-binder interaction, as well as the type and quantity of protein binder, and identification of the role that they play in the decay process affecting historical paintings subjected to atmospheric pollution.
3. Updating of a lipidomic analytical methodology which has great potential in the field of historic paintings, in order to optimize the analysis of the lipid binder – mineral pigment interaction when exposed to urban atmospheric pollution.
4. Application of colorimetric techniques to spectrophotometric data obtained from paint dosimeters that were aged naturally by exposure to different urban area scenarios in the city of Granada, in order to improve our understanding of the chromatic changes that these paints undergo and their development over time, associated with different pigment-binder interaction processes in a range of atmospheric pollution atmospheres.

Structure of the Doctoral Thesis

The research conducted in order to achieve the objectives proposed in this Doctoral Thesis has given rise to four research articles which are presented in Chapters 2, 3, 4 and 5 of this summary. Three of these articles have been published (chapters 2, 3 and 4), and the fourth (chapter 5) is in the process of publication. Earlier, in Chapter 1, we describe the paint materials and the scientific methods used in this research. Finally, we present the most important conclusions reached in this Doctoral Thesis.

Chapter 2: In this research, we present an analytical methodology based on MALDI-TOF-MS using a lipidomic approach for the study of fresh paint dosimeters and others that had been altered by exposure to the urban atmosphere (in the city of Granada). This enabled us to characterize and evaluate the impact of air pollution on the paint samples, paying particular attention to the pigment-binder interaction processes. This research gave rise to the following article:

- **Herrera, A., Navas, N. and Cardell, C. (2016)** *'An evaluation of the impact of urban air pollution on paint dosimeters by tracking changes in the lipid MALDI-TOF mass spectra profile'*, *Talanta*, 155, pp. 53–61. doi: 10.1016/j.talanta.2016.04.006. Índice de Impacto: 4.162 (2016). Posición revista en categoría: Analytical chemistry 9 / 75 (Q1).

Chapter 3: In this chapter we applied a multivariate data exploration technique (Principal Component Analysis) to discrete spectrophotometric data (about color), in order to detect color changes and tendencies in paint dosimeters exposed to the elements in (semi-) open monuments in the city of Granada for a period of 18 months. This enabled us to evaluate the specific chromatic parameters that cause the changes in color for each kind of paint dosimeter. We then assessed the influence of the nature of the binder and the pigment on

these changes in color, as well as the role of pigment grain size. This research was presented in the following article:

- **Herrera, A.**, Ballabio, D., Navas, N., Todeschini, R. and Cardell, C. (2017) '*Principal Component Analysis to interpret changes in chromatic parameters on paint dosimeters exposed long-term to urban air*', *Chemometrics and Intelligent Laboratory Systems*, pp. 113–122. doi: 10.1016/j.chemolab.2017.05.007. Índice de Impacto: 2.303 (2016). Posición revista en categoría: Mathematics, Interdisciplinary applications; 18/101 (Q1).

Chapter 4: In this research, we applied a range of complementary analytical techniques, including XRD, SEM-EDX, FTIR-ATR and micro-Raman spectroscopy, to characterize paint dosimeters made with azurite (different grain sizes) and rabbit glue. These dosimeters had either been naturally aged by exposure to different urban air scenarios in the city of Granada, or artificially aged in the laboratory using UV radiation. This research studies for the first time and demonstrates the influence of pigment grain-size on the pigment-binder interaction and therefore in the processes of decay of artists' paints. This research gave rise to the following article:

- Cardell, C., **Herrera, A.**, Guerra, I., Navas, N., Rodríguez Simón, L. and Elert, K. (2017) '*Pigment-size effect on the physico-chemical behavior of azurite-tempera dosimeters upon natural and accelerated photo aging*', *Dyes and Pigments*, 141, pp. 53–65. doi: 10.1016/j.dyepig.2017.02.001. Índice de Impacto: 3.473 (2016). Posición revista en categoría: Materials science, Textile 1/23 (Q1).

Chapter 5: In the last chapter, we evaluate the effects of SO₂ on paint dosimeters made with either calcite or calcite and portlandite (with different grain sizes) and a protein binder, e.g. egg yolk or rabbit glue. As in the previous chapter, we applied a multi-analytical approach to characterize the paint dosimeters, which were also subjected to natural (exposure to urban air) and artificial aging tests, placing special emphasis on the influence of the type of binder and the composition of the pigment in the sulfation process of the

paint samples. This research gave rise to the following article which is currently in the process of publication.

- **Herrera, A.**, Cardell, C., Pozo-Antonio, J.S., Burgos-Cara, A., Elert, K. (2018) '*Effect of proteinaceous binder on pollution-induced sulfation of lime-based tempera paints*', Progress in organic coating. (under revisión). Índice de Impacto: 2.858. Posición revista en categoría: Materials science, Coatings & Films 3/19 (Q1).

Resumen

En esta Tesis Doctoral se ha evaluado el impacto del aerosol atmosférico urbano en el deterioro físico-químico de dosímetros pictóricos (muestras pictóricas modelo) expuestos a largo plazo (hasta 40 meses) en monumentos piloto (semi)abiertos de Granada capital, profundizando en los procesos de interacción pigmento-aglutinante producidos en la interfase “pintura-ambiente de exposición”, que expliquen los cambios de color producidos en las pinturas debido a distintos escenarios de contaminación atmosférica. Estos resultados se han comparado con los obtenidos en distintos ensayos de alteración acelerada en laboratorio, por exposición de los dosímetros pictóricos a SO₂ y radiación UV. Además por primera vez en este tipo de investigación se aborda el análisis del efecto que tiene el tamaño de grano de los pigmentos y la cantidad de aglutinante pictórico en los procesos de degradación de las pinturas artísticas.

Para alcanzar los objetivos propuestos en esta Tesis Doctoral se ha realizado un estudio en detalle de los dosímetros pictóricos a distintas escalas (nano- hasta macroescala), aplicando un conjunto amplio de técnicas analíticas complementarias de uso tradicional en el patrimonio pictórico (e.g. SEM-EDX, FTIR-ATR, XRD, RS, espectrofotometría, etc). Asimismo, se presenta el diseño de protocolos de análisis novedosos y de alta potencialidad en la investigación de pinturas artísticas, como es la puesta a punto de estrategias analíticas lipídicas aplicadas al análisis de la interacción aglutinante lipídico-pigmento, y la aplicación de técnicas quimiométricas (PCA) a datos espectrofotométricos de pinturas modelo expuestas a la intemperie, para mejorar la interpretación de los cambios cromáticos de las mismas, y determinar tendencias de deterioro por exposición a diferentes escenarios de polución atmosférica.

En el primer trabajo de esta Memoria se caracterizan mediante MALDI-TOF-MS los lípidos presentes en las pinturas modelo patrón elaboradas mezclando yema de huevo y uno de los siguientes pigmentos: calcita, yeso, blanco de plomo, hematites, minio, cinabrio, azurita, lapislázuli y malaquita. Posteriormente se analizan los mismos dosímetros

pictóricos degradados tras ser expuestos 6 meses en distintos monumentos (semi)abiertos de la ciudad de Granada. La comparación de los espectros de masas de las muestras pictóricas frescas y alteradas ha permitido evaluar el impacto de la polución urbana en los lípidos del aglutinante yema de huevo de las pinturas, prestando especial atención a la interacción aglutinante-pigmento. Para poder realizar esta evaluación mediante MALDI-TOF-MS se optimizó el método de extracción de los lípidos de las muestras pictóricas. Los resultados revelaron que en los espectros de masas de los lípidos existen ciertas masas que se repiten en todos los dosímetros pictóricos (excepto aquellos que contienen blanco de plomo), y que por tanto se pueden usar como indicadores de la presencia de yema de huevo en el aglutinante. Además, se sugiere que el mecanismo de descomposición de los lípidos en todas las muestras de pintura envejecidas se debe a beta oxidaciones, excepto en aquellas elaboradas con el pigmento blanco de plomo.

En el segundo trabajo aquí presentado se realizaron medidas de color con un espectrofotómetro portátil a lo largo de 18 meses en dosímetros pictóricos expuestos a la intemperie en 7 monumentos piloto de la ciudad de Granada. Los dosímetros analizados fueron los elaborados con aglutinante de yema de huevo o cola de conejo mezclados con azurita (diferentes tamaños de grano), o lapislázuli o malaquita (mezclas binarias). Con los datos de color obtenidos se ensayó un enfoque multivariante de los parámetros discretos cromáticos en un estudio pionero que combina datos espectrofotométricos y análisis de componentes principales (PCA) para detectar cambios antiestéticos de color en pinturas modelo expuestas en distintos ambientes de aire urbano de una ciudad, en este caso Granada (España). Los resultados revelan que se pueden evaluar los parámetros cromáticos específicos que causan la variación de color para cada tipo de dosímetro pictórico, considerando la influencia de la naturaleza del aglutinante y del pigmento, y el tamaño de grano de este último. Este enfoque novedoso es capaz de discriminar muestras pictóricas según su composición, permitiendo una mejor interpretación de la evolución de su envejecimiento.

En el tercer trabajo que constituye esta Tesis Doctoral se aplica un enfoque multianalítico, que combina técnicas espectroscópicas y de superficie, para caracterizar dosímetros pictóricos patrón de cola de conejo y azurita con diferente tamaño de grano, y los correspondientes dosímetros envejecidos naturalmente (exposición a la intemperie) y artificialmente por radiación UV (laboratorio). En estas muestras pictóricas se ha analizado el papel que desempeña el tamaño de grano del pigmento en la interacción pigmento-aglutinante, poniendo los resultados de manifiesto su importancia en los procesos de degradación de las pinturas. Más aún, la investigación aporta nuevos datos sobre la probable formación de complejos proteína-cobre (compuestos organometálicos), que cambian las propiedades físico-químicas de las pinturas, y así su comportamiento frente al envejecimiento. Los ensayos de envejecimiento acelerado han revelado que los dosímetros conteniendo azurita con tamaño de grano más fino producen mayores cambios estructurales en el aglutinante. Además el tamaño de grano de la azurita también condiciona la formación de grietas en la pintura, que son más abundantes a medida que aumenta el tamaño del pigmento, pues existe mayor proporción de aglutinante en la pintura.

El último trabajo evalúa el efecto que tiene el SO₂ en dosímetros pictóricos confeccionados mezclando un aglutinante proteico (yema de huevo o cola de conejo) con calcita, o con calcita y portlandita. En estas muestras el tamaño de partícula de las fases minerales también es diferente. Como en el trabajo anterior, se han caracterizado los dosímetros pictóricos patrón y los envejecidos por exposición a la intemperie a largo plazo en la atmósfera urbana de la ciudad de Granada, y mediante un ensayo de alteración acelerada con SO₂ en laboratorio. Este estudio comparativo ha permitido profundizar en el proceso de sulfatación de pinturas artísticas al temple elaboradas con calcita, hasta el momento no abordado en la literatura.

Los resultados de laboratorio han revelado que el aglutinante retarda el proceso de sulfatación (formación de costra de yeso) de las pinturas elaboradas con calcita y calcita/portlandita, afectándose menos los dosímetros pictóricos elaborados a base

únicamente de calcita. Por su parte, no hay indicios claros de sulfatación en muestras pictóricas envejecidas de forma natural en los monumentos piloto de la ciudad de Granada, donde se han ubicado durante 40 meses.

Objetivo general

El objetivo general de esta Tesis Doctoral es profundizar en el conocimiento sobre los procesos de deterioro químico y físico que se producen en pinturas artísticas elaboradas al temple por exposición a la polución atmosférica urbana, abordando la investigación desde la perspectiva de la interacción pigmento-aglutinante, y analizando por primera vez el efecto que tienen el tamaño de grano de los pigmentos y la cantidad de aglutinante, en la alteración de dichas pinturas. Para la consecución de este objetivo general se han elaborado dosímetros pictóricos (muestras pictóricas modelo elaboradas según recetas históricas) que han sido sometidos a ensayos de envejecimiento natural (exposición a la intemperie en monumentos piloto (semi-)abiertos de Granada capital) y envejecimiento artificial en laboratorio. Este objetivo general se concreta en los siguientes objetivos específicos.

Objetivos específicos

1. Estudio en profundidad a distintas escalas (nano- hasta macroescala) de la interacción entre materiales pictóricos (pigmentos minerales y aglutinantes proteicos, i.e. cola de conejo y yema de huevo) bajo la influencia del aerosol atmosférico urbano. Para la consecución de este objetivo específico se han aplicado en dosímetros pictóricos un abanico de técnicas analíticas complementarias, y comparado los resultados obtenidos de ensayos de envejecimiento natural (exposición al aire urbano de Granada capital), con los resultados procedentes de ensayos de envejecimiento acelerado (exposición a SO₂ y radiación UV).
2. Determinación de la influencia que en la interacción pigmento-aglutinante tienen el tamaño de grano y la composición mineralógica del pigmento, así como el tipo y cantidad de aglutinante proteico, y en consecuencia, establecer el papel que éstos juegan frente a los fenómenos de degradación de las pinturas históricas sometidas a polución atmosférica.
3. Puesta a punto de una metodología analítica lipidómica de alta potencialidad en el campo del patrimonio pictórico, para optimizar el análisis de la interacción aglutinante lipídico-pigmento mineral bajo el impacto de la contaminación atmosférica urbana.
4. Aplicación de técnicas quimiométricas a datos espectrofotométricos obtenidos en dosímetros pictóricos envejecidos de forma natural por exposición a diferentes escenarios de aire urbano en la ciudad de Granada, con el fin de mejorar la interpretación de los cambios cromáticos sufridos por las pinturas modelo y su evolución en el tiempo, asociados a distintos procesos de interacción pigmento-aglutinante en diversos ambientes de polución atmosférica.

Estructura de la Tesis Doctoral

La consecución de los objetivos planteados en esta Tesis Doctoral ha dado lugar a cuatro artículos de investigación que se presentan en los capítulos 2, 3, 4 y 5 de la presente memoria. Tres de estos trabajos están publicados (capítulos 2, 3 y 4), y el cuarto (capítulo 5) se encuentra en proceso de publicación. Previamente, en el capítulo 1 se presentan los materiales pictóricos y la metodología científica empleada en su investigación. Finalmente se abordan las conclusiones más relevantes obtenidas en esta Tesis Doctoral.

Capítulo 2: En este trabajo se establece una metodología analítica mediante MALDI-TOF-MS empleando un enfoque lipidómico para el estudio de dosímetros pictóricos frescos y alterados a la intemperie en una atmósfera urbana (i.e. Granada capital). De esta manera se ha podido caracterizar y conocer el impacto de la contaminación del aire en muestras pictóricas, prestando especial atención a los procesos de interacción pigmento-aglutinante. Este trabajo ha dado lugar al artículo:

- **Herrera, A., Navas, N. and Cardell, C.** (2016) '*An evaluation of the impact of urban air pollution on paint dosimeters by tracking changes in the lipid MALDI-TOF mass spectra profile*', *Talanta*, 155, pp. 53–61. doi: 10.1016/j.talanta.2016.04.006. Índice de Impacto: 4.162 (2016). Posición revista en categoría: ANALYTICAL CHEMISTRY 9 / 75, (Q1).

Capítulo 3: En este capítulo se aplica un análisis multivariante de exploración de datos, i.e. Análisis de Componentes Principales, a datos espectrofotométricos (de color) discretos, para detectar variaciones y tendencias cromáticas en dosímetros pictóricos expuestos a la intemperie en monumentos (semi-abiertos) de la ciudad de Granada a lo largo de 18 meses. Así, se han podido evaluar los parámetros cromáticos específicos que causan la variación de color para cada tipo de dosímetro pictórico, considerando la influencia de la naturaleza del aglutinante y del pigmento, y del tamaño de grano de este último. Este trabajo ha dado lugar al artículo:

- **Herrera, A.**, Ballabio, D., Navas, N., Todeschini, R. and Cardell, C. (2017) '*Principal Component Analysis to interpret changes in chromatic parameters on paint dosimeters exposed long-term to urban air*', Chemometrics and Intelligent Laboratory Systems, pp. 113–122. doi: 10.1016/j.chemolab.2017.05.007. Índice de Impacto: 2.303 (2016). Posición revista en categoría: MATHEMATICS, INTERDISCIPLINARY APPLICATIONS; 18/101 (Q1).

Capítulo 4: En este trabajo se aplicó un abanico de técnicas analíticas complementarias, entre ellas XRD, SEM-EDX, FTIR-ATR y espectroscopia micro-Raman, para caracterizar dosímetros pictóricos elaborados con azurita (diferente tamaño de grano) y cola de conejo que fueron envejecidos naturalmente, por exposición a distintos escenarios de aire urbano de la ciudad de Granada, y artificialmente en laboratorio por radiación UV. Este trabajo aborda por primera vez, y pone de manifiesto, la influencia del tamaño de grano del pigmento en la interacción pigmento-aglutinante, y por consiguiente en los procesos de degradación de las pinturas artísticas. La investigación ha dado lugar al siguiente artículo:

- Cardell, C., **Herrera, A.**, Guerra, I., Navas, N., Rodríguez Simón, L. and Elert, K. (2017) '*Pigment-size effect on the physico-chemical behavior of azurite-tempera dosimeters upon natural and accelerated photo aging*', Dyes and Pigments, 141, pp. 53–65. doi: 10.1016/j.dyepig.2017.02.001. Índice de Impacto: 3.473 (2016). Posición revista en categoría: MATERIALES SCIENCE, TEXTILE 1/23 (Q1).

Capítulo 5: En el último capítulo se evalúa el efecto que tiene el SO₂ en dosímetros pictóricos elaborados con calcita, o con calcita y portlandita (con diferentes tamaños de grano) y un aglutinante proteico, i.e. yema de huevo o cola de conejo. Como en el capítulo anterior, se aplicó un enfoque multianalítico para caracterizar las muestras pictóricas que también fueron sometidas a ensayos de envejecimiento natural (exposición al aire urbano de Granada capital) y artificial, poniendo un especial énfasis en la influencia que tiene el tipo de aglutinante y la composición del pigmento en el proceso de sulfatación de las

muestras pictóricas. Este estudio ha dado lugar al siguiente artículo que se encuentra en fase de publicación:

- **Herrera, A.**, Cardell, C., Pozo-Antonio, J.S., Burgos-Cara, A., Elert, K. (2018) '*Effect of proteinaceous binder on pollution-induced sulfation of lime-based tempera paints*', Progress in organic coating, (under revisión). Índice de Impacto: 2.858. Posición revista en categoría: MATERIALS SCIENCE, COATINGS & FILMS 3/19. (Q1).

Introducción

La mayoría de la gente dice que el intelecto es lo que hace a un gran científico. Están equivocados: es el carácter.

Albert Einstein



Salvador Dalí-Muchacha en la ventana

I. Patrimonio pictórico

No existe una definición exacta para el término patrimonio pictórico. Según el origen etimológico de estas palabras, el vocablo patrimonio procede del latín *patrimonium* y se define como “... conjunto de bienes de una nación acumulado a lo largo de los siglos, que, por su significado artístico, arqueológico, etc., son objeto de protección especial por la legislación” (Real Academia Española, 2017). El término pictórico es un adjetivo que proviene de *pictor*, un término latino que puede traducirse como “pintor”, que se define como “perteneciente o relativo a la pintura” (Real Academia Española, 2017). Por lo tanto, se puede definir el patrimonio pictórico como el patrimonio que engloba las pinturas artísticas que han sido heredadas a lo largo de la historia.

La Figura I.1 muestra la clasificación de patrimonio según los documentos internacionales (Unesco, 2004). Así, el patrimonio pictórico se engloba dentro del patrimonio cultural tangible, perteneciendo al subgrupo de “inmuebles” donde se encuentran las pinturas murales, policromías, etc. Además, el patrimonio pictórico puede pertenecer al patrimonio cultural tangible “muebles” ya que en esta categoría se encuentran las obras de arte, esculturas, etc. Sin embargo, en esta Tesis Doctoral se enmarca en el grupo del patrimonio cultural tangible “inmuebles”; en concreto hace referencia a la pintura mural al temple.

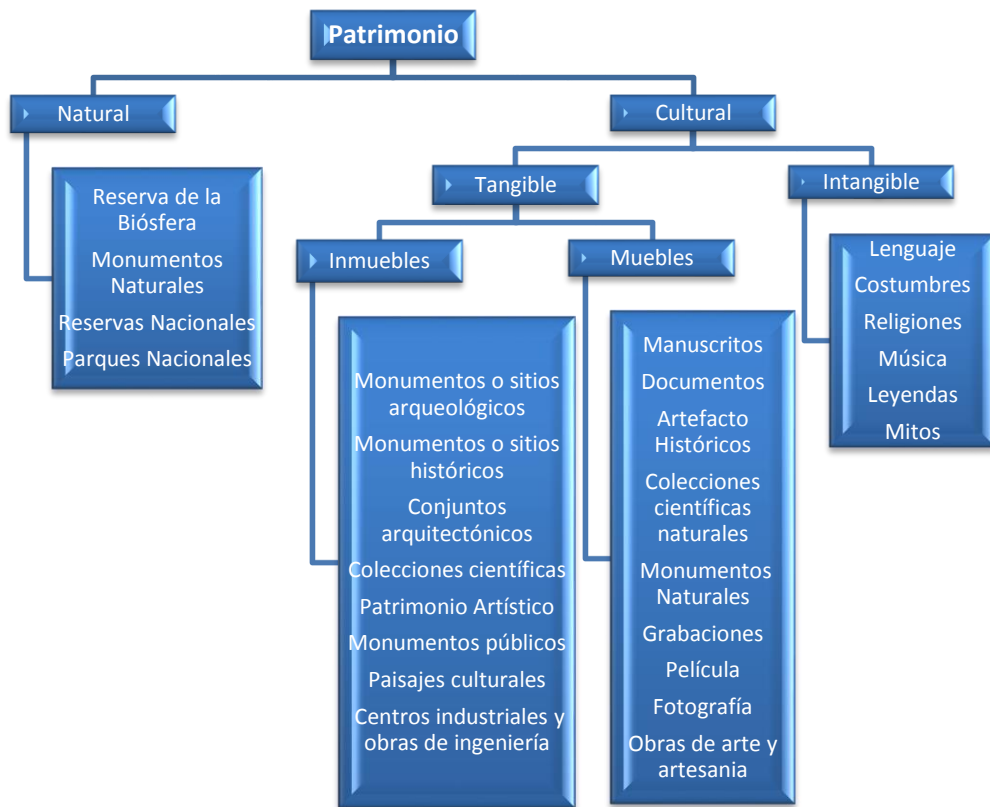


Figura I.1 Clasificación de patrimonio en base a la legislación internacional.

Desde el comienzo de los tiempos, la pintura mural ha sido una expresión cultural de la creación humana a lo largo de la historia, abarcando desde el arte rupestre hasta los murales actuales. Su deterioro, destrucción accidental o intencionalidad constituye una pérdida que afecta a una parte significativa del patrimonio cultural. Como documento importante a seguir en este contexto se puede citar la “Carta de Venecia” (1964), en la cual se pueden encontrar bases generales dirigidas fundamentalmente a la conservación y/o restauración del patrimonio cultural. Posteriormente, la denominada “Declaración de Amsterdam” (1975) introdujo el concepto de conservación integrada, ampliamente utilizado desde entonces; y ya más recientemente, el “Documento de Nara” (1994) está enfocado al concepto de la autenticidad. Estos documentos junto con otras contribuciones adicionales relevantes en este contexto, tales como el “Código de ética ICOM-CC” (1984),

el “Documento de Pavía” (1997) y las “E.C.C.O. directrices profesionales” (1997), así como la denominada “carta de ICOMOS” (International Council on Monuments and Sites) tienen como objetivo principal dotar a la comunidad internacional de principios más específicos y eficaces para la consecución de la protección, la preservación y la conservación y la restauración de pinturas murales.

Muchos de los problemas que afectan a las pinturas murales están vinculados a las malas condiciones del edificio o estructura que las sustentan, falta de mantenimiento de estos sustratos, y alteraciones y/o reparaciones frecuentes. También deben considerarse las intervenciones de consolidación y/o restauración incorrecta, y el uso de métodos y materiales inadecuados, que pueden causar daños irreparables si se acometen sin un estudio analítico previo de caracterización de las pinturas, y de sus procesos de degradación.

Por ello, uno de los objetivos de esta Tesis Doctoral es arrojar luz sobre las causas y mecanismos de deterioro que afectan a las pinturas artísticas elaboradas al temple, haciendo especial hincapié en los procesos de interacción pigmento-aglutinante que pueden ocasionar su alteración físico-química.

II. Deterioro de pinturas históricas por atmosferas urbanas

Impacto de atmósferas urbanas y cambio climático en el patrimonio pictórico

En las últimas décadas se ha producido un aumento de los estudios centrados en el deterioro del patrimonio pictórico, y se ha concedido una atención especial a sus condiciones ambientales de exposición porque son decisivas en su conservación (Staniforth et al .,2013). Existe una larga tradición de investigación en la caracterización de objetos artísticos en Europa (Cassar 1995; Camuffo 2001; Pavlogeorgatos 2003), de micro-ambientes de exposición (luz, temperatura, humedad relativa, luminosidad...) e incluso de calidad del aire (Brimblecombe 2003; Varotsos et al. 2009; Watt 2009; Horemans et al. 2011; Kontozova-Deutsch et al. 2011; Van Grieken and Worobiec 2011; Tidblad et al. 2012;

Pantavou et al., 2017). Estos estudios se han focalizado principalmente en los estudios de deterioro de materiales pétreo por efecto de atmósferas urbanas y/o marinas (Sabbionit et al., 1998; Urosevic et al., 2012; Moropoulou et al., 2018; Pozo-Antonio et al., 2018), y en los últimos años del cambio climático (Sabbioni et al., 2009; Sabbioni et al., 2010). En estos trabajos se ha determinado el efecto de gases atmosféricos contaminantes como SO₂, NO_x, O₃, y CO₂, y estimado indicadores y niveles de polución, estableciendo modelos de corrosión pétreo. No obstante, este tipo de estudios es más restringido en el patrimonio pictórico (Kontozova-Deutsch et al., 2011; Horemans et al., 2011; Patrón et al., 2017).

En el contexto de patrimonio pictórico y contaminación atmosférica, la conservación preventiva (estrategia dominante en la gestión del patrimonio cultural) se ha centrado casi exclusivamente en estudios de ambientes cerrados (museos, iglesias...), donde suelen controlarse las condiciones ambientales y de calidad del aire. Como parte de estos estudios, se han examinado los cambios sufridos en colecciones artísticas y pictóricas, y analizado agentes de alteración como el aerosol atmosférico (Van Grieken and Worobiec, 2011).

En numerosos casos, para realizar los estudios antes mencionados se ha hecho uso de muestras pictóricas modelo (elaboradas según recetas pictóricas tradicionales) denominadas dosímetros pictóricos (Bacci et al., 2000; Odlyha et al., 2000; Van den Brink et al., 2000). De hecho, son abundantes los trabajos que emplean dosímetros pictóricos envejecidos naturalmente en, por ejemplo, museos, para investigar el deterioro de materiales orgánicos y barnices (Bacci et al., 2000; Odlyha et al., 2000; Van den Brink et al., 2000; Godoi et al., 2008; Grøntoft et al., 2010). En cambio, los estudios de deterioro de pinturas expuestas a atmósferas contaminadas y/o marinas son escasos (Pérez-Rodríguez et al., 1998; Smith and Clark 2002; Cotte et al., 2006; Campos-Suñol et al., 2009; Navas et al., 2010; Horemans et al., 2011; Maguregui et al., 2014; Elert et al., 2018).

En las últimas décadas los niveles de SO₂ han descendido en Europa (por normativa, excepto en zonas volcánicas), en cambio ha incrementado la concentración de otros gases como NO_x, O₃, y NH₃, de compuestos orgánicos volátiles, y de partículas atmosféricas, creando nuevos escenarios de polución, a lo que además contribuye el cambio climático

(Bytnerowicz et al., 2007; Ramanathan and Feng, 2009; Titos et al., 2015; Chmutina et al., 2016; Patrón et al., 2017). Así, el deterioro de obras de arte expuestas a la intemperie está empeorando en zonas urbanas donde el tráfico es intenso, y en regiones cálidas como las Mediterráneas con orografías particulares, como es el caso de Granada capital (Patrón et al., 2017). Autores como Urosevic et al., 2012 pusieron de manifiesto que el aire de la ciudad de Granada está dominado por: i) partículas de polvo terrígeno y hollín que favorecen el oscurecimiento de sustratos pétreos y la formación de costras negras en monumentos, en menos de 2 años, ii) aerosoles marinos (NaCl, KCl), aerosoles inorgánicos secundarios (SO_4^{2-} y NO_3^- de Na/K/Mg/ NH_4), y iii) partículas complejas de Si-Al, metálicas ricas en Fe-C y metales pesados (V, Ni, Cr, Cu, Pb y Zn). Por su parte, Horemans et al., 2011 verificaron la interacción entre partículas atmosféricas cloruradas y pigmentos de policromías en el conjunto monumental de la Alhambra y Generalife, contribuyendo así a su cambio cromático.

Entre los objetivos de esta Tesis Doctoral se encuentra analizar los procesos de deterioro que sufren las pinturas artísticas por efecto de atmósferas urbanas. Para tal fin se han realizado ensayos de alteración natural de dosímetros pictóricos expuestos en monumentos piloto (semi-) abiertos en la ciudad de Granada, y los resultados se han comparado con los obtenidos en ensayos de alteración acelerada en laboratorio (atmósfera rica en SO_2 y radiación UV).

Degradación cromática de pinturas artísticas por contaminación atmosférica. Estudio a escala macroscópica

El cambio de color en una pintura artística es un efecto visible inmediato. Estos cambios pueden deberse al impacto del ambiente de exposición que puede originar transformaciones mineralógicas del pigmento inorgánico, oxidación del aglutinante, precipitación de nuevas fases (como sales), depósito de partículas atmosféricas, etc. A pesar de ello, aún son insuficientes los trabajos relacionados con los efectos del aerosol atmosférico (en concreto de material particulado mineral u orgánico) y del cambio

climático en pinturas (Smith and Clark 2002; Cotte et al., 2006; Lluveras et al., 2010; Fremout et al., 2011; Horemans et al., 2011; Bourges et al., 2014; Andersen et al., 2017). Algunas instituciones y galerías de arte han realizado grandes inversiones para monitorizar cambios cromáticos durante largos periodos de tiempo en sus colecciones artísticas (Saunders et al., 1996; Mazzeo et al., 2008). Sin embargo, aún son escasos los estudios de variación cromática de corta y/o larga duración de dosímetros pictóricos en condiciones de exposición a la intemperie, donde los cambios cromáticos más importantes pueden deberse al impacto de la polución y condiciones microclimáticas concretas, por ejemplo, el impacto directo de la radiación solar o de la lluvia.

El cambio de color en objetos del patrimonio histórico ha generado en los últimos años un gran interés, tanto por parte de expertos como de la sociedad en general (Bacci et al., 2008). A pesar de ello aún son escasos los estudios sobre variación cromática de pinturas artísticas expuestas al impacto de atmósferas contaminantes, aunque existen investigaciones pioneras como las realizadas por Aze et al., 2007, Horemans et al., 2011 y Maguregui et al., 2011, que han demostrado el efecto adverso de las partículas minerales y del NO₂ y SO₂ atmosféricos en policromías y pinturas murales. Igualmente siguen siendo insuficientes las investigaciones realizadas con dosímetros pictóricos expuestos a la intemperie en atmósferas urbanas, para analizar las variaciones cromáticas y el deterioro de los materiales pictóricos debido al aerosol atmosférico y el cambio climático (Patrón et al., 2017). Estos análisis permitirían determinar la función de daño de las pinturas y sus coeficientes de cambio de color (Brimblecombe and Grossi, 2004), como se ha realizado con éxito en piedra, plásticos, acero pintado y madera (Grossi et al. 2003; Brimblecombe and Grossi 2004; Urosevic et al. 2012).

Con el fin de contribuir a un mejor conocimiento de la problemática expuesta anteriormente, esta Tesis Doctoral se ha fijado como uno de sus objetivos desarrollar y optimizar metodologías analíticas que permitan predecir variaciones cromáticas en dosímetros pictóricos expuestos en diversos escenarios atmosféricos en una ciudad con variados índices de contaminación, como es Granada capital. Para ello se han situado

muestras pictóricas modelo en diversos monumentos (semi-)abiertos de la ciudad ubicados en zonas con diferente calidad del aire (centro ciudad y en colinas, i.e. Sabika donde se asienta el complejo monumental de la Alhambra y Generalife, y el Albayzín).

*Interacción entre materiales pictóricos bajo la influencia del aerosol atmosférico urbano.
Análisis a escala microscópica y molecular*

La mejor manera de plantear y ejecutar estrategias de conservación tradicional y preventiva del patrimonio pictórico es mediante una investigación multidisciplinar que aborde la caracterización de la obra pictórica, el ambiente donde está expuesta, y los procesos de deterioro que sufre, considerando la interacción entre sus materiales pictóricos. Las pinturas artísticas están formadas por mezclas complejas de componentes inorgánicos (pigmentos y cargas) y orgánicos (aglutinantes) de origen natural o artificial, aplicadas en capas heterogéneas sobre diferentes sustratos. Algunos de los componentes pictóricos pueden estar en cantidades traza en la pintura, o poseer un tamaño nano- o micrométrico (en el caso de los pigmentos minerales) (Cardell and Guerra, 2016). Además, pueden reaccionar entre sí sufriendo modificaciones a escala molecular o microescala como respuesta a un envejecimiento natural, debido a, por ejemplo, exposición a atmósferas contaminadas, radiación solar, impacto de lluvia, etc. Estas características, y el hecho adicional de que las pinturas artísticas poseen un carácter único, hacen que el análisis científico de las obras pictóricas sea un desafío científico (Romero-Pastor et al., 2011b).

Es por ello que la investigación científica de los mecanismos de alteración que sufren las pinturas históricas se ha realizado en las últimas décadas empleando dosímetros pictóricos envejecidos de forma natural y/o acelerada, y aplicando sobre ellos un abanico de técnicas analíticas tradicionales y avanzadas, diseñadas expresamente para caracterizar la pintura (Romero-Pastor et al. 2011a; Rivas et al., 2017; Pozo-Antonio et al., 2018). Esta dificultad antes mencionada ha favorecido que tradicionalmente la caracterización de los componentes pictóricos se hiciera por separado. Por tanto los trabajos que investigan la

interacción pigmento-aglutinante son escasos, aunque este panorama está cambiando en los últimos años (Doménech-Carbó et al. 2006; Grøntoft et al. 2010; Manzano et al. 2010; Romero-Pastor et al. 2011a; Ghezzi et al. 2015; Pozo-Antonio et al., 2018)

En consecuencia, otro de los objetivos abordados en esta Tesis Doctoral es presentar nuevas estrategias metodológicas para el análisis de obras pictóricas, que incluyen la aplicación de multitécnicas analíticas para conocer la composición, textura y morfología de los materiales pictóricos a distintas escalas (desde molecular a macroscópica), que arrojen luz sobre los procesos de interacción pigmento-aglutinante, y los mecanismos de degradación físico-química bajo ambientes de contaminación atmosférica. Por primera vez en este tipo de estudios se aborda el análisis del efecto de tamaño de grano en los pigmentos, y la cantidad de aglutinante presentes en la pintura.

III. Mecanismos de alteración físico-química de pinturas históricas

El estudio de los procesos de alteración físico-química que sufre el patrimonio pictórico es uno de los grandes retos que actualmente deben afrontar los investigadores y expertos dedicados a proteger tal legado cultural. Los procesos de degradación de los materiales pictóricos dependen de factores como la composición química del pigmento o aglutinante y sus propiedades físicas, el ambiente de exposición de la pintura (influencia del sol, lluvia, viento, contaminación atmosférica...), presencia de sales solubles y microorganismos en materiales adyacentes o sustrato, etc. (Lliveras et al., 2010; Salvadó et al., 2013; Baglioni et al., 2015; Andersen et al., 2017).

A continuación, se presentan algunas de las alteraciones más comunes que sufren los pigmentos inorgánicos y aglutinantes proteicos habitualmente usados en pintura artística al temple (Eastaugh et al., 2008), y que corresponden a algunos de los materiales pictóricos estudiados en esta Tesis Doctoral.

Alteración de pigmentos inorgánicos

❖ **Calcita**

La calcita (CaCO_3) se ha usado ampliamente como pigmento y como material de carga en pinturas artísticas. Una de las alteraciones más frecuente que sufre la calcita cuando está presente en una obra expuesta a la intemperie se produce por interacción con el SO_2 atmosférico.

Mientras que son abundantes los estudios de sulfatación de materiales pétreos por atmósferas contaminadas, son realmente escasos los estudios similares realizados en pinturas. Autores como Rodríguez-Navarro and Sebastián 1996 y Urosevic et al., 2012 encontraron que, en piedras calizas usadas en monumentos granadinos, el mecanismo de transformación de calcita en yeso se favorece por presencia de partículas carbonáceas y metálicas (Fe, Cr, Ni, Cu y Mn), éstas últimas procedentes principalmente de la combustión del tráfico rodado. Estos autores propusieron que dichos metales favorecen una mayor tasa de oxidación catalítica del SO_2 y, por lo tanto, aceleran la formación de costras de yeso.

Como ya se ha comentado, existe poca información acerca de los efectos del impacto de atmósferas contaminadas ricas en SO_2 en pinturas históricas compuestas por calcita y aglutinantes proteicos. Por ello, debido a la escasa información sobre los mecanismos de formación de yeso a partir de pinturas ricas en calcita, en esta Tesis Doctoral se han realizado, en dosímetros pictóricos elaborados con calcita y dos tipos de aglutinantes proteicos, ensayos de envejecimiento natural a la intemperie (exposición en atmósfera urbana contaminada), y ensayos de envejecimiento acelerado con SO_2 en laboratorio.

❖ **Yeso**

Al igual que la calcita, el yeso ($\text{CaSO}_4 \cdot 2\text{H}_2\text{O}$) es un material pictórico muy usado como pigmento, principalmente en las capas de preparación de pinturas. El yeso es muy susceptible a sufrir alteraciones por la presencia de humedad debido a su carácter higroscópico (Zehnder and Riederer, 1996). En las pinturas murales y esculturas

policromadas al temple del interior de la Iglesia de San Jerónimo en Granada, sobre el soporte de calcarenita se aplicaron capas de preparación de yeso muy porosas que potenciaron la alteración de las pinturas y su pérdida irreversible. Problemas estructurales del edificio y un inadecuado mantenimiento del mismo favorecieron la infiltración de agua a través de la calcarenita, propiciando la disolución y subsecuente cristalización del yeso de las capas de preparación. Posteriormente, la reacción entre el sulfato procedente del yeso y los cationes de los minerales que componen los pigmentos, originaron la neoformación de sales sulfatadas más complejas que actuaron de cuña entre el soporte y la pintura, produciendo su desprendimiento (Cardell-Fernández and Rodríguez-Gordillo, 2003)

❖ Blanco de Plomo

El blanco de plomo es un pigmento compuesto normalmente por una mezcla de cerusita (PbCO_3) e hidrocerusita ($\text{Pb}_3(\text{CO}_3)_2(\text{OH})_2$), utilizado durante muchos siglos en obras pictóricas tanto europeas como asiáticas (Eastaugh et al., 2008). Los fenómenos de degradación del blanco de plomo son a menudo descritos como ennegrecimiento, pero también viraje a colores rosa claro, marrón, gris moteado y negro (Lussier and Smith, 2007). Desde la antigüedad se conoce que el blanco de plomo se ve afectado por presencia de H_2S y compuestos sulfurosos. Smith and Clark 2002 demostraron que la cerusita era más resistente al oscurecimiento que el blanco de plomo. Por su parte otros estudios han revelado que pigmentos ricos en azufre como el oropimente (As_2S_3) y el rejalgam (As_4S_4) provocan el ennegrecimiento del blanco de plomo por favorecer su transformación a galena (PbS), circunstancia no producida en presencia de pigmentos como el cinabrio (HgS), el ultramar ($\text{Na}_8\text{Al}_6\text{Si}_6\text{O}_{24}\text{S}_{2-4}$) y el amarillo de cadmio (CdS). También se ha verificado la capacidad de los ácidos grasos de alterar el blanco de plomo a tonos rosados, rojizos o marrones en presencia de H_2S (Hoevel, 1985; Carlyle and Townsend, 1990).

Otro mecanismo de alteración que afecta al blanco de plomo es la transformación a plattnerita (PbO_2) en ambiente alcalino, por lo que su uso es desaconsejado en la técnica pictórica al fresco (Matteini and Moles, 1981; Koller et al., 1990). Matteini and Moles 1981

indican que el pH básico tan elevado que se alcanza cuando se prepara el *intonaco* en la técnica al fresco, es suficiente para reducir el potencial redox y que se oxide el blanco de plomo. Otros autores demostraron que la transformación del blanco de plomo a plattnerita puede producirse por acción microbiana (Petushkova and Lyalikova, 1986) o por el uso de fungicidas (Kotulanova et al., 2006).

En esta Tesis Doctoral se han investigado las transformaciones ocurridas en dosímetros pictóricos elaborados con blanco de plomo y yema de huevo envejecidos de forma natural a la intemperie. Se comprobó que el blanco de plomo tiene un efecto catalizador en la degradación oxidativa de las pinturas, siendo su deterioro muy diferente a otros dosímetros pictóricos elaborados con yema de huevo y diferente tipo de pigmentos (capítulo 2), probablemente debido a la facilidad que tiene el blanco de plomo en formar jabones en presencia de ácidos grasos (Cotte et al., 2017).

❖ Hematites

La hematites (Fe_2O_3) es uno de los pigmentos más antiguos que se conocen (Mayer and Sheehan, 1991). La bibliografía es escasa sobre los procesos de deterioro de la hematites, puesto que es un pigmento bastante estable. Sin embargo, en estudios realizados en pinturas murales en Pompeya se observaron unas costras ennegrecidas encima del pigmento de hematites. Estas costras estaban compuestas por magnetita (Fe_3O_4) y yeso (Maguregui et al., 2011). Posteriormente se realizaron experimentos de alteración acelerada con el fin de simular el posible deterioro de la hematites (Maguregui et al., 2014). Tras varios ciclos con SO_2 se confirmó la transformación de hematites a magnetita, y en presencia de niveles altos de SO_2 (similares a los alcanzados durante erupciones volcánicas del Vesubio) la sulfatación de la hematites transformándose en (para)coquimbita ($\text{Fe}_2(\text{SO}_4)_3 \cdot 9\text{H}_2\text{O}$).

❖ Minio

Los procesos de alteración que pueden afectar al minio (Pb_3O_4), considerado por algunos historiadores del arte como el pigmento manufacturado más antiguo (Gettens et al., 1986),

son diversos según la técnica pictórica utilizada en la obra de arte. Por ejemplo, el oscurecimiento del minio en numerosas esculturas policromadas (Doménech-Carbó et al., 2000) y pinturas murales (Daniilia et al., 2000) generalmente se atribuye a la formación de plattnerita (PbO_2). En cambio, en la mayoría de los estudios realizados en manuscritos, el minio sufre una transformación a galena (PbS) que podría deberse a la interacción del pigmento con el H_2S atmosférico (Smith and Clark, 2002). También se ha demostrado que la interacción de gases contaminantes como SO_2 y CO_2 con el minio origina su transformación a cerusita y anglesita (PbSO_4) (Aze et al., 2007). El minio además se describe como un pigmento fotosensible (Daniilia et al., 2000). Más aún, la interacción del láser con el minio durante el análisis con espectroscopía Raman puede inducir su fotodegradación (Burgio et al., 2001; Navas et al., 2010) y por tanto conducir a interpretaciones erróneas (Andalò et al., 2001). Igualmente se han realizado estudios sobre la acción que pueden ejercer gases como CO_2 , N_2 , O_2 en presencia de humedad y luz, en la posible transformación a plattnerita, y por tanto en el ennegrecimiento del minio (Hwang et al., 1993). En esta Tesis Doctoral, en dosímetros pictóricos elaborados con minio, se comprobó que la degradación producida por el impacto del láser de la espectroscopía Raman en condiciones muy energéticas, fue la transformación del minio a litargirio (PbO). En el ensayo de envejecimiento natural por exposición a la atmosfera urbana de Granada, en los dosímetros pictóricos elaborados con minio si se han producidos un cambio de color apreciable al ojo humano.

❖ Cinabrio

El cinabrio (HgS) ha sido un pigmento ampliamente utilizado desde la antigüedad (Eastaugh et al., 2008), y considerado resistente a los agentes ácidos y alcalinos, no reaccionando con otros pigmentos (Matteini et al., 2001). Sin embargo, se reconoce que es un pigmento fotosensible, describiéndose su oscurecimiento cuando aparece mezclado con diferentes aglutinantes, i.e. aceites, medios proteicos, y cal (Spring and Grout, 2002; Cotte et al., 2006).

Las hipótesis sobre los mecanismos de degradación del cinabrio que provocan su ennegrecimiento son muy variadas. Hasta hace poco la de mayor aceptación era la transformación del cinabrio rojo (sistema hexagonal, α -HgS) en metacinabrio negro (sistema cúbico, β -HgS) debido al impacto de la luz. Sin embargo, esta hipótesis nunca ha podido ser demostrada con seguridad en obras de arte (Feller, 1967). Dentro de la comunidad científica han surgido nuevas hipótesis sobre el oscurecimiento del cinabrio. Diversos investigadores (Cotte et al., 2006; Neiman et al., 2015) invocan el papel clave jugado por el NaCl en el proceso de oscurecimiento del cinabrio en pinturas históricas, a través de la formación de compuestos de cloruro de mercurio, o como un catalizador en la fotoquímica redox de Hg(II)S en Hg(0) y S(0). Otros trabajos en los que se analizaron muestras pictóricas modelo con distintos compuestos y bajo diferentes ambientes verificaron que la presencia de cloro es fundamental en el proceso de oscurecimiento del cinabrio (Radepon, 2013). En este trabajo no se identificó nunca metacinabrio, planteando la posibilidad de que el oscurecimiento del cinabrio se debe al mercurio en estado metálico.

A lo largo de esta Tesis Doctoral se han realizado algunos estudios preliminares sobre los mecanismos de degradación de dosímetros pictóricos elaborados con cinabrio. Los resultados, presentados en congresos internacionales, no sugieren que el oscurecimiento de los dosímetros de cinabrio expuestos a la intemperie esté relacionado con la presencia de cloro, pero sí con la intensa incidencia de la radiación solar, produciéndose ennegrecimiento en dosímetros de cinabrio elaborados tanto con yema de huevo como con cola de conejo.

❖ **Lapislázuli**

El lapislázuli es uno de los pigmentos más valorados, costosos y bellos que existen. El lapislázuli procede de la lazurita ($\text{Na}_3\text{Ca}(\text{Si}_3\text{Al}_3\text{O}_{12})\text{S}$), roca en cuya composición intervienen otros minerales como la calcita, el diópsido ($\text{CaMgSi}_2\text{O}_6$) y la piritita (FeS_2) (Eastaugh et al., 2008). El lapislázuli es un pigmento estable a la luz solar y aunque es bastante resistente a los agentes atmosféricos, se torna grisáceo por acción de la humedad relativa y el SO_2 . Por otra parte, se ha descrito otro tipo de deterioro relacionado con las impurezas que contiene

el pigmento natural. Así, en el tesoro egipcio de Tôd se encontraron abundantes bloques de lapislázuli, tallas y otros objetos creados con lapislázuli que mostraban en su superficie la presencia dispersa de cristalitos rojos. Se demostró que tales cristales se habían formado por la oxidación de la pirita contenida en el lapislázuli (Calligaro et al., 2014).

❖ Azurita

La azurita ($2\text{CuCO}_3 \cdot \text{Cu}(\text{OH})_2$) se empleó principalmente en pintura artística durante la Edad Media y el Renacimiento, tanto en Europa como en el Este (Mattei et al., 2008). La azurita es un pigmento susceptible de ser alterado por diversas causas. Así, se ha descrito su deterioro por exposición a medios alcalinos (Matteini et al., 2001), y por acción de la humedad y presencia de compuesto clorurados, como se encontró en las pinturas de San Antonio Abate en la iglesia de San Pietro en Quaracchi (Italia), donde se identificó paratacamita ($\text{Cu}_{1.5}\text{Zn}_{0.5}(\text{OH})_3\text{Cl}$) de color verde como producto de degradación de la azurita. Lluveras et al., 2010 también identificaron paratacamita además de atacamita ($\text{Cu}_2\text{Cl}(\text{OH})_3$) y oxalato de cobre (moolooíta, $\text{CuC}_2\text{O}_4 \cdot n\text{H}_2\text{O}$) como productos de alteración en pintura mural.

Por otra parte, en los ensayos de envejecimiento acelerado con H_2S en varios pigmentos de azurita, Smith and Clark (2002) observaron un ennegrecimiento de la azurita debido a su transformación en covelita (CuS). El oscurecimiento de la azurita también ha sido descrita por Mattei et al. (2008) en pinturas murales al fresco, debido al medio alcalino ($\text{pH}=12$) que origina esta técnica pictórica que utiliza $\text{Ca}(\text{OH})_2$ como consolidante. En este caso, el cambio de color se debe a la transformación de azurita en tenorita (CuO). Pero el deterioro más frecuente descrito en la azurita es su transformación a malaquita (Mansour, 1994), como ha ocurrido en las pinturas murales de la catedral de Siena (Italia) (Mugnaini et al., 2006).

En esta Tesis Doctoral se ha realizado un estudio en profundidad sobre los posibles mecanismos de deterioro de la azurita, con distinto tamaño de grano, y mezclada con aglutinante de cola de conejo. Los primeros indicios de transformación de azurita a

malaquita se produjeron a los 24 meses de exposición de los dosímetros pictóricos al aire urbano de la ciudad de Granada (ver capítulo 4)

❖ Malaquita

La malaquita $\text{Cu}(\text{OH})_2 \cdot \text{CuCO}_3$ es un mineral verde que suele estar asociado con la azurita. La fórmula molecular de ambos minerales es muy parecida, pero la malaquita difiere de la azurita en la cantidad de contenido de componentes básicos (Matteini et al., 2001). Por lo tanto, los mecanismos de degradación de la malaquita no son muy diferentes a los que tiene la azurita. Špec et al. (2014) realizaron ensayos de envejecimiento acelerado con radiación UV, y variaciones de temperatura y humedad relativa en réplicas pictóricas elaboradas con malaquita y distintos tipos de aglutinantes, encontrando que la malaquita con yema de huevo originó como producto de degradación tenorita (CuO). La posible formación de otro óxido de cobre, paramelaconita (Cu_4O_3) también fue tomada en consideración (Špec et al., 2014). Castro et al. (2008) también detectaron moolooíta ($\text{Cu}_2\text{O}_4 \cdot n\text{H}_2\text{O}$) como producto de degradación de la malaquita. En esta investigación los autores atribuyen la transformación mineralógica a la presencia de organismos vivos como líquenes y microorganismo, que tienen la capacidad de excretar ácido oxálico ($\text{H}_2\text{C}_2\text{O}_4$).

Alteración de aglutinantes proteicos

Este apartado aborda los fenómenos de alteración más comunes que sufren dos tipos de aglutinantes proteicos estudiados en esta Tesis Doctoral, i.e. la yema de huevo y la cola de conejo. Los aglutinantes proteicos son los usados en la técnica pictórica denominada al “temple”. Según se describe en (Matteini et al., 2001) “...Los términos italianos *tempera* y *temperare* -en castellano, *temple* y *templar*, respectivamente- designaban en origen la acción de mezclar los pigmentos en polvo con un aglutinante para obtener una pasta coloreada aplicable en forma de capas pictóricas sobre un soporte”. En la pintura al temple se pueden diferenciar dos tipos de aglutinantes según su naturaleza: i) los proteicos (e.g. huevo, caseína y colas animales) y, ii) los polisacáridos (e.g. gomas vegetales).

❖ Cola de conejo

La cola de conejo está constituida principalmente por colágeno, que es un polímero natural y la proteína más abundante en la estructura de los vertebrados (Pires et al., 2011). La función del colágeno es reforzar, sostener, dar forma y resistencia a todos los tejidos y órganos. El colágeno se organiza en forma de fibras formadas por un ramillete con giros a derechas, constituido por tres hélices paralelas tipo II de poliprolina, y a izquierdas, con las secuencias de aminoácidos (Gly-X-Y)_n (Brodsky and Ramshaw, 1997). En las posiciones X e Y se suelen encontrar la prolina y la hidroxiprolina (Gly= glicina) como se muestra en la Figura I.2.

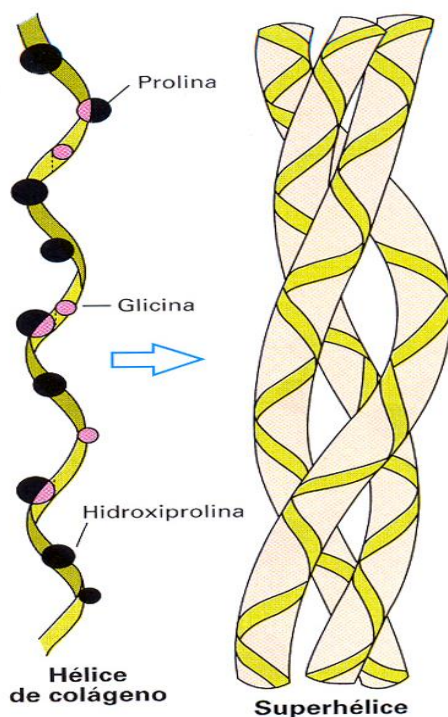


Figura I.2 Estructura secundaria del colágeno; hélice y superhélice.

El colágeno natural es insoluble en agua y se transforma en aglutinante mediante la desnaturalización del colágeno (Schellmann, 2007). El proceso de desnaturalización se

realiza durante el proceso de extracción. Esto se logra extrayendo el colágeno con agua caliente (descomposición hidrolítica) (Gudmundsson and Hafsteinsson, 1997; Schellmann, 2007; Skeist, 2007). A continuación, se le aplica un pre-tratamiento (ácido o básico) necesario para la mayoría de colágeno que se extrae de piel y hueso. Durante la extracción, los enlaces (predominantemente enlaces por puentes de hidrógeno) en la estructura de triple hélice del colágeno se rompen, por lo que se separa en bobinas desordenadas aleatoriamente de cadenas de proteínas, completando así la transición a gelatina (Privalov, 1979).

Aunque el proceso de desnaturalización es irreversible, es decir, el colágeno pierde la disposición de la triple hélice de la proteína, se pueden restaurar algunas estructuras helicoidales durante la gelificación y el secado del colágeno. Las bobinas desorganizadas son capaces de volver a reorganizarse parcialmente en una forma similar a la que tenía el colágeno. Las hebras que forman estas nuevas estructuras helicoidales están en desalineación con respecto al colágeno sin tratar. Además, también se pueden formar nodos entre las hebras, emergiendo nuevas formas de red tridimensional. El grado de re-naturalización depende de la composición química (contenido prolina e hidroxiprolina), la longitud de cadena de las moléculas (peso molecular), concentración en disolución y temperatura (Schellmann, 2007).

La cola de conejo, una vez extraída y tratada, tiene unas propiedades excelentes como aglutinante. Sin embargo, también se le atribuyen a la cola ciertos fenómenos de alteración en pinturas, normalmente debidas al envejecimiento, que pueden provocar el desprendimiento de las capas pictóricas. Los fenómenos de degradación en la cola no han sido totalmente aclarados, aunque sí se conocen tres tipos de alteración, i.e. física, química y microbiológica.

La degradación física está relacionada con la variación de la humedad y la presencia de agua en la cola de conejo, lo que puede provocar en ella fenómenos de dilatación y contracción. La pérdida de humedad por debajo de un 30% puede inducir la deshidratación de la cola. Esta deshidratación provoca variaciones a nivel estructural que hacen que se

vuelva rígida y quebradiza. Estas variaciones se han observado en el estudio realizado en dosímetros pictóricos de azurita con cola de conejo (ver capítulo 4).

La degradación química que más afecta a las proteínas se debe a variaciones de pH (ácido/básico), fuerza iónica, y ambientes oxidantes, que pueden proceder de ciertos compuestos o agentes empleados en la limpieza de las pinturas. También las proteínas se ven afectadas por la radiación (visible y UV). Sin embargo, como se ha comentado anteriormente, son escasos los estudios realizados para determinar los mecanismos de degradación que se producen en los aglutinantes a base de cola (Manzano et al., 2010; Romero-Pastor et al., 2012). Por ese motivo, en esta Tesis Doctoral se han estudiado las degradaciones que se producen en dosímetros pictóricos elaborados con cola de conejo cuando se someten a envejecimiento natural y artificial con radiación UV.

Por último, los fenómenos de degradación biológica están igualmente relacionados con la humedad, puesto que favorece el medio necesario para que se dé la proliferación de bacterias y microorganismos (Matteini et al., 2001).

❖ Yema de huevo

En la técnica pictórica al temple, el aglutinante más importante y empleado en la pintura mural ha sido el huevo, entero (clara y yema) o usando por separado sus componentes (yema o clara). Su uso se extiende a todas las épocas y culturas de la antigüedad (Matteini et al., 2001). En la técnica al temple se suele usar más comúnmente solo la yema de huevo como aglutinante, que ha sido el medio empleado en las pinturas elaboradas en esta Tesis Doctoral.

La yema de huevo está compuesta por aproximadamente un 30% de proteínas y un 70% de lípidos (Gil Hernández, 2010). Los lípidos son un grupo de sustancias insolubles en agua, pero solubles en disolventes orgánicos, que incluyen triglicéridos (comúnmente llamados grasas), fosfolípidos y esteroides (Tabla I).

Tabla 1 Fracción lipídica de la yema de huevo.

	Fracción Lipídica	Contenidos de Lípidos (%)	Contenido de fosfolípidos (%)
	Triglicéridos(TAG)	66	
Fosfolípidos	Fosfolípidos (PL):	28	
	Fosfatidilcolina (PC)		73
	Fosfatidiletanolamina (PE)		15,5
	Lisofosfatidilcolina (LPC)		5,8
	Esfingomielina (SM)		2,5
	Lisodofosfatidiletanolamina (LPE)		2,1
	Plasmalógenos		0,9
	Fosfatidilinositol (PI)		0,6
	Colesterol, ceramidas y otros (esteroles)	0.6	

Los triglicéridos y fosfolípidos mostrados en la Tabla 1 están formados por ácidos grasos insaturados, siendo los más abundantes en el huevo el ácido oleico ($C_{18}H_{34}O_2$), el ácido palmítico ($C_{16}H_{32}O_2$), el ácido esteárico ($C_{18}H_{36}O_2$) y el ácido linoleico ($C_{18}H_{32}O_2$). Los lípidos tienen que contener ácidos grasos insaturados (dobles enlaces) para que se produzca la oxidación por polimerización, que transforma a la yema de huevo en un material resistente y le proporciona una consistencia sólida. Este proceso comienza cuando los aceites de los triglicéridos y fosfolípidos empiezan a absorber cantidades de oxígeno. Los dobles enlaces de los ácidos grasos son el punto más susceptible para que se produzca una reacción. Como se observa en la Figura I.3, se forma un peróxido en el doble enlace de ácido graso por la reacción con el oxígeno. Los peróxidos son muy inestables y al romperse se forman radicales muy reactivos que reaccionan con los carbonos de los dobles enlaces de otras moléculas. Este proceso establece nuevos enlaces con otros ácidos grasos, formando una red tridimensional en forma de malla que envuelve a todos los materiales presentes en las capas pictóricas.

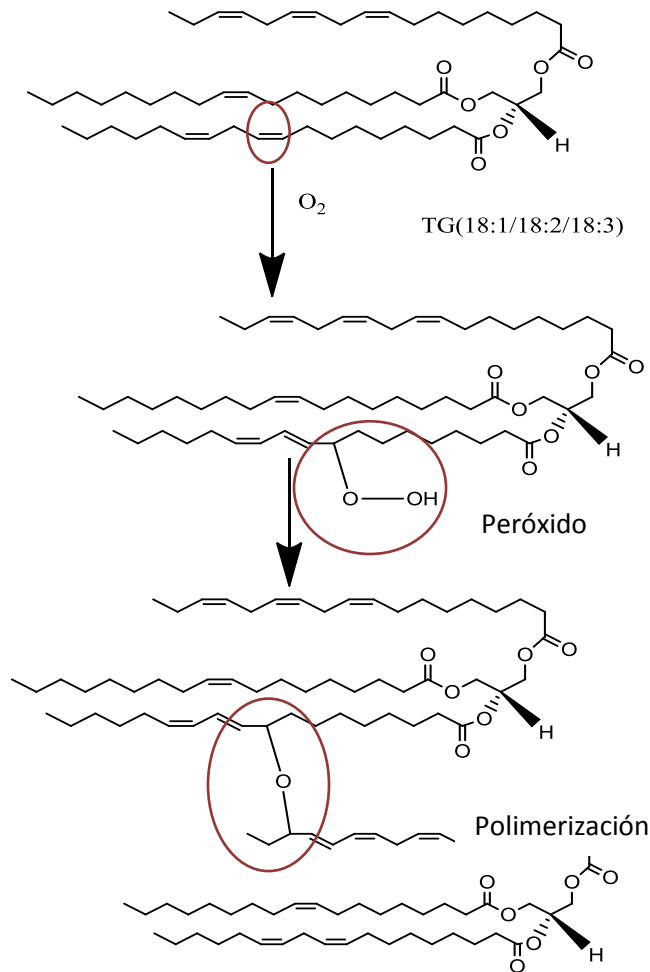


Figura I.3 Polimerización oxidativa de un triglicérido.

La oxidación en la polimerización es un efecto beneficioso en la pintura artística; sin embargo también existen fenómeno de oxidación que producen la degradación físico-química de la yema de huevo (Calvano et al., 2011; Van Der Werf et al., 2012). Durante el envejecimiento, el contenido de triglicéridos y fosfolípidos disminuye, mientras que aumenta la cantidad de diglicéridos, y además se forman cortes y oxidaciones en los ácidos grasos de los triglicéridos y fosfolípido. Como se muestra en la Figura I.4, se produce un corte en el doble enlaces en una de las cadenas de los ácidos grasos insaturados de un

fosfolípido o triglicérido. Después del corte en el doble enlace del ácido graso, se produce la oxidación, formándose un aldehído que no es un compuesto muy estable, y normalmente se oxida hasta finalmente formar un ácido carboxílico.

La oxidación de los lípidos de la yema de huevo es una de las degradaciones que más afectan a este aglutinante. En los procesos de envejecimiento oxidativo juegan un papel clave la temperatura y la radiación visible y UV. Sin embargo, existen pocos estudios al respecto (Van den Brink et al., 2001; Calvano et al., 2011; Van Der Werf et al., 2012), ya que los fenómenos involucrados en la degradación son complejos. Para profundizar en este tema, en esta Tesis Doctoral se ha realizado una optimización y puesta a punto de una metodología analítica de pinturas modelo elaboradas con yema de huevo, que ha permitido entender mejor los procesos de degradación de este aglutinante, abordando tal investigación desde la perspectiva de la interacción pigmento-aglutinante.

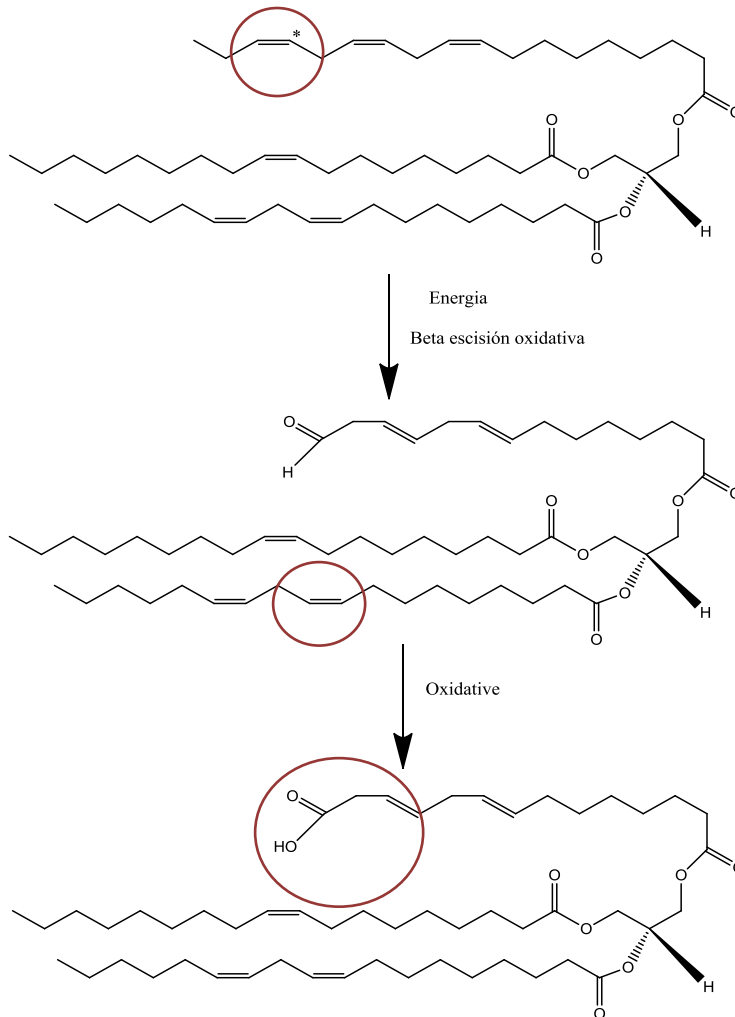


Figura 1.4 Esquema del corte y beta oxidación en los dobles enlaces de los ácidos grasos.

IV. Caracterización de pinturas históricas

El uso de una gran variedad de técnicas analíticas aplicadas al estudio del patrimonio pictórico ha aumentado notablemente en las últimas décadas, debido al creciente interés en identificar los materiales pictóricos utilizados en su elaboración (Cardell-Fernández and Navarrete-Aguilera, 2006; Van Grieken and Worobiec, 2011; Alfeld et al., 2013; Neiman et al., 2015; Papiiaka et al., 2017). Por otra parte, la conservación de las obras pictóricas solo se puede asegurar realizando un análisis riguroso y en profundidad de las causas, mecanismos y productos de degradación que les afectan, proporcionando así información valiosa para su conservación preventiva, y permitiendo establecer los procesos de intervención más adecuados (Pérez-Alonso et al., 2004; Vandenabeele et al., 2005; Baglioni et al., 2015; Marco et al., 2016; Cotte et al., 2017). Existe, para tal fin, una amplia gama de técnicas analíticas que abarcan desde técnicas microscópicas a espectroscópicas, vibracionales o cromatográficas y también técnicas de espectrometría de masas, cuyos datos pueden además ser evaluados con herramientas quimiométricas (e.g. análisis de componentes principales, PCA) para obtener –extraer- una mejor información de los resultados. La aplicación de técnicas analíticas en la investigación de pinturas artísticas continúa expandiéndose con la capacidad de analizar cantidades de muestras cada vez menores, y el uso de técnicas analíticas portátiles que permiten el estudio *in situ* de tales obras (Pérez-Alonso et al., 2004; Eveno et al., 2010; Colombari et al., 2012; Madariaga et al., 2016, Cardell and Guerra, 2016).

La elección de la metodología científica de investigación de dichas obras pictóricas se lleva a cabo cuidadosamente para garantizar que las técnicas de análisis elegidas aporten la mayor y mejor información posible a los propósitos del estudio. Entre las técnicas más empleadas en el análisis de obras del patrimonio pictórico se encuentran las técnicas de microscopía óptica y electrónica, , técnicas espectroscópicas (vibracionales y atómicas, y difracción de Rayos X), técnicas cromatográficas y de análisis térmico, así como en empleo de tratamientos quimiométricos de las señales analíticas obtenidas (Stuart 2007; Romero-Pastor et al., 2011b; Maguregui et al., 2014).

El estudio en detalle de una obra pictórica se inicia con una inspección visual con **lupa binocular o video-microscopio**. Ambas técnicas proporcionan una información valiosa de conjunto de la muestra analizada, así como detalles de su textura y/o morfología, color en superficie o de capas pictóricas, fenómenos y productos de degradación, etc. (Cardell-Fernández and Navarrete-Aguilera 2006) (Fig. 1.5). Los diferentes tipos de iluminación empleada en dichas técnicas pueden ayudar a un examen del objeto más pormenorizado. Por ejemplo, la iluminación estándar desde la parte frontal del mismo proporciona información sobre el color, la opacidad y el brillo en superficie; en cambio, con luz rasante se puede adquirir información de la textura, craquelados o rugosidad de la pintura artística.

La lupa binocular y el video-microscopio han sido utilizados ampliamente en los estudios realizadas en esta Tesis Doctoral, como herramientas de análisis visual preliminar de los dosímetros pictóricos patrón (Fig. 1.5a), y de los envejecidos por exposición a la intemperie (Fig. 1.5b) y mediante ensayos de alteración acelerada con SO₂ y radiación UV.

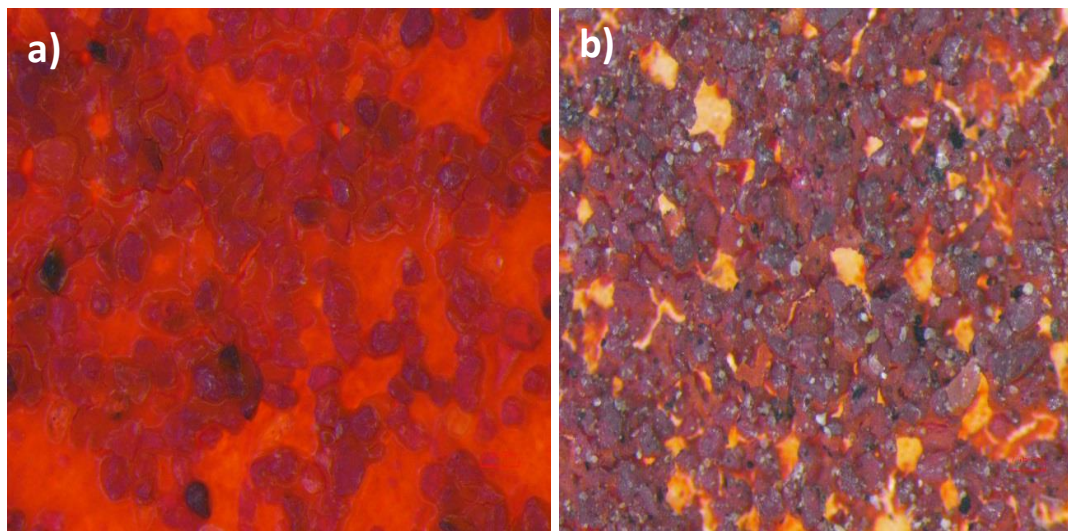


Figura 1.5. *Imágenes de lupa binocular del dosímetro pictórico elaborado con cinabrio y cola de conejo: a) dosímetro patrón, b) dosímetro envejecido naturalmente en el exterior de la Iglesia de Santo Domingo de Granada capital durante 24 meses.*

Una vez realizada una inspección visual global del objeto de estudio, se suele profundizar en su análisis utilizando el **microscopio electrónico de barrido** (SEM). En particular, el SEM de presión variable (VP-ESEM) permite estudiar las muestras en condiciones de bajo vacío (Cardell et al. 2009; Andersen et al., 2017), por lo que es de gran valor en la investigación de los procesos de deterioro que sufren las pinturas artísticas. En particular, es de gran interés la adquisición de mapas de rayos X en áreas de interés de la muestra pictórica, proporcionando información elemental, a partir de la cual se pueden obtener mapas de fases minerales (Campos-Suñol et al., 2009).

A lo largo de esta Tesis Doctoral, el SEM-EDX ha sido una herramienta básica para la caracterización morfológica, textural y composicional de los dosímetros pictóricos patrón y envejecidos. Se han obtenido imágenes con electrones secundarios y electrones retrodispersados, así como mapas de rayos X (Fig. I.6a) y mapas de fases minerales (Fig. I.6b) en dosímetros pictóricos patrón y envejecidos.

Por otro lado, una manera de observar las características cromáticas de las pinturas y su evolución en el tiempo, sin necesidad de usar un microscopio, es empleando un colorímetro o **espectrofotómetro**. En concreto, los espectrofotómetros son los instrumentos de medición de color más precisos y sofisticados, ya que realizan mediciones de un objeto en reflectancia total o transmitancia a lo largo del espectro visible (400 - 700nm). La precisión de estos instrumentos hace que sean los más utilizados para los estudios de variación cromática en patrimonio pictórico (Franceschi et al., 2006; Elert et al., 2018). En esta Tesis Doctoral el empleo de un espectrofotómetro portátil ha sido esencial para establecer los cambios cromáticos sufridos por los dosímetros pictóricos envejecidos en los monumentos piloto de la ciudad de Granada (ca. 40 meses) y en el laboratorio.

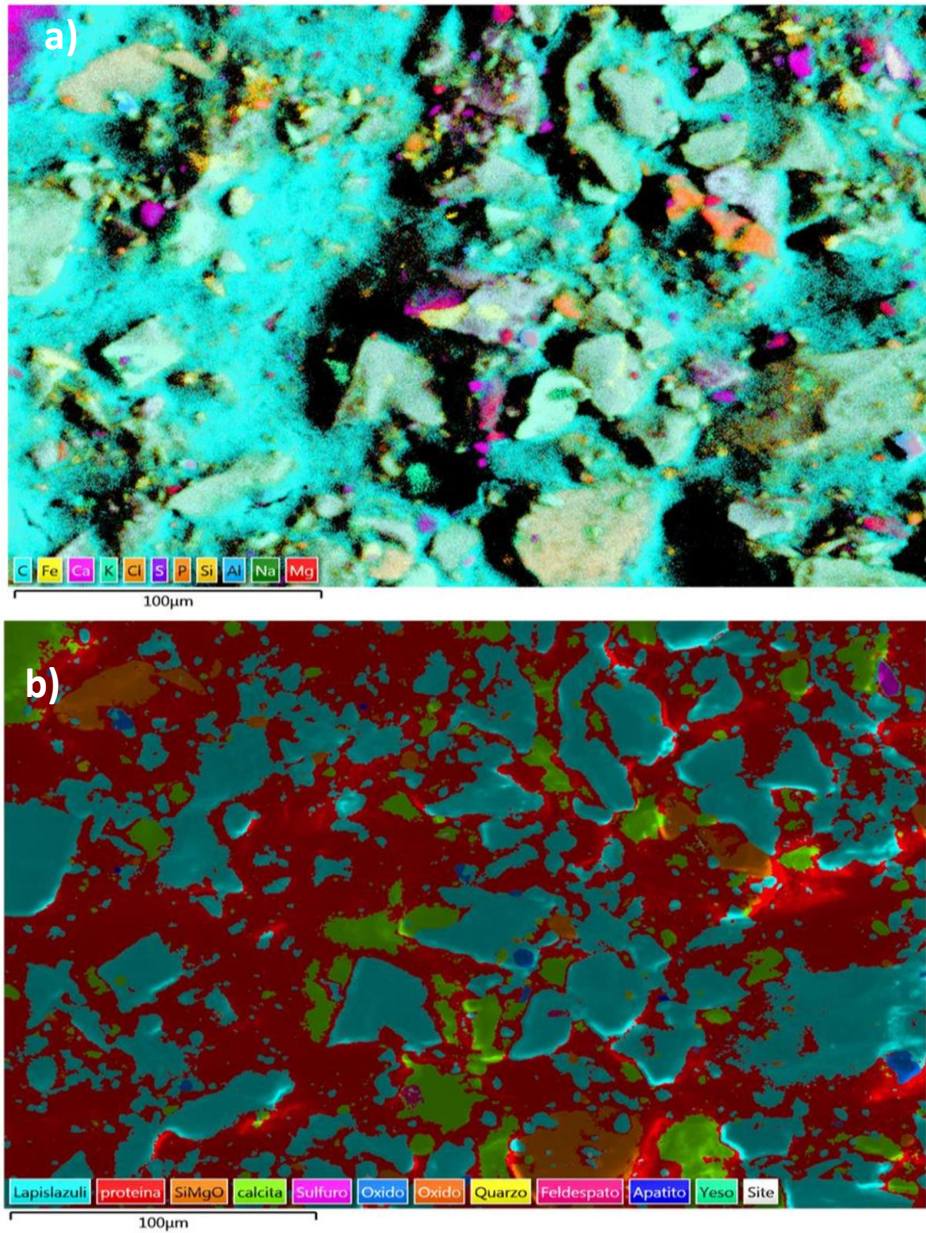


Figura 1.6 Mapas de falso color de zonas seleccionadas del dosímetro pictórico patrón de lapislazuli y yema de huevo: a) mapa de elementos, b) mapa de fases minerales elaborado a partir del mapa anterior de rayos X.

De gran interés en este campo de investigación son las técnicas analíticas vibracionales que proporcionan información conjunta de los componentes orgánicos (aglutinante) e inorgánicos (pigmento) que componen una pintura artística. Entre ellas la **espectroscopia de infrarrojos con transformada de Fourier (FTIR)** es comúnmente empleada para tal fin, proporcionando información cualitativa y semi-cuantitativa. Esta técnica de análisis puede operar en varios modos: i) FTIR por transmisión, donde la muestra es destruida y mezclada con KBr para formar una pastilla, por lo que no es el modo habitual de estudio en patrimonio pictórico; ii) FTIR por reflexión total atenuada (ATR), que puede estar o no acoplada a un microscopio, y que constituye la modalidad más usada para el análisis de pinturas ya, que la muestra pictórica no es destruida (Martin de Fonjaudran et al., 2008; Mahmoud, 2014); y iii) FTIR por reflexión o reflectancia difusa (DRIFTS), también empleada en el campo de estudio de muestras pictóricas (Navas et al., 2008; Maguregui et al., 2014) al ser un modo de análisis no destructivo.

Una de las limitaciones que presenta el análisis por FTIR es que pigmentos cuyas bandas diagnóstico están por debajo de 400 cm^{-1} no pueden ser detectadas, como por ejemplo los óxidos (hematites y minio), sulfuros (cinabrio), etc. Sin embargo, es una excelente técnica para analizar aglutinantes y pigmentos que no sean los referidos anteriormente (Navas et al., 2008; Manzano et al., 2009). En esta Tesis Doctoral se ha hecho uso de FTIR-ATR para la caracterización de pigmentos, aglutinantes, y sus procesos de interacción bajo la acción de diferentes agentes de alteración.

Otra técnica vibracional cualitativa de gran valor y complementaria a FTIR, capaz de analizar la materia orgánica e inorgánica de las pinturas artísticas es la **espectroscopía Raman (RS)**. De hecho es una de las técnicas analíticas más empleadas para caracterizar pinturas (Burgio et al., 2001; Frausto-Reyes et al., 2009; Cristini et al., 2010; Navas et al., 2010; Mateos et al., 2015). Los adelantos que ha experimentado esta técnica en los últimos años, con la incorporación de la microscopía óptica (RMS) y la mejora en los detectores, hacen de MR una herramienta muy adecuada para el análisis de materiales pictóricos, particularmente de pigmentos minerales. De hecho, es una técnica complementaria a FTIR, pues RS es capaz

de identificar las señales vibracionales de compuestos a longitudes de onda más cortas que FTIR, que corresponde a la zona del espectro donde aparecen las bandas características de pigmentos compuestos por óxidos y sulfuros (Fig. 1.7), siendo, además una técnica muy adecuada para detectar la degradación de los pigmentos inorgánicos (Burgio et al., 2001; Pérez-Alonso et al., 2004; Vandenabeele et al., 2005; Castro et al., 2008). La espectroscopia Raman ha sido una herramienta básica para la caracterización de los pigmentos en esta Tesis Doctoral. Con esta técnica se han detectado en los dosímetros pictóricos transformaciones minerales, existencia de polimorfos y procesos de carbonatación.

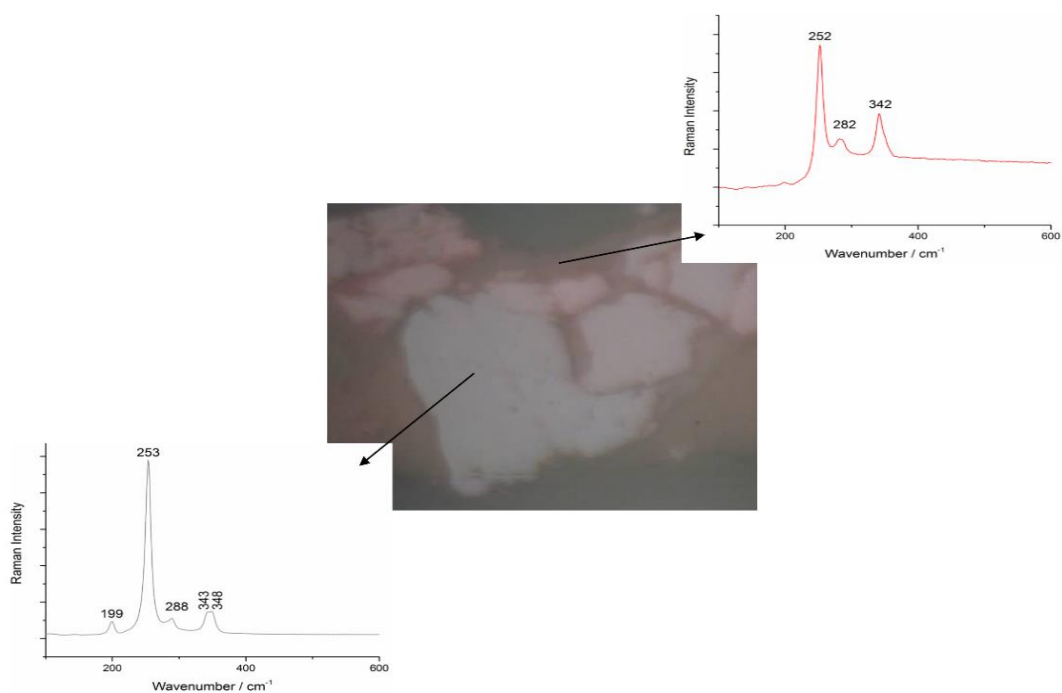


Figura 1.7 *Espectros Raman obtenidos en distintos granos minerales del dosímetro pictórico de cinabrio y yema de huevo elaborado como lámina delgada. Espectros adquiridos con láser rojo (785 nm).*

Por lo que se refiere a la caracterización mineral de las pinturas, una de las mejores técnicas para caracterizar e identificar la materia inorgánica (pigmento) es la **difracción de rayos X (XRD)** (Şerifaki et al., 2009; Manzano et al., 2010; Romero-Pastor et al., 2011b; Hradil et al., 2016). Esta técnica proporciona información mineral cualitativa y semicuantitativa, siendo

particularmente útil para distinguir polimorfos (De Leeuw and Parker, 1998). En esta Tesis Doctoral se ha empleado como herramienta fundamental para conocer la composición de los pigmentos y su degradación por distintos agentes de alteración.

En cuanto a la identificación y caracterizar en detalle de la materia orgánica de las pinturas históricas, una de las técnicas más adecuadas es la **espectrometría de masa (MS)**. Los materiales orgánicos pictóricos que es capaz de detectar la espectrometría de masa incluyen los aglutinantes, polímeros, aceites y barnices, entre otros (Van den Berg et al., 2004; Kuckova et al., 2005; Cottrell, 2011; Romero-Pastor et al., 2012; Van der Werf et al., 2012; Krizkova et al., 2014). Sin embargo, la espectrometría de masa no es más que un modo de detectar la materia, y ésta necesita ser ionizada para que pueda ser analizada. Existen muchas formas de ionizar la materia, entre ellas cabe destacar la ionización electrospray (ESI), por temperatura directa (DT), **desorción/ionización por láser asistida por matriz (MALDI)**, etc.

Antes de analizar la materia orgánica por espectrometría de masa (MS), normalmente ésta debe ser tratada, especialmente si la muestra objeto de estudio contiene proteínas. El gran tamaño molecular que tienen las proteínas es un inconveniente en su análisis, debido a la dificultad que presenta la detección de una masa grande con exactitud, además de los problemas asociados a obtener una adecuada ionización que permita su detección en el analizador de masas. Por este motivo se suelen realizar digestiones, normalmente con tripsina, consistente en cortar a la proteína por sitios específicos, obteniendo así una proteína en fragmentos más fácil de ser analizada mediante MS (Romero-Pastor et al., 2012). Existen diversos procedimientos para ionizar y detectar los compuestos orgánicos, de entre ellos, en esta Tesis Doctoral se ha optado por poner a punto un protocolo de análisis mediante desorción/ionización laser asistida por matriz acoplada a un espectrómetro de masas de tiempo de vuelo (MALDI-TOF/MS) para la caracterización de la fracción lipídica del aglutinante huevo presente en las pinturas al temple.

La MS puede cuantificar la materia orgánica, siempre que se puedan disponer de patrones para extrapolar la información en una recta de calibrado. Sin embargo, esto normalmente

no es factible en la mayoría de los casos porque no se dispone de patrones del material pictórico. Por este motivo, cuando se necesita una estimación cuantitativa de la materia orgánica o inorgánica de una pintura artística se pueden emplear otras técnicas analíticas como es el **análisis termogravimétrico (TGA)** (Gunasekaran and Anbalagan 2008; Şerifaki et al., 2009; Izzo et al., 2011). No obstante, el TGA presenta el inconveniente de que es también (como la MS) una técnica microdestructiva, debido a que el análisis se hace mediante descomposición térmica del material pictórico en función del tiempo y la temperatura. Al final del análisis TGA se obtienen los diferentes perfiles de descomposición que sufre el material pictórico analizado durante todo el proceso de calentamiento, obteniéndose información valiosa a partir de la descomposición del material.

El uso de TGA en esta Tesis Doctoral ha sido importante, debido a que los dosímetros pictóricos se realizaron según recetas de artistas medievales, basadas en percepciones organolépticas, y por tanto se desconoce la cantidad de aglutinante que contiene cada dosímetro pictórico. Con TGA se puede conocer la concentración de aglutinante que tienen los dosímetros pictóricos patrón, y por comparación, se puede establecer la cantidad de aglutinante que se ha perdido en los ensayos de envejecimiento natural y acelerado.

Con frecuencia, la información obtenida de las técnicas anteriormente descritas es compleja de analizar debido, por ejemplo, al gran volumen de datos que generan actualmente todos estos instrumentos. Por este motivo, en el campo del patrimonio pictórico existe un auge en el uso de técnicas quimiométricas, como el análisis de componentes principales (PCA) en datos obtenidos por técnicas de análisis como espectrofotometría, FTIR, RS, GC-MS, etc. (Manzano et al., 2010; Fremout et al., 2011; Romero-Pastor et al., 2011a; Karapanagiotis et al., 2013; Llorent-Martínez et al., 2014; Sessa et al., 2014; Carlesi et al., 2016) para extraer la máxima información de un gran volumen de datos. No obstante, son todavía escasos e innovadores los trabajos que aplican técnicas quimiométricas a estudios concretos de interacción de materiales pictóricos y degradación de pinturas artísticas (Bacci et al., 2000; Nevin et al., 2007, Romero-Pastor et al., 2012). En esta Tesis Doctoral se ha aplicado PCA a los datos espectrales obtenidos por

espectrofotometría de los dosímetros pictóricos colocados en diferentes monumentos piloto de la ciudad de Granada.

Referencias

- Alfeld, M., De Nolf, W., Cagno, S., Appel, K., Siddons, D.P., Kuczewski, A., Janssens, K., Dik, J., Trentelman, K., Walton, M., Sartorius, A., 2013. Revealing hidden paint layers in oil paintings by means of scanning macro-XRF: a mock-up study based on Rembrandt's "An old man in military costume." *J. Anal. At. Spectrom.* 28, 40–51. doi:10.1039/C2JA30119A
- Andalò, C., Bicchieri, M., Bocchini, P., Casu, G., Galletti, G.C., Mandò, P.A., Nardone, M., Sodo, A., Plossi Zappalà, M., 2001. The beautiful "Trionfo d'Amore" attributed to Botticelli: a chemical characterisation by proton-induced X-ray emission and micro-Raman spectroscopy. *Anal. Chim. Acta* 429, 279–286. doi:10.1016/S0003-2670(00)01292-7
- Andersen, C.K., Bonaduce, I., Andreotti, A., van Lanschot, J., Vila, A., 2017. Characterisation of preparation layers in nine Danish Golden Age canvas paintings by SEM–EDX, FTIR and GC–MS. *Herit. Sci.* 5, 34. doi:10.1186/s40494-017-0147-0
- Aze, S., Vallet, J.-M., Pomey, M., Baronnet, A., Grauby, O., 2007. Red lead darkening in wall paintings: natural ageing of experimental wall paintings versus artificial ageing tests. *Eur. J. Mineral.* 19, 883–890. doi:10.1127/0935-1221/2007/0019-1771
- Bacci, M., Boselli, L., Picollo, M., Pretzel, B., 2008. Colour measurement on paintings. *Res. Signpost.*
- Bacci, M., Picollo, M., Porcinai, S., Radicati, B., 2000. Evaluation of the museum environmental risk by means of tempera-painted dosimeters. *Thermochim. Acta* 365, 25–34. doi:10.1016/S0040-6031(00)00610-9
- Bacci, M., Picollo, M., Porcinai, S., Radicati, B., 2000. Tempera-painted dosimeters for environmental indoor monitoring: A spectroscopic and chemometric approach. *Environ. Sci. Technol.* 34, 2859–2865. doi:10.1021/es991437d
- Baglioni, P., Chelazzi, D., Giorgi, R., 2015. Cleaning of Wall Paintings and Stones BT-Nanotechnologies in the Conservation of Cultural Heritage: A compendium of materials and techniques, in: Baglioni, P., Chelazzi, D., Giorgi, R. (Eds.), Springer Netherlands, Dordrecht, pp. 61–82. doi:10.1007/978-94-017-9303-2_3
- Bourges, F., Genthon, P., Genty, D., Lorblanchet, M., Mauduit, E., & D'Hulst, D. 2014. Conservation of prehistoric caves and stability of their inner climate: Lessons from Chauvet and other French caves. *Science of The Total Environment*, 493, 79–91. <https://doi.org/10.1016/j.scitotenv.2014.05.137>
- Brimblecombe, P., 2003. The effects of air pollution on the built environment, Book. Imperial College Press. doi:10.1142/p243
- Brimblecombe, P., Grossi, C.M., 2004. The rate of darkening of material surfaces. *Air Pollut. Cult. Herit.* 193–198. doi:10.1201/b17004-30

Brodsky, B., Ramshaw, J.A.M., 1997. The collagen triple-helix structure. *Matrix Biol.* 15, 545–554. doi:10.1016/S0945-053X(97)90030-5

Burgio, L., Clark, R.J., Firth, S., 2001. Raman spectroscopy as a means for the identification of plattnerite (PbO₂), of lead pigments and of their degradation products. *Analyst* 126, 222–227. doi:10.1039/b008302j

Bytnerowicz, A., Omasa, K., Paoletti, E., 2007. Integrated effects of air pollution and climate change on forests: A northern hemisphere perspective. *Environ. Pollut.* 147, 438–445. doi:10.1016/j.envpol.2006.08.028

Calligaro, T., Coquinot, Y., Pichon, L., Pierrat-Bonnefois, G., De Campos, P., Re, A., Angelici, D., 2014. Characterization of the lapis lazuli from the Egyptian treasure of Tôd and its alteration using external μ -PIXE and μ -IBIL. *Nucl. Instruments Methods Phys. Res. Sect. B Beam Interact. with Mater. Atoms* 318, 139–144. doi:10.1016/j.nimb.2013.06.063

Calvano, C.D., Van der Werf, I.D., Palmisano, F., Sabbatini, L., 2011. Fingerprinting of egg and oil binders in painted artworks by matrix-assisted laser desorption ionization time-of-flight mass spectrometry analysis of lipid oxidation by-products. *Anal. Bioanal. Chem.* 400, 2229–40. doi:10.1007/s00216-011-4919-1

Campos-Suñol, M.J., De la torre-Lopez, M.J., Ayora-Cañada, M.J., Dominguez-Vidal, A., 2009. Analytical study of polychromy on exterior sculpted stone. *J. Raman Spectrosc.* 40, 2104–2110. doi:10.1002/jrs.2379

Camuffo, D., 2001. Environmental monitoring in four European museums. *Atmos. Environ.* 35, 127–140. doi:10.1016/S1352-2310(01)00088-7

Cardell-Fernández, C., Navarrete-Aguilera, C., 2006. Pigment and plasterwork analyses of Nasrid polychromed lacework stucco in the Alhambra (Granada, Spain). *Stud. Conserv.* 51, 161–176. doi:10.1179/sic.2006.51.3.161

Cardell-Fernández, C., Rodríguez-Gordillo, J., 2003. Policromías de la Iglesia del Monasterio de San Jerónimo de Granada: composición, alteración y técnicas de ejecución. *Bol. la Soc. Española Mineral.* 26, 118–121. doi:10.7597/acopios2171-7788.2012.35

Cardell, C., Guerra, I., 2016. An overview of emerging hyphenated SEM-EDX and Raman spectroscopy systems: Applications in life, environmental and materials sciences. *TrAC - Trends Anal. Chem.* 77, 156–166. doi:10.1016/j.trac.2015.12.001

Cardell, C., Rodríguez-Simón, L., Guerra, I., Sanchez-Navas, A., 2009. Analysis of Nasrid polychrome carpentry at the Hall of the Mexuar Palace, Alhambra complex (Granada, Spain), combining microscopic, chromatographic and spectroscopic methods. *Archaeometry* 51, 637–657. doi:10.1111/j.1475-4754.2008.00438.x

Carlyle, L. and Townsend, J. H. (1990). An investigation of lead sulphide darkening of nineteenth century painting materials, in *Dirt and pictures separated: papers given at a*

conference held jointly by UKIC and the Tate Gallery, January 1990. United Kingdom Institute of Conservation, pp. 40–43.

Carlesi, S., Ricci, M., Cucci, C., Lofrumento, C., Picollo, M., Becucci, M., 2016. Multivariate analysis of combined reflectance FT-NIR and micro-Raman spectra on oil-paint models. *Microchem. J.* 124, 703–711. doi:10.1016/j.microc.2015.10.023

Cassar, M., 1995. *Environmental Management: Guidelines for museums and galleries.*

Castro, K., Sarmiento, A., Martínez-Arkarazo, I., Madariaga, J.M., Fernández, L.A., 2008. Green copper pigments biodegradation in cultural heritage: From malachite to moolooite, thermodynamic modeling, X-ray fluorescence, and Raman evidence. *Anal. Chem.* 80, 4103–4110. doi:10.1021/ac800255w

Chmutina, K., Jigyasu, R., Boshier, L., 2016. Understanding the impacts of climate change on cultural heritage buildings: a case of York, UK.

Colomban, P., Tournié, A., Maucuer, M., Meynard, P., 2012. On-site Raman and XRF analysis of Japanese/Chinese bronze/brass patina - The search for specific Raman signatures. *J. Raman Spectrosc.* 43, 799–808. doi:10.1002/jrs.3095

Cotte, M., Checroun, E., De Nolf, W., Taniguchi, Y., De Viguerie, L., Burghammer, M., Walter, P., Rivard, C., Salomé, M., Janssens, K., Susini, J., 2017. Lead soaps in paintings: Friends or foes? *Stud. Conserv.* 62, 2–23. doi:10.1080/00393630.2016.1232529

Cotte, M., Susini, J., Metrich, N., Moscato, A., Gratzu, C., Bertagnini, A., Pagano, M., 2006. Blackening of Pompeian Cinnabar Paintings: X-ray Microspectroscopy Analysis. *Anal. Chem.* 78, 7484–7492. doi:10.1021/ac0612224

Cottrell, J.S., 2011. Protein identification using MS/MS data. *J. Proteomics* 74, 1842–1851. doi:10.1016/j.jprot.2011.05.014

Cristini, O., Kinowski, C., Turrell, S., 2010. A detailed micro-Raman spectroscopic study of wall paintings of the period AD 100-200: Effect of atmospheric conditions on the alteration of samples. *J. Raman Spectrosc.* 41, 1410–1417. doi:10.1002/jrs.2656

Daniilia, S., Sotiropoulou, S., Bikiaris, D., Salpistis, C., Karagiannis, G., Chrysoulakis, Y., Price, B.A., Carlson, J.H., 2000. Panselinos' Byzantine wall paintings in the Protaton Church, Mount Athos, Greece: a technical examination. *J. Cult. Herit.* 1, 91–110. doi:10.1016/S1296-2074(00)00164-3

De Leeuw, N.H., Parker, S.C., 1998. Surface Structure and Morphology of Calcium Carbonate Polymorphs Calcite, Aragonite, and Vaterite: An Atomistic Approach. *J. Phys. Chem. B* 102, 2914–2922. doi:10.1021/jp973210f

Doménech-Carbó, A., Doménech-Carbó, M.T., Moya-Moreno, M., Gimeno-Adelantado, J. V., Bosch-Reig, F., 2000. Identification of inorganic pigments from paintings and

polychromed sculptures immobilized into polymer film electrodes by stripping differential pulse voltammetry. *Anal. Chim. Acta* 407, 275–289. doi:10.1016/S0003-2670(99)00781-3

Doménech-Carbó, M.T., Kuckova, S., de la Cruz-Cañizares, J., Osete-Cortina, L., 2006. Study of the influencing effect of pigments on the photoageing of terpenoid resins used as pictorial media. *J. Chromatogr. A* 1121, 248–258. doi:10.1016/j.chroma.2006.04.005

Eastaugh N , Walsh V, Chaplin T, S.R., 2008. *Pigment Compendium*. Routledge. doi:10.4324/9780080943596

Elert, K., Herrera, A., Cardell, C., 2018. Pigment-binder interactions in calcium-based tempera paints. *Dye. Pigment*. 148, 236–248. doi:10.1016/j.dyepig.2017.09.013

Eveno, M., Duran, A., Castaing, J., 2010. A portable X-ray diffraction apparatus for in situ analyses of masters' paintings. *Appl. Phys. A* 100, 577–584. doi:10.1007/s00339-010-5641-0

Feller, R.L., 1967. Studies on the darkening of vermilion by light. *Rep. Stud. Hist. art* 1, 99–111. doi:10.2307/42618061

Franceschi, E., Letardi, P., Luciano, G., 2006. Colour measurements on patinas and coating system for outdoor bronze monuments. *J. Cult. Herit.* 7, 166–170. doi:10.1016/j.culher.2006.03.001

Frausto-Reyes, C., Ortiz-Morales, M., Bujdud-Pérez, J.M., Magaña-Cota, G.E., Mejía-Falcón, R., 2009. Raman spectroscopy for the identification of pigments and color measurement in Dugès watercolors. *Spectrochim. Acta - Part A Mol. Biomol. Spectrosc.* 74, 1275–1279. doi:10.1016/j.saa.2009.09.060

Fremout, W., Kuckova, S., Crhova, M., Sanyova, J., Saverwyns, S., Hynek, R., Kodicek, M., Vandenaabeele, P., Moens, L., 2011. Classification of protein binders in artist's paints by matrix-assisted laser desorption/ionisation time-of-flight mass spectrometry: an evaluation of principal component analysis (PCA) and soft independent modelling of class analogy (SIMCA). *Rapid Commun. Mass Spectrom.* 25, 1631–40. doi:10.1002/rcm.5027

Gettens, R.J., Feller, R.L., Chase, W.T., 1986. Artists' Pigments: A Handbook of Their History and Characteristics, in: *Artists' Pigments: A Handbook of Their History and Characteristics*. National Gallery of Art, pp. 159–182. doi:10.2307/1506614

Ghezzi, L., Duce, C., Bernazzani, L., Bramanti, E., Colombini, M.P., Tiné, M.R., Bonaduce, I., 2015. Interactions between inorganic pigments and rabbit skin glue in reference paint reconstructions. *J. Therm. Anal. Calorim.* 122, 315–322. doi:10.1007/s10973-015-4759-x

Gil Hernández, Á., 2010. Composición y calidad nutritiva de los alimentos., in: *Tratado de Nutricion*. Tomo II. Madrid, pp. 11–14.

Godoi, R.H.M., Potgieter-Vermaak, S., Godoi, A.F.L., Stranger, M., Van Grieken, R., 2008. Assessment of aerosol particles within the Rubens' House Museum in Antwerp, Belgium. *X-Ray Spectrom.* 37, 298–303.

Grøntoft, T., Odlyha, M., Mottner, P., Dahlin, E., Lopez-Aparicio Susana, S., Jakiela, S., Scharff, M., Andrade, G., Obarzanowski, M., Ryhl-Svendsen, M., Thickett, D., Hackney, S., Wadum, J., 2010. Pollution monitoring by dosimetry and passive diffusion sampling for evaluation of environmental conditions for paintings in microclimate frames. *J. Cult. Herit.* 11, 411–419.

Grossi, C.M., Esbert, R.M., Díaz-Pache, F., Alonso, F.J., 2003. Soiling of building stones in urban environments. *Build. Environ.* 38, 147–159. doi:10.1016/S0360-1323(02)00017-3

Gudmundsson, M., Hafsteinsson, H., 1997. Gelatin from cod skins as affected by chemical treatments. *J. Food Sci.* 62, 37–39. doi:10.1111/j.1365-2621.1997.tb04363.x

Gunasekaran, S., Anbalagan, G., 2008. Spectroscopic study of phase transitions in natural calcite mineral. *Spectrochim. Acta Part A Mol. Biomol. Spectrosc.* 69, 1246–1251. doi:10.1016/j.saa.2007.06.036

Hoevel, C.L., 1985. A study of the discoloration products found in white lead paint films. *B. Pap. Gr. Annu.* 4, 35–42.

Horemans, B., Cardell, C., Bencs, L., Kontozova-Deutsch, V., De Wael, K., Van Grieken, R., 2011. Evaluation of airborne particles at the Alhambra monument in Granada, Spain. *Microchem. J.* 99, 429–438. doi:10.1016/j.microc.2011.06.018

Hradil, D., Bezdička, P., Hradilová, J., Vašutová, V., 2016. Microanalysis of clay-based pigments in paintings by XRD techniques. *Microchem. J.* 125, 10–20. doi:10.1016/j.microc.2015.10.032

Hwang, I., Inaba, M., Sugisita, R., 1993. Discoloration of Lead Containing Pigments in Paintings. *Sci. Pap. Japanese Antiq.* 10–19.

Izzo, F.C., Zendri, E., Biscontin, G., Balliana, E., 2011. TG-DSC analysis applied to contemporary oil paints. *J. Therm. Anal. Calorim.* 104, 541–546. doi:10.1007/s10973-011-1468-y

Karapanagiotis, I., Mantzouris, D., Cooksey, C., Mubarak, M.S., Tsiamyrtzis, P., 2013. An improved HPLC method coupled to PCA for the identification of Tyrian purple in archaeological and historical samples. *Microchem. J.* 110, 70–80. doi:10.1016/j.microc.2013.02.008

Koller, M., Leitner, H., Paschinger, H., 1990. Reconversion of altered lead pigments in Alpine mural paintings. *Stud. Conserv.* 35, 15–20. doi:10.1179/sic.1990.35.1.15

Kontozova-Deutsch, V., Cardell, C., Urosevic, M., Ruiz-Agudo, E., Deutsch, F., Van Grieken, R., 2011. Characterization of indoor and outdoor atmospheric pollutants impacting

architectural monuments: the case of San Jerónimo Monastery (Granada, Spain). *Environ. Earth Sci.* 63, 1433–1445. doi:10.1007/s12665-010-0657-5

Kotulanova, E., Bezdicka, P., Grygar, T., Grunwaldova, S. V., Hradil, D., Hradilova, J., *IUCr*, 2006. Powder X-ray microdiffraction in research of wall painting damage by salts. *Acta Crystallogr. Sect. A Found. Crystallogr.* 62, s188–s188. doi:10.1107/S0108767306096255

Krizkova, M.C., Kuckova, S.H., Santrucek, J., Hynek, R., 2014. Peptide mass mapping as an effective tool for historical mortar analysis. *Constr. Build. Mater.* 50, 219–225. doi:10.1016/j.conbuildmat.2013.09.059

Kuckova, S., Nemeč, I., Hynek, R., Hradilova, J., Grygar, T., 2005. Analysis of organic colouring and binding components in colour layer of art works. *Anal. Bioanal. Chem.* 382, 275–82. doi:10.1007/s00216-005-3108-5

Llorent-Martínez, E.J., Domínguez-Vidal, A., Rubio-Domene, R., Pascual-Reguera, M.I., Ruiz-Medina, A., Ayora-Cañada, M.J., 2014. Identification of lipidic binding media in plasterwork decorations from the Alhambra using GC–MS and chemometrics: Influence of pigments and aging. *Microchem. J.* 115, 11–18. doi:10.1016/j.microc.2014.02.001

Lluveras, A., Boularand, S., Andreotti, A., Vendrell-Saz, M., 2010. Degradation of azurite in mural paintings: Distribution of copper carbonate, chlorides and oxalates by SRFTIR. *Appl. Phys. A Mater. Sci. Process.* 99, 363–375. doi:10.1007/s00339-010-5673-5

Lussier, S.M., Smith, G.D., 2007. A review of the phenomenon of lead white darkening and its conversion treatment. *Stud. Conserv.* 52, 41–53. doi:10.1179/sic.2007.52.Supplement-1.41

Madariaga, J.M., Maguregui, M., Castro, K., Knuutinen, U., Martínez-Arkarazo, I., 2016. Portable Raman, DRIFTS, and XRF Analysis to Diagnose the Conservation State of Two Wall Painting Panels from Pompeii Deposited in the Naples National Archaeological Museum (Italy). *Appl. Spectrosc.* 70, 137–146. doi:10.1177/0003702815616589

Maguregui, M., Castro, K., Morillas, H., Trebolazabala, J., Knuutinen, U., Wiesinger, R., Schreiner, M., Madariaga, J.M., 2014. Multianalytical approach to explain the darkening process of hematite pigment in paintings from ancient Pompeii after accelerated weathering experiments. *Anal. Methods* 6, 372–378. doi:10.1039/C3AY41741G

Maguregui, M., Knuutinen, U., Martínez-Arkarazo, I., Castro, K., Madariaga, J.M., 2011. Thermodynamic and spectroscopic speciation to explain the blackening process of hematite formed by atmospheric SO₂ impact: The case of Marcus Lucretius House (Pompeii). *Anal. Chem.* 83, 3319–3326. doi:10.1021/ac1029192

Mahmoud, H.H.M., 2014. Investigations by Raman microscopy, ESEM and FTIR-ATR of wall paintings from Qasr el-Ghuieta temple, Kharga Oasis, Egypt. *Herit. Sci.* 2, 18. doi:10.1186/s40494-014-0018-x

Mansour, S.A.A., 1994. Thermoanalytical investigations of decomposition course of copper oxysalts - I. Basic copper carbonate. *J. Therm. Anal.* 42, 1251–1263. doi:10.1007/BF02546934

Manzano, E., Navas, N., Checa-Moreno, R., L.Rodríguez-Simón, Capitán-Vallvey, L.F.F., 2009. Preliminary study of UV ageing process of proteinaceous paint binder by FT-IR and principal component analysis. *Talanta* 77, 1724–1731. doi:10.1016/j.talanta.2008.10.014

Manzano, E., Romero-Pastor, J., Navas, N., Rodríguez-Simón, L.R., Cardell, C., 2010. A study of the interaction between rabbit glue binder and blue copper pigment under UV radiation: A spectroscopic and PCA approach. *Vib. Spectrosc.* 53, 260–268. doi:10.1016/j.vibspec.2010.04.003

Marco, A., Moreira, P.R., Pintado, M., Vieira, E., 2016. Enzymatic degradation of fungal pigmentation from wall painting's isolates. *Color Res. Appl.* 41, 299–301. doi:10.1002/col.22025

Martin de Fonjaudran, C., Nevin, A., Piqué, F., Cather, S., 2008. Stratigraphic analysis of organic materials in wall painting samples using micro-FTIR attenuated total reflectance and a novel sample preparation technique. *Anal. Bioanal. Chem.* 392, 77–86. doi:10.1007/s00216-008-2111-z

Mateo, M.P., Ctvrtnickova, T., Nicolas, G., 2009. Characterization of pigments used in painting by means of laser-induced plasma and attenuated total reflectance FTIR spectroscopy. *Appl. Surf. Sci.* 255, 5172–5176. doi:10.1016/j.apsusc.2008.08.040

Mateos, L.D., Cosano, D., Mora, M., Muñiz, I., Carmona, R., Jiménez-Sanchidrián, C., Ruiz, J.R., 2015. Raman microspectroscopic analysis of decorative pigments from the Roman villa of El Ruedo (Almedinilla, Spain). *Spectrochim. Acta Part A Mol. Biomol. Spectrosc.* 151, 16–21. doi:10.1016/j.saa.2015.06.091

Mattei, E., de Vivo, G., De Santis, A., Gaetani, C., Pelosi, C., Santamaria, U., 2008. Raman spectroscopic analysis of azurite blackening. *J. Raman Spectrosc.* 39, 302–306. doi:10.1002/jrs.1845

Matteini, M., Moles, A., 1981. The reconversion of oxidized white lead in mural paintings: a control after a five year period, in: ICOM Committee for Conservation 6th Triennial Meeting: Ottawa, 21-25 September 1981: Preprints. Icom, p. 8.

Matteini, M., Moles, A., Bruno, E., Lain, G., 2001. La química en la restauración: los materiales del arte pictórico. Nerea.

Mayer, R., Sheehan, S., 1991. The artist's handbook of materials and techniques, The Viking. ed. New York.

Mazzeo, R., Prati, S., Quaranta, M., Joseph, E., Kendix, E., Galeotti, M., 2008. Attenuated total reflection micro FTIR characterisation of pigment–binder interaction in reconstructed paint films. *Anal. Bioanal. Chem.* 392, 65–76. doi:10.1007/s00216-008-2126-5

Moropoulou, A., Zacharias, N., Delegou, E.T., Apostolopoulou, M., Palamara, E., Kolaiti, A., 2018. OSL mortar dating to elucidate the construction history of the Tomb Chamber of the Holy Aedicule of the Holy Sepulchre in Jerusalem. *J. Archaeol. Sci. Reports* 19, 80–91. doi:10.1016/j.jasrep.2018.02.024

Mugnaini, S., Bagnoli, A., Bensi, P., Droghini, F., Scala, A., Guasparri, G., 2006. Thirteenth century wall paintings under the Siena Cathedral (Italy). Mineralogical and petrographic study of materials, painting techniques and state of conservation. *J. Cult. Herit.* 7, 171–185. doi:10.1016/j.culher.2006.04.002

Navas, N., Romero-Pastor, J., Manzano, E., Cardell, C., 2010. Raman spectroscopic discrimination of pigments and tempera paint model samples by principal component analysis on first-derivative spectra. *J. Raman Spectrosc.* 41, 1486–1493. doi:10.1002/jrs.2646

Navas, N., Romero-Pastor, J., Manzano, E., Cardell, C., 2008. Benefits of applying combined diffuse reflectance FTIR spectroscopy and principal component analysis for the study of blue tempera historical painting. *Anal. Chim. Acta* 630, 141–149. doi:10.1016/j.aca.2008.10.008

Neiman, M.K., Balonis, M., Kakoulli, I., 2015. Cinnabar alteration in archaeological wall paintings: an experimental and theoretical approach. *Appl. Phys. A Mater. Sci. Process.* 121, 915–938. doi:10.1007/s00339-015-9456-x

Nevin, A., Osticioli, I., Anglos, D., Burnstock, A., Cather, S. and Castellucci, E. (2007). Raman spectra of proteinaceous materials used in paintings: A multivariate analytical approach for classification and identificatio', *Analytical Chemistry*, 79(16), pp. 6143–6151. doi: 10.1021/ac070373j.

Odlyha, M., Cohen, N.S., Foster, G.M., 2000. Dosimetry of paintings: Determination of the degree of chemical change in museum exposed test paintings (small tempera) by thermal analysis. *Thermochim. Acta* 365, 35–44. doi:10.1016/S0040-6031(00)00611-0

Pantavou, K., Lykoudis, S., Psiloglou, B., 2017. Air quality perception of pedestrians in an urban outdoor Mediterranean environment: A field survey approach. *Sci. Total Environ.* 574, 663–670. doi:10.1016/j.scitotenv.2016.09.090

Papliaka, Z.E., Konstanta, A., Karapanagiotis, I., Karadag, R., Akyol, A.A., Mantzouris, D., Tsiamyrtzis, P., 2017. FTIR imaging and HPLC reveal ancient painting and dyeing techniques of molluskan purple. *Archaeol. Anthropol. Sci.* 9, 197–208. doi:10.1007/s12520-015-0270-3

Patrón, D., Lyamani, H., Titos, G., Casquero-Vera, J.A., Cardell, C., Močnik, G., Alados-Arboledas, L., Olmo, F.J., 2017. Monumental heritage exposure to urban black carbon pollution. *Atmos. Environ.* 170, 22–32. doi:10.1016/j.atmosenv.2017.09.030

Pavlogeorgatos, G., 2003. Environmental parameters in museums. *Build. Environ.* 38, 1457–1462. doi:10.1016/S0360-1323(03)00113-6

Pérez-Alonso, M., Castro, K., Martínez-Arkarazo, I., Angulo, M., Olazabal, M.A., Madariaga, J.M., 2004. Analysis of bulk and inorganic degradation products of stones, mortars and wall paintings by portable Raman microprobe spectroscopy. *Anal. Bioanal. Chem.* 379, 42–50. doi:10.1007/s00216-004-2496-2

Pérez-Rodríguez, J.L., Maqueda, C., Jiménez De Haro, M.C., Rodríguez-Rubio, P., 1998. Effect of pollution on polychromed ceramic statues. *Atmos. Environ.* 32, 993–998. doi:10.1016/S1352-2310(97)00337-3

Petushkova, J.P., Lyalikova, N.N., 1986. Microbiological Degradation of Lead-Containing Pigments in Mural Paintings. *Source Stud. Conserv.* 31214192, 65–69.

Pires, M.M., Przybyla, D.E., Rubert Pérez, C.M., Chmielewski, J., 2011. Metal-Mediated Tandem Coassembly of Collagen Peptides into Banded Microstructures. *J. Am. Chem. Soc.* 133, 14469–14471. doi:10.1021/ja2042645

Pozo-Antonio, J.S., Barral, D., Herrera, A., Elert, K., Rivas, T., Cardell, C., 2018. Effect of tempera paint composition on their superficial physical properties- application of interferometric profilometry and hyperspectral imaging techniques. *Prog. Org. Coatings* 117, 56–68. doi:10.1016/j.porgcoat.2018.01.007

Pozo-Antonio, J.S., Fernández-Rodríguez, S., Rocha, C.S.A., Carrera, F., Rivas, T., 2018. Marking petroglyphs with calcite and gypsum-based chalks: Interaction with granite under different simulated conditions and the effectiveness and harmfulness of cleaning methods. *Sci. Total Environ.* 612, 81–93. doi:10.1016/j.scitotenv.2017.08.223

Privalov, P.L., 1979. Stability of proteins: Small Globular Proteins. *Adv. Protein Chem.* 33, 167–241. doi:10.1016/S0065-3233(08)60460-X

Radepon, M., 2013. Understanding of chemical reactions involved in pigment discoloration, in particular in mercury sulfide (HgS) blackening.

Ramanathan, V., Feng, Y., 2009. Air pollution, greenhouse gases and climate change: Global and regional perspectives. *Atmos. Environ.* 43, 37–50. doi:10.1016/j.atmosenv.2008.09.063

Real Academia Española, 2017. Real Academia Española. *Dicc. Leng. Española*. URL <http://www.rae.es/> (accessed 1.11.18).

Rivas, T., Pozo-Antonio, J.S., Barral, D., Martínez, J., Cardell, C., 2017. Statistical analysis of colour changes in tempera paints mock-ups exposed to urban and marine environment. *Meas. J. Int. Meas. Confed.* doi:10.1016/j.measurement.2017.06.037

- Rodríguez-Navarro, C., Sebastian, E., 1996. Role of particulate matter from vehicle exhaust on porous building stones (limestone) sulfation. *Sci. Total Environ.* 187, 79–91. doi:10.1016/0048-9697(96)05124-8
- Romero-Pastor, J., Cardell, C., Manzano, E., Yebra-Rodríguez, Á., Navas, N., 2011a. Assessment of Raman microscopy coupled with principal component analysis to examine egg yolk-pigment interaction based on the protein CH stretching region (3100–2800 cm⁻¹). *J. Raman Spectrosc.* 42, 2137–2142. doi:10.1002/jrs.2977
- Romero-Pastor, J., Duran, A., Rodríguez-Navarro, A.B., Van Grieken, R., Cardell, C., 2011b. Compositional and quantitative microtextural characterization of historic paintings by micro-X-ray diffraction and Raman microscopy. *Anal. Chem.* 83, 8420–8428. doi:10.1021/ac201159e
- Romero-Pastor, J., Navas, N., Kuckova, S., Rodríguez-Navarro, A., Cardell, C., 2012. Collagen-based proteinaceous binder-pigment interaction study under UV ageing conditions by MALDI-TOF-MS and principal component analysis. *J. Mass Spectrom.* 47, 322–330. *J. Mass Spectrom.* 47, 322–330. doi:10.1002/jms.2966
- Rosi, F., Grazia, C., Gabrieli, F., Romani, A., Paolantoni, M., Vivani, R., Brunetti, B.G., Colomban, P., Miliani, C., 2016. UV–Vis-NIR and micro Raman spectroscopies for the non destructive identification of Cd 1–x Zn x S solid solutions in cadmium yellow pigments. *Microchem. J.* 124, 856–867. doi:10.1016/j.microc.2015.07.025
- Sabbioni, C., Brimblecombe, P., Cassar, M., 2010. *The Atlas of Climate Change Impact on European Cultural Heritage : Scientific Analysis and Management Strategies.* Anthem.
- Sabbioni, C., Cassar, M., Brimblecombe, P., Lefevre, R.A., 2009. Vulnerability of cultural heritage to climate change. *Pollut. Atmos.*
- Sabbioni, C., Zappiat, G., Ghedini, N., Gobbi, G., Favonis, O., 1998. Black crusts on ancient mortars. *Atmos. Environ.* 32, 215–223. doi:10.1016/S1352-2310(97)00259-8
- Salvadó, N., Butí, S., Cotte, M., Cinque, G., Pradell, T., 2013. Shades of green in 15th century paintings: Combined microanalysis of the materials using synchrotron radiation XRD, FTIR and XRF. *Appl. Phys. A Mater. Sci. Process.* 111, 47–57. doi:10.1007/s00339-012-7483-4
- Saunders, D., Chahine, H., Cupitt, J., 1996. Long-term colour change measurement: some results after 20 years. *Natl. Gall. Tech. Bull.* 17, 81–90.
- Schellmann, N.C., 2007. Animal glues: a review of their key properties relevant to conservation. *Stud. Conserv.* 52, 55–66. doi:10.1179/sic.2007.52.Supplement-1.55
- Şerifaki, K., Böke, H., Yalçın, Ş., İpekoğlu, B., 2009. Characterization of materials used in the execution of historic oil paintings by XRD, SEM-EDS, TGA and LIBS analysis. *Mater. Charact.* 60, 303–311. doi:10.1016/j.matchar.2008.09.016

Sessa, C., Bagán, H., García, J.F., 2014. Influence of composition and roughness on the pigment mapping of paintings using mid-infrared fiberoptics reflectance spectroscopy (mid-IR FORS) and multivariate calibration. *Anal. Bioanal. Chem.* 406, 6735–6747. doi:10.1007/s00216-014-8091-2

Skeist, I., 2007. *Handbook of adhesives*, Chapman & Hall. Springer US. doi:10.1073/pnas.0703993104

Smith, G.D., Clark, R.J.H., 2002. The role of H₂S in pigment blackening. *J. Cult. Herit.* 3, 101–105. doi:10.1016/S1296-2074(02)01173-1

Špec, T., Retko, K., Ropret, P., Meden, A., Bernard, J., 2014. The influence of UV-Vis radiation, and oscillations of temperature and relative humidity, on malachite alteration in the presence of different organic binders and varnishes. *J. Raman Spectrosc.* 45, 1068–1075. doi:10.1002/jrs.4518

Spring, M., & Grout, R. (2002). The Blackening of Vermilion: An Analytical Study of the Process in Paintings. *National Gallery Technical Bulletin*, 23, 50–61.

Staniforth, S., 2013. *Historical perspectives on preventive conservation*. Getty Conservation Institute.

Stuart, B., 2007. *Analytical techniques in materials conservation*. John Wiley & Sons.

Tidblad, J., Kucera, V., Ferm, M., Kreislova, K., Brüggerhoff, S., Doytchinov, S., Screpanti, A., Grøntoft, T., Yates, T., de la Fuente, D., Roots, O., Lombardo, T., Simon, S., Faller, M., Kwiatkowski, L., Kobus, J., Varotsos, C., Tzanis, C., Krage, L., Schreiner, M., Melcher, M., Grancharov, I., Karmanova, N., 2012. Effects of Air Pollution on Materials and Cultural Heritage: ICP Materials Celebrates 25 Years of Research. *Int. J. Corros.* 2012, 1–16. doi:10.1155/2012/496321

Titos, G., Lyamani, H., Drinovec, L., Olmo, F. J., Močnik, G. and Alados-Arboledas, L. 2015 Evaluation of the impact of transportation changes on air quality, *Atmospheric Environment*. 114, pp. 19–31. doi: <http://dx.doi.org/10.1016/j.atmosenv.2015.05.027>.

Unesco, 2004. *UNESCO world heritage*. Espac. Tour. Loisirs.

Urosevic, M., Yebra-Rodríguez, A., Sebastián-Pardo, E., Cardell, C., 2012. Black soiling of an architectural limestone during two-year term exposure to urban air in the city of Granada (Spain). *Sci. Total Environ.* 414, 564–575. doi:10.1016/j.scitotenv.2011.11.028

Van den Berg, J.D.J., Vermist, N.D., Carlyle, L., Holcapek, M., Boon, J.J., 2004. Effects of traditional processing methods of linseed oil on the composition of its triacylglycerols. *J. Sep. Sci.* 27, 181–99. doi:10.1002/jssc.200301610

Van den Brink, O.F., Boon, J.J., O'Connor, P.B., Duursma, M.C., Heeren, R.M., 2001. Matrix-assisted laser desorption/ionization Fourier transform mass spectrometric analysis of oxygenated triglycerides and phosphatidylcholines in egg tempera paint dosimeters used

for environmental monitoring of museum display conditions. *J. Mass Spectrom.* 36, 479–92. doi:10.1002/jms.145

Van den Brink, O.F., Eijkel, G.B., Boon, J.J., 2000. Dosimetry of paintings: determination of the degree of chemical change in museum-exposed test paintings by mass spectrometry. *Thermochim. Acta* 365, 1–23. doi:10.1016/S0040-6031(00)00609-2

Van Der Werf, I.D., Calvano, C.D., Palmisano, F., Sabbatini, L., 2012. A simple protocol for Matrix Assisted Laser Desorption Ionization- time of flight-mass spectrometry (MALDI-TOF-MS) analysis of lipids and proteins in single microsamples of paintings. *Anal. Chim. Acta* 718, 1–10. doi:10.1016/j.aca.2011.12.056

Van Grieken, R., Worobiec, A., 2011. X-ray spectrometry for preventive conservation of cultural heritage. *Pramana - J. Phys.* 76, 191–200.

Vandenabeele, P., Lambert, K., Matthys, S., Schudel, W., Bergmans, A., Moens, L., 2005. In situ analysis of mediaeval wall paintings: A challenge for mobile Raman spectroscopy. *Anal. Bioanal. Chem.* 383, 707–712. doi:10.1007/s00216-005-0045-2

Varotsos, C., Tzani, C., Cracknell, A., 2009. The enhanced deterioration of the cultural heritage monuments due to air pollution. *Env. Sci Pollut Res* 16, 590–592. doi:10.1007/s11356-009-0114-8

Watt, J., 2009. *The Effects of Air Pollution on Cultural Heritage*, Journal of Environmental Policy & Planning. Springer US, Boston, MA. doi:10.1007/978-0-387-84893-8

Zehnder, K., Riederer, J., 1996. Gypsum efflorescence in the zone of rising damp. Monitoring of slow decay processes caused by crystallizing salts on wall paintings, in: 8th International Congress on Deterioration and Conservation of Stone, Berlin, 30 Sept.-4 Oct. 1996: Proceedings. Moller Druck, pp. 1669–1678.

Parte Experimental

***Elimina de tu vida todo
aquello que te cause
estrés y te quite la
sonrisa.***

Paulo Coelho



**van Gogh-La noche
estrellada**

Capítulo 1

1. Materiales y métodos

1.1. Materiales

En esta Tesis Doctoral se han seleccionado para su estudio materiales pictóricos utilizados tradicionalmente en pintura al temple, según se describe en diversas recetas de la Edad Media y Renacimiento (Pacheco, 1954). Con dichos materiales pictóricos se han elaborado dosímetros pictóricos (muestras pictóricas modelo realizadas en el laboratorio) consistentes en una mezcla binaria de un pigmento mineral y un aglutinante proteico. A continuación se hace una descripción de los materiales pictóricos utilizados e investigados en esta Tesis Doctoral.

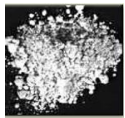






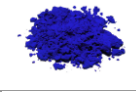
1.1.1. Pigmentos históricos inorgánicos

Los pigmentos minerales objeto de estudio en esta Tesis Doctoral se detallan en la Tabla 1. Los pigmentos fueron suministrados por *Kremer Pigments GmbH & Co. KG* (Madrid, España). Estos pigmentos han sido clasificados en tres grupos según su color, i.e. blanco, rojo y azul. Este último grupo también incluye el único pigmento verde estudiado.

Entre los pigmentos blancos se encuentra la **calcita** (CaCO_3), cuyo origen puede ser natural o sintético. Es un pigmento empleado desde la prehistoria, que ha sido descrito por primera vez en la literatura por Cennino Cennini (Cennini, 1960). En la actualidad no se emplea como pigmento en sentido estricto, sino como material de carga inerte para dar cuerpo a la capa pictórica. El **yeso** ($\text{CaSO}_4 \cdot 2\text{H}_2\text{O}$), que puede tener igualmente un origen natural o sintético, también es un pigmento empleado desde la antigüedad, principalmente en las capas de preparación de las pinturas (Cardell-Fernández and Rodríguez-Gordillo, 2003). El

blanco de plomo ($2\text{PbCO}_3 \cdot \text{Pb(OH)}_2$) es un pigmento de origen sintético muy utilizado desde la antigüedad.

Tabla 1. Características de los pigmentos minerales estudiados en esta Tesis Doctoral.

Color	Referencia del pigmento (proveedor)	Composición del pigmento (proveedor)	Código pigmento (Tesis Doctoral)	Tamaño de grano (μm) (proveedor)	Imagen
Blanco	Calcita K58720 (extra fina)	Calcita, CaCO_3	CA-EF	20	
	Bianco San Giovanni (estándar) K11415	Calcita, Portlandita, Ca(OH)_2	BSG-ST	120	
	Bianco San Giovanni (grueso) K11416	Calcita, Portlandita	BSG-C	120 – 1000	
	Yeso natural (selenita) K58300	Yeso, $\text{CaSO}_4 \cdot 2\text{H}_2\text{O}$	G-EF	80 % < 20 18 % < 25 1.94 % < 32	
	Blanco de plomo, K46000	Blanco de plomo, $\text{Pb(CO}_3)_2 \cdot \text{Pb(OH)}_2$	WL	< 45	
Rojo	Minio, K42500	Minio, Pb_3O_4	MIN	< 63	
	Hematites, K48651	Hematites, Fe_2O_3	HE-F	1.25	
	Cinabrio, K10628	Cinabrio	CIN-C	63 – 100	
Azul	Azurita estándar, K10200 (standard, deep greenish blue)	Azurita, $\text{Cu}_3(\text{CO}_3)_2(\text{OH})_2$	AZ-ST	< 20	
	Azurita MP, K10207 (sky blue)	Azurita	AZ-EF	< 38	
	Azurita MP, K10206 (pale)	Azurita	AZ-M	38 – 63	
	Azurita MP, K10204 (dark blue)	Azurita	AZ-C	63 – 80	
	Azurita MP, K10203 (extra profunda)	Azurita	AZ-EC	80 – 100	
	Lapislazuli, K10540 (cristalino)	Lapislazuli ($\text{Na}_{8-10}\text{Al}_6\text{Si}_6\text{O}_{24}\text{S}_{2-4}$)	LAP	< 80	
	Malaquita, K10300 (natural estándar)	Malaquita, $\text{Cu}_2\text{CO}_3(\text{OH})_2$	MAL	< 120 μm	

Nota: *Ca:* calcita; *BSG:* Bianco San Giovanni; *G:* yeso; *WL:* blanco de plomo; *MIN:* minio; *HE:* hematites; *CIN:* cinabrio; *AZ:* azurita; *LAP:* lapislazuli; *MAL:* malaquita; *EF:* extra fino; *ST:* standard; *C:* grueso (coarse); *M:* medio; *EC:* extra grueso (extra coarse).

El blanco de plomo fue mencionado por Plinio y por Vitrubio que describieron su preparación a partir de plomo metálico y vinagre (<http://www.webexhibits.org/pigments/>). El blanco de plomo fue el único blanco utilizado en las pinturas de caballete europeas hasta el siglo XIX, cuando su venenoso contenido de plomo restringió su fabricación y venta como pigmento artístico, y fue sustituido por el blanco de zinc, y por el blanco de titanio en el siglo XX.

Entre los pigmentos rojos estudiados se encuentra el minio (Pb_3O_4), que es uno de los primeros pigmentos sintéticos (Gettens et al., 1986; Aze et al., 2008). Este pigmento también puede aparecer de forma natural en yacimiento de galena (PbS) y cerusita ($PbCO_3$) en forma de alteración parcial con unas tonalidades rojizas o anaranjadas. El minio ha sido comumente empleado en la decoración de manuscritos (Eastaugh et al., 2008). El cinabrio (HgS) puede ser de origen natural (cinabrio s.s.) o sintético (bermellón), y fue un pigmento muy utilizado en China desde la antigüedad (II milenio antes de Cristo). El cinabrio era conocido por los griegos y romanos, y fue mencionado por Plinio en su tratado, que lo llamó "minium". La principal fuente de cinabrio se encuentra en Almaden (España) que ha sido explotada desde la época de los romanos (Eastaugh et al., 2008). La hematites (Fe_2O_3) es un pigmento que puede ser de origen natural o sintético. La hematites ha sido empleada en las pinturas murales desde la época de la prehistoria.

Entre los pigmentos azules utilizados en esta Tesis Doctoral se encuentra la **azurita** de origen natural ($2CuCO_3 \cdot Cu(OH)_2$). Este pigmento ha sido empleado en pinturas murales en China Central en la época de las dinastías Ming y Sung, así como en pinturas rupestres en Tun Huang en el oeste de China (Harley 1982) Existen registros de su uso también en Japón. Fue reemplazado por el azul de Prusia en el siglo XVIII. La azurita fue el pigmento azul más importante de la pintura Europea durante la Edad Media y el Renacimiento. El **lapislazuli** se obtiene de la gema semipreciosa que tiene el mismo nombre. El mineral que le confiere el color azul es la lazurita ($Na_{8-10}Al_6Si_6O_{24}S_{2-4}$). Se tiene constancia de su uso desde la

antigüedad (Afganistán, s. VIII) hasta el siglo XVIII (Calligaro et al., 2014). El pigmento verde **malaquita** ($\text{CuCO}_3 \cdot \text{Cu}(\text{OH})_2$) empleado en esta Tesis Doctoral es de origen natural. Se ha usado desde la antigüedad hasta el siglo XIX (Eastaugh et al., 2008; Han et al., 2016).

1.1.2. *Aglutinantes proteicos*

Los aglutinantes proteicos empleados para la elaboración de los dosímetros pictóricos han sido **cola de conejo** (colágeno), suministrado en forma de perlas por *Kremer Pigments GmbH & Co. KG* (Madrid, España) ref. 63028, y **yema de huevo**, procedente de huevos adquiridos en supermercados locales. Ambos aglutinantes se emplean normalmente en pintura mural. Se trata de aglutinantes proteicos que tienen propiedades de flexibilidad, viscosidad y elasticidad muy similares.

1.1.2.1. Dosímetros pictóricos: elaboración

Esta Tesis doctoral se enmarca en el proyecto de investigación “Impacto del aerosol atmosférico urbano en pinturas/policromías de monumentos arquitectónicos (semi-)abiertos. Predicción de cambios cromáticos y conservación preventiva” (AERIMPACT), del Ministerio de Educación y Ciencia (ref. CGL2012-30729). Los dosímetros pictóricos fueron elaborados por miembros integrantes de dicho proyecto con anterioridad al inicio de esta Tesis Doctoral. No obstante, el montaje en los soportes que fueron expuestos a la intemperie fue realizada por el doctorando.

a) Dosímetros pictóricos de cola de conejo

El aglutinante se preparó según recetas tradicionales (Pacheco, 1954). Para tal fin se pesaron aproximadamente ocho gramos de cola de conejo, que fueron puestos en remojo con 100 ml de agua desionizada durante 24 h con agitación periódica. Posteriormente la mezcla se calentó a una temperatura inferior a 50°C en baño de agua, y se agitó para obtener una mezcla homogénea. A continuación se dejó enfriar hasta temperatura ambiente (22°C) hasta obtener una consistencia similar a la de una gelatina.

Por lo que respecta a los pigmentos, cada pigmento se mezcló en primer lugar con agua desionizada, y seguidamente se le fueron agregando gotas de aglutinante de cola conejo hasta alcanzar una mezcla de consistencia adecuada. La pintura final se consideró que tenía la consistencia adecuada cuando las gotitas formadas en la punta del pincel no se desprendieron fácilmente. El último paso en la elaboración de los dosímetros pictóricos consistió en aplicar varias capas de cada mezcla pictórica en un portaobjetos de vidrio (76 x 26 x 1 mm), teniendo especial cuidado en que cada capa estuviera completamente seca antes de aplicar la siguiente (Fig 1.1). Para obtener el dosímetro de aglutinante puro, se aplicó la cola de conejo directamente sobre el portaobjeto de vidrio.



Figura 2.1 Preparación de los dosímetros pictóricos (autoría C. Cardell).

b) Dosímetros pictóricos de yema de huevo

Para preparar este aglutinante se separó la yema de huevo de la clara, utilizando el método habitual de verterla de un lado a otro en las medias cáscaras. Se tuvo especial cuidado en separar la clara del huevo adherida a la yema, así como la chalaza. A continuación se batió la yema del huevo y se guardó en un frasco cerrado. La preparación de los dosímetros pictóricos de yema de huevo fue la siguiente. Aproximadamente 0,5 g de cada pigmento en polvo se colocó en un tazón pequeño y se fueron añadiendo varias gotas del aglutinante yema de huevo previamente elaborado. Cada pigmento requirió diferente cantidad de yema de huevo para formar una pasta pictórica fluida. Se optó por este procedimiento para emular capas pictóricas de pinturas históricas. Finalmente, mediante el uso de un pincel se fueron extendiendo varias capas pictóricas (de las mezclas de pintura obtenidas) sobre un portaobjetos de vidrio. Para obtener el dosímetro pictórico de aglutinante puro, se extendió la yema de huevo batida directamente sobre el portaobjetos de vidrio.

Una vez secos todos los dosímetros pictóricos (de cola de conejo y de yema de huevo), se cortaron en un tamaño rectangular de 3 x 3 x 0.1 cm con un bolígrafo con punta de diamante. El siguiente paso consistió en pegar estas piezas, con cinta doble adhesiva de carbono, a un portaobjetos metálico típicamente empleado en microscopía electrónica de barrido. A continuación se almacenaron, en un orden preestablecido, en una caja de soporte de muestras usada igualmente en microscopía electrónica de barrido (Fig 1.2). Para la exposición de los dosímetros pictóricos a la intemperie, el soporte que los sustentaba fue fijado con una brida a un panel de cartón pluma, el cual fue pegado a un azulejo con pegamento resistente, para otorgar peso al conjunto tal que fuera resistente a las inclemencias atmosféricas.



Figura 1.2 Montaje de dosímetros pictóricos (autoría C. Cardell).

1.2. Metodología

Para alcanzar los objetivos propuestos en esta Tesis Doctoral se han empleado una variedad de técnicas analíticas complementarias, así como realizado una serie de ensayos de envejecimiento natural y acelerado en los dosímetros pictóricos, y aplicados tratamientos estadísticos a los datos obtenidos, que se describe a continuación.

1.2.1. Instrumentos de laboratorio

Los siguientes instrumentos básicos de laboratorio han sido empleados en la extracción de lípidos de los dosímetros pictóricos, para posteriormente ser analizados mediante MALDI-TOF/MS.

1.2.1.1. Balanza

La balanza se ha utilizado para pesar las muestras tomadas de los dosímetros pictóricos para ser analizado posteriormente su contenido lipídico mediante MALDI-TOF/MS. En la figura 1.3a se observa la balanza analítica empleada, modelo GH-252 de la marca A&D Company (Japón), y que tiene una precisión de 0.01 mg.

1.2.1.2. Ultrasonicador

Para el proceso de extracción de los lípidos de las muestras pictóricas, y posterior medida mediante MALDI-TOF/MS, ha sido necesario sonicar las muestras durante 20 minutos, para lo que se ha empleado un ultrasonicador modelo Ultrason-HD (Fig. 1.3b) de la marca JP Selecta S.A (España) con una frecuencia de 40 kHz y energía de 120 W.

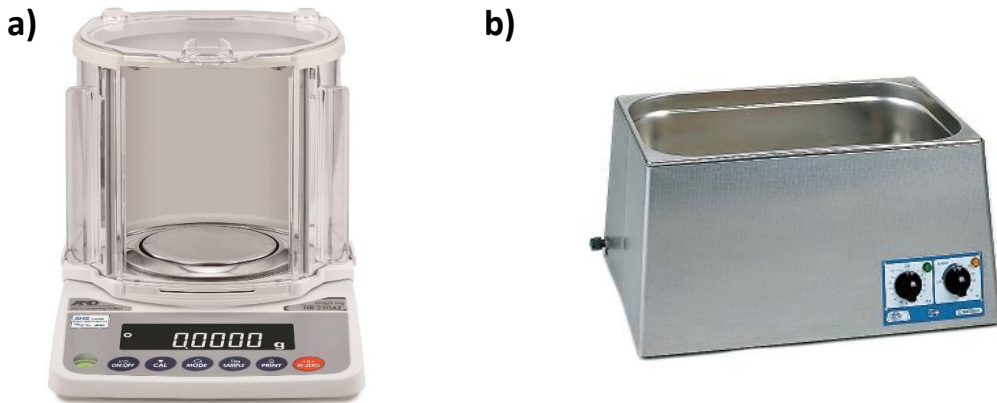


Figura 3.6 a) balanza analítica modelo GH-252; b) Ultrasonicador modelo Ultrason-HD

1.2.1.3 Centrifugadora

Para la separación de los lípidos y las proteínas de la yema de huevo, ha sido fundamental el uso de una centrifuga modelo 320 R de la marca Hettich Universal (Alemania) (Fig 1.4a). Las condiciones de trabajo fueron centrifugación de 3000 g de muestra durante 10 minutos a una temperatura de 25 °C.

1.2.1.4. Agitador

El agitador se empleó en la etapa inicial de la extracción de los lípidos de las muestras pictóricas. Concretamente se usó para mezclar durante 1 min y a una velocidad máxima de 3000 rpm los disolventes y las muestras pictóricas que contenían yema de huevo. El modelo empleado para agitar las muestras ha sido un IKA modelo Vortex 4 digital (Estados Unidos) (Fig 1.4b).

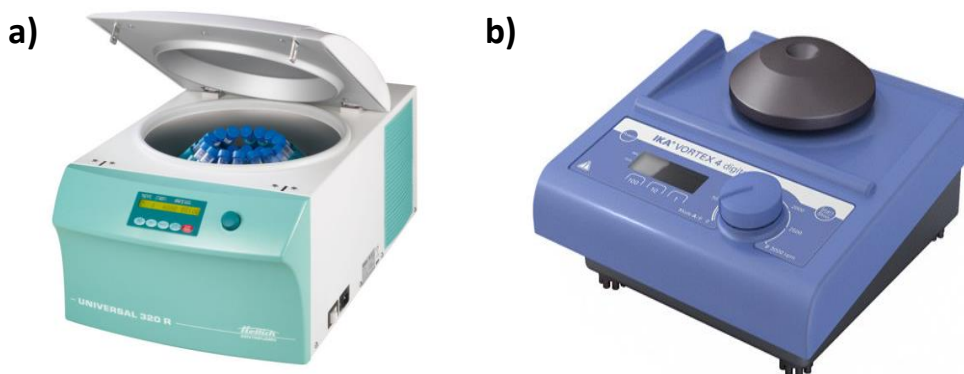


Figura 1.4 a) Centrifuga Hettich Universal 320 R; b) Agitador IKA vortex 4 digital.

1.2.1.5 Evaporizador o concentrador

Una vez separados los lípidos de las proteínas, se evaporaron o concentraron los analitos que contenían la fracción lipídica hasta sequedad, para posteriormente reconstituirla con un disolvente apropiado ($\text{CH}_3\text{CN}/\text{H}_2\text{O}/\text{TFA}$) para su análisis mediante MALDI-TOF/MS. El concentrador empleado fue un LabX modelo Stuart Scientific Sample Concentrator, SBHCONC/1 (Estados Unidos) (Fig 1.5) con un flujo de nitrógeno a una temperatura de 25°C.



Figura 1.5 Concentrador de muestras Stuart SBHCONC/1.

1.2.2. Caracterización composicional de los dosímetros pictóricos

1.2.2.1. Difracción de Rayos X (XRD)

La difracción de rayos X se ha empleado para la caracterización de la composición mineral de los pigmentos inorgánicos, y de los productos de degradación de éstos. Los análisis fueron realizados con un difractómetro Malvern Pananalytical's modelo X'Pert PRO (Reino Unido) (Fig 1.6) usando radiación Cu-K α , filtro de Níquel, voltaje de 45 kV, intensidad de 40 mA y en modo giro. Los difractogramas se registraron en un intervalo desde 3° a 60° 2 θ s⁻¹. La identificación y semicuantificación (5%) de los minerales se realizó usando el software Xpolder (Martín Ramos, 2004). La identificación de las fases cristalinas de los pigmentos se hizo mediante comparación con la base de datos *PDF-2 standards*.



Figura 1.6 Difractómetro X'Pert PRO Pananalytical's.

1.2.2.2. Microscopía electrónica de barrido (FESEM)

Se han empleado dos tipos de microscopios electrónicos de barrido para estudiar las características morfológicas y de composición química de los dosímetros pictóricos, tanto patrón como envejecidos. Para tal fin las muestras pictóricas se metalizaron parcialmente

con carbono. Los equipos usados fueron: i) un microscopio electrónico de barrido con emisión de campo (FESEM) Carl Zeiss modelo Auriga (Alemania), trabajando a vacío 10^{-4} Pa y entre 3 y 20 kV en modo imagen de electrones secundarios (BSE) (Fig. 1.7a), y ii) un microscopio electrónico de barrido con emisión de campo y presión variable (VP-FESEM) Carl Zeiss modelo Supra 40Vp (Alemania) equipado con un detector Aztec 3 EDX y X-Max 50 mm (Fig 1.7b). Las condiciones de trabajo fueron: vacío de 40-66 Pa y voltaje de aceleración del haz de 15-20 kV. Con VP-SEM se obtuvieron mapas de rayos X de alta resolución (1024 x 768 píxeles) en áreas seleccionadas no metalizadas de los dosímetros pictóricos. Las condiciones de trabajo fueron 100 *frames*, un tiempo de permanencia de 10 ms (adquisición de 2,5 horas), corriente de filamento 3 nA y resolución de 20 eV/ch. Para determinar la naturaleza de las fases cristalinas y las amorfas presentes en los dosímetros pictóricos, los mapas de fase mineral se compilaron a partir de mapas de distribución elemental mediante la aplicación de la herramienta *FindPhases* implementada en software Aztec versión 3. Este procedimiento permitió resaltar la ubicación, la morfología y la cantidad de fases presentes en los dosímetros pictóricos.

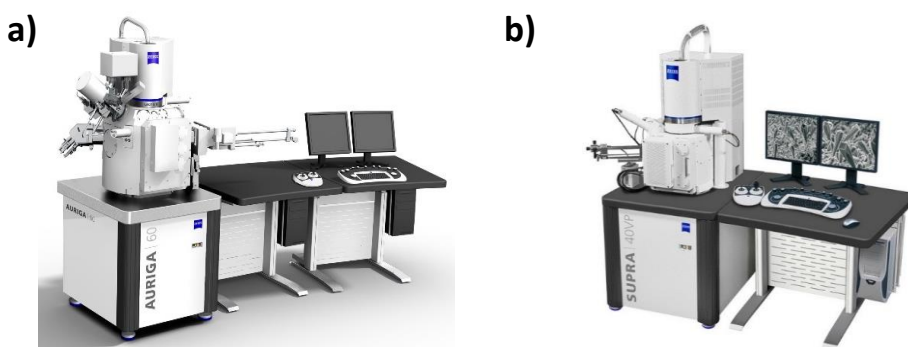


Figura 1.7 a) Microscopio electrónico de barrido FESEM (Auriga, Carl Zeiss); b) Microscopio electrónico de barrido y presión variable VP-FESEM (Carl Zeiss, Supra 40Vp).

1.2.2.3. Espectroscopía micro-Raman (RMS)

La espectroscopia microRaman (Jasco modelo NRS-5100 confocal Raman spectrometer (Reino Unido)) (Fig.1.8a) se ha aplicado a los dosímetros pictóricos patrón para caracterizar su composición (pigmento y aglutinantes), así como detectar los posibles cambios sufridos por envejecimiento natural o acelerado. Las muestras se han excitado con láser verde a 532 nm (Elford light G4-30; Nd:YAG) y laser rojo a 785 nm (Torsana Starbright) y se han registrado en el rango espectral de 100 -3000 cm^{-1} con una resolución de 2 cm^{-1} y una abertura de 50 μm . Las condiciones de análisis han sido diferentes según el tipo de dosímetro pictórico estudiado. El software para visualizar los espectros ha sido *Spectra Manager II* versión 2.08.04 desarrollado por Jasco es.

1.2.2.4. Espectroscopia infrarroja con transformada de Fourier (FTIR) con reflectancia total atenuada (ATR)

La técnica FTIR-ATR (Jasco Analytical instruments, Japón) se ha aplicado a dosímetros pictóricos patrón y envejecidos (Fig 1.8b), para caracterizar tanto los pigmentos como los aglutinantes, determinar el estado de conservación de los mismos (particularmente del aglutinante), y profundizar en las interacciones entre pigmento y aglutinante bajo distintas condiciones de exposición. Para el análisis, los dosímetros pictóricos se presionaron contra el cristal de diamante ATR. Los espectros de infrarrojos se registraron con una resolución de 2 cm^{-1} , 100 acumulaciones y en un intervalo espectral de 400-4000 cm^{-1} . El software para visualizar los espectros es *Spectra Manager II* versión 2.08.04 desarrollado por Jasco.

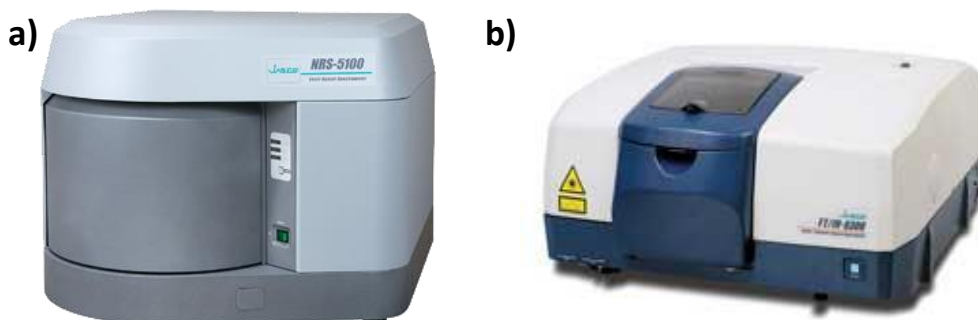


Figura 1.8 a) *Micro Raman Jasco NRS-5100*; b) *FTIR-ATR Jasco 6200*

1.2.2.5. Espectrometría de masas de tiempo de vuelo con desorción/ionización láser asistida por matrix o (MALDI-TOF/MS)

Para estudiar el contenido lipídico de los dosímetros pictóricos patrón y envejecidos se utilizó un equipo de MALDI-TOF/MS. Concretamente se empleó un espectrómetro de masas Bruker Biflex MALDI-TOF (Bruker-Franzen Analytik GMBH, Alemania) (Fig 1.9a). El instrumento tiene un láser de nitrógeno a 337 nm (OEM VSL-337i, Laser Science Inc., Estados Unidos) atenuado aproximadamente el 75% de su potencia máxima (250 μ), con un ancho de pulso de 3 ns para desorción/ionización. Los espectros de masas positivos se obtuvieron promediando 50 espectros individuales, registrados mediante extracción retardada, en modo reflector y una tensión de aceleración de 19,6 kV.

1.2.2.6. Termogravimetría (TGA)

El análisis termogravimétrico (Fig 1.9b) se empleó para cuantificar el aglutinante que contienen los dosímetros pictóricos. Los análisis se realizaron en un equipo Shimadzu modelo TGA-50H (Japón) en flujo de aire (100ml/min) a una velocidad de calentamiento constante de 10 ° C min⁻¹ (25-950°C).

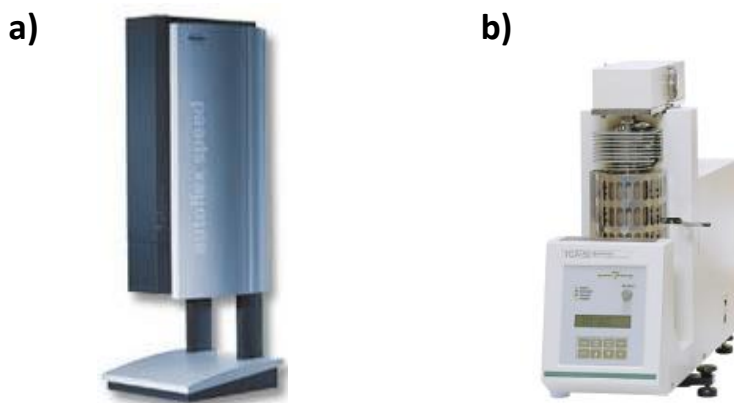


Figura 1.9 a) MALDI-TOF-MS de Bruker-Franzen Analytik GMBH; b) TGA de Shimadzu TGA-50H

1.2.3. Determinación de propiedades físicas y superficiales

1.2.3.1. Granulómetro

La medida del tamaño de partícula de los pigmentos se ha realizado con un granulómetro (Malvern Panalytical modelo Mastersizer 2000 LF (Reino Unido)). Este equipo realiza medidas en el intervalo de 0.02 -1500 μm , y las partículas de los pigmentos son detectadas por difracción de láser (Fig 1.10a).

1.2.3.2. Espectrofotómetro

Los parámetros de color de los dosímetros pictóricos patrón y envejecidos fueron medidos con un espectrofotómetro portátil (Konica Minolta modelo CM-700d (España)) (Fig 1.10b) usando un observador de 10° , apertura de 8 mm y el iluminante estándar D65 (color de temperatura: 6504 K). Los parámetros de color fueron guardados en modo SCI (componente especular incluida) y modo SCE (componente especular excluida). Los datos se han expresados en el espacio de color CIEL*a*b* y CIEL h*C*L*. Para el sistema

CIEL*a*b*, L* es luminosidad (negro=0 y blanco= 100); a* puede ser rojo (+a) o verde (-a) y b* puede ser amarillo (+b) o azul (-b). El sistema de color CIEL h*C*L* está representado por tres coordenadas cilíndricas: h* que es el tono de color referido a la longitud de onda dominante, C* que es el croma o saturación relacionado con la intensidad de color, y L* que es luminosidad del color. Para calcular la diferencia de color se emplea la fórmula $\Delta E = ((\Delta L^*)^2 + (\Delta a^*)^2 + (\Delta b^*)^2)^{1/2}$. En términos generales, se considera que la diferencia de color es perceptible al ojo humano con una variación de más de tres unidades ($\Delta E > 3$) (Mokrzycki and Tatol, 2011). El software para visualizar los datos cromáticos ha sido *Color Data Software CM-S100W Spectra Magic NX versión 2.10.0004* desarrollado por Konica Minolta sensing, Inc.



Figura 1.10 a) Granulómetro Malvern Master sizer 2000 LF; b) Espectrofotómetro Konica Minolta CM-700d

1.2.3.3. Estereomicroscopio o Lupa binocular

El estereomicroscopio (Nikon modelo SMZ 1000 (Japón)) se usó para examinar la textura, estructura y características superficiales de los dosímetros pictóricos patrón y envejecidos (Fig 1.11a). El estudio se realizó empleando pocos aumentos (8-40x), lo que permitió tener una visión de conjunto de las muestras pictóricas (Fig 3.9a).

1.2.3.4. Video-microscopio óptico

Los cambios texturales en la superficie de los dosímetros pictóricos se examinaron con un video-microscopio (Leica modelo DVM2000 (Alemania)) alcanzando una magnificación entre 40 y 400x aumentos (Fig 1.11b). Las imágenes se procesaron usando el software *Leica versión 3.8.0* desarrollado por Leica Microsystems©.

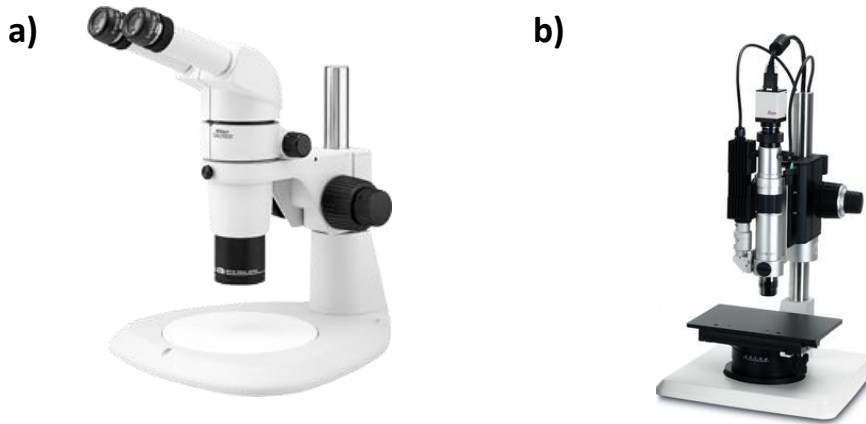


Figura 1.11 a) *Estereomicroscopio Nikon SMZ 100*; b) *Video-microscopio Leica DVM2000*.

1.3. Ensayos de envejecimiento de dosímetros pictóricos

1.3.1. Envejecimiento natural por exposición a la atmosfera urbana de Granada capital

Los dosímetros pictóricos se expusieron a la intemperie en monumentos piloto (semi)abiertos de la ciudad de Granada, en distintos escenarios de calidad de aire urbano (Fig 1.12). En concreto los dosímetros se ubicaron en: A) la Iglesia de Santa Domingo (barrio del Realejo, centro histórico ciudad), B) y C) el complejo monumental de la Alhambra y Generalife en la colina de la Sabika (Fig.1.13 a), D) Hospital de San Juan de Dios (centro histórico ciudad), E) La Catedral (centro histórico ciudad), F) Palacio del Almirante (colina del Albayzín (Fig 1.13b)), y G) Corral del Carbón (centro histórico ciudad).



Figura 1.12 Localización de los dosímetros pictóricos en los monumentos piloto de la ciudad de Granada.



Figura 1.13 Dosímetros pictóricos colocados en a) el Harem de la Alhambra; b) Palacio del Almirante en Albayzin

1.3.2. Ensayos de envejecimiento acelerado

1.3.2.1 Envejecimiento acelerado con radiación Ultravioleta (UV)

El envejecimiento artificial o acelerado de los dosímetros pictóricos se realizó con un tubo de radiación UV (Philips Lighting Holding B.V modelo TL 40W / 12 RS SLV / 25 (Países Bajos)) durante 1000 h en una cámara ventilada a 24 ± 3 ° C y $25 \pm 10\%$ de HR. La lámpara UV emite más de 85% de su energía en el intervalo de longitud de onda UV-B con un pico a ~ 320 nm. El nivel de irradiancia se fijó en 765 W / m². La luz del día fue bloqueada con papel de aluminio.

1.3.2.2 Ensayos de envejecimiento acelerado con SO₂

Actualmente no existe una normativa específica para los ensayos de envejecimiento acelerado con SO₂ en muestras pictóricas modelo. Por ello, para realizar este ensayo en los dosímetros pictóricos, se adaptó el método utilizado para la determinación de la resistencia

de la piedra natural al envejecimiento inducido por SO_2 en presencia de alta humedad (AENOR, Madrid 2003). El ensayo empleado en esta Tesis Doctoral consistió en colocar los dosímetros pictóricos en un recipiente de plástico herméticamente cerrado (7,5 l) junto con ácido sulfuroso diluido (1,35 % en peso de SO_2 , 104 ml) para generar una atmósfera saturada de SO_2 a $\sim 100\%$ de HR y durante 82h (Burgos-Cara et al., 2017). El contenedor se mantuvo en un ángulo de 45° durante el ensayo con el fin de facilitar la escorrentía de las gotas de condensación acumuladas en la tapa del recipiente. Los dosímetros pictóricos se colocaron sobre un soporte de plástico (rejilla cuadrículada) para evitar el contacto directo con el ácido diluido.

1.4 Tratamiento estadístico de datos

1.4.1 Quimiometría

La quimiometría se puede definir de muchas maneras, y no existe una definición que sea la más aceptada por toda la comunidad internacional. Sin embargo una de las definiciones que tiene más consenso dentro de la comunidad científica es dada por (Otto, 2017) :“... *la disciplina química que utiliza métodos matemáticos y estadísticos, (a) para diseñar o seleccionar procedimientos y experimentos óptimos de medición, y (b) para proporcionar información química máxima analizando datos químicos*”. No obstante, e independientemente de la definición, la quimiometria se basa en el análisis de datos multivariantes, para lo cual emplea diversos enfoques y herramientas matemáticas con diferentes grados de complejidad. Una de estas herramientas matemáticas de análisis de datos multivariante es el método del análisis de las componentes principales, conocido comúnmente como PCA por sus siglas derivadas del acrónimo en inglés (Principal Componente Analysis). Este método ha adquirido una gran aceptación en el análisis de patrimonio cultural por ser de los más sencillos desde el punto de vista del proceso matemático que emplea a la vez que aporta información muy valiosa referida a la muestra pictórica estudiada (Manzano et al 2010). PCA, además de ser un método de exploración de datos sin supervisión –sin imposición de condiciones o reglas- permite simultáneamente

reducir los datos originales transformándolos en nueva información más fácilmente interpretable en función de la información buscada. Por tanto, mediante PCA se puede poner de manifiesto la relación que existe entre las diferentes muestras y reducir los datos originales, ya que elimina la información redundante y la variabilidad debido al ruido de la técnica analítica empleada (Blanco and Cerdà, 2007).

En esta Tesis Doctoral se ha hecho uso de la quimiometría, concretamente del PCA. Este método se ha empleado por primera vez para analizar los datos discretos de color obtenidos con un espectrofotómetro portátil al medir dosímetros pictóricos expuestos al ambiente contaminante de la ciudad de Granada a lo largo de un periodo prolongado de tiempo. Mediante el PCA se pudo discriminar y agrupar las muestras según pigmento, aglutinante y tamaño de grano y evaluar su estado o tendencia de color. Además, se determinó mediante esta estrategia la tendencia en la variación cromática de los dosímetros pictóricos, evaluándose así tendencias de color no detectables a simple vista, y con capacidad de proponer modificaciones o tendencias en el tiempo del color. (Capítulo 3).

1.4.2 Tecnologías ómicas

Los grandes avances obtenidos en recientes años tanto en el ámbito de la biología y la salud como en el de la bioinformática, han permitido un nuevo enfoque en el que se aplica una visión global para el estudio de los procesos biológicos. El sufijo “oma” es de origen latino y hace referencia a “conjunto de”. Las denominadas “ciencias ómicas” tienen en común analizar una cantidad enorme de datos generados mediante instrumentación analítica avanzada, generalmente espectrometría de masas. El análisis integrado de una estrategia de comparación permite el estudio global de procesos biológicos y su relación, entre otros, con la salud. Disciplinas como la genómica, proteómica, transcriptómica, metabolómica y lipidómica (una rama de la metabolómica) forman parte de estas ciencias ómicas, que aplican unas herramientas comunes actualmente reconocidas como estrategias y/o tecnologías ómicas (Amaro et al. 2015; Quiroga 2016). Dentro de estas se encuentra el

empleo de la espectrometría de masas para la generación de complejos espectros de masas que son posteriormente analizados haciendo uso de grandes y complejas bases de datos a disposición de la comunidad internacional.

Este enfoque ómico es normalmente empleados en la investigación sobre todo médica, pero también en la biotecnológica, farmacéutica, bioquímica (Rolim et al., 2015) y alimentaria (Picariello and Mamone, 2012) . Sin embargo, su uso se ha empezado a expandir en campo del patrimonio cultural (Van den brink et al., 2001; Van der werf et al., 2012). Particularmente en las últimas dos décadas se ha experimentado un gran avance en el patrimonio pictórico donde se han empezado a realizar estudios de proteínas, lípidos, etc, que constituyen el aglutinante de las pinturas pictóricas empleando técnicas ómicas (Romero-Pastor et al., 2012).

En concreto, en esta Tesis Doctoral se ha empleado una estrategia lipidómica para estudiar las interacciones que se producen en los dosímetros pictóricos al temple entre el pigmento y el aglutinante (yema de huevo). Dosímetros pictóricos de referencia se caracterizan mediante su huella dactilar lipídica para posteriormente evaluar mediante comparación el impacto que tiene en las pinturas el ambiente contaminante de la ciudad de Granada. Para tal fin, se han analizado los dosímetros pictóricos frescos y degradados naturalmente durante 6 meses en la ciudad de Granada mediante MALDI-TOF/MS y se ha utilizado la base internacional de datos *www.lipidmaps.org* (Capítulo 2).

Referencias

AENOR, Natural Stone Test Methods. Determination of Resistance to Ageing by SO₂ Action in the Presence of Humidity., 2003. (UNE-EN 13919:2003, Madrid)

Amaro, A., Petretto, A., Angelini, G. and Pfeffer, U. 2015. Advancements in Omics Sciences, in *Translational Medicine: Tools and Techniques*, pp. 67–108. doi: 10.1016/B978-0-12-803460-6.00004-0.

Aze, S., Vallet, J.-M., Pomey, M., Baronnet, A., Grauby, O., 2007. Red lead darkening in wall paintings: natural ageing of experimental wall paintings versus artificial ageing tests. *Eur. J. Mineral.* 19, 883–890. doi:10.1127/0935-1221/2007/0019

Burgos-Cara, A., Ruiz-Agudo, E. and Rodríguez-Navarro, C., 2017. Effectiveness of oxalic acid treatments for the protection of marble surfaces. *Materials & Design*, 115, pp. 82–92. doi: 10.1016/j.matdes.2016.11.037

Blanco, M. and Cerdà, V. 2007. Temas avanzados de quimiometría, *Materials didàctics*. Universitat de les Illes Balears.

Calligaro, T., Coquinot, Y., Pichon, L., Pierrat-Bonnefois, G., De Campos, P., Re, A., & Angelici, D., 2014. Characterization of the lapis lazuli from the Egyptian treasure of Tôd and its alteration using external μ -PIXE and μ -IBIL. *Nuclear Instruments and Methods in Physics Research*, 318, 139–144. <https://doi.org/10.1016/j.nimb.2013.06.063>

Cardell-Fernández, C., & Rodríguez-Gordillo, J., 2003. Policromías de la Iglesia del Monasterio de San Jerónimo de Granada: composición, alteración y técnicas de ejecución. *Boletín de La Sociedad Española de Mineralogía*, 26, 118–121. <https://doi.org/10.7597/acopios2171-7788.2012.35>

Cennino C., 1960). *The Craftsman's Handbook* (Dover edit).

Eastaugh N, Walsh V, Chaplin T, S. R., 2008. *Pigment Compendium*. Routledge. <https://doi.org/10.4324/9780080943596>

Gettens, R.J., Feller, R.L., Chase, W.T., 1986. Artists' Pigments: A Handbook of Their History and Characteristics, in: *Artists' Pigments: A Handbook of Their History and Characteristics*. National Gallery of Art, pp. 159–182. doi:10.2307

Han, K., Nam, J.-Y., Ji, J.-E., Kang, D., Lee, H., Baek, N., ... Yang, I.-S., 2016. Existence of nanoparticles in azurite and malachite pigments – Raman spectroscopy and X-ray diffraction studies. *Dyes and Pigments*, 133, 232–237. <https://doi.org/10.1016/j.dyepig.2016.06.004>

Harley, R. D., 1982. *Artists' Pigments c. 1600-1835: A Study in English Documentary*

Sources. second edi. London: Butterworth Scientific.

Martin-Ramos, J. D., 2004. Using X Powder: A software package for Powder X-Ray diffraction analysis. DL GR (Vol. 1001). Retrieved from www.xpowder.com

Mokrzycki, W. S., & Tatol, M., 2011. Colour difference dE- A survey. *Machine Graphics and Vision*, 20(4), 383–411.

Otto, M., 2017. *Chemometrics: statistics and computer application in analytical chemistry*. Wiley-VCH.

Pacheco, F., 1954. *El arte de la pintura (Cátedra)*. Madrid.

Picariello, G. and Mamone, G., 2012. Novel Mass Spectrometry-Based Applications of the 'Omic' Sciences in Food Technology and Biotechnology, *Food Technology and Biotechnology*, 50(3), pp. 286–305.

Quiroga, C. (2016) 'Las tecnologías «ómicas»: situación actual y desafíos futuros', *Revista Argentina de Microbiología*. Elsevier, 48(4), pp. 265–266. doi: 10.1016/j.ram.2016.12.001.

Rolim, A. E. H., Henrique-Araújo, R., Ferraz, E. G., de Araújo Alves Dultra, F. K. and Fernandez, L. G., 2015. Lipidomics in the study of lipid metabolism: Current perspectives in the omic sciences', *Gene*, 554(2), pp. 131–139. doi: 10.1016/j.gene.2014.10.039.

Romero-Pastor, J., Navas, N., Kuckova, S., Rodríguez-Navarro, A. and Cardell, C. 2012. Collagen-based proteinaceous binder-pigment interaction study under UV ageing conditions by MALDI-TOF-MS and principal component analysis', *Journal of Mass Spectrometry*, 47(3), pp. 322–330. doi: 10.1002/jms.2966.

Van den brink, O. F., Boon, J. J., O'Connor, P. B., Duursma, M. C. and Heeren, R. M. 2001. Matrix-assisted laser desorption/ionization Fourier transform mass spectrometric analysis of oxygenated triglycerides and phosphatidylcholines in egg tempera paint dosimeters used for environmental monitoring of museum display conditions. *Journal of Mass Spectrometry*, 36(5), pp. 479–92. doi: 10.1002/jms.145.

Van der werf, I. D., Calvano, C. D., Palmisano, F. and Sabbatini, L. 2012. A simple protocol for Matrix Assisted Laser Desorption Ionization- time of flight-mass spectrometry (MALDI-TOF-MS) analysis of lipids and proteins in single microsamples of paintings, *Analytica Chimica Acta.*, 718, pp. 1–10. doi: 10.1016/j.aca.2011.12.056.

**Resultados y discusión:
*caracterización de la interacción
pigmento-aglutinante bajo
atmosfera contaminada***

***El conocimiento y la
habilidad suman, pero la
actitud multiplica***

Victor Küpper



**Pablo Picasso-Mujer en
azul**

Capítulo 2

An evaluation of the impact of urban air pollution on paint dosimeters by tracking changes in the lipid MALDI-TOF mass spectra profile

A.Herrera⁽¹⁾, N.Navas⁽²⁾ and C.Cardell^{(1)*}

(1) Dept. of Mineralogy and Petrology, Faculty of Science, University of Granada, Campus Fuentenueva s/n, 18071 Granada, Spain.

(2) Dept. Analytical Chemistry, and Biomedical Research Institute of Granada (IBIG), University of Granada, Faculty of Science, Campus Fuentenueva s/n, 18071 Granada, Spain.

Talanta 155 (2016)53 61 <http://dx.doi.org/10.1016/j.talanta.2016.04.006>

Article history:

Received 21 January 2016

Received in revised form

2 April 2016

Accepted 4 April 2016

Available online 6 April 2016

Hipótesis de partida

Recientemente las investigaciones dedicadas al análisis simultáneo de pigmentos y aglutinantes orgánicos en muestras pictóricas (reales o modelo) han aumentado, centrándose en la descripción de los procesos de interacción entre los materiales pictóricos bajo diversos escenarios de alteración. Los estudios de caracterización de pigmentos minerales y sus procesos de deterioro suelen ser, en general, más rápidos y precisos que los realizados en aglutinantes orgánicos, por varios motivos. En las pinturas artísticas los aglutinantes se encuentran en proporción inferior a los pigmentos (i.e. razón pigmento-aglutinante es ca. 3:1), complicando así su correcta identificación. Por otra parte, los aglutinantes orgánicos son menos estables a los agentes de alteración, y por tanto se deterioran con mayor facilidad, lo que a su vez complica su estudio.

De entre los aglutinantes orgánicos empleados en obras pictóricas, los de naturaleza proteica, como la yema de huevo, han sido muy usados por los artistas durante siglos. La yema de huevo se compone aproximadamente por un 70% de lípidos y un 30% de proteínas. Por tanto, su correcta caracterización supone analizar ambos componentes.

De entre las numerosas técnicas analíticas empleadas en la investigación de aglutinantes proteicos, en las últimas décadas se ha producido un auge en la aplicación de la espectrometría de masas de tiempo de vuelo con fuente de desorción/ionización laser asistida por matriz (MALDI-TOF/MS). Los especialistas en este campo han propuesto diversos protocolos analíticos basados en diferentes métodos de extracción, seguidos por el análisis con MALDI-TOF/MS, para investigar las pinturas al temple elaboradas con yema de huevo. La reproducción de los protocolos analíticos publicados solo es posible al aplicar el modo lineal MALDI-TOF/MS, pero ello origina espectros de baja resolución, y por consiguiente, baja precisión en los análisis de masas. En muestras complejas de pintura histórica es mejor realizar un análisis del aglutinante en profundidad usando datos de masas de mayor resolución en modo reflectron, para obtener huellas dactilares de péptidos más precisas y fiables.

Objetivo de la investigación

Presentar un método optimizado para el análisis de la fracción lipídica de los dosímetros pictóricos elaborados con yema de huevo mediante MALDI-TOF/MS. De esta manera, aplicando dicho método al análisis de las muestras pictóricas se puede realizar un seguimiento de los cambios producidos en la fracción lipídica debido al envejecimiento natural (muestras pictóricas no expuestas a la intemperie), y debido a distintos escenarios de polución atmosférica en la ciudad de Granada (muestras pictóricas expuestas a la intemperie). Además, es también objetivo del estudio determinar cómo afecta a los resultados y a su interpretación la procedencia del huevo de pollo (variedad de gallina ponedora) empleado para la elaboración de los dosímetros pictóricos. El objetivo final es proporcionar una estrategia y/o protocolo analítico preciso que permita identificar y asilar los cambios producidos en la composición lipídica de la yema de huevo en los dosímetros pictóricos asociados específicamente a la interacción entre pigmento y aglutinante.

Abstract

We evaluated the impact of urban air pollution on egg yolk tempera paint dosimeters (binary mixture samples made with historic artist's blue, red and white pigments) by tracking changes over time in their lipid matrix-assisted laser desorption ionization time-of-flight mass spectra (MALDI-TOF-MS) profiles. We studied triacylglycerols (TGs), phospholipids (PLs) and their oxidation by-products from paint dosimeters that had been exposed outdoors for six months to the polluted atmosphere in the city center of Granada (Spain). Four types of chickens' eggs were also analyzed to find out whether their lipid mass spectra (lipid fingerprints) varied significantly. The ultimate goal of this research is to provide a precise analytical protocol to show whether the changes in the egg yolk identified in paint dosimeters are due to pigment-binder interactions. The Bligh-Dyer (BD) method was optimized for the extraction of the lipids. This innovative procedure included a washing-step prior to the mass spectrometric analysis, which proved crucial for obtaining higher quality lipid fingerprints. A novel interpretation of the results is proposed by applying the BD method, which suggests that transesterification processes occurred in the lipid fractions that were catalyzed by the pigments in the paint dosimeters. In blank dosimeters specific ions produced by oxidative cleavage of PLs and/or TGs may be used as markers of the presence of egg yolk binders. The composition and structure of the specific lipid compounds are also tentatively proposed. In aged dosimeters the intact content of the TGs and PLs decreased; however, we propose that short-chain oxidative products arising from TGs and PLs are present in all the samples, except for the white lead-based dosimeter. We end with a new explanation as to why this dosimeter behaves differently from the others.

2.1. Introduction

One of the greatest hazards for open-air paintings on the buildings that form part of our architectural heritage is the darkening and degradation of colors caused by urban pollution, aggressive marine atmospheres and climate change. This problem is intensified in hot Mediterranean coastal cities with heavy traffic, such as those in southern Spain. Color changes can be caused by chemical or mineralogical transformation of pigments, oxidation of organic binders, precipitation of new mineral phases (including salts) and dust or pollen accumulation on the surface of the paintings, often producing irreversible aesthetic damage [1]. Preventive conservation of these ancient paintings is becoming increasingly important nowadays, requiring complete characterization of the artwork, its microclimatological and atmospheric environment, and of the interactions at the artwork-atmosphere interface using a multi-analytical and multidisciplinary approach. However, and in spite of the clear financial savings associated with preventive conservation as compared to restoration once damage has been done, few studies have addressed the effects of atmospheric aerosols (gas and particulate matter) and/or climate change on the surface of outdoor paintings [1-5]. Moreover, up to now, preventive conservation to deal with the impact of atmospheric pollution has focused almost exclusively on indoor research in museums, churches, art galleries, etc. where the environmental conditions (temperature, relative humidity and luminosity) and air quality are closely controlled, and any color changes in the paintings can be evaluated [3, 6, 7].

The characterization of historical paintings is quite challenging as they often have a complex composition and structure, in which painting materials such as inorganic/organic pigments, mineral fillers and organic binders are closely mixed, in addition to the small amount of sample permitted for use in research. These limitations mean that scientific research can only advance with the aid of model paint samples, known as paint dosimeters or mock-ups. Various studies have focused on the use of naturally aged paint dosimeter inside museums, aimed at characterizing organic compounds and varnish [3, 6, 7].

However, to our knowledge there are no papers on the use of paint dosimeters to evaluate the damage caused by outdoor exposure to urban air pollution.

The simultaneous characterization of pigments and organic binders in the same paint (layer) sample, either original or laboratory prepared, is also unusual. Only recently have researchers begun to describe the processes of interaction between pigments and binders in both historical paintings and dosimeters –artificially aged under UV irradiation-, examining the role of inorganic pigments in the weathering process of organic binders [8-14]. While pigments can be characterized quickly and accurately, the identification of organic binders and their ageing in paint samples is quite problematic for various reasons: i) they appear in smaller amounts than inorganic pigments in the paint layers (the normal pigment to binder ratio is ca. 3:1), thus the occurrence of a high quantity of pigments, mineral fillers and desiccants could complicate accurate identification of the binder, and ii) organic binders are less stable than mineral pigments and hence deteriorate faster, making identification more complex.

The identification of the organic binders used in paintings is crucial when it comes to identifying the technique used by the artist and deciding on the most suitable conservation/restoration treatments. Although numerous studies have addressed the question of how to identify the different organic binders (i.e. oils, proteins, waxes or gums), less research has been done on the in-depth characterization of their ageing processes, particularly for proteinaceous binders as a result of their intricate composition and structure [8, 14-19].

To date, proteinaceous binders have been studied using an array of analytical techniques such as Fluorescence Spectroscopy, Fourier Transform Infrared Spectroscopy (FTIR), Raman Microscopy (RM), Gas Chromatography (GC) and Liquid Chromatography (HPLC) [6,8,14,18,20,21]. Mass spectrometry (MS) also plays an important role in their characterization [14,22-25]. Of the various ionization techniques used in the analysis of proteinaceous binders, Matrix-Assisted Laser Desorption Ionization (MALDI) coupled with Time of Flight Mass Spectrometers (MALDI-TOF-MS) has become increasingly popular over

the last decade in the characterization of organic binders used in artwork [12,14,26]. Pioneering research applying this technique to paint samples used specific enzymatic cleavage (trypsin) to break the bonds of the amino acid compounds of those proteins, so obtaining peptides. The peptides were then compared using the relevant databases to discover the source of the proteins found in the paint samples [12,27]. More recent authors applied MALDI-TOF-MS to analyze various kinds of binders, for instance rabbit blue, in paint dosimeters artificially aged with UV radiation [14] and oils from real easel paint samples [28].

A common organic binder used by artists for many centuries is egg yolk, which is about 70% lipid and 30% protein [29]. The correct characterization of egg-yolk therefore involves analyzing both components. Specialists in this field have proposed several analytical protocols based on different extraction methods followed by MALDI-TOF-MS analysis to investigate egg yolk-based (tempera) paintings [22,23,30]. In the framework of two Research Projects aimed at analyzing pigment-binder interactions in real polychromes and paint dosimeters exposed at open and semi-open monuments in the polluted urban atmosphere of Granada (southern Spain), we applied these analytical procedures to typify tempera dosimeters (binary mixtures of pigments mixed with pure egg-yolk) that we had made in the laboratory. Replication of published protocols was only possible when the linear mode of MALDI-TOF-MS was applied, but this provided limited resolution spectra leading to low mass accuracy. In complex paint mixtures it is better to perform in-depth analyses of organic binders using higher resolution MS data in reflectron mode for more accurate, more reliable peptide mass fingerprinting (PMF) [14,27].

The aim of this paper is therefore to present an optimized extraction method for MALDI-TOF mass spectrometry in order to analyze the lipid fraction of blank egg-yolk-based paint dosimeters and to track changes when they are naturally aged for long periods in an urban atmosphere. We also analyzed four types of chickens' eggs to find out whether their lipid fingerprints varied significantly. The final goal is to provide a precise accurate analytical

protocol, which proves that the changes in the egg yolk identified in the paint samples are due to pigment-binder interactions.

2.2. Materials and Methods

2.2.1. Chemicals and reagents

All reagents were of analytical reagent grade unless stated otherwise. Reverse-osmosis quality water (purified with a Milli-RO plus Milli-Q station from Millipore Corp., Madrid, Spain) was used throughout. Methanol, chloroform, acetonitrile, ammonium phosphate dibasic and diammonium citrate were supplied by Panreac (Barcelona, Spain). α -cyano-4-hydroxycinnamic acid (A-CHCA) matrix, sinapinic acid (SA) matrix, 2,5-dihydroxybenzoic acid (DHB) matrix and trifluoroacetic acid (TFA) were all from Sigma Aldrich (Barcelona, Spain).

2.2.2. Paint dosimeters

Twenty paint dosimeters were prepared according to 'Old Master recipes' to obtain egg yolk tempera painting standards similar to those used by medieval artists [31]. Tempera is a painting technique in which finely ground pigments are first mixed with water and later blended with a solidifying proteinaceous binding agent, in our case egg yolk [32]. The first nine model samples were pure pigments and the tenth was the pure egg yolk binder. The ten remaining model samples were binary mixture paint samples composed of each of the pure pigments mixed with the egg yolk binder. We selected three blue pigments (azurite, malachite and lapis lazuli), three red pigments (cinnabar, minium and hematite), and three white pigments (lead white, calcite and gypsum) for analysis. All pigments were purchased from Kremer Pigments GmbH & Co. KG (Madrid, Spain).

To prepare the binder, the egg yolk was separated from the white using the usual method of pouring it back and forth in the half shells. It was then rolled onto a paper tissue to remove the layer of clinging egg white and most of the chalazae. The skin was punctured

at the bottom using a pin and the liquid content poured into a jar. The preparation of the tempera paint dosimeters was as follows: approximately 0.5 g of each pigment powder was placed in a small bowl and several drops of beaten egg yolk (different amounts for each pigment) were added to form a fluid paste. This procedure was adapted to emulate real paint layers with variable pigment concentrations as found in ancient paintings. Then, we used a paintbrush to spread several layers of the paste in a fine coat on a glass slide. To obtain the pure binder model sample, the beaten egg yolk was spread directly onto the glass slide [33]. Four different types of eggs were included in the study, i.e. brown, white, organic and free-range eggs, all of them from the domestic market. Paint dosimeters were prepared as explained above for pure binder model samples.

2.2.3. Natural ageing test

The paint dosimeters were placed in the courtyard of the church of “San Juan de Dios” in the city (historic center) of Granada (Spain), where they were exposed to environmental pollution for six months, including heavy construction works, heavy traffic and extreme sun, heat and cold, in addition to rain and wind conditions.

2.2.4. Lipid extraction procedure

The lipid fraction in the paint dosimeters was extracted using optimized Bligh-Dyer (BD) method (Fig. 1 supplementary material Appendix I) [6,22]. Briefly: a small amount of sample was scraped off the paint dosimeters, crushed and placed in an Eppendorf. 150 μL of $\text{CHCl}_3/\text{MeOH}$ (1:2) were added to 150-200 μg of sample followed by vigorous vortex-mixing (IKA Vortex 4 digital, USA) and 20 min ultrasonication (Ultrasons-HD Model, Spain; Power 120 W/frequency 40 kHz). Then, 50 μL of CHCl_3 were added, followed by 50 μL of H_2O and the mixture was vortexed and ultra-sonicated again (20 min) after each addition [2]. To facilitate phase separation, the mixture was centrifuged (10 min at 3000 $\times g$). The bottom organic layer where the lipid fraction was expected to be extracted was collected,

concentrated under a gentle nitrogen stream and reconstituted into 0.5 mL of a CH₃CN/H₂O/TFA (50:49.9:0.1) solution for later analysis.

2.2.5. MALDI-TOF-MS and data analysis

The lipid extracts were mixed with matrix solution in volume ratio 1:1 (2 μ L) and applied on a stainless steel MALDI target (Bruker Daltonik GmbH, Bremen, Germany). The matrix was a solution of A-CHCA (25 mM in a solution of ammonium phosphate dibasic 8 mM), 1 μ L of the lipid fraction/matrix mixture was deposited on the spot of the MALDI plate and left to dryness (Fig. 1 supplementary material Appendix I)[34]. Before recording the MALDI-TOF mass spectra, the MALDI samples were spot-washed to suppress the A-CHCA matrix cluster and to reduce the chemical noise in the subsequent spectra [34]. To this end, 1.5 μ L of ammonium washing buffer was dropped on the spot containing the dry extracted sample. After 3-5 s, the supernatant retained on the spot was removed using a 2 μ L pipet. The MS analysis was performed on this washed MALDI sample as explained below.

The MALDI-TOF-MS spectra were obtained using a Bruker Biflex MALDI-TOF mass spectrometer (Bruker-Franzen Analytik GMBH, Bremen, Germany). The instrument used a nitrogen laser at 337 nm (OEM VSL-337i, Laser Science, Inc., Newton, MA, USA) attenuated to about 75% of its maximum power (250 μ J), with a 3 ns pulse width for desorption/ionization. Positive MALDI spectra were obtained by averaging 50 individual spectra, recorded using delayed extraction, the reflector mode and an accelerating voltage of 19.6 kV, unless otherwise stated. Angiotensin II [M+H]⁺ (m/z =1046.5), angiotensin I (m/z =1296.6), Substance P [M+H]⁺ (m/z = 1347.7), Bombesin [M+H]⁺ (m/z = 1619.8) and Renin substrate [M+H]⁺ (m/z =1758.9) mixtures with an average molecular weight of 400 and 2000, respectively, were used for internal calibration.

For the data analysis, the registered mass spectra were exported as txt files and edited with mMass software [35]. This program was used for the sequential data processing performed on the mass spectra before the lipidomic analysis. Figure 2 supplementary material Appendix I shows the work-flow of these procedures. Smoothing using the Savitzky-Golay

method was applied with a window size of 0.05 m/z and 5 cycles. The baseline was corrected with approximately 75% accuracy. The deisotoping step was also executed with this program and was followed by the peak-picking procedure, thereby obtaining the corresponding lipid mass spectra profile of the paint dosimeters by MALDI-TOF-MS in the interval between 500-2000 Daltons (m/z) with an accuracy of 0.6 Da [8]. Afterwards the mass spectra were exported in txt format with data pairs representing the m/z and its relative intensity signal. The lipid assignment in the mass spectrum was performed using international lipidomic databases, i.e. www.lipidmaps.org., using a command included in the mMass software [35]. The particular criteria for accepting the lipid assignment are discussed below in the “results and discussion” section.

2.3. Results and discussion

2.3.1. Optimization of the lipid extraction procedure

The first step in this research was the optimization of the overall lipid extraction protocol, which includes solution of the solid dosimeter sample, extraction and isolation from other components, bearing in mind that the extracted samples will be further analyzed by MALDI-TOF-MS. Although several dissolving procedures were checked (agitation, sonication, mixtures of organic solvents, etc) that described by Bligh and Dyer [22] showed the best results. Therefore the solubilization of the samples was achieved using the BD method, i.e. with a mixture of chloroform/methanol 1:2 (v/v), with sonication in an ultrasonic bath for 20 min with a further addition of chloroform and water in a proportion of 1:1 (v/v). This method is widely used for the extraction of organic compounds with different polarities, and in our case for the extraction of the lipids and proteins from the organic fraction of the paint dosimeters. Figure 1 supplementary material Appendix I sets out the procedure.

The concentration of the analytes in the solid sample taken from the paint dosimeters is another important issue in that high intensities in the signals could saturate the mass spectra and/or affect the ionization process. It is therefore necessary to control the

concentration in the samples. To this end, different concentrations of the lipids content ranging over 5.0 mg/L to 5000.0 mg/L were tested. These concentrations were adjusted by the volume used to reconstitute the samples in the step prior to adding the matrix for MALDI-TOF-MS analysis. The best results were obtained with a concentration of 500 mg/L [25]. Once we had optimized both the composition of the solution used to dissolve the solid sample and the amount of sample to be used, we then extracted the lipids fraction using a modification of the Bligh and Dyer method [22]; the most common method for separating lipids and proteins. The proposed modification is the use of acetonitrile/water in a 1:1 (v/v) ratio instead of chloroform and methanol in a 1:1 (v/v) ratio to reconstitute the sample after being taken to dryness with a gentle stream of nitrogen. The purpose of this change is to allow the further use of Zip TIPC18® filters, widely used to clean the samples immediately before analysis by MS. This type of filter does not support media with chloroform levels of over 1 %. After experiments using these filters showed that they had no significant effects on the mass spectra, we decided not to use them. However we decided to continue using the mixture of acetonitrile/water in a 1:1 (v/v) ratio, due to its excellent results for dissolving lipids with different grades of polarities.

2.3.2. Optimization of the MALDI-TOF-MS procedure

The optimization of the MALDI-TOF-MS analysis focused above all on the selection of the most suitable matrix for the ionization of the samples and on optimizing the spot-washing step, which had been shown to improve the quality of the mass spectra [13,22,36]. The ionization of the compounds to be analyzed by MALDI-TOF-MS depends to a large extent on the matrix, which means that correct selection is crucial. In this research, we selected the three matrices most commonly used in the bibliography, namely DHB (2,5 dihydroxybenzoic acid), SA (sinapinic acid) and A-CHCA (alpha cyano - 4 -hydroxy – cinnamic acid) [37]. All these matrices were prepared with acetonitrile and H₂O at different percentages, and trifluoroacetic at 0.1 %. The concentration of the matrix was close to the level of saturation of the organic medium. Of these three, we opted for A-CHCA because it provided the best mass spectra based on the number and quality of the signals obtained

(m/z). The selected conditions of this matrix were: A-CHCA at a concentration of 25 mM in 50% acetonitrile, 49.9% H₂O and 0.1 % TFA (trifluoroacetic). Phosphate dibasic ammonium (8 mM) was added to the matrix to produce a final concentration ranging from 8 mM to 10 mM.

As mentioned earlier, a major problem affecting the quality of the mass spectra is the presence of sodium and potassium salts. These salts have to be removed to avoid complex mass spectra that are difficult to interpret due to the presence of adducts and also to avoid potential deletion of important signals. Smirnov [34] proposed a method for removing adducts involving a change in the matrix composition and washing with ammonium citrate. For this reason, we decided to add ammonium hydrogen phosphate to the matrix at a concentration of 8 mM, keeping the final concentration of the A-CHCA at 25 mM. This procedure proved decisive when the reflectron mode was used, because it improved the quality of the mass spectra. If the MALDI spot had not been washed prior to the analysis, only the linear mode could have been used, since the number of signals in the mass spectra was very poor in reflectron mode. This may be due to the suppression of signals in reflectron mode caused by the formation of adducts by the salts.

2.3.3. Characterization of the blank paint dosimeters

In order to assess whether the kind of egg used in the paint dosimeters affected the results, egg yolks from eggs with different colored shells were analyzed, i.e. brown shell and white shell, and from different origin, i.e. organic and free-range eggs (both with brown shells). The results indicated that the mass spectra were closed both in terms of the signals (m/z) and the intensities, and no important differences were detected. Even the paint dosimeters prepared using only binder media produced mass spectra similar to those. As an example of this, Figure 1 shows the mass spectra of the lipid fraction of three different kinds of eggs (i.e. white and brown shells, and free range eggs) and the mass spectra of a blank egg yolk based paint dosimeter) where can be corroborated close lipid mass spectra profile. We detected phospholipids and triglycerides that were very close in class but with differences

in their fatty acids composition. This shows that the particular kind of egg used in the dosimeter did not affect the mass spectra and could not, therefore, be considered a discriminate parameter. This meant that further analysis of the mass spectra for the dosimeters had to be based on the pigment.

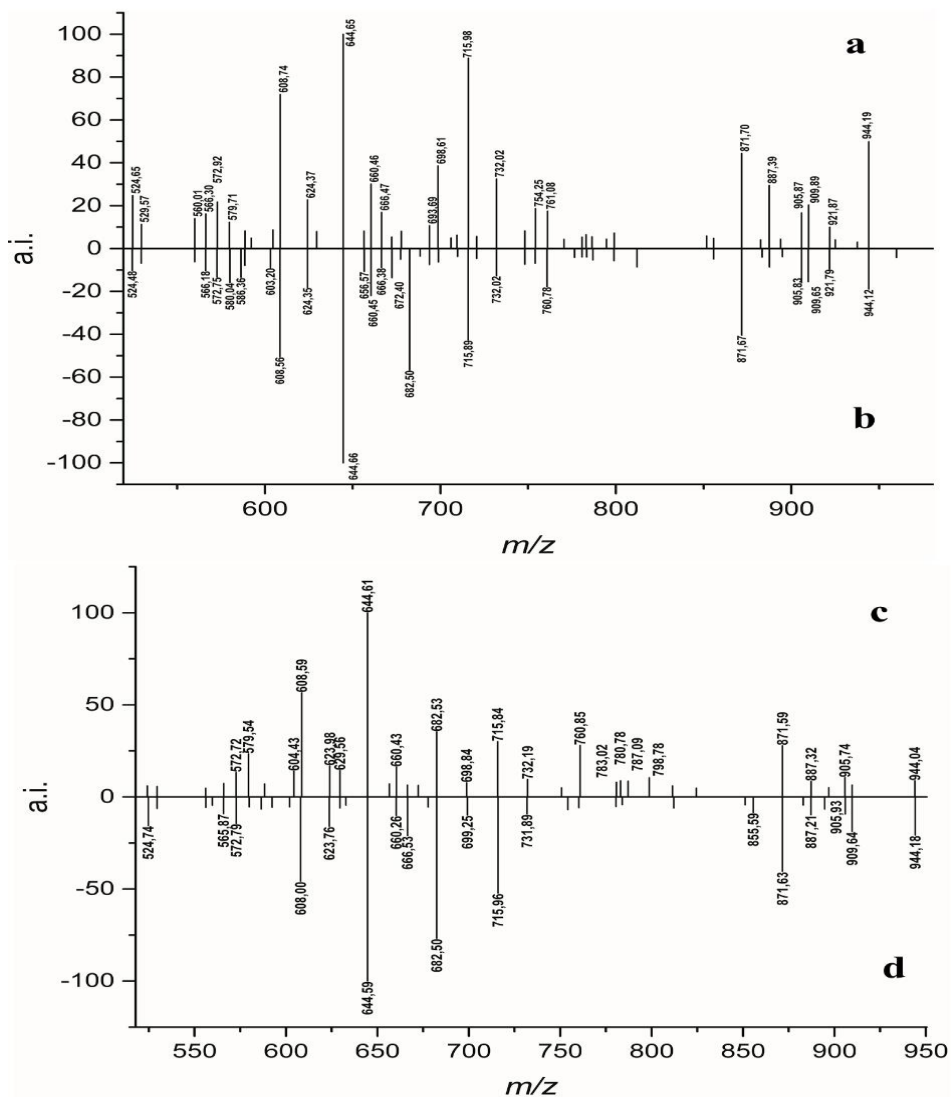


Figure 1 MALDI-TOF mass spectra of the lipid fractions in the paint dosimeters (a) Free-range egg yolk (b) White shell egg yolk (c) Brown shell egg yolk (d) Egg yolk-based paint dosimeter.

The next stage was to analyze the mass spectra in greater depth to find out more about the particular composition of the paint dosimeters. Peak assignment in mass spectrometry is a difficult task. As indicated above, in this research initial lipid assignment was performed using the most frequently used international lipidomic data base [35]. This was followed by a specific and meaningful analysis of the results. Lipid assignment of the m/z signals started from a survey analysis of the most important classes of lipids in egg yolk. Table 4 supplementary Appendix I material shows the lipid classes that previous researchers considered most likely to be present in the egg yolk [29]. We also specifically looked for the most common fatty acids in egg yolk: 14:0 myristic acid, 16:0 palmitic acid, 16:1 palmitoleic acid, 18:0 stearic acid, 18:1 oleic acid, 18:2 linoleic acid, 18:3 linolenic acid, 20:4 arachidonic acid, behenic acid 22:0 (only sphingomyelin) and 22:6 docosahexaenoic acid (DHA), all of them in positive ionization mode [22,29,30,36,37]. We will now discuss the particular results of the application of this procedure for accepting the lipid assignment in all the paint dosimeters.

Each paint dosimeter has a unique fingerprint, which is different from the fingerprint of the egg yolk (Fig. 5 supplementary material Appendix I). We suggest that the differences in the spectral profiles for each paint dosimeter are due to the interaction between the binder and the particular pigment in the paint dosimeter since, as indicated above, the binder itself is not a discriminate parameter. Although the fingerprint for each blank paint dosimeters is unique and depends on the pigment composition, the inspection of the entire mass spectra revealed the grouping of the m/z signals into three main areas. Radicals from lipids and lysophospholipids were detected from 524 m/z to 700 m/z ; intact phospholipids and sphingomyelins from 700 m/z to 850 m/z ; and intact triglycerides from 850 to 1000 m/z . Consequently, we suggest the most characteristic lipids that we found in these mass ranges.

The results obtained for the paint dosimeters after applying the criteria for lipid signal assignment in the 524-700 m/z interval are shown in Table 1 supplementary material Appendix I. Previous authors [22] identified radicals from phospholipids and triglycerides

in this zone. We suggest here for the first time that these m/z signals are the results of transesterification reactions or alcoholysis [38-40] with methanol, because the latter was used in the extraction process (see Fig. 1 supplementary material Appendix I). As shown in supplementary material Figure 3 Appendix I, the transformation of triglyceride (TG) into diglyceride occurs due to breakage of the ester bond and subsequent protonation. In addition, we propose that the differences we observed between the lipid mass spectra profiles for the blank paint dosimeters are due to the particular pigments in the dosimeter that may act as catalysts, favoring (or not) the transesterification reactions, therefore acting throughout this reaction. This behavior was not observed in the mass spectra from the blank paint dosimeter prepared using only the binder, i.e. egg yolk, in which mass spectra profiles were analogous and unaffected by this reaction.

The outcomes of the lipidomic approach (Tables 1, 2 and 3 supplementary material Appendix I) were further investigated to justify the proposed identification of each lipid selecting one target for each lipid class. The signal at 524.73 m/z was assigned to LPC 18:0/0:0 as indicated in the bibliography [36], which is known to come from PC. The signal at 556.12 m/z was assigned to LPC 18:3(6Z,9Z,12Z)/0:0 K^+ and the signal at 566.46 m/z to LPC 20:4 (5Z,8Z,11Z,14Z)/0:0 Na^+ , both of which are LPC with different fatty acids forming potassium and sodium adducts respectively. These LPC were detected in all the blank paint dosimeters, including the dosimeters with only binder, as can be seen in Table 1 supplementary material Appendix I.

The application of the lipidomic approach also identified several ceramides even though they are not present in egg yolk, nor have they been previously identified or proposed in samples from historic paintings. We propose that the ceramides (Cer) could come from sphingomyelin (SM) [41] by a rupture of the ether linkage between the phosphate and the group head during the extraction step through the transesterification reactions with methanol. For example, signals at 586.57 m/z and 598.51 m/z can be attributed to Na^+ and K^+ of Cer d18:1/18:1(9Z), respectively. Other lipid compounds identified, but again not typically found in egg, are diglycerides (DG). These lipids come from triglycerides by the

rupture of the ester linkage in one of the three fatty acids promoted by the aforementioned transesterification reaction (see supplementary material Figure 3 Appendix I). As triglycerides are the most abundant lipids in egg yolk (see supplementary material Table 4 Appendix I), DG are the most abundant signals in this first interval, i.e. 524 m/z to 698 m/z (see Table 1 supplementary material Appendix I), in all the blank paint dosimeters, both with and without pigment. Also in this zone, i.e. 524-698 m/z , we suggest that radicals from phospholipids (usually detected at around 700-837 m/z) are detected as results of the loss of the group head caused by the transesterification reaction followed by protonation. If we accept this procedure, the following signals can be explained: 644.59 m/z PA 16:1(9Z)/16:1(9Z) or PA 14:0/18:2(9Z,12Z) and 693.85 m/z PA 14:0/22:6(4Z,7Z,10Z,13Z,16Z,19Z) or PA 18:3(9Z,12Z,15Z)/18:3(9Z,12Z,15Z). These compounds appear with great intensity in all the spectra.

In addition to ceramides, we also propose the identification of another class of lipids that have never been described in cultural heritage samples, namely plasmalogens [29,42]. These were detected in the 524-698 m/z zone at low intensity values (see Table 1 supplementary material Appendix I). We propose the presence of two types of plasmalogens: the 'O' prefix, which is used to indicate the presence of an alkyl ether substituent, and the 'P' prefix, which is used for the 1Z-alkenyl ether. For example at 687.45 m/z PA P-18:0/18:1(9Z) and PA O-18:0/18:2(9Z, 12Z) are the results of the loss of the corresponding group head of the plasmalogens, similarly as explain above but for the loss of the phospholipids group head (see supplementary material Figure 4 Appendix I). Intact phospholipids were also detected in the size window between 700-837 m/z . (see Table 2 supplementary material Appendix I). The first type of this class of lipids identified in the blank paint dosimeters were sphingomyelins at 700.11 m/z , i.e. SM (d18: 2/16: 0), and at 702.90 m/z SM d18: 1/16:0. An ion at 740.03 m/z matched the potassium adduct SM d16: 1/18:0. In this m/z interval, PC and PE were also detected in the blank paint dosimeters, such as mass at 754.37 m/z PC 18:3(6Z,9Z,12Z)/16:1(9Z) and 760.17 m/z PE 18:3(9Z,12Z,15Z)/18:2(9Z,12Z) or PE 16:1(9Z)/20:4(5Z,8Z,11Z,14Z) Na⁺. As expected, TGs were detected in the higher mass interval, between 837-1000 m/z (see Table 3

supplementary material Appendix I). These lipids are the most abundant in the blank samples, as they are the most abundant in the egg yolk binder. Of special interest was the signal at 871.68 m/z , which was detected with high intensity in all the blank samples; this signal is assigned to the TG 16: 1 (9Z)/18: 0/18:0 K^+ or TG 16: 0/18:1(9Z)/18:0 K^+ .

2.3.4. Outdoor aged paint dosimeters characterization

The last step in this research was the evaluation of the mass spectra lipid profile of the paint dosimeters exposed to atmospheric long-term natural ageing in an urban atmosphere. Our aim here was to find out more about the ageing process due to exposure and assess the role of the different pigments in this process. With this in mind, we began by evaluating the mass spectra for several paint dosimeters, which considered possible short-chain products and more likely oxidative β -cleavage of bonds in the lipids previously proposed for the blank dosimeters. To this end we conducted a comparative study between blank and naturally aged paint dosimeters in the three mass spectral intervals described for the blank paint dosimeters.

The lowest degree of similitude in the paint dosimeter mass spectra was in the mass interval between 524-698 m/z , which displays transesterification and alcoholysis reaction compounds that originated in the lipid extraction processes. However, there are two masses at 527.22 m/z and at 685.64 m/z which are detected in all the mass spectra, except for white lead, which will be discussed later because it is unusual. The identification of these two peaks was very complicated as they resulted from degraded products yielded by the particular lipid extraction procedure. Nevertheless, they were always detected and with a significant level of intensity in all the naturally aged paint dosimeters (less for Pb-based dosimeter). Although still unidentified, these two masses can therefore be proposed as markers of degradation.

In the mass range from 698-1000 m/z , where intact lipids were found in the blank paint dosimeters, (see Table 4), beta oxidative cleavage and fragmentation from those proposed in the blank sample were suggested for the naturally aged paint dosimeter. As shown in

Table 4, in this mass spectral range, five signal masses were detected in all the naturally aged paint dosimeters (except white lead): 719.52 m/z , 725.15 m/z , 913.78 m/z , 948.58 m/z , 954.90 m/z . We suggest that the signal at 719.52 m/z comes from the TG 14:0/16:1(9Z)/22:6 (4Z,7Z,10Z,13Z,16Z,19Z) Na⁺ (871.68 m/z in blank paint dosimeters) as a sodium adduct [M+Na⁺]. This TG was detected in all the blank paint dosimeters. As shown in Figure 2a, there is short-chain and subsequent oxidation at the carbon 11 in the docosahexaenoic acid, obtaining the corresponding aldehyde, due to instability of the aldehyde and its tendency to continue to oxidize. It is located in its most stable form, carboxylic acid, which was found without a sodium adduct in the form [M+H⁺]. A similar breakup pattern is proposed to explain signals at 725.15 m/z and at 851.71 m/z ; in this case they could come from TG 16:0/16:0/18:3 (9Z,12Z,15Z)Na⁺ which undergoes beta oxidation and subsequent oxidation to its most stable form, as shown in Figure 2b. We suggest that the signal at 913.78 m/z comes from 921.69 m/z TG (16:1(9Z)/18:3(9Z, 12Z, 15Z)/22:6(4Z,7Z,10Z,13Z,16Z,19Z)Na⁺), in which a fatty acid loses a double bond followed by beta oxidation, with further oxidation occurring at carbon 16 of linolenic acid.

The evaluation of the lipid mass spectra in the higher values of the 850-1000 m/z showed the presence of two signals at 948.58 m/z and at 954.90 m/z in all the naturally aged paint dosimeters (Fig. 2c). We tried to interpret these two signals according to the mechanism of degradation cited above for the compounds previously identified in the blank paint dosimeters. Neither of these compounds matches these signals. It is possible however that these signals are the same as those detected in the blank paint dosimeters with the addition or subtraction of sodium. These compounds would therefore be resistant to natural ageing by exposure to the urban atmosphere. If 22 mass units are subtracted from the signal at 948.58 m/z detected in all the naturally aged paint dosimeters, the resulting value matches the signal at 926.52 m/z from the blank paint dosimeters; this last signal was assigned to TG 18:1(9Z)/18:3(9Z,12Z,15Z)/ 22:6(4Z,7Z,10Z,13Z,16Z,19Z) (see Table 4 supplementary material Appendix I). We therefore suggest that what we are witnessing is the breakup of the sodium adduct and that no alteration process occurs. Something similar occurs in the case of the signal at 954.90 m/z albeit in the opposite direction. In this case,

the signals correspond to the protonated form while in the blank paint dosimeters the sodium adduct was detected at 976.05 m/z TG 18:1(9Z)/20:4(5Z,8Z,11Z,14Z)/22:6(4Z,7Z,10Z,13Z,16Z,19Z)Na⁺.

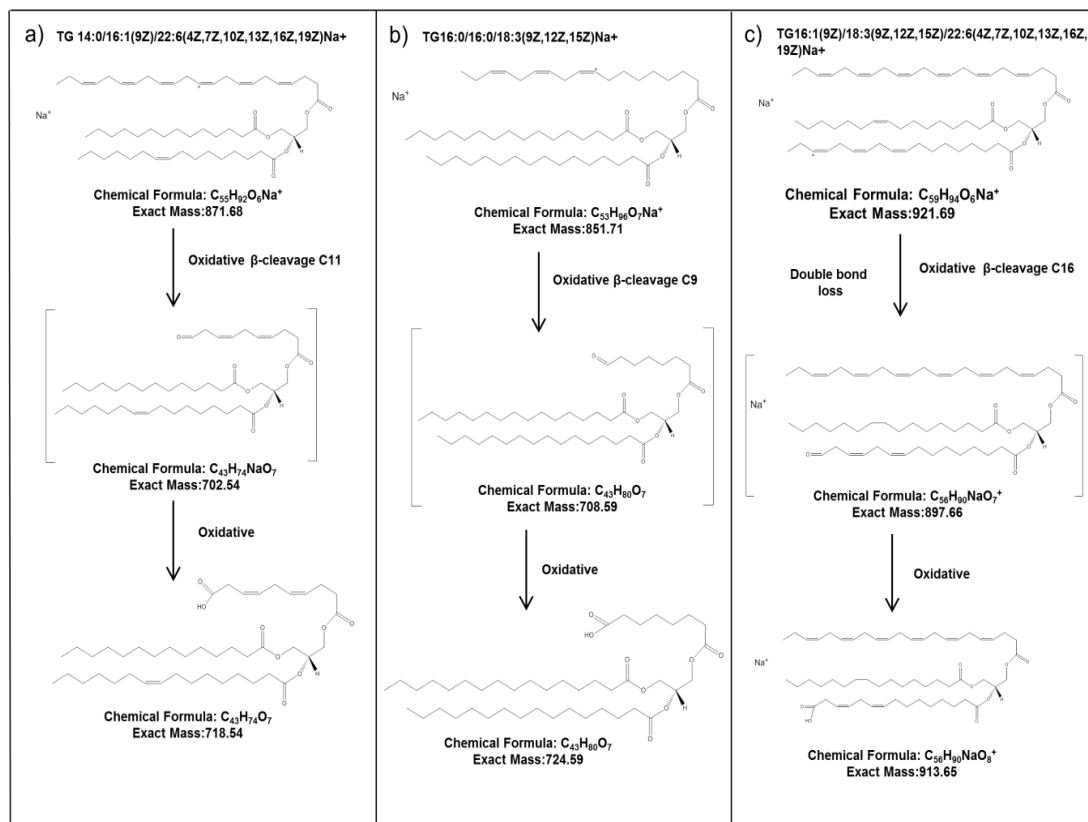


Figure 2 Proposed formation of short-chain products from triacylglycerols after oxidative β-cleavage.

In general there are significantly fewer signals (m/z) in the lipid mass spectra of the naturally aged paint dosimeters than in those for the blank paint dosimeters. This finding could be attributed to the degradation of many lipids resulting from exposure of the paint dosimeters to the polluted urban atmosphere, so demonstrating the serious damage that this can cause. In addition to the degradation patterns described above, there may be others that could not be detected due, for example, to low ionization properties.

2.3.5. White lead-based paint dosimeter as an exceptional case

White lead-based dosimeters behave differently from all the other paint dosimeters in that the number of signals (m/z) in the lipid mass spectrum increases with pollution exposure while a fall is detected in the other paint dosimeters (Figure 3). It is well known that lead is a catalyst which accelerates oxidation, and tends to form lead soaps. We suggest that this increase in the number of signals (m/z) occurs due to an increase in β -oxidative cleavage at the double bonds of the PL and TG that contain unsaturated fatty acids. We based this suggestion on our analysis of the PL or TG identified in the blank paint dosimeters, to which we applied the oxidative reactions catalyzed by lead in search of the compounds resulting from the oxidative reactions on the naturally aged paint dosimeters. For example, in Figure 4, the ion at m/z 754.38 corresponding to PC 18:3(6Z,9Z,12Z)/16:1(9Z) is one of the most abundant phospholipids, (see Table 2 supplementary material Appendix I) and is present in almost all the blank paint dosimeters we studied. When a β -cleavage oxidative reaction was performed at the C15 of the linolenic acid, an aldehyde with m/z 714.47 was obtained, which was detected only in the lipid mass spectrum of the naturally aged lead white based paint dosimeters

Likewise when the same oxidative reaction was performed at the C9 of the same linolenic acid, a signal at 634.41 m/z was observed, which continued to oxidize until it reached its more stable form, i.e. carboxylic acid, corresponding to a signal at 650.40 m/z . This signal was also detected in the naturally aged white lead paint dosimeter. None of these signals were detected in the other naturally aged paint dosimeters. Finally, in the other fatty acid of this phospholipid, palmitic acid, we propose β -cleavage oxidative at C9, obtaining the corresponding aldehyde 9, matching the observed signal at 672.42 m/z in the naturally aged white lead paint dosimeter.

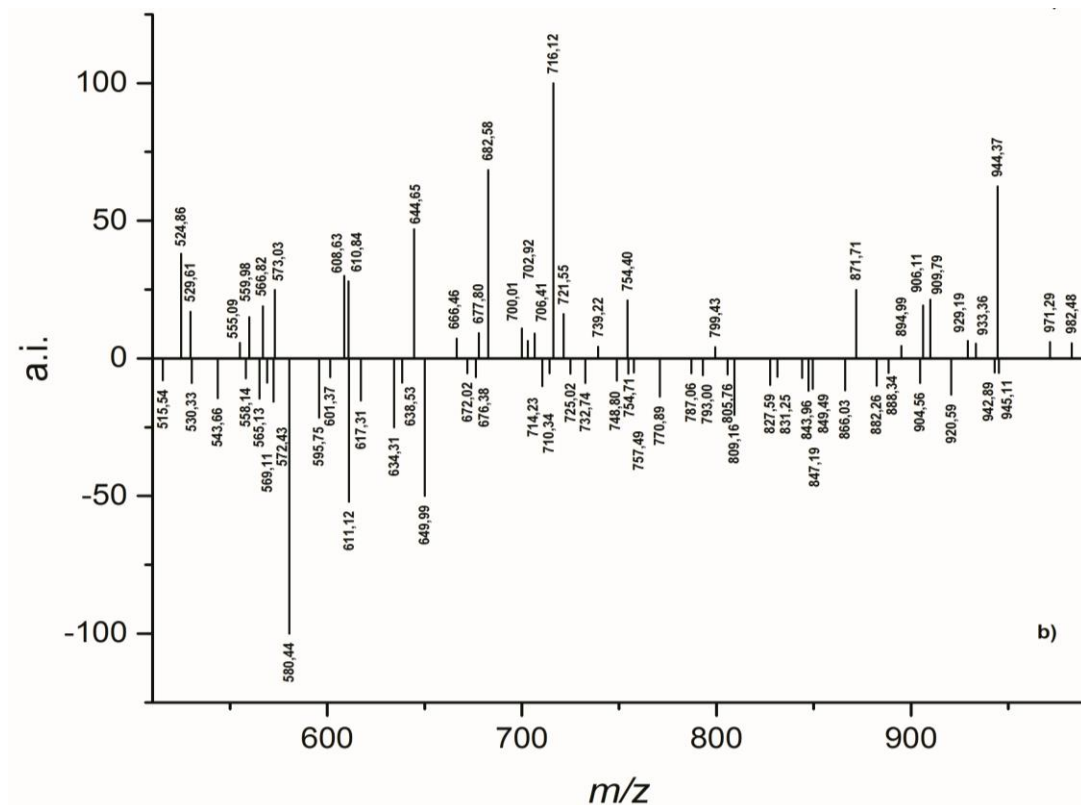


Figure 3 MALDI-TOF mass spectra of the lipid fractions in the white lead-based paint dosimeters (a) Naturally aged (b) Blank dosimeter.

According to these reactions, the increase in the number of signals in the lipid mass spectra for the naturally aged white lead-based dosimeter seems logical because from a phospholipid detected in the homologous blank paint dosimeter, up to four different signals (m/z) could be suggested (and detected) in the lipid mass spectra of the naturally aged dosimeter. It is well-known that unsaturated fatty acids oxidate from double bonds to carboxylic acid (with the aldehyde before the carboxylic compound). Thus the aldehyde proposed at this ageing stage will probably be detected as carboxylic acid due to the oxidation effect of the urban atmosphere.

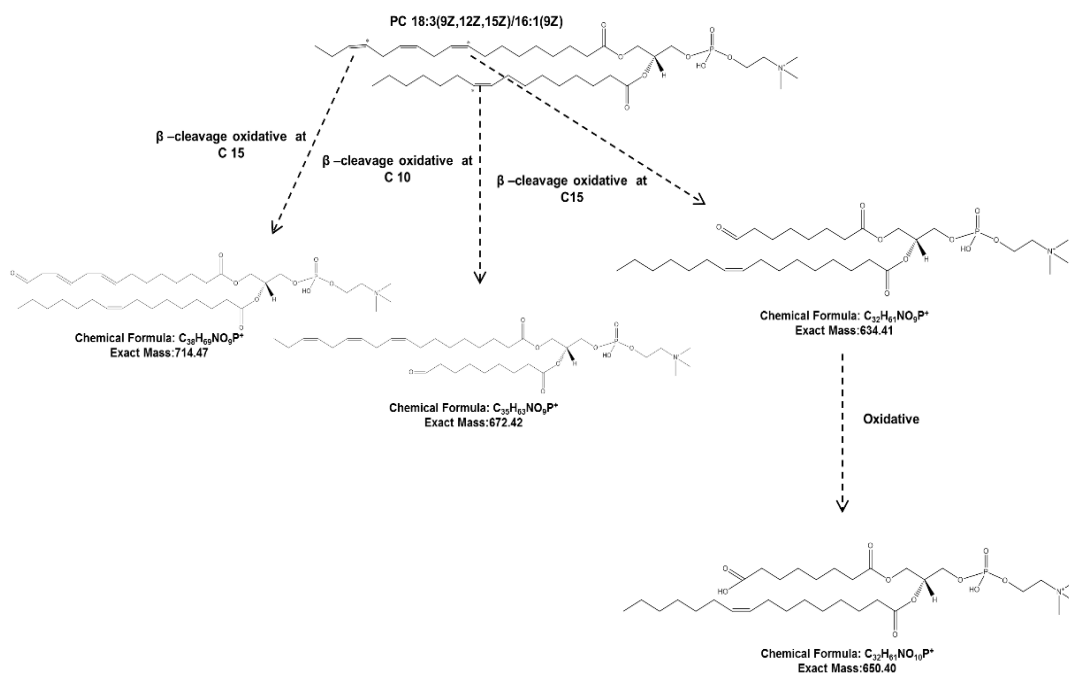


Figure 4 Proposed formation of short-chain products from PC 18:3(9Z,12Z,15Z)/16:1(9Z) after oxidative β -cleavage.

2.4. Conclusions

In this research we applied and optimized the Bligh-Dyer (BD) method, one of the most commonly used for the extraction and separation of protein and lipid material. This included a new step in which the adducts were removed. The results suggest that a transesterification process occurs due to the organic solvent (methanol) used in the extraction step. The products of this reaction are detected above all in the mass interval between 500-700 m/z . Results can therefore be erroneous if this reaction is not taken into account. We propose that the signals detected in the mass range (500-700 m/z) come from transesterification reactions between reactants, lipids and pigments. As a result, and in order to interpret the changes in the lipid fraction of the paint dosimeters, we decided to focus the study on the mass region between 700-1000 m/z , evaluating the changes caused by

urban pollution in the paint samples, and not those occurring during the extraction method.

The lipid fingerprints for the different kinds of eggs were very similar. From this, we deduced that the differences in the spectral profiles of the blank paint dosimeters are mainly due to the presence of the particular pigment that promotes a characteristic interaction between the binder and the pigment. We propose that these interactions (binder-pigment) depend on the particular pigment in each binary paint dosimeter, as they each had a unique fingerprint.

The naturally aged paint dosimeters also have a unique fingerprint, but we propose that they have similar degradation processes (β -cleavage oxidative and short-chain) because a decrease in the m/z signals is observed in a similar range. The mass spectrum for the white lead-based dosimeter by contrast showed an increased number of m/z signals. We suggest that this is due to the fact that oxidation in white lead is slower than in the other pigments studied, and that these reactions occur in almost all the double bonds of unsaturated fatty acids.

Another important conclusion is that five m/z signals, i.e. 719.52 m/z , 725.15 m/z , 913.78 m/z , 948.58 m/z and 954.90 m/z , were detected in all the paint dosimeters (except the white lead-based dosimeter). We propose these signals as markers for the presence of egg yolk as a binder in both blank and aged paint dosimeters. Finally, we propose the presence of several compounds in our egg yolk-paint dosimeters that have hitherto never been detected in paint samples from the cultural heritage field. These include plasmalogens, ceramides and sphingomyelin.

Acknowledgements

Financial support was provided by Spanish Research Projects AERIMPACT (CGL2012-30729) and EXPOAIR (P12-FQM-1889), the European Regional Development Fund (ERDF), and the Andalusian Research Groups RNM-179 and FQM-118. Analyses were performed in the Scientific Instrumentation Centre (CIC) of the University of Granada (Spain). J.A. Herrera Rubia is funded by a Spanish grant from the AERIMPACT Project (ref. BES-2013-065507). The authors thank N. Walkington for English revision.

References

- [1] M. Cotte, J. Susini, N. Metrich, A. Moscato, C. Gratziu, A. Bertagnini, et al., Blackening of Pompeian cinnabar paintings: X-ray microspectroscopy analysis, *Anal. Chem.* 78 (2006) 7484–92. doi:10.1021/ac0612224.
- [2] G.D. Smith, R.J.H. Clark, The role of H₂S in pigment blackening, *J. Cult. Herit.* 3 (2002) 101–105. doi:10.1016/S1296-2074(02)01173-1.
- [3] M. Bacci, M. Picollo, S. Porcinai, B. Radicati, Evaluation of the museum environmental risk by means of tempera-painted dosimeters, *Thermochim. Acta.* 365 (2000) 25–34. doi:10.1016/S0040-6031(00)00610-9.
- [4] B. Horemans, C. Cardell, L. Bencs, V. Kontozova-Deu6tsch, K. De Wael, R. Van Grieken, Evaluation of airborne particles at the Alhambra monument in Granada, Spain, *Microchem. J.* 99 (2011) 429–438. doi:10.1016/j.microc.2011.06.018.
- [5] S. Potgieter-Vermaak, B. Horemans, W. Anaf, C. Cardell, R. Van Grieken, Degradation potential of airborne particulate matter at the Alhambra monument: a Raman spectroscopic and electron probe X-ray microanalysis study, *J. Raman Spectrosc.* 43 (2012) 1570–1577. doi:10.1002/jrs.4052.
- [6] O.F. van den Brink, J.J. Boon, P.B. O’Connor, M.C. Duursma, R.M. Heeren, Matrix-assisted laser desorption/ionization Fourier transform mass spectrometric analysis of oxygenated triglycerides and phosphatidylcholines in egg tempera paint dosimeters used for environmental monitoring of museum display conditions., *J. Mass Spectrom.* 36 (2001) 479–92. doi:10.1002/jms.145.
- [7] M. Odlyha, N.S. Cohen, G.M. Foster, Dosimetry of paintings: Determination of the degree of chemical change in museum exposed test paintings (small tempera) by thermal analysis, *Thermochim. Acta.* 365 (2000) 35–44. doi:10.1016/S0040-6031(00)00611-0.
- [8] E. Manzano, J. Romero-Pastor, N. Navas, L.R. Rodríguez-Simón, C. Cardell, A study of the interaction between rabbit glue binder and blue copper pigment under UV radiation: A spectroscopic and PCA approach, *Vib. Spectrosc.* 53 (2010) 260–268. doi:10.1016/j.vibspec.2010.04.003.
- [9] M. Jackson, L.-P. Choo, P.H. Watson, W.C. Halliday, H.H. Mantsch, Beware of connective tissue proteins: Assignment and implications of collagen absorptions in infrared spectra of human tissues, *Biochim. Biophys. Acta - Mol. Basis Dis.* 1270 (1995) 1–6. doi:10.1016/0925-4439(94)00056-V.

- [10] K. Dif, C. Pepe, J. Peduzzi, B. Lavedrine, C. Chahine, An approach of a study of the interaction between collagen and sulphur dioxide by using ESI and MALDI-TOFMS, *J. Cult. Herit.* 3 (2002) 317–323. doi:10.1016/S1296-2074(02)01241-4.
- [11] P.R. Palaniappan, V. Vijayasundaram, Fourier transform infrared study of protein secondary structural changes in the muscle of *Labeo rohita* due to arsenic intoxication, *Food Chem. Toxicol.* 46 (2008) 3534–3539. doi:10.1016/j.fct.2008.09.001.
- [12] S. Kuckova, I.C.A. Sandu, M. Crhova, R. Hynek, I. Fogas, S. Schafer, Protein identification and localization using mass spectrometry and staining tests in cross-sections of polychrome samples, *J. Cult. Herit.* 14 (2013) 31–37. doi:10.1016/j.culher.2012.03.004.
- [13] S. Kuckova, R. Hynek, M. Kodicek, Identification of proteinaceous binders used in artworks by MALDI-TOF mass spectrometry., *Anal. Bioanal. Chem.* 388 (2007) 201–6. doi:10.1007/s00216-007-1206-2.
- [14] J. Romero-Pastor, N. Navas, S. Kuckova, A. Rodríguez-Navarro, C. Cardell, Collagen-based proteinaceous binder-pigment interaction study under UV ageing conditions by MALDI-TOF-MS and principal component analysis, *J. Mass Spectrom.* 47 (2012) 322–330. doi:10.1002/jms.2966.
- [15] M.P. Colombini, A. Carmignani, F. Modugno, F. Frezzato, A. Olchini, H. Brecoulaki, et al., Integrated analytical techniques for the study of ancient Greek polychromy, *Talanta.* 63 (2004) 839–848. doi:10.1016/j.talanta.2003.12.043.
- [16] J. Gimeno-Adelantado, R. Mateo-Castro, M. Doménech-Carbó, F. Bosch-Reig, a. Doménech-Carbó, M. Casas-Catalán, et al., Identification of lipid binders in paintings by gas chromatography, *J. Chromatogr. A.* 922 (2001) 385–390. doi:10.1016/S0021-9673(01)00914-1.
- [17] M.T. Doménech-Carbó, S. Kuckova, J. de la Cruz-Cañizares, L. Osete-Cortina, Study of the influencing effect of pigments on the photoageing of terpenoid resins used as pictorial media, *J. Chromatogr. A.* 1121 (2006) 248–258. doi:10.1016/j.chroma.2006.04.005.
- [18] A. Nevin, I. Osticioli, D. Anglos, A. Burnstock, S. Cather, E. Castellucci, Raman Spectra of Proteinaceous Materials Used in Paintings : A Multivariate Analytical Approach for Classification and Identification Raman Spectra of Proteinaceous Materials Used in Paintings : A Multivariate Analytical Approach for Classification and Id, *Anal. Chem.* 79 (2007) 6143–6151. doi:10.1021/ac070373j.

- [19] E. Manzano, N. Navas, R. Checa-Moreno, L.R. Rodríguez-Simón, L. Capitan-Valley, Preliminary study of UV ageing process of proteinaceous paint binder by FT-IR and principal component analysis, *Talanta*. 77 (2009) 1724–1731. doi:10.1016/j.talanta.2008.10.014.
- [20] A. Nevin, D. Comelli, G. Valentini, R. Cubeddu, Total synchronous fluorescence spectroscopy combined with multivariate analysis: Method for the classification of selected resins, oils, and protein-based media used in paintings, *Anal. Chem.* 81 (2009) 1784–1791. doi:10.1021/ac8019152.
- [21] M.P. Colombini, F. Modugno, E. Menicagli, R. Fuoco, A. Giacomelli, GC-MS characterization of proteinaceous and lipid binders in UV aged polychrome artifacts, *Microchem. J.* 67 (2000) 291–300. doi:10.1016/S0026-265X(00)00075-8.
- [22] I.D. Van Der Werf, C.D. Calvano, F. Palmisano, L. Sabbatini, A simple protocol for Matrix Assisted Laser Desorption Ionization- time of flight-mass spectrometry (MALDI-TOF-MS) analysis of lipids and proteins in single microsamples of paintings, *Anal. Chim. Acta.* 718 (2012) 1–10. doi:10.1016/j.aca.2011.12.056.
- [23] B. Fuchs, J. Schiller, R. Süß, M. Schürenberg, D. Suckau, A direct and simple method of coupling matrix-assisted laser desorption and ionization time-of-flight mass spectrometry (MALDI-TOF MS) to thin-layer chromatography (TLC) for the analysis of phospholipids from egg yolk., *Anal. Bioanal. Chem.* 389 (2007) 827–34. doi:10.1007/s00216-007-1488-4.
- [24] J.S. Cottrell, Protein identification using MS/MS data, *J. Proteomics.* 74 (2011) 1842–1851. doi:10.1016/j.jprot.2011.05.014.
- [25] B. Fuchs, R. Süß, J. Schiller, An update of MALDI-TOF mass spectrometry in lipid research., *Prog. Lipid Res.* 49 (2010) 450–75. doi:10.1016/j.plipres.2010.07.001.
- [26] S. Kuckova, I. Nemeč, R. Hynek, J. Hradilova, T. Grygar, Analysis of organic colouring and binding components in colour layer of art works., *Anal. Bioanal. Chem.* 382 (2005) 275–82. doi:10.1007/s00216-005-3108-5.
- [27] M.C. Krizkova, S.H. Kuckova, J. Santrucek, R. Hynek, Peptide mass mapping as an effective tool for historical mortar analysis, *Constr. Build. Mater.* 50 (2014) 219–225. doi:10.1016/j.conbuildmat.2013.09.059.
- [28] E. Manzano, L.R. Rodriguez-Simón, N. Navas, R. Checa-Moreno, M. Romero-Gámez, L.F. Capitan-Vallvey, Study of the GC-MS determination of the palmitic-stearic acid ratio for the characterisation of drying oil in painting: La Encarnación by Alonso Cano as a case study, *Talanta*. 84 (2011) 1148–1154. doi:10.1016/j.talanta.2011.03.012.

- [29] M.D. Ruiz, Huevos y ovoproductos, in: A. Gil (Eds.), *Composición y calidad nutritiva de los alimentos*, Médica Panamericana, Madrid, 2010: pp. 232–234
- [30] K. Teuber, J. Schiller, B. Fuchs, M. Karas, T.W. Jaskolla, Significant sensitivity improvements by matrix optimization: a MALDI-TOF mass spectrometric study of lipids from hen egg yolk., *Chem. Phys. Lipids.* 163 (2010) 552–60. doi:10.1016/j.chemphyslip.2010.04.005.
- [31] F. Pacheco, *El arte de la pintura*, Cátedra, Madrid, 1990.
- [32] L. Masschelein-Kleiner, *Ancient binding varnishes adhesives*, second ed., ICCROM, Rome, 1995.
- [33] R. Mayer, *The Artist's Handbook of Materials and Techniques*, fifth ed., Viking, New York, 1991.
- [34] I.P. Smirnov, X. Zhu, T. Taylor, Y. Huang, P. Ross, I. a Papayanopoulos, et al., Suppression of alpha-cyano-4-hydroxycinnamic acid matrix clusters and reduction of chemical noise in MALDI-TOF mass spectrometry., *Anal. Chem.* 76 (2004) 2958–65. doi:10.1021/ac035331j.
- [35] M. Strohm, D. Kavan, P. Novák, M. Volný, V. Havlíček, MMass 3: A cross-platform software environment for precise analysis of mass spectrometric data, *Anal. Chem.* 82 (2010) 4648–4651. doi:10.1021/ac100818g.
- [36] C.D. Calvano, I.D. van der Werf, F. Palmisano, L. Sabbatini, Fingerprinting of egg and oil binders in painted artworks by matrix-assisted laser desorption ionization time-of-flight mass spectrometry analysis of lipid oxidation by-products., *Anal. Bioanal. Chem.* 400 (2011) 2229–40. doi:10.1007/s00216-011-4919-1.
- [37] O.F. van den Brink, G.B. Eijkel, J.J. Boon, Dosimetry of paintings: determination of the degree of chemical change in museum-exposed test paintings by mass spectrometry, *Thermochim. Acta.* 365 (2000) 1–23. doi:10.1016/S0040-6031(00)00609-2.
- [38] Z. Helwani, M.R. Othman, N. Aziz, J. Kim, W.J.N. Fernando, Solid heterogeneous catalysts for transesterification of triglycerides with methanol: A review, *Appl. Catal. A Gen.* 363 (2009) 1–10. doi:10.1016/j.apcata.2009.05.021.
- [39] X. Zhang, S. Yan, R.D. Tyagi, P. Drogui, R.Y. Surampalli, Ultrasonication aided biodiesel production from one-step and two-step transesterification of sludge derived lipid, *Energy.* 94 (2016) 401–408. doi:10.1016/j.energy.2015.11.016.

- [40] E. Martinez-Guerra, V.G. Gude, Alcohol effect on microwave-ultrasound enhanced transesterification reaction, *Chem. Eng. Process. Process Intensif.* 101 (2016) 1–7. doi:10.1016/j.cep.2015.12.003.
- [41] J.B. Massey, Interaction of ceramides with phosphatidylcholine, sphingomyelin and sphingomyelin/cholesterol bilayers, *Biochim. Biophys. Acta - Biomembr.* 1510 (2001) 167–184. doi:10.1016/S0005-2736(00)00344-8.
- [42] R. Maeba, M. Nishimukai, S. Sakasegawa, D. Sugimori, H. Hara, Chapter Two – Plasma/Serum Plasmalogens: Methods of Analysis and Clinical Significance, in: *Adv. Clin. Chem.*, 2015: pp. 31–94. doi:10.1016/bs.acc.2015.03.005.

Capítulo 3

Principal Component Analysis to interpret changes in chromatic parameters on paint dosimeters exposed long-term to urban air

A. Herrera⁽¹⁾, D. Ballabio⁽²⁾, N. Navas⁽³⁾, R. Todeschini⁽²⁾, C. Cardell⁽¹⁾

(1) Dept. of Mineralogy and Petrology, Faculty of Science, University of Granada, Campus Fuentenueva s/n, 18071 Granada, Spain

(2) Dept. of Earth and Environmental Sciences, University of Milano-Bicocca, P.za dellaScienza 1, 20126 Milano, Italy.

(3) Dept. Analytical Chemistry, and Biomedical Research Institute of Granada (IBIG), University of Granada, Faculty of Science, Campus Fuentenueva s/n, E 18071 Granada, Spain.

Chemometric and Intelligent Laboratory Systems 167 (2017) 113–122

Article history:

Received 17 February 2017;

Received in revised form 7 April 2017;

Accepted 6 May 2017

Available online 19 May 2017

0169-7439/© 2017 Elsevier B.V. All rights reserve

Hipótesis de partida

En las últimas décadas la política de conservación de los objetos que componen el patrimonio cultural se ha centrado principalmente en estrategias de conservación preventiva, y en actuaciones para reducir la necesidad de realizar intervenciones más costosas y complejas. Uno de los efectos más evidentes del impacto de agentes agresivos en las obras de arte es su cambio de color. Por ello comúnmente se realizan medidas cromáticas en tales obras para evaluar el daño estético que produce el tiempo. Son numerosas las policromías de obras de arte y pinturas de monumentos (semi)-abiertos que están expuestas a la intemperie en zonas urbanas, donde la contaminación atmosférica puede ser importante. Aun así, actualmente son escasos los estudios que abordan el impacto de atmósferas contaminadas en el deterioro de este patrimonio pictórico. Igualmente son pocos los trabajos que analizan la degradación de dosímetros pictóricos expuestos durante tiempo prolongado en zonas urbanas. Estos trabajos permitirían monitorear los cambios cromáticos acaecidos como consecuencia de, por ejemplo, transformaciones mineralógicas, oxidación de aglutinantes, o depósito de partículas atmosféricas.

En el campo del patrimonio cultural, los análisis estadísticos multivariantes, tales como el Análisis de Componentes Principales (PCA), se han aplicado con profusión en las últimas décadas a datos espectrales obtenidos con diversas técnicas analíticas, puesto que tales análisis permiten manejar miles de datos, y extrapolar los más significativos. No obstante la bibliografía es escasa en relación a trabajos que combinen técnicas quimiométricas con datos de reflectancia obtenidos con espectrofotometría en la región del espectro visible (400-700 nm). La hipótesis de partida es que determinando la variación cromática de dosímetros pictóricos expuestos a la intemperie en diferentes escenarios de aire urbano, se podrían predecir modelos evolutivos del color, debido a la influencia de las diversas

condiciones de exposición a la intemperie. Tal información será relevante en la toma de decisiones de conservación preventiva de pinturas expuestas al exterior.

Objetivos de la investigación

Aplicar una metodología multivariante novedosa basada en la aplicación de PCA a datos discretos de parámetros cromáticos de los sistemas de color CIEL*a*b* and CIEL*C*h* (L^* , a^* , b^* , h^* , C^* and ΔE). El objetivo es evaluar los parámetros cromáticos específicos que causan el cambio de color en los diferentes dosímetros pictóricos expuestos, durante tiempo prolongado, a la intemperie en la ciudad de Granada. Se tendrán en cuenta la influencia del aglutinante (yema de huevo o cola de conejo), la naturaleza del pigmento, y por primera vez en este tipo de estudios el tamaño de grano del pigmento. Se pretende demostrar que este enfoque es capaz de discriminar, de forma más efectiva y precisa, las pinturas modelo en función de su composición. Ello permitirá interpretar los procesos de envejecimiento en las muestras pictóricas, y su tendencia evolutiva en distintos escenarios de contaminación atmosférica en la ciudad de Granada. Este tipo de aproximación metodológica podrá aplicarse a datos espectrofotométrico obtenidos en otras obras de arte expuestas en otros escenarios atmosféricos urbanos.

Abstract

Atmospheric pollutants can originate the decay of historic paintings exposed to the outdoor elements. This is a cause of great concern, since such contaminants can produce physical-chemical alterations manifested initially in undesirable color change. This paper tests an unsupervised multivariate approach on discrete data color parameters in a pioneering study which combines spectrophotometric data and principal components analysis to detect unaesthetic color change on paint dosimeters in (semi)open-air monuments exposed long-term to the urban atmosphere of the city of Granada (South Spain). To this end the chromatic parameter of the CIEL*a*b* and CIEL*C*h* systems (L^* , a^* , b^* , h^* , C^* and ΔE) were used as variables for subsequent multivariate analysis in order to determine the intrinsic color change trends. The aim is to evaluate the specific chromatic parameter(s) that cause the unaesthetic damage for each type of paint dosimeter, while also considering the influence of the binder (egg yolk/rabbit glue), the pigment (azurite, malachite and lapis lazuli) and for the first time, the grain size of the studied pigments (azurite). Results demonstrated that this approach is capable of discriminating samples on the basis of dosimeter composition, so enabling interpretation of their aging process. Azurite and lapis lazuli-laden dosimeters tended to turn green over time as a result of exposure to city air regardless of binder composition and location. By contrast, all malachite-laden dosimeters became bluer over time. Luminosity remained stronger in dosimeters prepared with collagen, an important parameter in binder discrimination. This information is also of great value for restoration purposes.

3.1. Introduction

Over the last two decades cultural heritage conservation (e.g. historic buildings, wall paintings, sculptures, mosaics, archaeological sites, etc.) has focused on preventive conservation policies and procedures to reduce the need for more complex and costly restoration work [1]. To accomplish this, a range of conservation activities have been carried out inside buildings such as museums, churches and art galleries, and even in caves and catacombs, to prevent damage to artworks. This work normally includes assessment of the environmental conditions, typically temperature (T), relative humidity (RH), light and UV levels, as well as the effects of pollutants, microorganisms and visitors [2–4], and their impact on the artworks [5–7]. Given that a large amount of indoor artworks are paintings or have polychrome decoration, model samples (paint dosimeters or mock-ups) made with artists' materials (pigments and binders) that replicate the composition of the paint used by the original artists have been used to evaluate the damage they suffer, due to the effects of different indoor environments [8–10]. Since color change is the most evident effect of the impact of these environmental parameters on paint, chromatic measurements are commonly performed to assess the degree of aesthetic damage over time [11–13].

Although most works of art are stored indoors in museums and galleries, some important paintings, for example on the façades of historical buildings, are directly exposed to the outdoor city air. The atmospheric pollutants it contains can cause physical-chemical alterations in the paint that are manifested in undesirable color change. Nonetheless few studies have addressed the impact of polluted atmospheres on artworks of this kind [6,14–17]. Similarly, very little research has been done on paint dosimeters exposed long-term to urban polluted air, so as to monitor color changes that manifest underlying changes in the mineralogical composition of the pigments, binder oxidation and the precipitation of new crystalline phases or dust deposition [17–19].

In the last decades, in the field of Cultural Heritage, statistical multivariate analyses such as Principal Component Analysis (PCA) have been applied to spectral data produced by diverse analytical techniques conducted on samples from real artworks or from reproductions made in the laboratory, such as e.g. Raman micro-spectroscopy (RMS), Fourier transform infrared spectroscopy (FTIR), Gas chromatography–mass spectrometry (GC-MS), Matrix-Assisted Laser Desorption Ionization Time of Flight Mass Spectrometry (MALDI-TOF-MS), Fiber optics reflectance spectroscopy (FORS). These multivariate analyses can handle large data bases and extrapolate the most meaningful information from the data. PCA has proved to be a useful tool for fast data representation and interpretation [13,20], identification of pigments and binders [21–24], assessing their state of conservation and distinguishing between natural and synthetic pigments [25]. However papers combining chemometric techniques with reflectance spectra obtained from spectrophotometers in the visible region (400-700 nm) are still rare in any field of science [26,27]. To the authors' knowledge this is the first paper to use PCA to analyze color changes in paint dosimeters exposed to the outdoor elements.

This paper presents a pioneering study which combines spectrophotometric data (in situ portable spectrophotometer) and PCA to detect undesirable color changes on paint dosimeters exposed long-term to the urban atmosphere in the city of Granada (South Spain). To this end the chromatic parameters of the CIEL*a*b* and CIEL*C*h* systems (L^* , a^* , b^* , h^* , C^* and ΔE) were used as variables for subsequent multivariate analysis. The aim is to identify the specific chromatic parameter(s) that cause the unaesthetic damage for each type of paint dosimeter, while also considering the influence of the binder (egg yolk/rabbit glue) and, for the first time, the grain size of the studied pigments (azurite, malachite and lapis lazuli).

The final goal is to provide useful information that can be used to draw up preventive conservation strategies to safeguard these artworks. This problem is worse in hot cities with heavy traffic near the Mediterranean coast, such as Granada [4,5,30,31], famous for the Alhambra Palace, which contains a number of (semi)outdoor paintings. Granada's old

quarter also has historical buildings with outdoor wall paintings, as does its Albayzín district, a UNESCO world heritage site.

3.2. Materials and methods

3.2.1. *Painting materials*

We selected two proteinaceous binders and three historical pigments to prepare the paint dosimeters. They were chosen after being identified in paint used in diverse artworks in (semi)open-air monuments in the city of Granada [30,31]. The painting materials were purchased from Kremer Pigments GmbH & Co. KG (Madrid, Spain). The natural pigments were malachite ($\text{Cu}_2\text{CO}_3(\text{OH})_2$), lapis lazuli ($\text{Na}_{8-10}\text{Al}_6\text{Si}_6\text{O}_{24}\text{S}_{2-4}$) and azurite ($\text{Cu}_3(\text{CO}_3)_2(\text{OH})_2$), whose references and grain sizes (according to the manufacturer) are: malachite natural standard with $\phi < 120 \mu\text{m}$ (ref: K10300), lapis lazuli $\phi < 80 \mu\text{m}$ (ref: K10540), and azurite with five different grain sizes which include various “azurite MP” and the “azurite natural standard”; these are: azurite MP extra deep (ref: K10203, $\phi = 80\text{-}100 \mu\text{m}$), azurite MP deep (ref: K10204, $\phi = 80\text{-}63 \mu\text{m}$), azurite MP pale (ref: K10206, $\phi = 63\text{-}38 \mu\text{m}$), azurite MP sky-blue (ref: K10207, $\phi = < 38 \mu\text{m}$), and azurite natural standard deep greenish blue (ref: 10200, $\phi = < 120 \mu\text{m}$). MP refers to Michel Price, who in 1997 established a method for the separation of powdered azurite into different grades, representing different hues of blue [32]. This method was adopted by Kremer Pigments GmbH & Co. KG in 1998 to prepare a new variety of azurite pigments called “azurite MP.”

The chosen proteinaceous binders were rabbit glue (fine grind pearls from Kremer Pigments GmbH & Co. KG, ref. 63028) and natural egg yolk (from eggs purchased at the local market). Both binders were widely used during the Middle Ages and the Renaissance, and have been found in outdoor paintings in the city of Granada [31]. The names for the paint dosimeters were formed by adding the letters G (for glue) and E (for egg yolk) to the pigment labels (see Table 1), so as to clearly differentiate the powder pigments from the binary (pigment/binder) paint mixtures.

Table 1. Features of the analyzed blue pigments.

Kremer pigment reference	Kremer pigment size	Grain size according to [30]	Authors pigments reference	Paint dosimeter reference (authors)
Malachite natural standard N° 10300	<120 µm	2.5 µm very extra fine	MAL-VEF	MAL-VEF-E
				MAL-VEF-G
Azurite MP extra deep N° 10203	100-80 µm	90 µm extra coarse	AZ-EC	AZ-EC-E
				AZ-EC-G
Azurite MP deep N° 10204	80-63 µm	70 µm coarse	AZ-C	AZ-C-E
				AZ-C-G
Azurite MP pale N° 10206	63-38 µm	45 µm medium	AZ-M	AZ-M-E
				AZ-M-G
Azurite MP sky-blue N° 10207	< 38 µm	25 µm extra fine	AZ-EF	AZ-EF-E
				AZ-EF-G
Azurite natural standard N° 10200	< 120 µm	< 22 µm very extra fine	AZ-VEF	AZ-VEF-E
				AZ-VEF-G
Lapis lazuli N° 10540	< 80 µm	47 µm medium	LAP-M	LAP-M-E
				LAP-M-G

Note: VEF= very extra fine; EC= extra coarse; C= coarse; M= medium; EF=extra fine; E=Egg Yolk; G= Rabbit Glue.

3.2.2. Paint dosimeters

Fourteen paint dosimeters were prepared according to old master recipes to mimic the real egg yolk-based or rabbit glue-based tempera used by medieval artists. In the tempera painting technique, pigments are finely ground and mixed with water, then solidified by blending with a proteinaceous binder. Seven paint dosimeters were composed of a pure pigment blended with the egg yolk binder, while the other seven dosimeters were blended with the rabbit glue binder [33]. The procedure to prepare the egg yolk binder can be found in Herrera et al.[17] and the rabbit glue binder in Cardell et al.[19]. To obtain the pure binder dosimeters each fluid paste was spread directly onto a glass slide.

The tempera paint dosimeters were prepared as follows: circa 0.5 g of each pigment powder was placed in a small bowl and several drops of the binder (each pigment requires different amounts) were added to form a fluid paste. Then, to prepare the binary paint dosimeter, several fine layers of the pastes were spread onto a glass slide with a paintbrush, so as to emulate the real paint layers found in ancient paintings.

3.2.3. Natural air pollution aging test

The paint dosimeters were naturally aged by exposing them to the urban atmosphere of the city of Granada (South Spain). To this end, sets of dosimeters were placed in selected (semi)open-air monuments with varying air quality (Figure 1). Some of the monuments are situated in the city center (~ 650 meter above sea level), and thus are more affected by heavy traffic; these are the Cathedral, the *Corral del Carbón*, the Hospital of *San Juan de Dios*, and the Church of *Santo Domingo*. The rest of the dosimeters were positioned in monuments on the city's two hills, the Albayzín and al-Sabika. The dosimeters in the Albayzin were placed in the *Palacio del Almirante* (~100m above the city center), while three sets of dosimeters were installed in the *Alhambra and Generalife* monumental complex (on the al-Sabika hill, ~200m above the city center), as follows: one set in the Harem (Alhambra) and two sets in the Generalife in two rooms at slightly different altitudes

(Figure 1). These dosimeters were exposed to the urban air for 18 months. In situ non-invasive color measurements were performed with a portable spectrophotometer after 1, 2, 3, 4, 6, 10 weeks, 6 months, 12 months and 18 months. During the exposure period the paint dosimeters were subjected to the effects of major construction works, heavy traffic, sunlight irradiation, rain, cold, heat and wind.



Figure 1. (a) Aerial view of the city of Granada (South Spain) showing the location of the paint dosimeters at (semi)open monuments; (b) set of paint dosimeters placed in the Harem of the Alhambra monument.

3.2.4. Color measurements

The chromatic characteristics of the paint dosimeters were studied with a Minolta CM-700d portable spectrophotometer using an 8mm measuring aperture. The standard daylight illuminant D65 (color temperature: 6504 K) was applied. Results are presented in alphanumeric color codes of the CIEL*a*b* and CIEL*C*h* systems. In the CIEL*a*b* system, L* represents luminosity, varying from black (0) to white (100); a* ranges from -a* (green) to +a* (red), and b* from -b* (blue) to +b* (yellow).

In the CIEL*C*h* color system each color is represented by means of three angular parameters or cylindrical coordinates, most closely related to the psychophysical perception of the color: L*, lightness or luminosity of color, also defined in both scalar and angular color sets; chroma or saturation ($C^* = (a^{*2} + b^{*2})^{1/2}$) related to the intensity of color and the hue angle ($h^* = \arctan(b^*/a^*)$) or tone of color, which refers to the dominant wavelength and indicates redness, yellowness, greenness or blueness on a circular scale, starting at 0° and increasing counterclockwise, i.e. 0° is "red", 90° is "yellow", 180° is "green" and 270° is "blue" [34]. CIEL*a*b* color difference (ΔE) is the Euclidean distance between two points in the color space [34]. This distance is typically expressed as ΔE , where: $\Delta E = (\Delta L^*)^2 + (\Delta a^*)^2 + (\Delta b^*)^2)^{1/2}$. Note that when ΔE has three units or more, it is considered to be a color change that can be perceived by the human eye.

3.2.5. Principal component analysis (PCA)

Data were arranged in a numerical matrix with samples on the rows and variables (L*, a*, b*, H*, C* and ΔE) on the columns. In order to detect data patterns and clusters, the data structure was analyzed using PCA, which is a well-known multivariate pattern recognition technique [35]. PCA was calculated on auto-scaled data (mean-centering and unit variance scaling) since variables had different scales and units, such that auto-scaling was needed in order to standardize them and make them comparable for the subsequent multivariate analysis [13,36]. Principal Component Analysis was performed by means of the PCA toolbox

for MATLAB [35] and SpectraMagic X (spectrophotometer) for the data obtained from color measurements.

3.3. Results and discussion

PCA is a well-known chemometric technique for unsupervised data analysis by projecting data in a reduced space, defined by orthogonal principal components, i.e. PCs [37]. With this in mind, we used all the samples analyzed in the entire study to look for similarities and differences beyond the obvious color characteristics, i.e. green for malachite-laden dosimeters and blue for lapis lazuli and azurite-laden dosimeters. To this end, PCA was performed on a data matrix comprising 1086 measured of colors (rows), each described by the 6 variables (columns) related with the intrinsic color parameters, i.e. L^* , a^* , b^* , H^* , C^* and ΔE .

In previous studies, PCA has been applied on continuous color data, i.e. using reflectance spectra [38]. In this paper, we propose an innovative way to track color changes based on the use of discrete data, i.e. the chromatic parameters L^* (luminosity), a^* (red/green), b^* (yellow/blue), H^* (tone of color), C^* (chroma or saturation) and ΔE (total color difference), which are used in the $CIE L^*a^*b^*$ and $CIE L^*C^*h^*$ systems. The information obtained by applying PCA to these color parameters enables easier visualization and interpretation of the color change trends occurring in all the dosimeters.

Table 1 supplementary material Appendix II shows the statistical parameters of the PCA performed on this entire data set. PC1 had a high explained variability value of 62 %, and similarly high values were obtained for PC2 (19 %) and PC3 (16 %). PC4 and PC5 only accounted for 1 % and 0.6% of total explained variability respectively. We therefore decided to base the interpretation of the data on the first three PCs (98 % of the variability included in the original data set).

The information encoded in these three PCs is shown in Figure 2. The loading plot of PC1 vs PC2 (Figure 2a) indicated that L^* and b^* (yellow/blue hues) have the highest positive

Principal Component Analysis to interpret changes in chromatic

weight on PC1, while the color tone (H^*) and a^* (red/green hues) have the highest negative values. The two remaining variables i.e. C^* and ΔE , have little influence on this PC1 and have higher weight on PC2. Figure 2b (loading plot of PC1 vs PC3) shows that ΔE has the highest weight on PC3, followed by L^* and C^* .

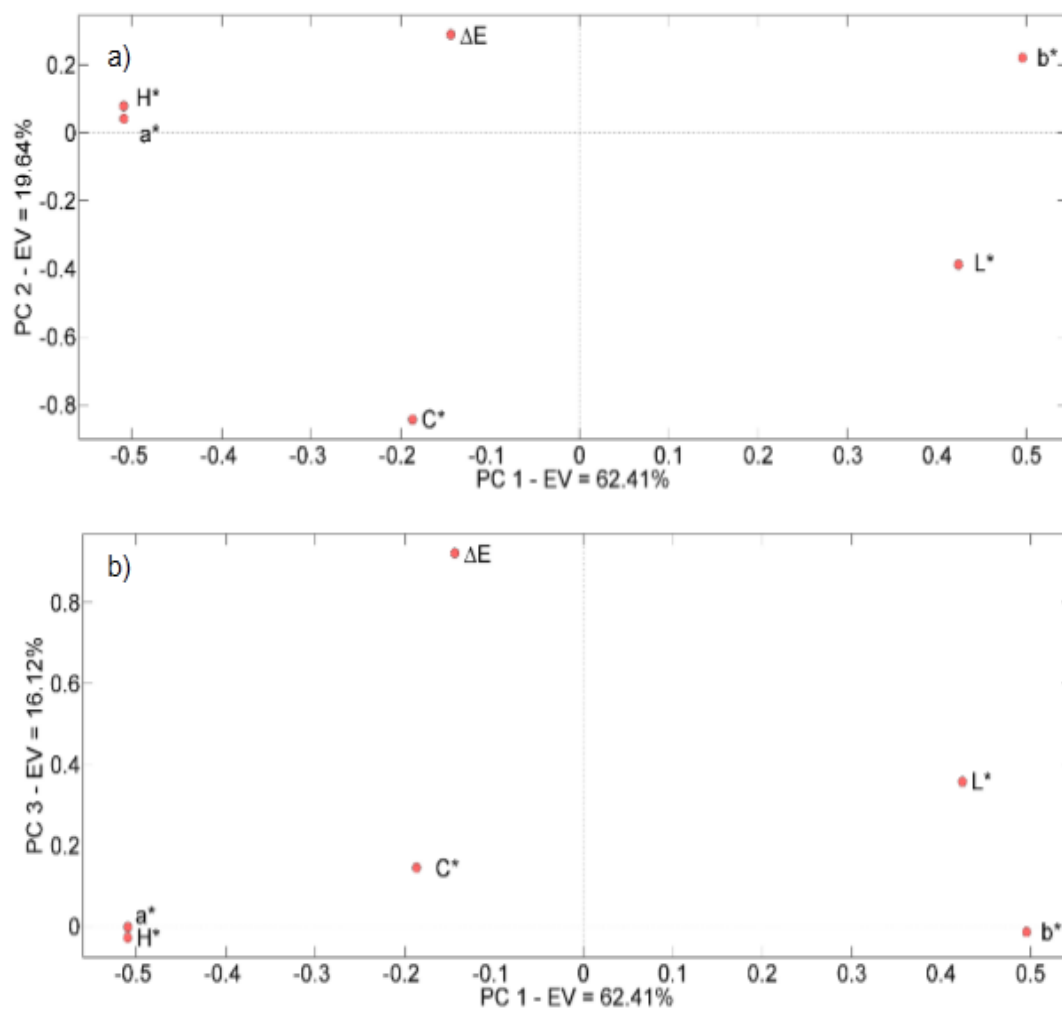


Figure 2. Loading plot of the PCA performed using all the paint dosimeters: (a) loading plot of PC1 vs PC2; (b) loading plot of PC1 vs PC3.

Figure 3a displays changes in the color parameters of all the paint dosimeters (at the various selected monuments), which shows the score of the dosimeters on the first three PCs. Each point on the score plot represents a dosimeter, which means that relationships and similarities between the dosimeters can be deduced from the clusters. For a better comprehension of the Figures, hereafter the scores have been colored differently based on the specific factors being studied in this paper, i.e. pigment composition, pigment particle size, type of binder mixed with the pigment, and exposure time to urban air. In Figure 3, sample scores were colored on the basis of the pigment composition of the paint dosimeter. Figure 3a shows that the paint dosimeters were clearly grouped together according to their respective colors using the information contained in the three first PCs, which accounted for 98 % of the explained variability. This initial inspection indicates that the color of the pigment in the dosimeter is the key factor enabling us to discriminate between the dosimeters, rather than exposure time to urban air or the type of binder used in the paint. Hence, as shown in Figure 3a, all malachite-laden dosimeters (green) were clearly clustered at the highest values on PC1 (at positive values), far away from the other samples (blue).

As Figure 3a reveals, azurite and lapis lazuli-based dosimeters were well clustered and were close to each other. In these samples a clear tendency was observed in the analysis of the PC1 and PC2 as shown in Figure 3b. The score for the lapis lazuli-laden dosimeters increased with exposure time to urban air such that after 18 months it had reach similar values to those of the azurite-laden dosimeters at the beginning of the experiment. The scores for azurite-laden dosimeters on PC1 and PC2 also increased with exposure time to air pollution.

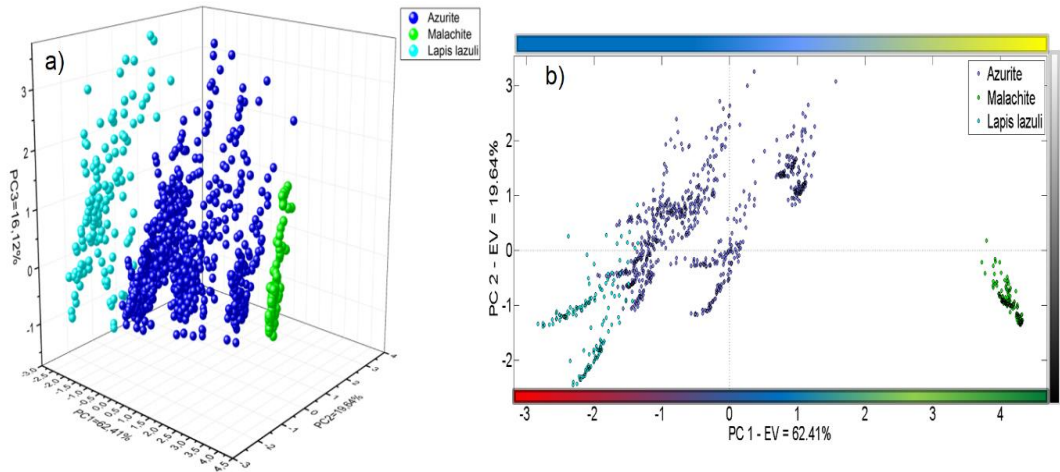


Figure 3. PCA results for all the paint dosimeters (each pigment colored differently): (a) score plot PC1 vs PC2 vs PC3; (b) score plot PC1 vs PC2.

Figure 3b also clearly shows that in the blue dosimeters (made of either lapis lazuli or azurite) there is a noticeable effect that distributes them in PC1 and PC2 in the same direction with increasing exposure time to urban air. Thus, parameters such as H^* , C^* , ΔE and the tendency to yellow hues ($+b^*$) and green hues ($-a^*$) increase with exposure to urban air. As regards discrimination among the three types of pigments, although the three PCs are related with a total discrimination based on the pigment used in the paint dosimeter, they can be partially grouped by using the score samples on PC1. This indicates that color parameters such as a^* (red/green), b^* (yellow/blue), H^* and L^* have greater weight than ΔE and C^* to discriminate these dosimeters based on the pigment composition (see Figure 2a).

We performed a more detailed analysis of the results using two-dimensional score plots of the first three PCs as shown in Figure 4a-d. In each Figure the scores were colored differently according to the particular variable that could influence color change in the paint dosimeters. These variables were: i) the type of binder - the scores were colored either blue (rabbit glue) or red (egg yolk) (Figure 4a, 4b); ii) the time exposed to urban air - the different exposure times were given different colors (Figure 4c); and iii) the pigment

grain size - the scores for the different crystal sizes of the pigments were colored differently.

As regards the type of binder, a close inspection of the clusters was carried out in order to ascertain whether the binders could produce a sufficient degree of discrimination to enable us to group the dosimeters according to exposure time to urban air. Figure 4a shows that PC1 and PC2 could discriminate the type of binder (egg yolk or rabbit glue) in certain paint dosimeters. The AZ-VEF (i.e. azurite standard according to Kremer manufacturer, see Table 1) dosimeters were clustered according to binder composition, i.e. egg yolk or rabbit glue. Indeed, those with egg yolk content had slightly lower scores on PC1 than the samples with rabbit glue binder. This means that AZ-VEF-E dosimeters tend to become more yellow and green than AZ-VEF-G dosimeters (Figure 4a). However, as shown in Figure 4b, when the scores are represented on PC1 and PC3, only malachite-laden samples are grouped according to the type of binder. Hence MAL-VEF dosimeters have the highest b^* and L^* values and a^* exhibit the most negative values as expected for the green malachite color (Figure 2b). The MAL-VEF-G dosimeters are the greenest and brightest of all the samples studied.

PCA results assessing the ageing of the samples at different times over the 18 months experimental period are shown in Figure 4c. In this case the combination of PC1 and PC3 was also checked and it proved to be even more informative than PC1 vs PC2, as it allowed us to discern a relationship with exposure over time. Results showed that at the beginning of the outdoor aging test LAP-M dosimeters scored high values on PC1 (red hues, i.e. a^* values and tone, H^*) and low values on PC3 (total color differences, ΔE) (see Figure 2b for loading interpretation). At the beginning of the aging test these dosimeters were bluer but over time tended to become greener. The malachite-laden samples by contrast had high scores at the beginning of the test for the yellow parameter ($+b^*$) and L^* , and very low green hues ($-a^*$), tone (H^*) and color differences (ΔE), which resulted in a more yellowish color and higher luminosity than the other pigments. These dosimeters, which display the lowest total color variations (ΔE), are also the least damaged. In addition, in azurite-laden

Principal Component Analysis to interpret changes in chromatic

dosimeters the a^* , b^* , H^* and L^* loading values on PC1 and PC2 are neither very positive or very negative. Instead, these dosimeters have the highest C^* and ΔE values on PC3. This means that the azurite-laden dosimeters experienced the highest changes in saturation and total color of all the paints we studied.

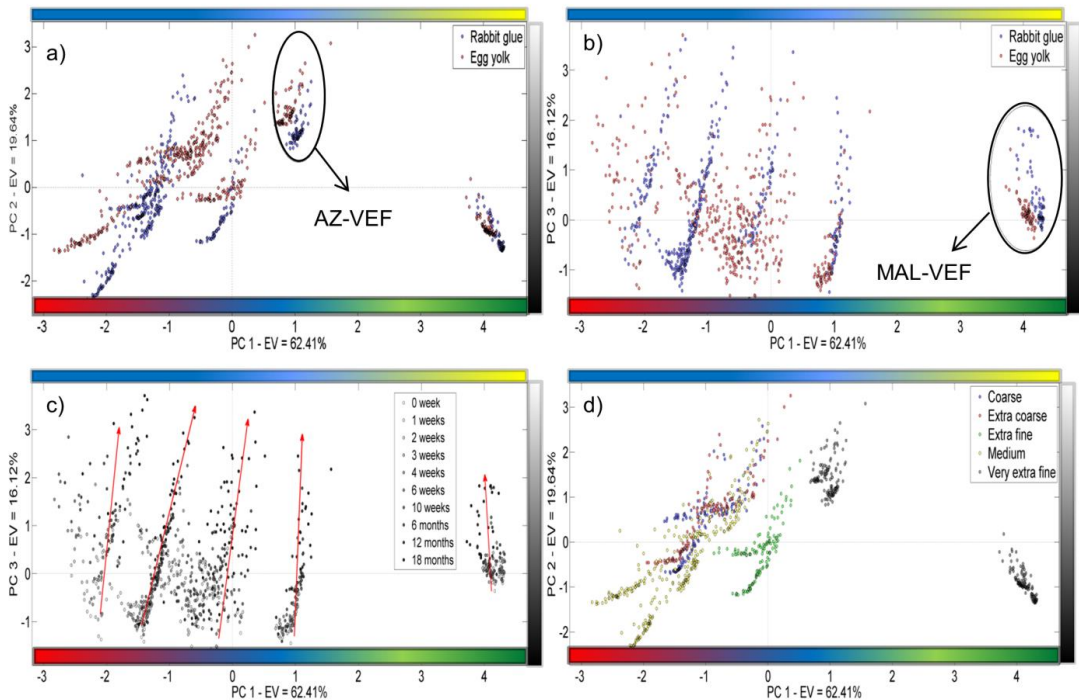


Figure 4. Score plots for all paint dosimeters: (a) samples colored by binder represented in PC1 and PC2; (b) samples colored by binder represented in PC1 and PC3; (c) samples colored by exposure time represented in PC1 and PC3; (d) samples colored by grain size represented in PC1 and PC2. AZ=azurite; MAL=malachite; VEF=very extra fine grain size.

The effect of the pigment grain size on variation of color parameters is shown in Figure 4d. Five different grain sizes were checked to evaluate whether there is any relationship between pigment particle size and the tendency to age in the urban air of Granada. If we examine the score plots in Figure 4d, it is clear that the AZ-EF and AZ-VEF samples are separated in PC1, irrespective of the binder used, as AZ-VEF samples have scores greater

than 0, while AZ-EF samples have scores lower than 0. If we look at the loading plots (see Figure 2a), the AZ-VEF dosimeters tend to be the greenest (highest $-a^*$ values) of all the azurite-laden dosimeters. AZ-VEF and AZ-EF also show the highest total color variation of all the paint samples we studied.

When the sample scores were colored according to the sites of the dosimeters in different open-air monuments in Granada (see Figure 1 supplementary material Appendix II), PCA was unable to extract any information regarding the impact of the different air quality scenarios, in that sample score distribution was not related with the location of the dosimeters. This indicates that the location of the paint dosimeters is less important in producing color changes than the type of pigment present in the paint, at least over the period of the natural ageing test, and for the pigments we studied. One exceptional, major visible color change was noticed after six months in the dosimeters AZ-EC-G, AZ-M-G and AZ-EF-G situated in the Generalife (see Figure 1, label C), the highest point in the Alhambra monument complex and surrounded by gardens. This color change turned out to be unrelated with the aging process, and was caused by a discontinuous layer of pollen on the surface of the dosimeters that was visible with the naked eye.

A similar approach was used to extract information on each set of paint dosimeters containing the same pigment, i.e. malachite, lapis lazuli and azurite based dosimeters. Results are discussed below by pigment.

3.3.1. *Malachite*

When performing PCA on malachite-laden samples, we used a data matrix defined by 158 rows (malachite-laden dosimeters) and 6 columns (color parameters as variables). PCA indicated that the first two PCs explained 90% of total data variance (Table 2 supplementary material Appendix II). Figure 5 shows the corresponding loading (Figure 5a) and score plots. In order to better search for some kind of pattern in the results, dosimeters are represented according to the binder (Figure 5b) and the exposure time (Figure 5c).

The loading plot shown in Figure 5a revealed that the color parameters were clearly separated into four groups (easier score plot interpretation). Figure 5b, which examines the influence of the binder in the dosimeters, shows that the type of binder was discriminated well enough in PC2, as most of the dosimeters containing egg yolk obtained scores greater than 0, while rabbit glue gave scores of less than 0. This is an interesting result as the MAL-VEF-E and MAL-VEF-G dosimeters cannot be distinguished with the naked eye. The loading plot (Figure 5a) showed that all chromatic parameters have a high influence in PC1 with the exception of L*, which is the most influential in PC2. Consequently, luminosity appears to be the most important factor for discriminating the type of binder.

Figure 5c shows a relationship between PC1 and exposure time, as samples are distributed according to their exposure time. In MAL-VEF-E, the tendency to yellow hues (+b*) is one of the key color parameters related to color change over time, as it presents positive loadings in both PCs, i.e. PC1 and PC2. We also noticed this in all egg yolk-based dosimeters measured at the highest exposure times. Thus, the values for MAL-VEF-E at the start of the natural aging test are characterized low b* values (blue hues), which increase in line with exposure time. This means that dosimeters containing egg yolk become yellower over time. Likewise, dosimeters containing rabbit glue binder were characterized by low b* values at the lowest measurement times. However, the chromatic parameters a* (red/green) and ΔE (total color change) appear as the decisive factors affecting color variations over time, in that the greatest changes took place in these parameters. Results show that ΔE is higher for MAL-VEF-G than for MAL-VEF-E. MAL-VEF-G also turns redder with increasing exposure times.

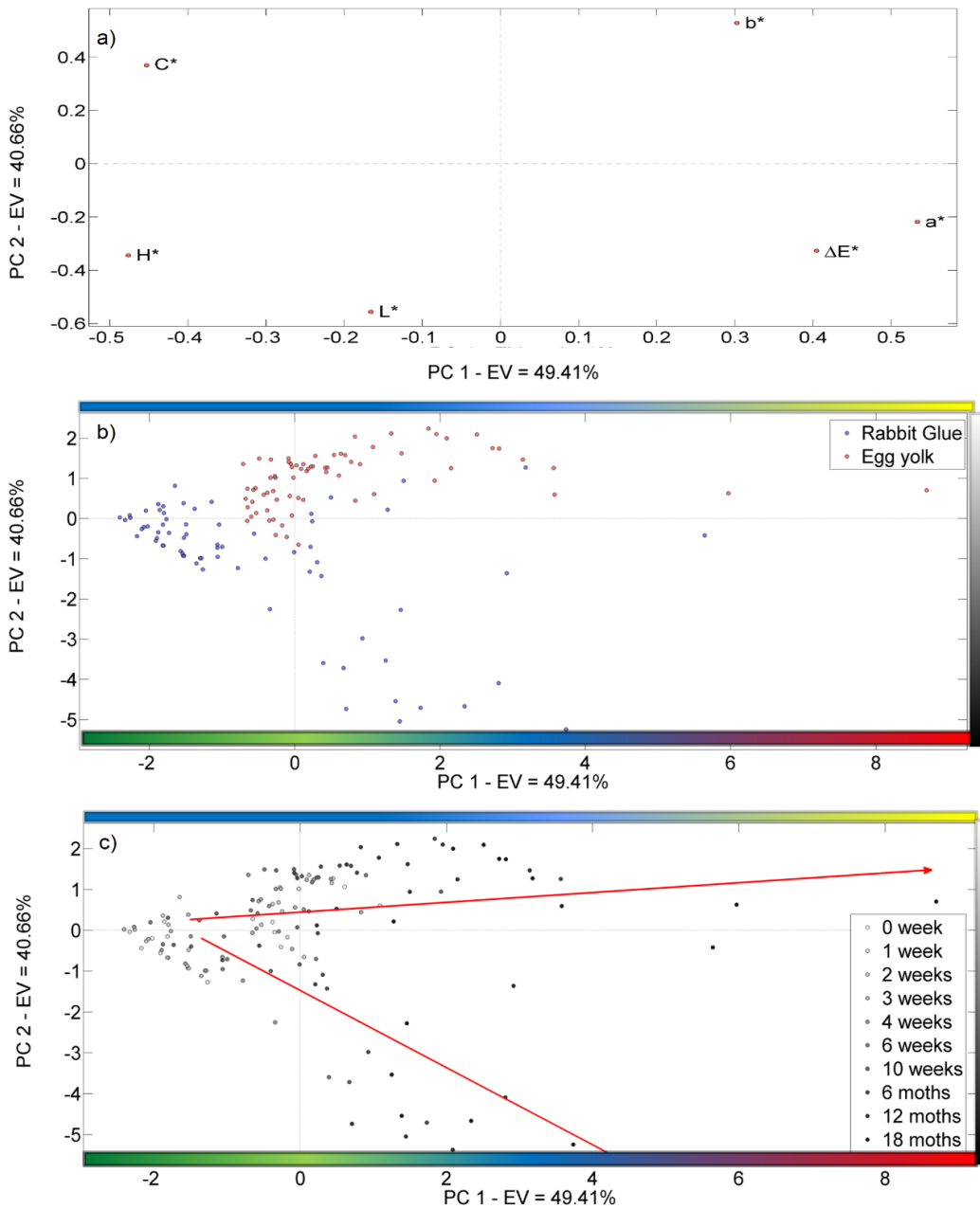


Figure 5. PCA results for malachite-laden dosimeters: (a) loading plot PC1 vs PC2; (b) score plot PC1 vs PC2 (scores colored according to the kind of binder); (c) score plot PC1 vs PC2 (scores colored according to exposure times).

3.3.2. Azurite

PCA was performed on a data matrix with 774 rows (azurite-laden samples) and 6 columns (color variables). In this multivariate analysis the first three components explained 94% of the total data variance (Table 2 supplementary material Appendix II). The loading plots are shown in Figure 6. The PC1 vs PC2 loading plot (Figure 6a) once again displays that the color parameters are grouped into four types, i.e. those defined by the x/y axes. C^* , H^* and a^* color parameters have the highest negative values on PC1, while b^* has the highest positive values. The PC1 scores could therefore be related with the tendency of the paint dosimeters to turn yellower. The two remaining variables, i.e. L^* and ΔE have little influence on this PC1, showing higher weights on PC2. Figure 6b shows the loading plot for PC1 and PC3. Although all the chromatic parameters show a certain dependence on PC3 with loading values far above or below zero, ΔE has the highest weight on this PC. This suggests that PC3 scores are mainly related with total color change (ΔE). Hence, dosimeters with high scores on this PC will have undergone important color modifications.

To better understand the pattern in the data, the scores were again colored according to the different parameters being investigated (Figure 7), i.e. the kind of binder used in the paint dosimeters (Figure 7a), exposure time (Figure 7b) and pigment particle size (Figure 7c and 7d).

Results suggested that the combination of PC1 and PC2 allowed us to distinguish the type of binder present in the dosimeters. Two clearly differentiated groups can be observed on the score plot (Figure 7a). One group comprises all the azurite MP samples, and the other includes the azurite standard (i.e. AZ-VEF see Table 1). This second group has two clearly distinguishable sub-groups according to the binder used in the dosimeters. At the start of the natural ageing test on the dosimeters all the azurite samples were characterized by high C^* , H^* and $+a^*$ (red hues) values and low L^* and ΔE values (i.e. ca. 4 weeks); all these parameters increased with exposure time to the urban atmosphere (Figure 7a). This means

that the azurite MP dosimeters containing rabbit glue become greener and more luminous over time.

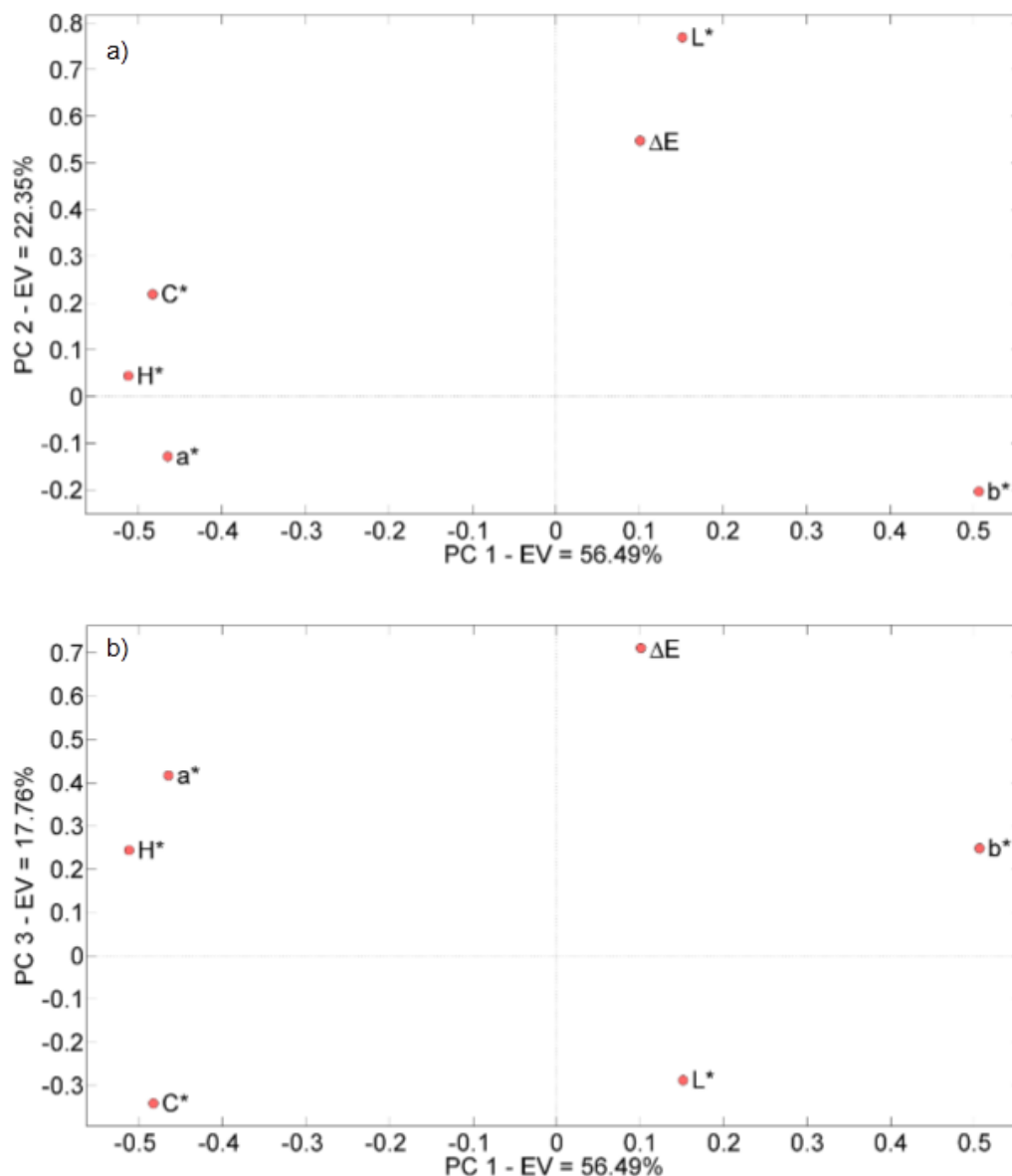


Figure 6. Loading plots for the azurite-laden dosimeters: (a) PC1 vs PC2; (b) PC1 vs PC3.

Principal Component Analysis to interpret changes in chromatic

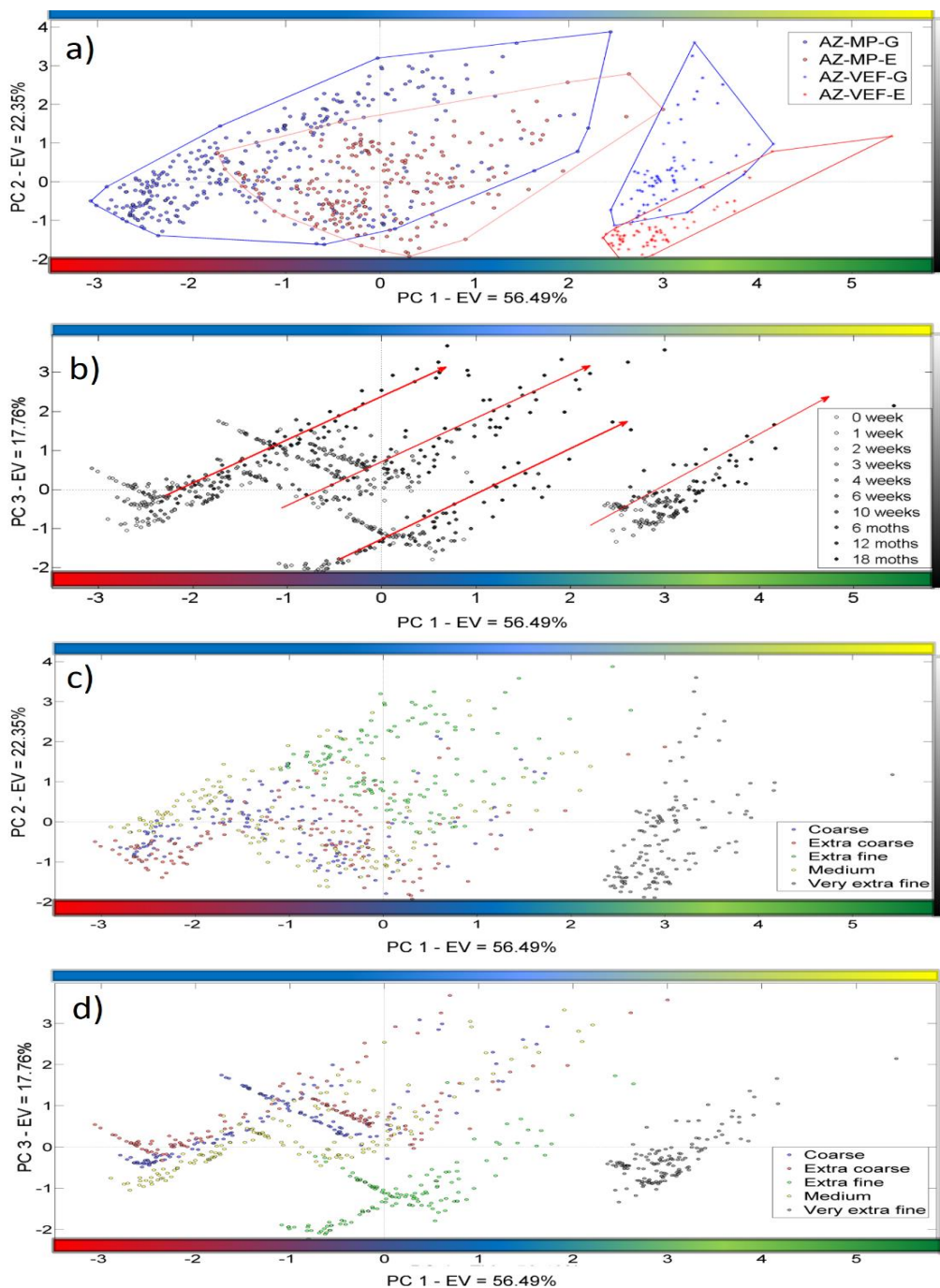


Figure 7. Score plots for the azurite-laden dosimeters: (a) PC1 vs PC2 (scores colored according to the kind of binder); (b) PC1 vs PC3 (scores colored according to exposure times); (c) PC1 vs PC2 (scores colored according to grain size); (d) PC1 vs PC3 (scores colored according to grain size). AZ-MP means all the azurites MP (see Table 1).

By contrast, all the azurite MP samples mixed with egg yolk have scores closer to zero than those mixed with glue (Figure 7a). The azurite MP dosimeters showed more dispersed chromatic parameters compared to the AZ-VEF dosimeters measured over time. They also have some overlap with the other grain sizes in rabbit glue-based samples since the corresponding scores appear nearby. The azurite MP dosimeters therefore have similar H^* , C^* and a^* (red/green) values but they have higher values of L^* and ΔE with respect to the paint dosimeters with long exposure times. The AZ standard samples (i.e. AZ-VEF, see Table 1) have the highest values of $+b^*$ (yellow hues) at the shortest exposure times, in particular the AZ-VEF-E dosimeter. The score plot (Figure 6a) and loading plot (Figure 7a) show that as time passes the chromatic parameters L^* and ΔE are the decisive factors affecting color changes over time. This means that AZ-VEF-G samples become bluer and more luminous over time, as well as experiencing the greatest net change in color, as detected by Cardell et al [21] who noted dissolution of the glue exposing azurite crystals. For its part AZ-VEF-E was characterized by high $+b^*$ (yellow hues) values at the shortest exposure times, although over time it underwent less change in L^* and ΔE than AZ-VEF-G.

The score plot for PC1 vs PC3 contains information about color changes over different exposure times (see Figure 7b). The loading plot (Figure 6b) showed that all the chromatic parameters had a high weight in PC1 with the exception of ΔE , which had a higher influence on PC3. ΔE appears to be the most important factor for discriminating color change due to exposure time.

Figure 7c and 7d show how PC1 separates AZ-VEF dosimeters (i.e. azurite standard according to Kremer, see Table 1) from the other MP azurites (extra coarse, coarse, medium, and extra fine grain sizes). AZ-VEF samples were characterized by high $+b^*$ (yellow hues) values, with both AZ-VEF-E and AZ-VEF-G samples having high b^* positive scores and loading on PC1, respectively. Furthermore, the score plot on PC1 and PC3 (Figure 7d) separated AZ-VEF dosimeters and AZ-EF dosimeters. AZ-VEF dosimeters became yellower ($+b^*$) and greener ($-a^*$) than the azurite MP dosimeters. In addition, AZ-EF dosimeters

showed the highest brightness values and represent the grain size that contributed most to color change in all the azurite dosimeters.

3.3.3. *Lapis lazuli*

PCA was performed on a data matrix with 154 rows (*lapis lazuli*) and 6 columns (color variables) containing the information about all the *lapis lazuli*-laden dosimeters. After applying PCA, results indicated that the first two components together explained 79% of the original data variance (Table 2 supplementary material Appendix II), and were thus retained for data interpretation. The corresponding loading and score plots are shown in Figure 2 supplementary material Appendix II. To better analyze the data patterns, the scores for the *lapis lazuli*-laden dosimeters are presented according to their binder content and the different exposure times.

Although in our initial inspection these paint dosimeters did not appear to be clustered, results suggest that there is a “hidden” relationship between the six color variables and the exposure time. The type of binder is also discriminated on PC2. The loading plot (Figure 2 supplementary material Appendix II) indicated that all the chromatic parameters had a high influence on PC1, with the exception of b^* and C^* , which are more important on PC2. Consequently, b^* (yellow/blue) and C^* (chroma) are the most important factors for discriminating the type of binder in *lapis lazuli*-laden dosimeters. As regards sample LAP-M-E, all the color parameters were related to the color change over time (Figure 2c supplementary material Appendix II), since the corresponding paint dosimeters had positive loadings on both PCs. This was also observed in the egg yolk-laden samples when measured at the highest exposure times. Thus, LAP-M-E dosimeters whose colors were measured at the start of the natural ageing test, were characterized by low $-b^*$ (blue hues) values, which increased in line with the time exposed to the urban air. This means that paint dosimeters containing egg yolk become yellower over time. Likewise, LAP-M-G samples were characterized by low $-b^*$ (blue hues) and high $+a^*$ (red hues) values at the

lowest exposure times. However in this case the chromatic parameters L^* and ΔE are the decisive factors affecting color changes over time.

3.4. Conclusions

The information obtained by applying this innovative reliable approach based on PCA to discrete color parameters enabled us to visualize and interpret the color change trends (over time) of dosimeters exposed long-term to the urban atmosphere more easily, as well as to discriminate paint dosimeters based on their pigment/binder characteristics and composition.

The results confirmed successful discrimination of the pigment when all the dosimeters were studied together. After long periods of exposure to the polluted urban environment, lapis lazuli-laden dosimeters acquired the distinctive blue of the azurite-laden dosimeters. PCA also allowed us to discriminate between the two proteinaceous binders (egg or rabbit glue) and the different grain sizes (in the azurite-laden dosimeters). This approach thus offers an efficient, fast and non-expensive exploratory procedure to obtain important information about paint composition.

A closer, more detailed study of each of the pigment-laden dosimeters revealed sufficient differences in luminosity to discriminate the binder in azurite and malachite-laden dosimeters, in which those prepared with rabbit glue showed high luminosity values. In the case of lapis lazuli-laden dosimeters the yellowness was the discriminant parameter for the paints containing egg-yolk binder, which became yellower as exposure time increased. As a general tendency for the binder, results indicated that paint dosimeters prepared with rabbit glue tended to become brighter and those prepared with egg yolk went yellower over time. In addition, lapis lazuli and azurite-laden dosimeters tended to a slightly greener shade, especially in the presence of the egg yolk binder. By contrast, the initially green malachite-laden dosimeters turned bluer.

Results indicated that grain size was important in the greenish tendency. Thus, in the different grain sizes studied in the azurite pigments, the greenish tendency was only observed in the dosimeters with small grain azurite. The color change tendencies were similar in the dosimeters with extra coarse, coarse and medium grain sizes, as the multivariate approach could not discriminate between them.

In summary, we evaluated the natural ageing of paint dosimeters when exposed to polluted urban air, offering a clear, in-depth, detailed description of the different chromatic changes that took place. The results indicate that the azurite-laden samples underwent the most important color changes over time while the malachite and lapis lazuli-laden dosimeters were the least affected. In addition to the new approach we used, all these results provide very useful, detailed information that is of great value when considering preventive strategies for the conservation of outdoor paintings.

Acknowledgements

Financial support was provided by Spanish Research Projects AERIMPACT (CGL2012-30729) and EXPOAIR (P12-FQM-1889), the European Regional Development Fund (ERDF), the Andalusian Research Groups RNM-179 and FQM-118, and the Milano Chemometrics and QSAR Research Group. J.A. Herrera Rubia is funded by a Spanish grant from the AERIMPACT Project (ref.BES-2013-065507). The authors thank Nigel Walkington for English revision.

References

- [1] R. Van Grieken, A. Worobiec, X-ray spectrometry for preventive conservation of cultural heritage, *Pramana - J. Phys.* 76 (2011) 191–200.
- [2] D. Camuffo, Environmental monitoring in four European museums, *Atmos. Environ.* 35 (2001) 127–140. doi:10.1016/S1352-2310(01)00088-7.
- [3] S. Sanchez-Moral, L. Luque, S. Cuezva, V. Soler, D. Benavente, L. Laiz, J.M. Gonzalez, C. Saiz-Jimenez, Deterioration of building materials in Roman catacombs: The influence of visitors, *Sci. Total Environ.* 349 (2005) 260–276.
- [4] V. Kontozova-Deutsch, C. Cardell, M. Urosevic, E. Ruiz-Agudo, F. Deutsch, R. Van Grieken, Characterization of indoor and outdoor atmospheric pollutants impacting architectural monuments: the case of San Jerónimo Monastery (Granada, Spain), *Environ. Earth Sci.* 63 (2011) 1433–1445. doi:10.1007/s12665-010-0657-5.
- [5] N.A. Katsanos, F. De Santis, A. Cordoba, F. Roubani-Kalantzopoulou, D. Pasella, Corrosive effects from the deposition of gaseous pollutants on surfaces of cultural and artistic value inside museums, *J. Hazard. Mater.* 64 (1999) 21–36.
- [6] B. Horemans, C. Cardell, L. Bencs, V. Kontozova-Deutsch, K. De Wael, R. Van Grieken, Evaluation of airborne particles at the Alhambra monument in Granada, Spain, *Microchem. J.* 99 (2011) 429–438. doi:10.1016/j.microc.2011.06.018.
- [7] J. Grau-Bové, M. Strlič, Fine particulate matter in indoor cultural heritage : a literature review, *Herit. Sci.* 1 (2013) 1–17.
- [8] M. Bacci, M. Picollo, S. Porcinai, B. Radicati, Tempera-painted dosimeters for environmental indoor monitoring: A spectroscopic and chemometric approach, *Environ. Sci. Technol.* 34 (2000) 2859–2865. doi:10.1021/es991437d.
- [9] M. Odlyha, N.S. Cohen, G.M. Foster, Dosimetry of paintings: Determination of the degree of chemical change in museum exposed test paintings (small tempera) by thermal analysis, *Thermochim. Acta.* 365 (2000) 35–44. doi:10.1016/S0040-6031(00)00611-0.
- [10] R. Mazzeo, S. Prati, M. Quaranta, E. Joseph, E. Kendix, M. Galeotti, Attenuated total reflection micro FTIR characterisation of pigment–binder interaction in reconstructed paint films, *Anal. Bioanal. Chem.* 392 (2008) 65–76. doi:10.1007/s00216-008-2126-5.
- [11] D. Saunders, H. Chahine, J. Cupitt, Long-term colour change measurement: some results after 20 years, *Natl. Gall. Tech. Bull.* 17 (1996) 81–90.
- [12] M. Bacci, L. Boselli, M. Picollo, B. Pretzel, Colour measurement on paintings, *Res. Signpost.* (2008).
<http://www.create.uwe.ac.uk/membership/Colourmeasurementonpaintings.pdf>.

- [13] E. Manzano, J. Romero-Pastor, N. Navas, L.R. Rodríguez-Simón, C. Cardell, A study of the interaction between rabbit glue binder and blue copper pigment under UV radiation: A spectroscopic and PCA approach, *Vib. Spectrosc.* 53 (2010) 260–268. doi:10.1016/j.vibspec.2010.04.003.
- [14] G.D. Smith, R.J.H. Clark, The role of H₂S in pigment blackening, *J. Cult. Herit.* 3 (2002) 101–105. doi:10.1016/S1296-2074(02)01173-1.
- [15] M. Cotte, J. Susini, N. Metrich, A. Moscato, C. Gratziu, A. Bertagnini, M. Pagano, Blackening of Pompeian Cinnabar Paintings: X-ray Microspectroscopy Analysis, *Anal. Chem.* 78 (2006) 7484–7492. doi:10.1021/ac0612224.
- [16] S. Potgieter-Vermaak, B. Horemans, W. Anaf, C. Cardell, R. Van Grieken, Degradation potential of airborne particulate matter at the Alhambra monument: a Raman spectroscopic and electron probe X-ray microanalysis study, *J. Raman Spectrosc.* 43 (2012) 1570–1577. doi:10.1002/jrs.4052.
- [17] A. Herrera, N. Navas, C. Cardell, An evaluation of the impact of urban air pollution on paint dosimeters by tracking changes in the lipid MALDI-TOF mass spectra profile, *Talanta.* 155 (2016) 53–61. doi:10.1016/j.talanta.2016.04.006.
- [18] T. Rivas, J. Pozo-Antonio, D. Barral, J. Martínez, C. Cardell, Vectorial versus functional statistical approaches to evaluate colour variations of tempera paints exposed to real environment., in: *Conf Metrol. Archaeol. Cult. Herit. (MetroArchaeo 2016)*, 2016.
- [19] C. Cardell, A. Herrera, G. Isabel, N. Navas, L. Rodríguez Simón, K. Elert, Pigment-size effect on the physico-chemical behavior of azurite-tempera dosimeters under natural and accelerated photo aging, *Dye. Pigment.* (2016).
- [20] L. Medeghini, S. Mignardi, C. De Vito, A.M. Conte, Evaluation of a FTIR data pretreatment method for Principal Component Analysis applied to archaeological ceramics, *Microchem. J.* 125 (2016) 224–229. doi:10.1016/j.microc.2015.11.033.
- [21] A. Nevin, I. Osticioli, D. Anglos, A. Burnstock, S. Cather, E. Castellucci, The analysis of naturally and artificially aged protein-based paint media using Raman spectroscopy combined with Principal Component Analysis, *J. Raman Spectrosc.* 39 (2008) 993–1000. doi:10.1002/jrs.1951.
- [22] C. Miguel, J.A. Lopes, M. Clarke, M.J. Melo, Combining infrared spectroscopy with chemometric analysis for the characterization of proteinaceous binders in medieval paints, *Chemom. Intell. Lab. Syst.* 119 (2012) 32–38. doi:10.1016/j.chemolab.2012.09.003.
- [23] K. Rajer-Kanduč, J. Zupan, N. Majcen, Separation of data on the training and test set for modelling: A case study for modelling of five colour properties of a white pigment, *Chemom. Intell. Lab. Syst.* 65 (2003) 221–229. doi:10.1016/S0169-

7439(02)00110-7.

- [24] S. Mas, C. Miguel, M.J. Melo, J.A. Lopes, A. de Juan, Screening and quantification of proteinaceous binders in medieval paints based on μ -Fourier transform infrared spectroscopy and multivariate curve resolution alternating least squares, *Chemom. Intell. Lab. Syst.* 134 (2014) 148–157. doi:10.1016/j.chemolab.2014.03.012.
- [25] I. Osticioli, N.F.C. Mendes, S. Porcinai, A. Cagnini, E. Castellucci, Spectroscopic analysis of works of art using a single LIBS and pulsed Raman setup, *Anal. Bioanal. Chem.* 394 (2009) 1033–1041. doi:10.1007/s00216-009-2653-8.
- [26] E. Franceschi, P. Letardi, G. Luciano, Colour measurements on patinas and coating system for outdoor bronze monuments, *J. Cult. Herit.* 7 (2006) 166–170. doi:10.1016/j.culher.2006.03.001.
- [27] G. Luciano, R. Leardi, P. Letardi, Principal component analysis of colour measurements of patinas and coating systems for outdoor bronze monuments, *J. Cult. Herit.* 10 (2009) 331–337. doi:10.1016/j.culher.2008.10.004.
- [28] M. Urosevic, A. Yebra-Rodríguez, E. Sebastián-Pardo, C. Cardell, Black soiling of an architectural limestone during two-year term exposure to urban air in the city of Granada (S Spain), *Sci. Total Environ.* 414 (2012) 564–575. doi:10.1016/j.scitotenv.2011.11.028.
- [29] G. Titos, H. Lyamani, L. Drinovec, F.J. Olmo, G. Močnik, L. Alados-Arboledas, Evaluation of the impact of transportation changes on air quality, *Atmos. Environ.* 114 (2015) 19–31. doi:http://dx.doi.org/10.1016/j.atmosenv.2015.05.027.
- [30] C. Cardell-Fernández, C. Navarrete-Aguilera, Pigment and plasterwork analyses of Nasrid polychromed lacework stucco in the Alhambra (Granada, Spain), *Stud. Conserv.* 51 (2006) 161–176. http://www.jstor.org/stable/20619445.
- [31] C. Cardell, L. Rodriguez-Simón, I. Guerra, A. Sanchez-Navas, Analysis of Nasrid polychrome carpentry at the Hall of the Mexuar Palace, Alhambra complex (Granada, Spain), combining microscopic, chromatographic and spectroscopic methods, *Archaeometry.* 51 (2009) 637–657. doi:10.1111/j.1475-4754.2008.00438.x.
- [32] M. Price, A Renaissance of Color: Particle Separation and Preparation of Azurite for Use in Oil Painting, *Leonardo.* 33 (2000) 281–288. doi:10.1162/002409400552667.
- [33] R. Mayer, S. Sheehan, *The artist's handbook of materials and techniques*, The Viking, New York, 1991.
- [34] J. Schanda, *Colorimetry: Understanding the CIE System*, John Wiley and Sons, 2007.
- [35] D. Ballabio, A MATLAB toolbox for Principal Component Analysis and unsupervised exploration of data structure, *Chemom. Intell. Lab. Syst.* 149 (2015) 1–9.

doi:10.1016/j.chemolab.2015.10.003.

- [36] R. Bro, A.K. Smilde, Principal component analysis, *Anal. Methods*. 6 (2014) 2812. doi:10.1039/c3ay41907j.
- [37] I.T. Jolliffe, Principal Component Analysis, Second Edition, *Encycl. Stat. Behav. Sci.* 30 (2002) 487. doi:10.2307/1270093.
- [38] E. Sánchez-Zapata, E. Fuentes-Zaragoza, C. Navarro-Rodríguez de Vera, E. Sayas, E. Sendra, J. Fernández-López, J.A. Pérez-Alvarez, Effects of tuna pâté thickness and background on CIEL*a*b* color parameters and reflectance spectra, *Food Control*. 22 (2011) 1226–1232. doi:10.1016/j.foodcont.2011.01.022.

Capítulo 4

Pigment-size effect on the physico-chemical behavior of azurite-tempera dosimeters under natural and accelerated photo aging

C. Cardell ⁽¹⁾, A. Herrera ⁽¹⁾, I. Guerra ⁽²⁾, N. Navas ⁽³⁾, L. Rodríguez Simón ⁽⁴⁾ and Kerstin Elert ⁽¹⁾

(1) Dept. of Mineralogy and Petrology, Faculty of Science, University of Granada, Campus Fuentenueva s/n, E 18071 Granada, Spain.

(2) Scientific Instrumentation Centre, University of Granada, Campus Fuentenueva s/n, E 18071 Granada, Spain.

(3) Dept. of Analytical Chemistry, and Biomedical Research Institute of Granada (IBIG), Faculty of Science, University of Granada, Campus Fuentenueva s/n, E 18071 Granada, Spain.

(4) Dept. of Paint and Restoration, Faculty of Fine Arts, University of Granada, Av. Andalucía s/n, 18071 Granada, Spain.

Dyes and Pigments 141 (2017) 53e65

<http://dx.doi.org/10.1016/j.dyepig.2017.02.001>

Article history:

Received 17 October 2016

Received in revised form

21 December 2016

Accepted 2 February 2017

Available online 4 February 2017

Hipótesis de partida

El impacto de la radiación solar en pinturas artísticas (expuestas en el interior de recintos o a la intemperie) es particularmente importante en promover reacciones físico-químicas entre sus componentes, cuya consecuencia última es un cambio de color antiestético en las mismas. Por consiguiente, en países donde la incidencia de la luz solar es amplia, como es el caso de los países de la cuenca del Mediterráneo, debe prestarse especial atención a la alteración de obras de arte pictóricas inducida por la radiación del sol. La alteración es más intensa si las pinturas están expuestas a la intemperie en atmósferas urbanas contaminadas, recibiendo el impacto directo de la luz solar.

Aunque son numerosos los trabajos que examinan el deterioro de pigmentos y aglutinantes debido a la radiación UV y Vis, principalmente en el interior de edificios, aún son escasos los que abordan el envejecimiento de las pinturas artísticas bajo ambientes soleados y de polución atmosférica, considerando la interacción entre materiales pictóricos.

Por otra parte es sabido que los diferentes pigmentos poseen distinta estabilidad frente a la radiación solar dependiendo de su naturaleza y tipo de aglutinante con el que se mezclan. No obstante, aún debe profundizarse en la contribución del tamaño de grano del pigmento en la interacción pigmento-aglutinante, y en consecuencia, como afecta a los procesos de alteración que sufren las pinturas, en particular, cuando están expuestas a la contaminación atmosférica.

Objetivos de la investigación

El objetivo de este trabajo es investigar la influencia que tiene el tamaño de grano del pigmento, el cual condiciona la cantidad de aglutinante, en los cambios físicos y químicos (color, composición y textura) ocurridos en pinturas. Para ello se han analizado dosímetros pictóricos elaborados con azurita de distinto tamaño y aglutinante proteico de cola de conejo, envejecidos de forma natural y artificial. En el primer caso los dosímetros pictóricos se expusieron durante dos años en diversos monumentos (semi)-abiertos de la ciudad de Granada, en los que las condiciones de calidad de aire y el impacto de la radiación solar fueron diferentes. En el segundo caso, los dosímetros pictóricos se sometieron a un ensayo de envejecimiento acelerado en laboratorio con luz UV. La comparación de los resultados obtenidos en ambos ensayos permitirá profundizar en el conocimiento que se tiene sobre los procesos de foto-degradación de pinturas, estableciendo las similitudes y discrepancias entre la degradación natural (solar) y la acelerada por luz UV.

Abstract

This paper presents the first comprehensive study on the role played by pigment particle size in pigment-binder interactions, and thus susceptibility to aging of azurite-rabbit glue paint dosimeters upon accelerated UV-aging versus natural outdoor sunlight exposure. A complementary multi-analytical approach, including spectroscopic and surface analytical techniques, was applied to characterize commercial azurite pigments, as well as blank and aged dosimeters. Results show the crucial role played by azurite particle size on protein-copper complex formation, which governed physico-chemical properties of paints and their aging behavior under different light-aging conditions. On UV-aged dosimeters, finer particles promoted stronger binder structural changes, inducing more severe color changes ($\Delta E=4-17$). Azurite size also controlled crack formation which was more severe as pigment grain increased due to greater accumulation of binder in inter-pore spaces. Outdoor exposure caused important binder loss (50-60%) and initial transformation of azurite into malachite. Since analyzed pigment composition and particle size differed from manufacturer data, we recommend their characterization prior to use in conservation works and scientific studies. Based on these results, paints made of coarse azurite particles are preferable since they are less prone to color change. Moreover, a small addition of fine-grained pigments might reduce crack development upon aging.

4.1. Introduction

The increasing interest in historical painting techniques and artist materials over recent decades has led to numerous publications dealing with the use and characterization of traditional painting materials, i.e., in-/organic pigments and organic binders, utilized prior to the 18th century. Research on these materials is key to: i) unravel artistic and technical issues of historic paintings [1-4], ii) establish dating, authorship or forgery of artworks [5-8], iii) understand aging mechanisms [9-13], and thus, iv) promote preventive conservation strategies and suitable conservation/restoration treatments [14-16].

To investigate damage processes, model paint samples (dosimeters or mock-ups), that mimic the composition and structure of real paintings, are often used to evaluate the effects of temperature (T), relative humidity (RH), ultraviolet/visible (UV/Vis) irradiation, and pollutant gases and particles, through in situ and/or accelerated aging tests [10,17-20]. Sunlight is particularly important in promoting physico-chemical reactions on paintings causing fading or darkening [21-23]. Thus, in countries where the incidence of solar light is significant, such as those of the Mediterranean Basin, light-induced decay on paint artworks is an important issue to take into account.

Light-induced damage to a great variety of dyes, pigments and organic binders has been the topic of many investigations over the last decades [23-25]. Only more recently studies have tackled the paintings aging considering the interaction between pigments and binders [10, 13, 18, 19]. For instance, Odlyha et al. [18] examined the effect of accelerated and natural indoor light aging on azurite-egg-yolk tempera dosimeters. They found that azurite induced binder oxidation although dosimeters suffered only minor changes in their thermal stability upon light aging. Manzano et al. [10] also detected slight changes in reflectance values of azurite-rabbit glue tempera dosimeters exposed to accelerated UV-aging. These changes were not influenced by the different binder amount present in the tempera paints.

To further elucidate the pigment-binder interaction on the weathering behavior of azurite tempera (i.e., color changes, pigment and binder composition, and texture of paint dosimeters), we have included azurite pigments of various particle sizes in this study. The effect of particle size on pigment features (e.g. color, hiding power, appearance and optimum surface finish) is widely recognized [26-29]. However, the contribution of pigment size on paint alteration has seldom been addressed [27]. Hence, in this work azurite-rabbit glue tempera dosimeters were exposed to artificial UV light (laboratory aging test) and outdoor sunlight radiation (two-year outdoor test in Granada, southern Spain) in order to gain knowledge about similarities and discrepancies in their photo-physicochemical decay.

Long-term outdoor exposure was performed since previous studies mainly focused on photodegradation of pigments and paints under controlled indoor/museum conditions [17, 18] and results are not easily applicable to wall paintings and polychrome artworks located in (semi)-open monuments/buildings exposed to the Mediterranean climate. These are part of many important monuments of Granada, including the known worldwide Alhambra and Generalife [1, 4, 7, 14] and the wall paintings in the Carrera del Darro [30]. Their state of conservation varies greatly and the here obtained results will serve as the basis for the determination of prevailing degradation mechanisms and the selection of suitable materials for their restoration. Prior to aging tests, the selected commercial azurite pigments were fully characterized. On all samples an array of complementary spectroscopic and surface analytical techniques were applied.

4.2. Materials and Methods


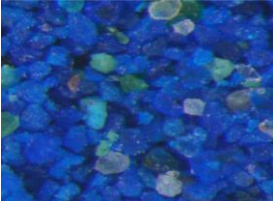
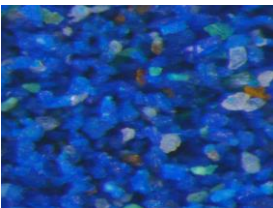

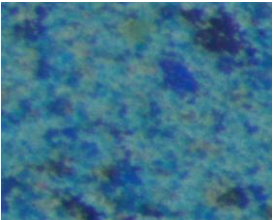
4.2.1. Materials

Azurite ($\text{Cu}_3(\text{CO}_3)_2(\text{OH})_2$) was the most widely used blue pigment in European paintings from the 15th to the middle of the 17th century [31]. Traditionally, azurite has been used coarsely ground since it becomes pale and unsuitable as a coloring material when very finely ground [32]. In 1997 Michel Price (MP) developed a method for the separation of ground azurite into different pigment sizes corresponding to diverse hues of blue, from a

deep rich blue to a pale sky blue [28]. This method consists of consecutive washings in an egg yolk medium, separating different particle sizes based on Stokes' law. This treatment also confers to azurite protection against acid reactions in oil media by surrounding pigment particles with a protein coating. In 1998 Kremer Pigments GmbH & Co. KG adopted this method to prepare a new range of azurite pigments, called "azurite MP." These pigments are available in seven grades (according to their average particle size) from a deep royal blue to a pale sky blue.

In this study we analyzed Kremer azurite pigments with different particle sizes which include various "azurite MP" and the "azurite natural standard" (color index PB3077420) (Table 1). Pearls of rabbit glue (Kremer Pigments GmbH & Co. KG, ref. 63028) were used to prepare proteinaceous-based paint dosimeters. The binder was prepared according to traditional recipes. Eight grams of rabbit glue were soaked in 100 ml of deionized water for 24 h, under periodic stirring. Afterwards the mixture was heated below 50°C in a water bath and stirred to obtain a homogeneous mixture. The rabbit glue was cooled to room T (22°C) until a gel-like consistency was obtained.

Table 1. *Characteristics of commercial azurite pigments.*

Kremer pigment reference	Stereomicroscope image of pigments Scale: <u>0.6 mm</u>	Kremer pigment size	Authors azurite reference
Azurite MP extra deep. No. 10203 (intense dark blue)		80-100 μm	AZ-EC: azurite extra coarse
Azurite MP, deep. N° 10204 (dark blue)		63-80 μm	AZ-C: azurite coarse
Azurite MP, pale, N° 10206 (light blue)		38-63 μm	AZ-M: azurite medium
Azurite MP, sky-blue. N° K10207 (light greenish blue)		< 38 μm	AZ-EF: azurite extra fine
Azurite standard. N° 10200 (deep greenish blue)		< 120 μm	AZ-ST: azurite standard

4.2.2. Paint dosimeters preparation

During the Middle Ages and the Renaissance, pigments were ground into particles of properly uniform size to obtain a smooth spreading paint. Afterward the pigments were mixed with the correct amount of binder to make an easily workable paint. Though there are manuscripts, treatises and books with painting recipes [33-35], in practice the precise amount of binder to be mixed with a pigment varied since it depends on the crystal size attained during the pigment grinding.

Hence, in this work the paint dosimeters were prepared according to traditional procedures, used by medieval painters, considering organoleptic parameters. Each pigment was first mixed with deionized water. Then, droplets of prepared rabbit glue were added until an adequate consistency was reached. It was found adequate when droplets formed at the tip of the brush would not fall off easily. Subsequently, several layers of paint mixture were applied by brush to glass slides (76x26x1mm). Care was taken that each layer be completely dry before the next was applied. Then, glass slides were cut with a diamond knife into 15x15x1 mm pieces to conduct the aging tests. To obtain the pure rabbit glue binder dosimeter, the glue paste was directly applied onto the glass slide.

Paint dosimeters are named adding the letter C (which refers to rabbit glue, cola in Spanish) to the pigments label (see Table 1), to clearly differentiate powder pigments from binary (pigment/binder) paint mixtures.

4.2.3. UV-accelerated aging test

The artificial aging test was performed during 1000 h in a ventilated chamber at $24\pm 3^{\circ}\text{C}$ and $25\pm 10\%$ RH. A tubular UV lamp (TL 40W/12 RS SLV/25, Philips Lighting Holding B.V.) was operated continuously during the test. The lamp emits more than 85% of its energy in the UV-B wavelength range with a peak at ~ 320 nm. Irradiance level was fixed at 765 W/m². Day light was blocked using aluminum foil.

4.2.4. Outdoor sunlight exposure test

The paint dosimeters were placed vertically in an exterior eave (protected from direct rainfall) of the Granada Cathedral (South Spain), in the historic center of the city where traffic is restricted. Samples faced SW and were exposed for two years to direct sunlight ~5 h in winter and ~10 h in summer, under urban air conditions. It was estimated that the overall sunlight exposure duration was ~5500 h at an irradiance level of ~1090 W/m² [36]. During the exposure, T reached 40°C in summer and -3°C in winter (www.ugr.es/~velilla/meteo-albayzin/resumen.htm, accessed 7.7.16). The average maximum T in Granada being ~30-35°C in summer and ~10-15°C in winter, with diurnal variations up to 20°C. The average RH was ~40% in summer and ~75% in winter, with average monthly precipitation ranging from ~5 mm in summer to ~40 mm in winter (www.granada.climatemps.com, accessed 5.7.16). Data on average concentrations of atmospheric aerosols during winter and summer 2015 are reported in Table 2. Although Granada is a non-industrialized city, concentrations of NO₂, O₃ and particulate matter with 10 µm average size (PM₁₀) in 2015 frequently exceeded the threshold values set by the EU directive 2008/50EC. The SO₂ concentration was generally below the established limit. Particle matter is primarily constituted by soil dust (quartz, calcite, dolomite, phyllosilicates, iron oxides/hydroxide), black carbon, secondary inorganic aerosols, and sea salt [14, 37].

Table 2. Average air contamination and particulate matter (PM₁₀) concentration (µg m⁻³) during winter and summer 2015 in the city center of Granada.

Dates	SO ₂	NO ₂	O ₃	PM ₁₀
15/1/2015-9/1/2015	15.8±6.1	40.2±21.0	31.6±22.7	22.2±14.3
22/6/2015-8/7/2015	6.9±7.0	29.9±21.7	82.5±31.1	40.6±20.1

Data: from www.juntadeandalucia.es/medioambiente/site/rediam/menuitem, 1.12.16

4.2.5. Analytical techniques

The azurite pigments, organic binder, and all paint dosimeters (i.e. blank and aged) were analyzed with the following analytical techniques:

A stereomicroscope (SMZ 1000, Nikon) was used to examine the textural, structural and chromatic features of blank and aged paint dosimeters. Granulometry (Mastersizer 2000LF, Malvern Instruments) was performed to verify the particle size of the azurite pigments in the range 0.02 – 1500 μm using laser diffraction. Samples were dispersed in ethanol. Thermogravimetric analysis (TG) was used to quantify both the egg yolk present in the commercial azurite MP pigments and the rabbit glue binder added to each azurite to prepare the corresponding paint dosimeter. Analyses were performed on a Shimadzu TGA-50H (Shimadzu Corporation) in flowing air (100 ml/min) at a constant heating rate of 10 $^{\circ}\text{C min}^{-1}$ (25 - 950 $^{\circ}\text{C}$). One analysis per sample was performed. The binder content of paint dosimeters was calculated considering the weight loss of the corresponding azurite pigment and the pure binder in the same temperature range. Using X-ray diffractometer (X'Pert PRO PANalytical B.V.), the mineralogical composition of azurite pigments and all paint dosimeters was identified. Analyses were performed using Cu-K α radiation, Ni filter, 45 kV voltage, 40 mA intensity and spinner. The exploration range was 3 $^{\circ}$ to 60 $^{\circ}$ 2 θ and goniometer speed 0.05 $^{\circ}$ 2 θ s $^{-1}$. Identification and semi-quantification (~ 5%) of minerals were carried out using Xpoflower [38].

To analyze the micro-texture and chemical composition of pigments and all paint dosimeters, two high-resolution (Schottky-type field emission) scanning electron microscopes (FESEM) coupled to an energy dispersive X-ray spectrometer (EDX) were used. Samples were mounted on Al stubs with double-sided adhesive C tape. The instruments were: i) an Auriga (Carl Zeiss, Germany) joined to an INCA-200 EDX working at 10 $^{-4}$ Pa vacuum and 2 kV beam accelerating voltage (secondary electron imaging mode; carbon-coated samples); and ii) a variable pressure FESEM (VP-FESEM, Supra 40Vp Carl Zeiss, Germany) equipped with an Aztec 3 EDX and X-Max 50mm detector. Working conditions

were 40-66 Pa vacuum, 15-20 kV (imaging mode) and 20 kV beam accelerating voltage (samples not carbon coated). High-resolution X-ray maps (1024X768 pixels) were obtained from selected areas with 100 frames and a dwell time of 10 ms (2.5 h acquisition) using 3 nA filament current and 20 eV/ch resolution. To determine the nature of the crystalline/amorphous phases present in the dosimeters, phase maps were compiled from elemental distribution maps by applying the *Find Phases* tool implemented in the Aztec 3 version used in this work. This procedure allowed us to highlight the location, morphology and amount of phases present in the paint dosimeters. Linear crack density (mm^{-1}) was calculated using $0.1 \times 0.95 \text{ mm}^2$ SEM images according to the following equation: crack length (mm)/image size (mm^2) = linear crack density (mm^{-1}).

A portable reflectance spectrophotometer (Minolta CM-700D) was used to measure the chromatic features of the paint dosimeters. Color data were collected in SCI (specular component included) and SCE (specular component excluded) modes from 400 to 700 nm at 10 nm intervals for the standard D65 daylight illuminant (color temperature 6504 K) using 10° observer and an 8 mm measuring aperture. Note that the difference between SCI and SCE measurements was ≤ 0.2 units for all color parameters, and only the former are reported in this study. Data were expressed in the CIE $L^*a^*b^*$ and CIE $h^*C^*L^*$ color spaces. In the CIE $L^*a^*b^*$ system, L^* is luminosity which varies from black with a value of 0 to white with a value of 100; a^* varies from $+a^*$ (red) to $-a^*$ (green) and b^* ranges from $+b^*$ (yellow) to $-b^*$ (blue). In the CIE $h^*C^*L^*$ color system each color is represented by three cylindrical coordinates: hue or tone (h^*) which refers to the dominant wavelength, chroma or saturation (C^*) related to the intensity of color, and L^* which is lightness or luminosity of color. The CMC (2:1) version of the color difference formula (i.e., $\Delta E^* = \sqrt{(\Delta L^*)^2 + (\Delta a^*)^2 + (\Delta b^*)^2}$) was used to colorimetrically compare dosimeters [39]. In general terms, these differences will be visually perceptible when the values change by more than three units [40]. Average values are based on a minimum of 5 measurements per samples.

A confocal Raman spectrometer (Jasco NRS-5100) fitted with an Olympus microscope and a Peltier-cooled CCD detector (Andor DU 420 OE) was used to recognize the molecular

composition of powder pigments, rabbit glue binder and all the paint dosimeters. Samples were observed using the 5X, 20X and 100X objectives. The video camera was used to identify particular locations in the samples, which were excited with lasers at 532 nm (green, Elforlight G4-30;Nd:YAG) and 785 nm (red, Torsana Starbright). The scattered Raman light was collected in a 180° backscattering geometry by a Charge Coupled Device (CCD) after having passed through a 50µm entrance slit. Spectra were collected with an average resolution of 2 cm⁻¹ within the wavenumber range of 100-3000 cm⁻¹. To improve the signal/noise ratio and avoid laser-induced degradation of samples, a series of recorded spectra (n=6-10) were collected from each sample spot and averaged, with exposure times from 20 to 30s for green (100% power, Max Power Density W·cm⁻² = 6.37e⁻⁷), and from 30 to 40s for red laser (10 % power, Max Power Density W·cm⁻² = 8.40e⁻⁸). To ensure statistical representativity, a minimum of 5 spots were analyzed in each sample.

Attenuated Total Reflection – Fourier transform infrared spectroscopy (ATR-FTIR) was performed on powder samples of pigments and binder, as well as on blank and aged dosimeters using a Jasco 6200 (JASCO Analytical Instruments, Japan). The dosimeters were pressed against the ATR diamond crystal window and the infrared (IR) spectra were recorded at a 2 cm⁻¹ resolution over 100 scans from 400 to 4000cm⁻¹. The ATR correction was applied on selected FTIR spectra using Spectra Manager II software. Results showed no peak shifts as compared to uncorrected FTIR spectra. The results reported here are based on uncorrected ATR-FTIR data.

4.3. Results and discussion

4.3.1. Stereomicroscope study of paint dosimeters

The stereomicroscope images revealed that all azurite pigments contained impurities, showing colorless and green colored crystals (Fig. 1), identified as quartz (SiO₂) and malachite (Cu₂(CO₃)(OH)₂) using XRD (see section 3.4). Additionally, a few orange-brown/black crystals were observed and recognized as iron oxides/hydroxides (Fig. 1h)

with VP-FEMEM-EDX (see section 3.5). In AZ-ST-C only the larger individual azurite particles could be distinguished, whereas the finer grains were completely covered by egg yolk/rabbit glue, added either during the pigment or the paint preparation. Some large circular pockmarks could be observed on the paint surface, as relics of air bubbles.

After the UV-aging test, dosimeters with the coarser pigments (Fig. 1b, 1e, 1h) displayed a whitish glaze with a slight yellowish tint on the surface, which was more pronounced in AZ-M-C. Instead AZ-EF-C (Fig. 1k) suffered severe discoloration towards yellow, while a less significant color change took place on AZ-ST-C (Fig. 1n). Here, part of the organic binder was lost, thus a larger amount of the fine grained azurites was now discernible. Furthermore, some surface micro-pitting was observed which at first might seem surprising considering the low RH conditions (i.e., $25\pm 10\%$ RH) during the artificial UV-aging test. However, in this RH range the amount of water absorbed by the glue changes drastically. Karpowicz [41] reported that below 30% RH, the protein molecule surface was covered only by a monomolecular layer of water. In contrast, above this RH the proteins contained more water, reaching 0.3-0.5 g of water per 1 g of protein at 30-90% RH. With this in mind, and considering that the paint dosimeters were at times exposed to RH >30%, a significant increase in moisture content of the glue binder could be expected, which facilitated dissolution processes leading to the formation of micro-pitting on the sample surface.

The two-year outdoor exposure caused binder and pigment loss in all paint dosimeters, being more significant in AZ-EF-C and AZ-ST-C (Fig. 1l, 1o). AZ-ST-C revealed a very distinct surface appearance compared with the blank dosimeter (Fig. 1o). Individual pigments were no longer covered by egg yolk/rabbit glue binders, thus morphological features of crystals were perfectly seen. The surface also suffered micro-pitting and formation of fine fissures.

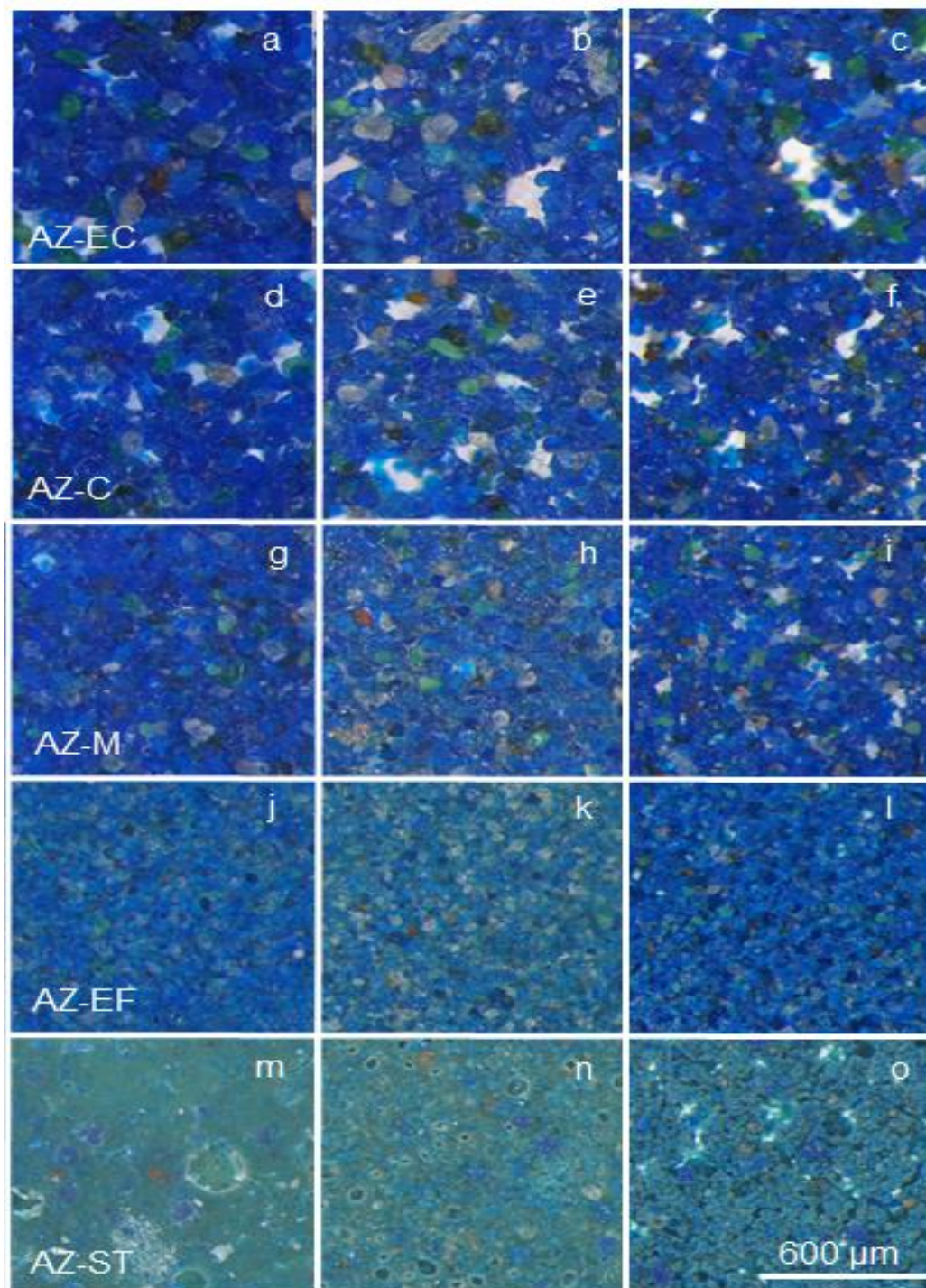


Figure 1. Stereomicroscope photographs of azurite-proteinaceous paint dosimeters: (a, d, g, j, m) blank, (b, e, h, k, n) artificial UV-aged, (c, f, i, l, o) outdoor sunlight exposed.

4.3.2. Particle size analysis of powder pigments

Particles in powder pigments are hardly uniform in size. Results revealed a wider particle size range (Fig. 2, Table 3) as compared to manufacturer’s data (see Table 1). However, it should be said that this technique might provide larger particle sizes, due to the aggregation of smaller particles. Indeed, note that stereomicroscope and SEM observation did not show particles >100 μm . Generally, the finer pigments (AZ-EF and AZ-ST) have wider particle size ranges than do coarser pigments (Fig. 2), especially in the case of AZ-ST which has many particles <10 μm , down to ca. 0.2 μm . Our results agree with the finding of Han et al. [27] who noticed the existence of nanometer-sized particles in diverse historical azurite pigment grades; these were more abundant and finer in size in the smaller particle-size azurites and greatly influence their luminosity.

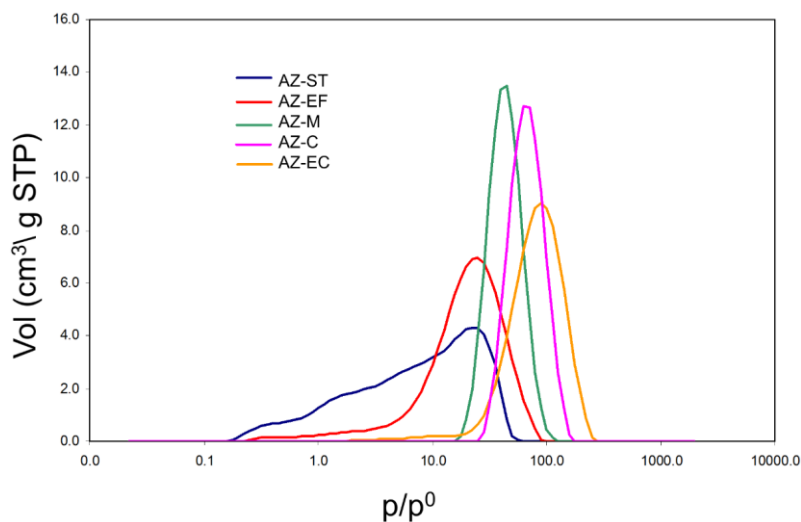


Figure 2. Particle size distribution of azurite pigments.

Table 3. Particle size (μm) of azurite pigments studied in this work.

Pigment	Main Maximum (Authors)	Range (Authors)	Range (Kremer)
AZ-EC	90	20-280	80-100
AZ-C	70	25-180	63-80
AZ-M	45	20-110	38-63
AZ-EF	25	4-90	<38
AZ-ST	22	0.2-55	<120

4.3.3. Thermogravimetric analysis of pigments and dosimeters

Using TG analyses the egg yolk content added to the azurites during the Michel Price method, as well as the rabbit glue binder added to prepare the paint dosimeters were determined. The former was estimated taking into account the weight loss upon heating from 50 to 200°C, considering the weight loss of pure egg yolk in the same temperature range (Table 4). Note that weight loss data <50°C were not considered for calculating the egg yolk content because loss is mainly caused by adsorbed water. Results showed that the egg yolk content was highest in AZ-ST (10.5 wt%) compared with the other pigments (ranging from 2 to 3.5 wt%).

The rabbit glue binder content was calculated from the TG weight loss data (50 to 950°C) considering the weight loss of the corresponding pigment and pure binder in the same temperature range. It was found that binder content generally increased with decreasing pigment size (Table 4). However, the calculated amount of rabbit glue binder was unexpectedly low in AZ-ST-C (i.e. 8.4 wt%), considering that this dosimeter is made of the finest particles. Nevertheless, it has to be kept in mind that the AZ-ST pigment already contained a high quantity of egg yolk (10.5 wt%), added during its preparation by the manufacturer; hence the AZ-ST-C dosimeter had the highest amount of total organic media (18 wt%).

After the two-year outdoor exposure, paint dosimeters suffered a decrease in organic content of ~50-60%. Note that this technique did not allow determining whether the reduction was primarily due to egg yolk or rabbit glue loss. No relation was observed between organic content decrease and pigment.

Table 4. *Egg yolk content (wt%) of commercial pigments and rabbit glue binder content (wt%) of blank and outdoor exposed dosimeters, calculated based on TG data.*

Commercial Pigments	Egg yolk content of commercial pigments	Dosimeters	Rabbit glue binder content in blank dosimeters	Total organic content in blank dosimeters	Organic content of dosimeters after 2-year outdoor exposure
AZ-EC	2.3	AZ-EC-C	7.9	10.0	6.1
AZ-C	2.9	AZ-C-C	7.7	10.4	5.4
AZ-M	3.5	AZ-M-C	8.8	12.0	6.9
AZ-EF	2.0	AZ-EF-C	9.3	11.1	5.3
AZ-ST	10.5	AZ-ST-C	8.4	18.0	10.0

4.3.4. XRD of pigments and dosimeters

The diffraction patterns of azurite pigments revealed the presence of mineral phases matching the following Joint Committee on Powder Diffraction Standards (JCPDS): azurite (JCPDS card nº 701579), malachite (JCPDS card nº 760660) and quartz (JCPDS card nº 331161), these last two present as impurities. Semi-quantitative (~5%) XRD analyses (Table 5) showed that the azurite content was highest in AZ-ST (90%) and lowest in AZ-EF (70%). Note that XRD analyses of two different batches of AZ-ST are shown in Table 5, displaying different mineralogical composition, which indicates that quality control for this pigment could be improved. In this work only AZ-ST-1 was used.

XRD analyses showed that no mineralogical changes took place upon UV-aging. Bragg peak positions of sunlight exposed samples did not change either; thus evidence for an azurite to malachite transformation was not detected using this technique. However, XRD patterns

Pigment-size effect on the physico-chemical behavior of azurite-

of the latter revealed an additional peak at $\sim 3.03 \text{ \AA}$ indicating the presence ($\sim 10 \text{ wt\%}$) of calcite (CaCO_3 , JCPDS card n^o 050586), likely due to the deposition of particulate matter on the dosimeters' surface. Note that Ca and Mg carbonates are among the major mineral phases detected in soil dust in Granada [14, 37]. Considering the low reactivity and hygroscopicity of calcite, alteration processes are not likely to be accelerated by its presence. However, it will affect the esthetic perception of the painted surface.

Table 5. Mineralogical composition (wt%) of azurite pigments according to semi-quantitative ($\sim 5\%$) XRD analysis.

Pigment	Azurite (JCPDS 701579)	Malachite (JCPDS 760660)	Quartz (JCPDS 331161)
AZ-EC	80	10	10
AZ-C	85	5	10
AZ-M	85	5	10
AZ-EF	70	>5	20
AZ-ST-1	90	<5	<5
AZ-ST-2	50	10	40

Note: 1 and 2 refer to two different batches of "azurite natural standard" pigment acquired from Kremer Pigments GmbH & Co. KG.

4.3.5. SEM-EDX of paint dosimeters

SEM-EDX analyses of blank azurite dosimeters revealed the presence of mainly copper (Cu) and in minor amounts silicon (Si), aluminum (Al), iron (Fe), barium (Ba), sulfur (S), calcium (Ca), potassium (K) and titanium (Ti). A general spectrum based on five EDX analyses taken from the AZ-C-C dosimeter is shown in Figure 3a. Using false-color phase mapping (Figure 3b) these elements were related with the following mineral phases: azurite, quartz, aluminum silicates (ascribed to clay minerals as impurities) [42], barite (BaSO_4), calcite

(CaCO₃), iron-bearing oxides/hydroxides, and dolomite (CaMg(CO₃)₂). Mapping also provided information on binder distribution.

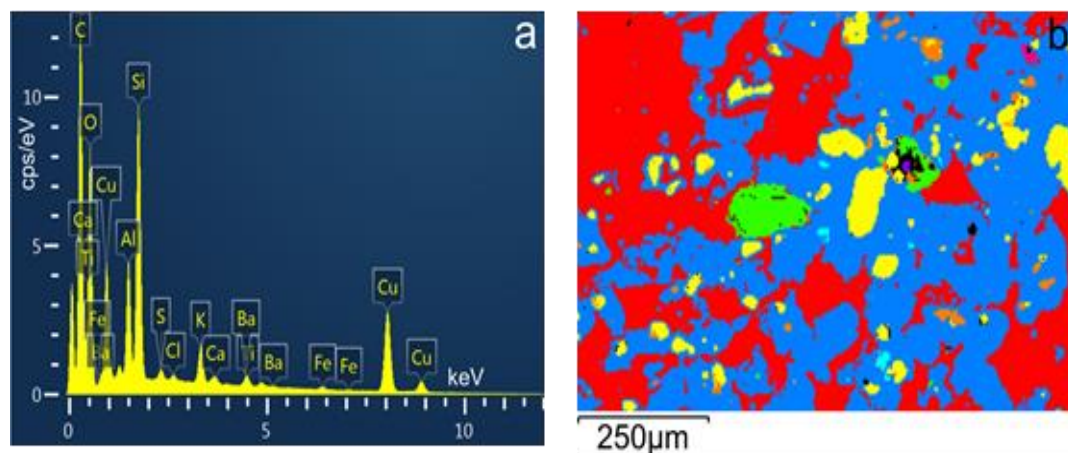


Figure 3. AZ-C-C dosimeter: a) general EDX spectrum, b) SEM-EDX false-color mineral map. Blue = azurite, red = glue, yellow = quartz, orange = aluminum silicates, green = barite, violet = dolomite, pink = iron-bearing oxides/hydroxides, and light blue = KCl phase.

SEM images of blank dosimeters revealed that the coarser pigments were covered with a thin rabbit glue binder layer which conferred a smooth, rounded aspect to the originally sharp edges of azurite particles (Fig. 4a, 4d, 4g). The relatively large pores between individual azurite particles were filled with binder. In the case of dosimeters prepared with finer pigments (AZ-EF-C and AZ-ST-C), discrete pigment particles could rarely be distinguished, thus the paint appeared as a homogeneous mixture of pigments and binder (Fig. 4j, 4m). Additionally some drying cracks were observed in AZ-EF-C (Fig. 4).

The artificial UV-aging test caused severe first- and second-order polygonal cracking in the glue binder present in dosimeters prepared with the coarser pigments (Fig. 4b, 4e, 4h). In contrast, crack formation was very limited in dosimeters containing the finest pigments (Fig. 4k, 4n). Cracks were quantified using image analysis (Table 6). Calculated data showed that the linear crack density decreased with decreasing particle size. Quantification could

not be done in AZ-ST-C since this paint suffered significant superficial binder loss. AZ-EF-C also suffered some binder loss during UV-irradiation. Consequently in both dosimeters discrete azurite particles were distinguished. Moreover, in AZ-ST-C some micro-pitting was observed which has also been detected in stereomicroscopic images (Fig.1n).

Crack formation can be attributed to RH fluctuations during the UV-aging test. It can, to a large degree, be correlated with the binder distribution in paint dosimeters. The accumulation of larger amounts of glue in pores of dosimeters prepared with coarse pigments resulted in severe cracking upon UV-aging. Finer pigment particles ($\phi < 25 \mu\text{m}$, present in e.g. AZ-ST-C), in contrast, facilitated a more homogeneous pigment and binder distribution, thus reducing crack development caused by volume changes of the binder. Cracking, causing an increase in the paint's surface area, further facilitates accelerated chemical and physical attack. Moreover, organic and inorganic particle matter can accumulate in these cracks, enhancing or catalyzing degradation.

After two-year outdoor exposure all paint dosimeters (except AZ-ST-C) suffered severe binder loss. Hence pigments appeared completely uncovered by glue, and thus sharp particle edges, as well as empty pores, could now be observed (Fig. 4c, 4f, 4i, 4l). AZ-ST-C also experienced some superficial binder loss, and likewise, larger azurite particles ($\sim 10 \mu\text{m}$) are now discernible. However, due to the high organic content of this paint, some egg yolk/rabbit glue were still retained and cemented small azurite particles (i.e., $< 1 \mu\text{m}$), which formed compact aggregates (Fig. 4o). Overall, SEM did not reveal any alteration of azurite pigments; only the organic binder (egg yolk or rabbit glue) seemed to have been affected by the artificial UV-aging or the long-term outdoor exposure.

Table 6: Crack formation (linear crack density, mm^{-1}) in paint dosimeters upon UV aging.

Paint dosimeter	Linear crack density
AZ-EC-C-UV	88
AZ-C-C-UV	68
AZ-M-C-UV	51
AZ-EF-C-UV	34
AZ-ST-C-UV	Not available

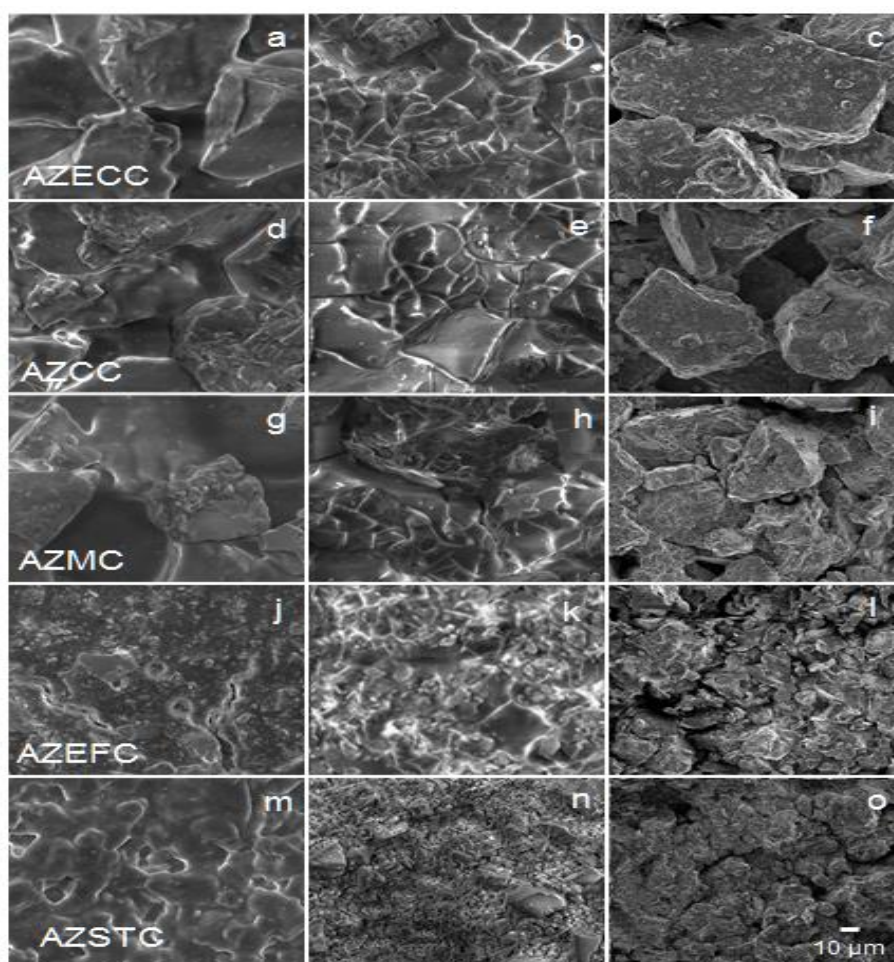


Figure 4. SEM photographs of blank (a, d, g, j, m), UV-aged (b, e, h, k, n) and 2-year outdoor exposed (c, f, i, l, o) azurite-proteinaceous dosimeters.

4.3.6. Chromatic features of paint dosimeters

Spectrophotometry results revealed that L^* and C^* of blank dosimeters generally increased with decreasing particle size of azurite pigments (Table 7). The exception was AZ-ST-C which showed the lowest values ($L^* = 37.12$ and $C^* = 15.82$), in spite of its particle size. This behavior was attributed to its high organic content (both egg yolk and rabbit glue). Diminishing crystal size also induced dosimeters to turn more greenish, since a^* values vary from 2.59 (AZ-EC-C) to -10.13 (AZ-ST-C). Data also showed that AZ-M-C was the bluest sample ($b^* = -32.45$) while AZ-ST-C was the greenest ($a^* = -10.13$). The particularly high a^* value of AZ-ST-C is also attributed to the high organic content, particularly due to the egg yolk amount added during its preparation by the manufacturer. Thus AZ-ST-C is very dissimilar in color parameters to the other dosimeters (see Fig. 1).

Color changes were more severe in dosimeters exposed to 1000 h of artificial UV radiation as compared to samples after two-year outdoor exposure (Fig. 1). The former samples experienced $\Delta E = \sim 10$ to 17 units, which increased with decreasing pigment particle size. This color change was attributed to deterioration of the organic binders added to the azurites, which caused a substantial decrease in a^* and an increase in b^* (i.e., a shift towards green/yellow). However, AZ-ST-C behaved differently and only suffered $\Delta E = 6$ units. In this paint the yellowish color of the original pigment containing $\sim 10\%$ egg yolk, may have partially masked the green/yellow color change induced by rabbit glue aging.

The two-year outdoor exposure of dosimeters resulted in $\Delta E = 4$ to 6 units which could not be correlated with the pigment particle size, and was induced by a decrease in a^* (towards green) and a minor increase in b^* (towards yellow). Moreover L^* increased with decreasing particle size, mostly in AZ-EF-C and AZ-ST-C (values ~ 47); also L^* was in most cases slightly higher than that attained in the UV-aged dosimeters. Again, AZ-ST-C behaved differently, experiencing a $\Delta E = 10$ units caused by a significant increase in L^* which was attributed to the binder/egg yolk loss in the dosimeter's surface, leaving pigments uncovered.

Table 7. Chromatic parameters: luminosity (L^*), a^* and b^* (chromatic coordinates), chroma (C^*), h^* (hue), and their corresponding shift, i.e. ΔL^* (lightness/darkness), Δa^* (redness/greenness), Δb^* (yellowness/blueness), ΔC^* (saturation), and total color variation (ΔE) for blank and aged dosimeters exposed to artificial UV irradiation and outdoor sunlight. Standard deviations are included.

sample	L^*	a^*	b^*	C^*	h^*	ΔL^*	Δa^*	Δb^*	ΔC^*	ΔE
AZ-EC-C	33.11 ±0.22	2.59 ±0.21	-28.26 ±0.28	28.38 ±0.30	275.23 ±0.38					
AZ-C-C	34.70 ±0.26	3.24 ±0.16	-29.54 ±0.38	29.72 ±0.23	276.25 ±0.23					
AZ-M-C	37.28 ±0.20	2.33 ±0.05	-32.45 ±0.22	32.54 ±0.07	274.10 ±0.07					
AZ-EF-C	42.37 ±0.19	-5.82 ±0.05	-29.60 ±0.12	30.17 ±0.13	258.89 ±0.13					
AZ-ST-C	37.12 ±0.03	-10.13 ±0.01	-12.16 ±0.09	15.82 ±0.22	230.20 ±0.22					
AZ-EC-UV	33.19 ±0.48	-2.01 ±0.37	-19.41 ±0.72	19.51 ±0.70	264.06 ±1.19	0.17 ±0.51	-4.60 ±0.36	8.88 ±0.71	-8.89 ±0.69	10.02 ±0.73
AZ-C-UV	35.55 ±0.43	-2.88 ±0.13	-18.52 ±0.30	18.75 ±0.31	261.17 ±0.37	0.93 ±0.43	-6.10 ±0.13	11.03 ±0.29	-10.99 ±0.29	12.65 ±0.25
AZ-M-UV	38.38 0.86	-5.04 0.12	-17.91 0.33	18.61 0.29	254.29 0.60	1.09 0.86	-7.36 0.12	14.54 0.33	-13.93 0.29	16.36 0.38
AZ-EF-UV	45.04 0.25	-11.77 0.23	-13.67 0.26	18.04 0.17	229.26 0.92	2.67 0.25	-5.96 0.23	15.93 0.26	-12.12 0.17	17.22 0.30
AZ-ST-UV	37.99 ±0.49	-11.23 ±0.31	-6.19 ±0.48	12.83 ±0.43	208.85 ±1.66	0.87 ±0.49	-1.10 ±0.31	5.97 ±0.48	-3.00 ±0.43	6.15 ±0.47
AZ-EC-2Y	35.70 ±0.25	0.88 ±0.07	-25.72 ±0.29	25.74 ±0.29	271.96 ±0.17	2.59 ±0.25	-1.71 ±0.07	2.54 ±0.29	-2.64 ±0.29	4.03 ±0.14
AZ-C-2Y	36.69 ±0.20	0.60 ±0.04	-24.55 ±0.27	24.56 ±0.27	271.39 ±0.09	1.99 ±0.20	-2.64 ±0.04	4.99 ±0.27	-5.16 ±0.27	5.99 ±0.18
AZ-M-2Y	36.56 ±0.34	0.15 ±0.13	-27.33 ±0.55	27.33 ±0.55	270.31 ±0.27	-0.72 ±0.34	-2.18 ±0.13	5.12 ±0.55	-5.21 ±0.55	5.62 ±0.59
AZ-EF-2Y	47.70 ±0.43	-6.22 ±0.14	-29.12 ±0.66	29.78 ±0.62	257.94 ±0.53	5.33 ±0.43	-0.40 ±0.14	0.48 ±0.66	-0.39 ±0.62	5.40 ±0.53
AZ-ST-2Y	47.01 ±0.40	-10.99 ±0.32	-11.14 ±0.51	15,65 ±0,58	225.39 ±0.53	9.89 ±0.40	-0.86 ±0.32	1.02 ±0.51	-0.17 ±0.58	10.00 ±0.39

Assuming that color change is mainly caused by binder degradation, the superficial binder loss explains the smaller color change experienced by dosimeters after two-year outdoor exposure, as compared to samples exposed to artificial UV aging where, in general, no important binder loss has been detected.

4.3.7. Raman analysis

Raman analysis was performed on pigments, binder and dosimeters. Low quality spectra were acquired from pure organic rabbit glue binder with the two laser excitations. Results from azurite-glue dosimeters showed that bands corresponding to this binder – appearing in the region between 2800 and 3000 cm^{-1} – were only visible in blank dosimeters when spectra were acquired with the green laser (Fig. 5). These bands, which can be related to the $\nu(\text{CH})$ stretching mode of proteins from the proteinaceous glue, did not appear in any of the aged dosimeters, irrespective of the laser excitation used. Hence ATR-FTIR was used to study in-depth changes taking place within the organic binder (see section 3.8).

Raman spectra of powder pigments were similar in all azurite grades. Moreover, we could not relate the line-width of the Raman band at $\sim 400 \text{ cm}^{-1}$ with particle size as proposed elsewhere [27]. The azurite Raman bands could be detected in blank and aged dosimeters using both lasers. However, bands were better seen with the green laser, despite the high fluorescence compared with that observed in spectra acquired with the red laser. Here we show the Raman spectra of the blank and aged AZ-C-C dosimeters (representative of all samples) acquired with the green laser.

Azurite Raman bands (Fig. 5a) were assigned according to published data [27, 43, 44]. Fig. 5b displays the Raman spectrum of the UV-aged AZ-C-C dosimeter, and shows clearly that fluorescence masks the azurite Raman bands, displaying lower intensity. Also, a shift towards higher wavenumbers is observed in certain azurite bands (i.e. 248, 285, 761, 829, 933 cm^{-1}) up to 1096 cm^{-1} . Above this wavenumber the azurite bands are missing, as are those credited to the organic binder. The patent shift of these bands could be due to a

variation in the chemical bond length of certain bonds in the azurite molecule (causing a structural change) triggered by the UV irradiation.

Fig. 5c shows the Raman spectrum of the outdoor exposed AZ-C-C dosimeter. Here the fluorescence is lower than that found in both the blank and the UV- aged dosimeters. This striking result can easily be explained when observing the SEM images of the corresponding dosimeters (Fig. 4). In all blank and UV-aged dosimeters, the azurite pigments are surrounded by the binder (different extension according to azurite grade), which contributes to Raman fluorescence. In addition, in the UV-aged dosimeters cracks formed (to different degrees, according to crystal size) in the binder. UV-induced protein fragmentation causes an increased amount of short chains which should have contributed to the increase in fluorescence. By contrast, in outdoor aged dosimeters severe binder loss is observed in SEM images, such that uncovered azurite crystals are clearly seen. Thus, the spectra of these dosimeters show the lowest fluorescence and the most intense azurite bands of all dosimeters.

Fig. 5c also reveals that some blue crystals gave spectra where two extra Raman signals appeared at 466 and 1049 cm^{-1} , which correspond to malachite. The Raman spectra of malachite and azurite are very similar. According to literature, the three typical bands of malachite are identified at 435 cm^{-1} corresponding to the lattice modes $T(\text{Cu},\text{CO}_3)$; not seen here), and at 1049 and 1097 cm^{-1} related to the ν_1 symmetric stretching modes (of two different CO_3 groups - doubly degenerate mode) [45].

Malachite is a natural impurity present in azurite mineral. Indeed, in this work malachite has been identified with XRD in all pigments (Table 5). Malachite can also be a weathering product of azurite since it is more stable than azurite under atmospheric conditions [46]. That is, azurite is more prone to oxidation processes, and, in the presence of water slowly transforms into malachite. Malachite is a pseudomorph of azurite that holds the same external form as the original azurite crystal, but the unit cells of azurite are gradually

replaced by those of malachite. Thus, during this process crystals with intermediate chemical compositions between azurite and malachite can be found, as recognized here.

The Raman spectra acquired from paint dosimeters exposed during two-year to the urban atmosphere of Granada, show a mineral phase intermediate in composition between that of azurite and malachite (Fig. 5c), as also found by Salvadó et al [47]. We discount the hypothesis that this intermediate phase was part of the original pigment since it was not found in the blank dosimeters or in the UV-aged ones (Fig. 5). Malachite formation should have been minimal since semi-quantitative XRD analysis (~5%) on two-year aged paints detected no changes compared to the blank dosimeters.

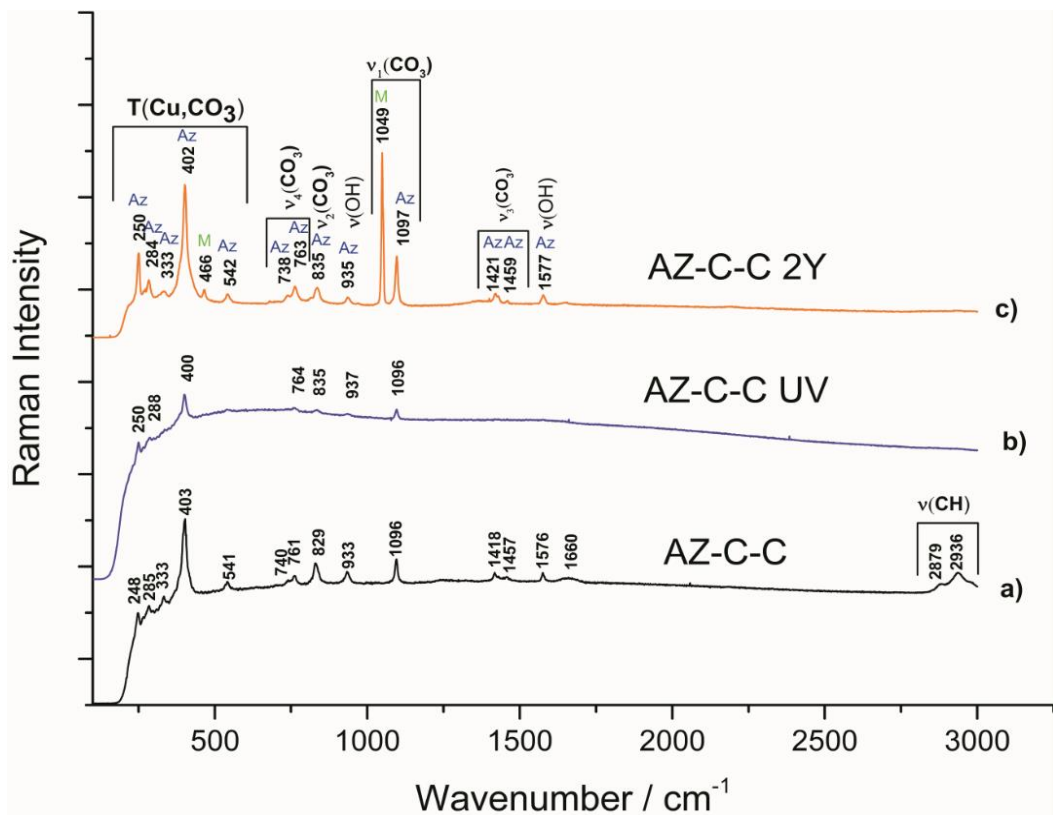


Figure 5. Raman spectra (green laser) of blank, UV-aged and sunlight-aged AZ-C-C dosimeters. T = torsion, M = malachite, Az = azurite.

4.3.8. ATR-FTIR analysis

ATR-FTIR results revealed that the amide I band (carbonyl stretching) and amide II band (N-H bending) of the proteinaceous binder were modified in blank dosimeters. The amide I band at 1627 cm^{-1} shifted to $1640\text{-}1645\text{ cm}^{-1}$ when blended with the different azurite grades (Table 8). This band is caused mainly (~80%) by C=O stretching vibrations of the peptide linkages of amino acids [48], and is absent in pure azurite pigments (see AZ-EC in Fig. 6). The shift corresponds to a blue shift associated with a frequency increase ($\Delta\sigma = 20\text{ cm}^{-1}$) which indicates increased bond strength of C=O groups (i.e., the bond dissociation strength increases) [49].

Table 8. ATR-FTIR wavenumbers of amide I and amide II bands (cm^{-1}) identified on blank, UV-aged, and outdoor-aged glue and paint dosimeters.

Dosimeter	Amide I	Amide II
Rabbit Glue	1627	1529
Rabbit Glue-UV	1628	1531
Rabbit Glue 2Y	1628	1528
AZ-EC-C	1640	1498
AZ-EC-C-UV	1651	1497
AZ-EC-C-2Y	1653 (vw)	1488
AZ-C-C	1642	1494
AZ-C-C-UV	1651	1506
AZ-C-C-2Y	1653 (vw)	1488
AZ-M-C	1642	1502
AZ-M-C-UV	1647	1502
AZ-M-C-2Y	1656 (vw)	1488
AZ-EF-C	1645	1492
AZ-EF-C-UV	1649	1497
AZ-EF-C-2Y	1651	1488
AZ-ST-C	1645	1492
AZ-ST-C-UV	1651	1488
AZ-ST-C-2Y	1653 (vw)	1490

vw = very weak.

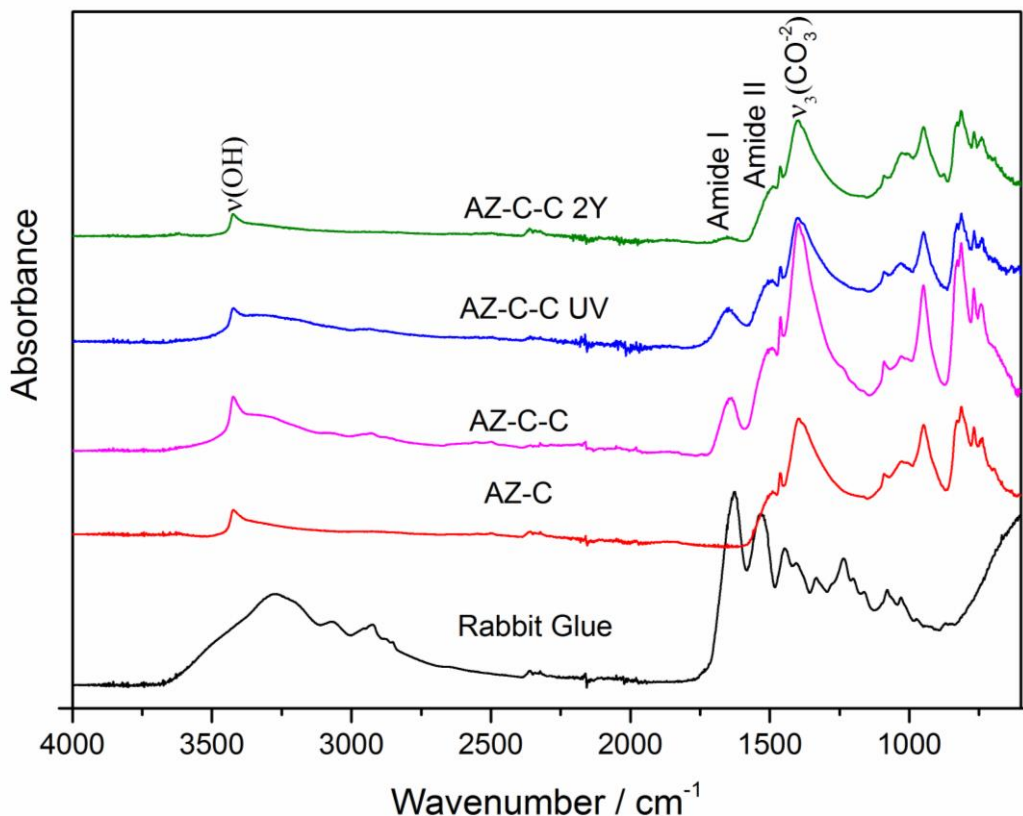


Figure 6. ATR-FTIR spectra of blank rabbit glue, and blank, UV-aged and two year sunlight-aged AZ-EC-C dosimeters.

The frequency of the amide I band, and thus, the bond strength of C=O groups, is influenced by intra- and intermolecular hydrogen bonding of peptides [50]. When a reduction in hydrogen bonds between N-H and C=O groups of protein chains takes place, the frequency increases subsequently. According to Kong and Yu [48] this shift indicates changes in the secondary structure from β -sheets to random coils. Hence, the decrease in hydrogen bonds in the azurite-glue paints, as compared to pure glue, can be explained by the formation of protein-Cu²⁺ complexes occupying N-H groups of the protein chains, thus reducing sites for hydrogen bonding [19]. Our results agree with the findings of Odlyha et al. [18], who stated

that copper catalyzed the oxidation of the egg yolk binder prior to light aging of azurite tempera dosimeters.

FTIR data showed that the amide I band shift was slightly larger in paints prepared with fine grained pigments than with coarser pigments. Although observed differences are small, all pigments followed the same tendency; thus, results suggest that the binder-pigment interaction might have been stronger in the case of fine grained pigments. This seems reasonable considering that smaller pigment particles offer a larger surface area for reaction with amino acids in the glue binder as compared with coarser pigments. On the other hand, the amide II band at 1529 cm^{-1} shifted to $1492\text{-}1502\text{ cm}^{-1}$ when blending the binder with the different azurites (Table 8). The observed significant red shift is considered to be a clear indication of the complexation of Cu^{2+} ions with the amide group, a process that reduces the frequency of the bending vibrations of these C-N bonds through the attachment of heavier atoms [51,52].

Upon UV-exposure for 1000 h, the amide I and amide II bands of the pure rabbit glue dosimeters did not suffer any important shift (Table 8). Thus, the spectra of the blank and UV-aged glue samples are quite similar (Fig. 7). However, changes in the intensity ratio of bands at ~ 1028 and $\sim 1076\text{ cm}^{-1}$, associated with C-O bonds occurred, indicating a modification of the conformational structure of the rabbit glue binder.

The amide I band appearing in the paint dosimeters suffered a shift to higher frequencies (Table 8, Fig. 6), which indicates a decrease in hydrogen bonding due to the UV irradiation. This suggests that the presence of azurite induced the breaking of hydrogen bonds since the position of the amide I band in pure glue did not change. The shift was more noticeable in paint dosimeters made of larger particle size. Note that the breaking of hydrogen bonds will influence the glue's adhesive power and elasticity negatively [53]. These results are in agreement with findings by Ghezzi et al. [54], who also detected changes in the glue's behavior upon mixing with azurite pigment. According to these authors, the glue-azurite mixture showed less thermal stability than pure glue, which they attributed to

conformational changes. In azurite paint dosimeters the amide I band and the band at $\sim 3300\text{ cm}^{-1}$ corresponding to N-H stretching did not change significantly as compared with the blank paint dosimeters (Fig. 6). This suggests that binder loss was limited in paint dosimeters exposed to 1000 h UV radiation, as observed in SEM images.

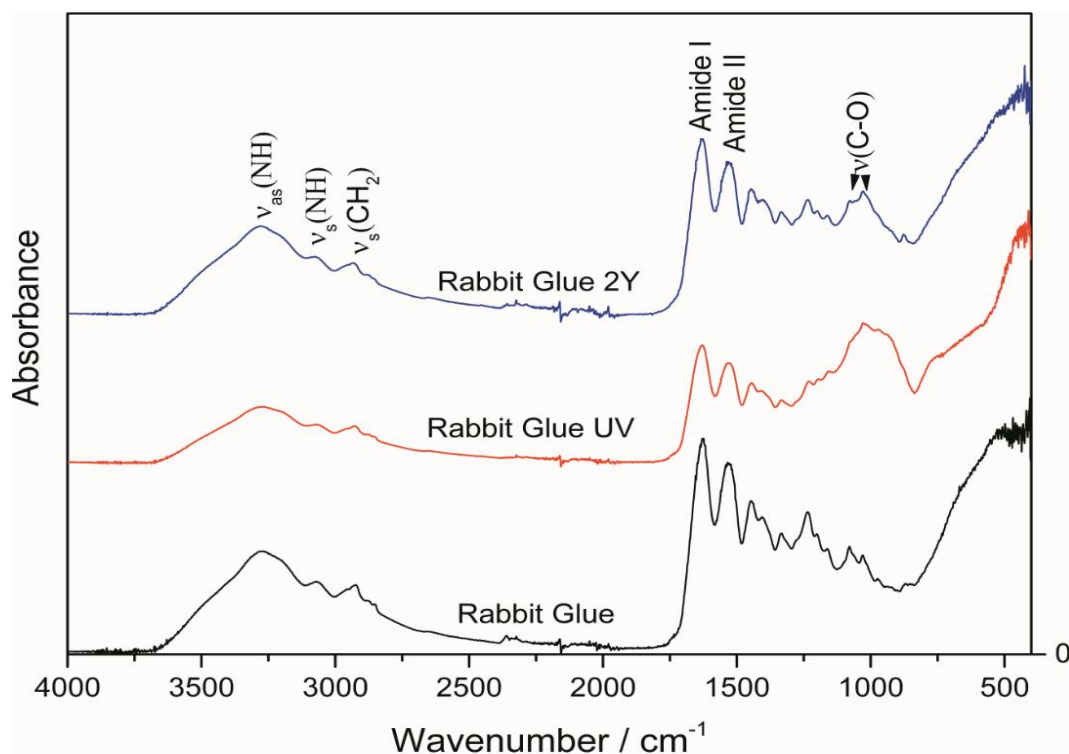


Figure 7. ATR-FTIR spectra of blank, UV-aged and two year sunlight-aged rabbit glue dosimeters.

The two-year outdoor test caused a significant alteration of the rabbit glue binder in the paint dosimeters, as shown by a drastic decrease or even absence of several bands related to peptide linkage (the amide I band and the band at $\sim 3300\text{ cm}^{-1}$) (Fig. 6). These results agree with the stereomicroscopic and SEM observations (Fig. 4c, 4f, 4i, 4l, 4o) and TG results, revealing a severe binder loss in outdoor-exposed dosimeters, which could be attributed to dissolution caused by condensation. Nonetheless, the shifts detected in the

very low intensity amide I bands in outdoor-aged dosimeters were in most cases similar to those detected in the UV-aged dosimeters (Table 8), even though the light exposure duration and irradiance level were significantly higher during the two-year outdoor exposure.

4.4. Conclusions

Particle size influenced the binder distribution in azurite paints, which controlled crack formation in paints during accelerated UV-aging. Paints made of coarse pigments were especially prone to crack formation. Thus we conclude that mixing these pigments with a small quantity of fine-grained azurites (i.e., AZ-EF) would be beneficial to avoid crack formation. Finer grains can fill pore spaces between coarse pigments, preventing large accumulations of rabbit glue, and thus reducing binder volume changes caused by RH and/or T variations. However, the amount added must be kept to a minimum in order to preserve the color properties and limit binder-pigment interactions since, as revealed by FTIR data, interactions were stronger in fine-grained azurite paints leading to conformational structural changes of the binder. Changes in the binder structure are most likely responsible for the color variation towards yellow/green of the UV-aged paints, which was more severe as the pigment particle size decreased, since the binder demand increased.

Overall, color changes of paint dosimeters were related to binder degradation. Although color variations perceptible to human eye were found in all light-aged paints, they were lower in outdoor exposed dosimeters due to binder loss exposing unaltered azurite crystals. However, the identified transformation of azurite into malachite in paints exposed outdoors might add to the color change upon long-term exposure, as well as deposition of calcite particles from soil dust.

Experimental results also show the importance of a detailed characterization of painting materials prior to scientific investigations or applications in conservation treatments. Until

now little has been published in this respect, although optical, chemical and physical properties might vary significantly with impurities or quality variations among different batches of pigments or binders, which will influence pigment-binder interactions, and thus, the paint aging behavior. These aspects deserve special consideration since they will have important implications in the outcome of aging studies and also affect the durability of conservation treatments of (wall)paintings.

Acknowledgements

Financial support was provided by Spanish Research Projects AERIMPACT (CGL2012-30729) and EXPOAIR (P12-FQM-1889), the European Regional Development Fund (ERDF), and the Andalusian Research Groups RNM-179. Analyses were performed in the Scientific Instrumentation Centre (CIC) of the University of Granada (Spain). J.A. Herrera is funded by a Spanish grant from the AERIMPACT Project (ref.BES-2013- 065507), and K. Elert is a post-doctoral researcher in the EXPOAIR Project. The authors thank R. Gutiérrez for helping with the UV-aging test, and A. Kowalski for English revision.

References

- [1] Cardell C, Rodríguez-Simón L, Guerra I, Sánchez-Navas A. Analysis of Nasrid polychrome carpentry at the Hall of the Mexuar palace, Alhambra complex (Granada, Spain) combining microscopic, chromatographic and spectroscopic methods. *Archaeometry* 2009; 51:637-657.
- [2] Comelli D, Nevin A, Valentini G, Osticioli I, Mario Castellucci E, Toniolo L, Gulotta D, Cubeddu R. Insights into Masolino's wall paintings in Castiglione Olona: Advanced reflectance and fluorescence imaging analysis. *J. Cult. Herit.* 2011; 12:11–18.
- [3] Romero-Pastor J, Durán A, Rodríguez-Navarro AB, Van Grieken R, Cardell C. Compositional and quantitative microtextural characterization of historic paintings by means of micro-X-ray diffraction and Raman microscopy. *Anal. Chem.* 2011; 83:8420-8428.
- [4] Gómez-Morón MA, Ortiz P, Martín-Ramírez JM, Ortiz R, Castaing J. A new insight into the vaults of the kings in the Alhambra (Granada, Spain) by combination of portable XRD and XRF. *Microchem. J.* 2016; 125:260–265.
- [5] Durán A, Franquelo ML, Centeno MA, Espejo T, Pérez-Rodríguez JL. Forgery detection on an Arabic illuminated manuscript by micro-Raman and X-ray fluorescence spectroscopy. *J. Raman Spectrosc.* 2011; 42:48–55.
- [6] Hradil D, Píšková A, Hradilová J, Bezdicka P, Lehrberger G, Gerzer S. Mineralogy of bohemian green earth pigment and its microanalytical evidence in historical paintings. *Archaeometry* 2011; 53:563–586.
- [7] Cardell C. Painting materials and technical evolution of Islamic polychrome art of the Nasrid Dynisty in Granada, Spain. In: Hradil D, Hradilová J, editors. *Acta Artis Academica: Knowledge and Experience in the Fine Art*, Prague: Academy of Fine Arts; 2012, p. 9-24.
- [8] Wang N, He L, Egel E, Simon S, Rong B. Complementary analytical methods in identifying gilding and painting techniques of ancient clay-based polychromic sculptures. *Microchem. J.* 2014; 114:125–140.
- [9] Dei L, Ahle A, Baglioni P, Dini D, Ferroni E. Green degradation products of Azurite in wall paintings: identification and conservation treatment. *Stud. Conserv.* 1998; 43:80-88.
- [10] Manzano E, Romero-Pastor J, Navas N, Cardell C. A study of the interaction between rabbit glue binder and blue copper pigment under UV radiation: a spectroscopic and PCA approach. *Vibrat. Spectrosc.* 2010; 53:260-268.

- [11] Anaf W, Trashin S, Schalm O, van Dorp D, Janssens K, De Wael K. Electrochemical photodegradation study of semiconductor pigments: influence of environmental parameters. *Anal. Chem.* 2014; 86:9742–9748.
- [12] Giacometti L, Satta A. Degradation of Cd-yellow paints: Ab initio study of native defects in {10.0} surface CdS. *Microchem. J.* 2016; 126:214–219.
- [13] Herrera Rubia A, Navas N, Cardell C. An evaluation of the impact of urban air pollution on paint dosimeters by tracking changes in the lipid MALDI-TOF mass spectra profile. *Talanta* 2016; 155:53–61.
- [14] Horemans B, Cardell C, Bencs L, Kontozova-Deutsch V, DeWael K, Van Grieken R, Evaluation of airborne particles at the Alhambra monument in Granada, Spain. *Microchem. J.* 2011; 99:429–438.
- [15] Douglas-Jones R, Hughes JJ, Jones S, Yarrow T. Science, value and material decay in the conservation of historic environments. *J. Cult. Herit.* 2016; 21:823-833.
- [16] Mohanu I, Mohanu D, Gomoiu I, Barbu O-H, Fechet R-M, Vlad N, et al. Study of the frescoes in Ionești Govorii wooden church (Romania) using multi-technique investigations. *Microchem. J.* 2016; 126:332–340.
- [17] Bacci M, Picollo M, Porcinai S, Radicati, B. Evaluation of the museum environmental risk by means of tempera-painted dosimeters”, *Thermochim. Acta.* 2000; 365:25-34.
- [18] Odlyha M, Cohen NS, Foster GM, West RH. Dosimetry of paintings: determination of the degree of chemical change in museum exposed test paintings (azurite tempera) by thermal analysis and spectroscopic. *Thermochim. Acta* 2000; 365:53–63.
- [19] Romero-Pastor J, Navas N, Kuckova S, Rodríguez-Navarro AB, Cardell C. Collagen-based proteinaceous binder-pigment interaction study under UV aging conditions by MALDI-TOF-MS and principal component analysis. *J. Mass Spectrom.* 2012; 47:322–330.
- [20] Villafana TE, Delaney JK, Warren WS, Fischer MC. High-resolution, three-dimensional imaging of pigments and supporting paper and textiles. *J. Cult. Herit.* 2016; 20:583-588.
- [21] Ballirano, P, Maras A., In-situ X-ray transmission powder diffraction study of the kinetics of the light induced alteration of realgar (α -As₄S₄). *Eur. J. Miner.* 2006; 18: 589-599.
- [22] Aze S, Vallet JM, Pomey M, Baronnet A, Grauby O, Red lead darkening in wall paintings: natural aging of experimental wall paintings versus artificial aging tests. *Eur. J. Miner.* 2007; 19: 883-890.

- [23] Mazzeo R, Prati S, Quaranta M, Joseph E, Kendix E, Galeotti M. Attenuated total reflection micro FTIR characterisation of pigment–binder interaction in reconstructed paint films. *Anal. Bioanal. Chem.* 2008; 392:65–76.
- [24] Saunders D, Chahine H, Cupitt J. Long-term colour change measurement: some results after twenty years. *National Gallery Techn. Bull.* 1996; 17:81-90.
- [25] Ghelardi E, Degano I, Colombini MP, Mazurek J, Schilling M, Khanjian H, Learner T, A multi-analytical study on the photochemical degradation of synthetic organic pigments. *Dyes and Pigments* 2015; 123: 396-403.
- [26] Mattei E, Vivo G, Santis A, Gaetani C, Pelosi C, Santamaria U. Raman spectroscopic analysis of azurite blackening. *J. Raman Spectrosc.* 2008; 39:302-306.
- [27] Han K, Nam JY, Ji JE, Kang D, Lee H, Baek N, Song Y, Yang IS. Existence of nanoparticles in azurite and malachite pigments by Raman spectroscopy and X-ray diffraction studies. *Dyes and Pigments* 2016; 133:232-237.
- [28] Price M. A Renaissance of Color: Particle Separation and Preparation of Azurite for Use in Oil Painting. *Leonardo* 2000; 33:281–288.
- [29] Gueli AM, Bonfiglio G, Pasquale S, Troja Sebastiano O. Effect of particle size on pigments colour. *Color Research & Application* 2016; DOI: 10.1002/col.22062.
- [30] Manzano E, Bueno AG, González-Casado A, Del Olmo M. Mortars, pigments and binding media of wall paintings in the ‘Carrera del Darro’ in Granada, Spain. *J Cult Herit.* 2000; 1:19–28.
- [31] Eastaugh N, Walsh V, Chaplin T, Siddall R. *Pigment Compendium: A Dictionary and Optical Microscopy of Historic Pigments.* Oxford: Elsevier Butterworth-Heinemann; 2004.
- [32] Kühn H. *Erhaltung und Pflege von Kunstwerken und Antiquitäten 1.* München: Keyserische Verlagsbuchhandlung. 1981.
- [33] Merrifield M. *Original Treatises on the Arts of Painting. v. I.* New York: Dover Publications Inc.; 1967.
- [34] Cennini C. *The Craftsman’s Handbook “Il Libro dell’Arte”.* New York: Dover Publications Inc.; 1968.
- [35] Pacheco F. *Arte de la pintura.* Madrid: Cátedra; 1990.
- [36] *Atlas Weathering Testing Guidebook, Atlas Material Testing Technology, Illinois, USA, 2001.*

[37] Urosevic M, Yebra-Rodríguez A, Sabastián-Pardo E, Cardell C. Black soiling of an architectural limestone during two-year term exposure to urban air in the city of Granada (S Spain). *Sci. Total Env.* 2012; 414:564-575.

[38] Martín-Ramos JD. *Using X Powder: A Software Package for Powder X-Ray Diffraction Analysis.* (GR 1001/04. ISBN 84-609-1497-6) 2004.

[39] AATCC Test Method 173-1989. CMC: Calculation of small colour differences for acceptability. In: *AATCC Technical Manual.* North Carolina: American Association of Textile Chemists and Colorists; 1989.

[40] Mokrzycki WS, Tatol M. Colour change ΔE – A survey. *Machine Graphics and Vision* 2011; 20:383-411.

[41] Karpowicz, A, Aging and deterioration of proteinaceous media. *Stud. Conserv.* 1981; 26:153-160.

[42] Aru M, Burgio L, Rumseu MS., Mineral impurities in azurite pigments: artistic or natural selection. *J. Raman Spectrosc.* 2014; 45:1013-1018.

[43] Frost RL, Martens WN, Rintoul L, Mahmutagic E, Kloprogge JT. Raman spectroscopic study of azurite and malachite at 298 and 77 K. *J. Raman Spectrosc.* 2002; 33: 252-259.

[44] Nakamoto K. *Infrared and Raman Spectra of Inorganic and Coordination Compounds. Part A: Theory and Applications in Inorganic Chemistry.* New York: John Wiley and Sons; 1997.

[45] Buzgar N, Apopei AI. The Raman study on certain carbonates. *Analele Stiintifice ale Universitatii "Al. I. Cuza" - Iasi* 2009; 55:97-112.

[46] Vink B W. Stability relations of malachite and azurite. *Mineral. Magazine.* 1986; 50: 41-47.

[47] Salvadó N, Butí S, Aranda MAG, Pradell T. New insights on blue pigments used in 15th century paintings by synchrotron radiation-based micro-FTIR and XRD. *Anal. Methods* 2014; 6:3610–3621.

[48] Kong J, Yu S. Fourier Transform infrared spectroscopic analysis of protein secondary structures. *Acta Biochim Biophys Sinica* 2007; 39:549-559.

[49] Kirillov SA. Novel approaches in spectroscopy of interparticle inter-actions. Vibrational line profiles and anomalous non-coincidence effects. In: Samios J, Durov VA, editors. *Novel Approaches to the Structure and Dynamics of Liquids: Experiments, Theories and Simulations.* NATO Science Series, The Netherlands: Springer; 2004, p. 193-227.

[50] Zhao J, Shi J, Wang J. Amide-I characteristics of helical β -peptides by linear infrared measurement and computations. *J. Phys. Chem. B* 2014; 118:94-106.

[51] SIAS, *Infrared Spectroscopy (IR)*, Royal Society of Chemistry. 2009.

[52] Jhaumeer-Laulloo S, Bhowon MG, Reddi K. Synthesis and characterization of benzamide metal complexes. *Asian Journal of Chemistry* 2000; 12:1296-1300.

[53] Von Endt DW, Baker MT, The chemistry of filled animal glue systems. In: Bigelow D, editor. *Guided Wood: Conservation and History*, Madison, Conn.: Sound View Press; 199, p. 155-162. 1991

[54] Ghezzi L, Duce C, Bernazzani L, Bramanti E, Perla Colombini M, Tiné MR, Bonaduce H. Interaction between inorganic pigments and rabbit skin glue in reference paint reconstructions. *J. Thermal Calor.* 2015; 122:315-322.

Capítulo 5

Effect of proteinaceous binder on pollution-induced sulfation of lime-based tempera paints

A. Herrera¹, C. Cardell¹, J. S. Pozo-Antonio², Alejandro Burgos-Cara^{1,3} and K Eiert^{1*}

(1) Dept. of Mineralogy and Petrology, Faculty of Science, University of Granada, Campus Fuentenueva s/n, 18071 Granada, Spain.

(2) Dept. de Enxeñaría de Recursos Naturais e Medio Ambiente. Escola de Enxeñaría de Minas e Enerxía. University of Vigo, 36310 Vigo, Spain.

(3) Sensient Colors UK Ltd., Oldmedow Road, King's Lynn, Norfolk, PE30 4LA, UK.

Progress in Organic Coatings

Article history:

Under review

Hipótesis de partida

Desde hace décadas se reconoce que la polución atmosférica es una de las causas más importantes de alteración del patrimonio histórico construido. Uno de los ejemplos clásicos de deterioro inducido por la contaminación atmosférica es el desarrollo de costras (negras) de yeso en calizas y morteros de cal debido a la sulfatación de la calcita. A pesar de que los niveles de SO_2 se han reducido hasta un ca. 75 % en los países Europeos desde 1990, la sulfatación de materiales pétreos sigue siendo un gran problema, que afecta principalmente a monumentos localizados en áreas urbanas, pero también a obras de arte pictóricas expuestas a la intemperie. En este sentido, mientras que la literatura ha abordado la sulfatación de los enlucidos de cal preparatorios de la pintura mural, poco se conoce, en concreto, sobre los efectos del SO_2 en pinturas murales propiamente dichas, elaboradas con pigmentos inorgánicos a base de cal y aglutinantes orgánicos proteicos.

Objetivos de la investigación

Investigar en profundidad el efecto que tienen atmósferas contaminadas en SO_2 en pinturas artísticas elaboradas al temple mediante mezcla de un aglutinante proteico y un pigmento elaborado con cal (calcita y/o portlandita), prestando especial interés en la contribución que tienen la naturaleza del pigmento y la presencia o ausencia del aglutinante, en los posibles procesos de sulfatación de la pintura. Para tal fin se comparan los resultados obtenidos en dosímetros pictóricos envejecimiento de forma natural, tras exposición de 40 meses a la intemperie en diversos monumentos (semi)-abiertos de Granada capital, y envejecidos de forma acelerada mediante ensayo de SO_2 en el laboratorio.

Abstract

Even though, atmospheric SO₂ contamination has been reduced over the last decades in Europe, practical experience has shown that sulfation of lime-based materials (i.e., lime-based tempera paint, lime mortar and plaster, as well as limestone) is still of importance, affecting monuments exposed to polluted air in urban centers. In order to evaluate the effect of organic binders (i.e., rabbit glue or egg yolk) on the chemical weathering resistance of lime-based materials, tempera paint dosimeters (i.e., paints containing calcite or mixtures of portlandite and calcite) were subjected to long-term outdoor exposure and accelerated SO₂-aging. Accelerated-aging test results revealed that sulfation was significantly delayed in the presence of the organic binder. Furthermore, paints containing portlandite and calcite transformed faster into calcium sulfite hemihydrate and gypsum than paints containing only calcite. Calcium sulfite hemihydrate formation onto calcite always preceded non-epitaxial gypsum crystallization after dissolution of the sulfite precursor phase. These results suggest that a passivating product layer will not form onto calcite, and so sulfation will continue under suitable environmental conditions until all calcite is transformed into gypsum. However, the organic binder strongly affected the mineralogical evolution of paints containing portlandite (*Bianco di San Giovanni*), resulting in the formation of organic-inorganic hybrid materials similar to biominerals with superior weathering resistance which did not show any clear signs of sulfation after prolonged outdoor exposure. The selection of lime-based tempera paints for conservation interventions must be made considering the prevailing exposure conditions. In polluted dry environments where carbonation of portlandite will be significantly delayed, the use of calcite-based tempera paints might be preferable, while tempera paints prepared with Bianco di San Giovanni (i.e., mixture of portlandite and calcite) would be more suitable in humid climates where carbonation is fast, resulting in the formation of weather resistant hybrid materials.

5.1. Introduction

For decades atmospheric pollution has been recognized as one of the mayor threats to cultural heritage (Schaffer, 1932). More recently, scientists have established that the damaging effects of pollution are enhanced by climate change, affecting a wide range of materials of the built heritage (Smith et al. 2008, Patrón et al., 2017). One of the classical examples of pollution-induced deterioration includes the formation of gypsum-rich black-crusts on limestone and lime mortars due to sulfation of calcite (Rodriguez Navarro and Sebastian, 1996; Maravelaki-Kalaitzaki, 2005, Török, 2008, Cultrone et al., 2008).

Even though, SO₂ concentration has been reduced drastically by ~75% since 1990 according to the European Environment agency (European Environment Agency 2013a), pollution-induced sulfation is still affecting monuments located in polluted metropolitan areas (Urosevic et al., 2012). Actually, some experts suggest that there might not be any safe threshold and that resulfation of previously cleaned monuments could occur relatively rapidly. The formation of gypsum crusts is well documented for many monuments and historic buildings in Granada (southern Spain) (Rodriguez Navarro and Sebastian, 1996). However, sulfation is not limited to building materials and also affects painting materials. Sayre et al. (1963) detected large amounts of gypsum (CaSO₄·2H₂O) in decayed lime plaster from the Giotto frescoes in the Scrovegni Chapel, Italy, which they identified as a reaction product of calcium carbonate with atmospheric sulfur oxides (i.e., sulfur di- and trioxide) in the presence of moisture. While some research has been dedicated to the sulfation of pure lime in wall paintings (Sayre et al., 1963, Zehnder, 1996), little is known on the effect of atmospheric SO₂ on lime-based binary systems, such as tempera paints, which contain an inorganic pigment and an organic binder.

Tempera paints applied in the fresco-secco technique have been extensively used in southern Spain and important examples include the wall paintings of the Hospital of “San Juan de Dios” located in semi-open courtyards or the mural paintings of the Alhambra and the Moorish quarter (Albaycin, Granada) (Capitán-Vallvey et al., 1993; Manzano et al.,

2000). These wall paintings are exposed to relatively high levels of atmospheric pollution (Kontozova-Deutsch et al., 2011; Urosevic et al., 2012). The high porosity of tempera paints and the underlying mortars make wall paintings very vulnerable to pollution-induced chemical weathering. Common damage patterns observed upon crystallization of gypsum include disaggregation, microflaking, and the formation of surface bloom (Matteini, 1991).

In order to get a better insight into SO₂-induced deterioration of lime-based tempera paints, paint dosimeters were exposed outdoors for 40 months in the historic city center of Granada. A second set of dosimeters was exposed to an accelerated SO₂-aging test to further study mineralogical and morphological changes upon sulfation of lime-based pigments in the presence and absence of an organic binder (i.e., rabbit glue and egg yolk). To this end a wide range of analytical techniques were applied, including x-ray diffraction (XRD), laser particle size analysis, nitrogen adsorption, field emission scanning electron microscopy (FESEM), Raman spectroscopy, and spectrophotometry. Analytical results revealed a significant effect of the organic binders on the mineralogical evolution of lime-based tempera paints and their susceptibility to sulfation. The outcome of this investigation furthers the understanding of the chemical weathering process of lime-based tempera paints and allows for recommendations regarding the selection and preparation of adequate materials, not only for paintings conservation but also for applications involving the use of lime mortars or plasters exposed to polluted urban air.

5.2. Materials and Methods

5.2.1. Pigments and binders

Three different lime-based pigments of different grain size (see Table 1) were purchased from Kremer Pigment GmbH & Co. (Germany): *Bianco di San Giovanni* standard (Ref. 11415) with a mean particle size of ~60 µm, *Bianco di San Giovanni* coarse (Ref. 11416) with a mean particle size of ~120 µm, and extrafine calcite (Ref. 58720) with mean particle size of ~25 µm (Elert et al. 2018). Note that *Bianco di San Giovanni* has been historically

prepared by sun-drying small “cakes” of slaked lime in order to obtain a partial carbonation of portlandite upon reaction with atmospheric CO₂ (Cennini, 1988). Consequently, these pigments contain a mixture of calcium carbonate (i.e. calcite, CaCO₃) and calcium hydroxide (i.e. portlandite, Ca(OH)₂). Pigments were mixed with two different organic binders: rabbit glue (Ref. 63028, Kremer Pigment GmbH & Co) or locally purchased egg yolk.

5.2.2. Preparation of paint dosimeters

Paint dosimeters were prepared following traditional recipes in order to mimic the egg yolk- and rabbit glue-based tempera paints used by medieval artists (Pacheco, 1990). These techniques are based on the mixing of white pigments with the aforementioned proteinaceous binders in varying amounts in order to obtain paints with adequate consistency. For details regarding the preparation of egg yolk- and rabbit glue-based paints see Herrera et al. (2016) and Cardell et al. (2017), respectively. Freshly prepared paints were spread directly onto glass slides with a paintbrush. The paint was applied in several layers once the previous layer was completely dry.

For the accelerated SO₂-aging test a second set of samples was prepared with a fixed water-pigment-rabbit glue ratio of 2:1:0.1 wt/wt. Paints prepared with analytical grade calcium hydroxide (Ca(OH)₂, Guinama S.L.U., Spain) and calcium carbonate (CaCO₃, Labkem, Spain) were included in this study as reference materials. The former was also prepared without the addition of rabbit glue, maintaining the same water-pigment ratio. Note that only samples prepared with rabbit glue were included in the accelerated SO₂-aging test because they can be expected to be more susceptible to chemical weathering than their egg yolk-based counterparts. Dosimeters were labeled by adding to the pigments label the letter EY for egg yolk-based paints, RG for rabbit glue-based paints, and H₂O for dosimeters prepared with water. See Table 1 for the complete nomenclature of samples.

Table 1. Nomenclature of samples

Pigments	Material
CA-EF	Extrafine calcite
BSG-ST	Bianco di San Giovanni (standard)
BSG-C	Bianco di San Giovanni (coarse)
CaCO ₃	Analytical grade calcium carbonate (calcite)
Ca(OH) ₂	Analytical grade calcium hydroxide (portlandite)
Outdoor-exposed dosimeters	Test duration
CA-EF-EY*	6, 12, 24, 36, 40 months
BSG-ST-EY	
BSG-C-EY	
CA-EF-RG*	
BSG-ST-RG	
BSG-C-RG	
SO ₂ -aged dosimeters	Test duration
CA-EF-RG	5, 10, 34, 82, 240 h
BSG-ST-RG	
BSG-C-RG	
CaCO ₃ -RG	
Ca(OH) ₂ -RG	
Ca(OH) ₂ -H ₂ O*	

* Paint dosimeters prepared with egg yolk (EY), rabbit glue (RG), or deionized water (H₂O).

5.2.3. Outdoor exposure test

Dosimeters were placed vertically in an exterior eave of the Hospital of San Juan de Dios in Granada which faces SW and is adjacent to a highly trafficked street. Samples were exposed for up to 40 months (i.e., from January 2014 to July 2017) to direct sunlight but partially protected from rain. Sunlight exposure was ~10 h in summer and ~5 h in winter, the maximum T being 40 °C in summer and the minimum T being -3 °C in winter. The climate

in Granada is characterized by significant diurnal T and RH variations of 20 °C and 50%, respectively. Average RH is ~40% in summer and ~75% in winter (Velilla, 2017). Granada is a non-industrialized city surrounded by up to 3500 m high mountains. As a result of its topography, low wind speeds, heavy traffic and intensive construction work, O_3 and particulate matter frequently exceeded the threshold values set by the EU directive 2008/50EC and the World Health Organization (WHO) (Urosevic et al., 2012; Ecologistas en Acción, 2015-2017). Even though, SO_2 concentration was below the limit established by the Directive 2008/50/EC it exceeded that recommended by the WHO in several occasions (Ecologistas en Acción, 2015-2017). Moreover, based on the annual mean concentration (i.e., 11.85 $\mu\text{g}/\text{m}^3$ SO_2 in 2013), Granada is among the cities with the highest SO_2 contamination in Western Europe according to the European Environment agency (European Environment Agency 2013b). Data on average concentrations of atmospheric contaminants during the outdoor exposure test are reported in Table 2. Previous studies (Rodríguez-Navarro and Sebastian 1996, Horemans et al. 2011, Kontozova-Deutsch et al., 2011, Urosevic et al., 2012,) showed that atmospheric particulate matter was primarily constituted of soil dust (quartz, calcite, dolomite, gypsum, phyllosilicates, iron oxides/hydroxides), antropogenic black and organic carbon, metallic particles from fossil fuels, and sea salt.

Table 2. Average air contamination values (NO_2 , O_3 , SO_2 , and particulate matter (PM_{10} and $PM_{2.5}$) during the outdoor exposure of dosimeters in the city center of Granada (Ecologistas en acción 2014-16).

Year	NO ₂	O ₃		SO ₂	PM ₁₀		PM _{2.5}	
	Annual average	8 hours values	8 hours values	Daily value	Annual average	Daily value	Annual average	Daily value
	µg/m ³	Nº days >120µg/m ³	Nº days >100 µg/m ³	Nº days >20 µg/m ³	µg/m ³	Nº days >50 µg./m ³	µg/m ³	Nº days >25 µg/m ³
	Dir.*: max=40 WHO**: max=40	Dir.: max=25	-	Dir.: max=35 WHO: max=3	Dir.: max=40 WHO: max=20	Dir.: max=35 WHO: max=3	Dir.: max=20 WHO: max=10	Dir.: max=20 WHO: max=3
2014	32	15	76	2	25	2	11	5
2015	36	17	85	17	33	8	15	16
2016	36	12	76	4	33	7	12	8

* Dir. = Directive 2008/50/EC** WHO = recommendations issued by the World Health Organizations (Grey color indicates values which exceed the threshold values set by the WHO)

5.2.4 Accelerated SO₂-aging test

Currently, no specific normative for accelerated SO₂-aging tests of pictorial samples is available. For this reason a test method used for the determination of the resistance of natural stone to SO₂-induced aging in the presence of high humidity (AENOR, Madrid 2003) was adapted. To this end, samples were enclosed in a hermetically sealed plastic container (7.5 l) together with diluted sulfurous acid (1.35 wt% SO₂, 104 ml) to generate a saturated SO₂ atmosphere and ~100% RH. The container was maintained at a 45° angle during testing in order to facilitate the run-off of condensation droplets accumulating at the container ceiling, which would otherwise have impacted the paint dosimeters. Samples were placed on a grid above the diluted acid and kept in the container for a total of 82 h. The mineralogical evolution was monitored by XRD after 5, 10, 34, and 82 h. Each time the container was opened the acid solution was replaced to assure a saturated SO₂ atmosphere.

5.2.5. Analytical techniques

X-ray diffraction (X'Pert PRO PANalytical B.V.) was used to determine the mineralogical composition of blank dosimeters and to identify compositional changes in outdoor-exposed/SO₂-aged samples. Analyses were performed using Cu-K α radiation, Ni filter, 45 kV voltage, 40 mA intensity and spinner. The exploration range was 3 to 60 °2 θ and goniometer speed 0.05 °2 θ s⁻¹. Identification and semi-quantification (± 5 wt%) of minerals were carried out using Xpovder software (Martin Ramos 2004).

Nitrogen sorption isotherms of powdered pigment samples were obtained at 77 K on a TriStar 3000 (Micromeritics) and the specific surface area was determined applying the BET method (Brunauer et al., 1938). About 0.2 g of sample was degassed at 80 °C for 24 h prior to analysis using a sample degas system (VacPrep 061, Micromeritics).

Textural changes were studied using an optical microscope (Leica DVM2000) with 50-400x lens. The data were processed using the Leica Application Suite v3.8.0 (Leica Microsystems©).

Color parameters of blanks and dosimeters exposed outdoors for 1, 6, 12, 24, and 40 months were measured with a Minolta CM-700d portable spectrophotometer using a 10° observer, 8 mm measuring aperture, and standard daylight illuminant D65 (color temperature: 6504 K). Data were expressed in CIEL*a*b* color space, where L* is luminosity or lightness (black = 0 and white = 100); a* from +a* (red) to -a* (green), and b* from +b* (yellow) to -b* (blue). Color changes were expressed as ΔL^* , Δa^* , Δb^* , and ΔE^* ($\Delta E^* = (\Delta L^{*2} + \Delta a^{*2} + \Delta b^{*2})^{1/2}$) (CIE S014-4, 2007). Average values based on two measurements are reported. Note that ΔE^* higher than three units is considered the threshold of perceptible detection for the human eye (Berns, 2000).

Morphological features and chemical composition of blank and exposed dosimeters were studied by means of a Field Emission Scanning Electron Microscopy (FESEM, Auriga, Carl Zeiss, Germany) working at 10⁻⁴ Pa vacuum and 3 kV in secondary electron imaging mode.

Samples were carbon coated. Additionally, elemental mapping was performed using a Supra 40Vp (FESEM, Carl Zeiss-Germany equipped with an Aztec 3 EDX and X-Max 50 mm detector). The working conditions were: 40-66 Pa vacuum, 15-20 kV beam accelerating voltage. High-resolution X-ray maps (1024 x 768 pixels) from selected areas of uncoated samples were obtained using 100 frames, a dwell time of 10 ms (2.5 h acquisition), 3 nA filament current, and 20 eV/ch resolution.

Micro-Raman analysis was performed using a Jasco NRS-5100 confocal Raman spectrometer in order to detect possible compositional changes in paint dosimeters upon outdoor exposure and accelerated SO₂-aging. Spectra were recorded by placing the samples on the OLYMPUS microscope stage and observing them with a 20x objective. Samples were excited with a solid state Torsana Starbright laser (785 nm). A series of recorded spectra (n = 6-10) were collected from each sample spot and averaged, with exposure times from 60 to 90 s (100 % power). The Raman signal was collected in a 180° backscattering geometry by a Charge Coupled Device (CCD) after having passed through a 50 μm entrance slit. The Raman spectra were recorded in the 3000-100 cm⁻¹ range with a spectral resolution of 1.6 cm⁻¹. The Raman spectra were processed using JASCO Spectra Manager™ II software.

5.3. Results and Discussion

5.3.1. XRD analysis of pigments and dosimeters before and after accelerated SO₂-aging test and outdoor exposure

Pigments

Semiquantitative XRD analyses showed that BSG pigments contained ~15 wt% calcite and ~85 wt% portlandite. The analytical grade Ca(OH)₂ contained >95 wt% portlandite and a small amount of calcite (<5 wt%). The CA-EF pigment contained mainly calcite and ~10 wt% dolomite (CaMg(CO₃)₂), while analytical grade calcite revealed no detectable impurities.

Paint dosimeters

The mineralogical composition of BSG-based paints did not change significantly upon mixing with either egg yolk or rabbit glue (i.e., the amount of newly formed calcite due to the carbonation of portlandite was below the detection limit (~5 wt%) of this technique, and the possible formation of amorphous calcium carbonate cannot be detected with XRD. Paint dosimeters recently prepared with analytical grade Ca(OH)_2 and dried for 2 days under laboratory conditions contained 70 wt% calcite and 30 wt% portlandite in the absence of rabbit glue, and only 15 wt% calcite and 85 wt% portlandite in its presence. The later results indicate that the presence of rabbit glue resulted in an important delay in carbonation by the formation of a superficial film around portlandite particles, which hindered the diffusion of ambient CO_2 to the carbonation front (Elert et al. 2018). CA-EF-based paints only contained calcite and dolomite, which underwent only minor dissolution/precipitation upon paint preparation. Consequently, no mineralogical changes were detected upon paint preparation.

Outdoor exposure

During outdoor exposure, BSG-based paints suffered important compositional changes. In samples prepared with rabbit glue an almost complete carbonation was observed after 6 months, and only trace amounts of portlandite were detected (Fig. 1a). Egg yolk binder, on the other hand, partially inhibited carbonation, and BSG-ST-EY and BSG-C-EY dosimeters still contained 45 and 30 wt% portlandite, respectively. It is known that egg yolk transforms into a fairly water- and weathering resistant binder over time (Kühn 1981). Apparently, the egg yolk was more efficient in forming a long lasting superficial film around portlandite particles and impeded the diffusion of ambient CO_2 as compared to the more water soluble rabbit glue. After 1-year exposure of the BSG-based paints carbonation was generally completed with the exception of paints prepared with BSG-ST and egg yolk, where a trace amount of portlandite was still present. After 2 years of outdoor exposure, however, portlandite was no longer detected in any of the tempera paint samples. The presence of

portlandite has an important effect on the susceptibility of these paints towards sulfation as revealed by accelerated SO_2 -aging test results, increasing the rate of transformation (see below). CA-EF-based paints, in contrast, showed only small mineralogical changes over the course of the outdoor exposure (Fig. 1b).

In the majority of outdoor exposed paint dosimeters small amounts of quartz, dolomite, and clay minerals (note that CA-EF originally contained dolomite as an impurity) were detected, which originated from the deposition of atmospheric particulate matter and increased in concentration over time (Fig. 1b). The concentration of gypsum was generally below the XRD detection limit. Only in CA-EF-EY a small amount of gypsum was detected, which might either originate from the deposition of particulate matter (i.e., gypsum being part of the soil dust) or from sulfation of the calcite-based pigment by atmospheric SO_2 .

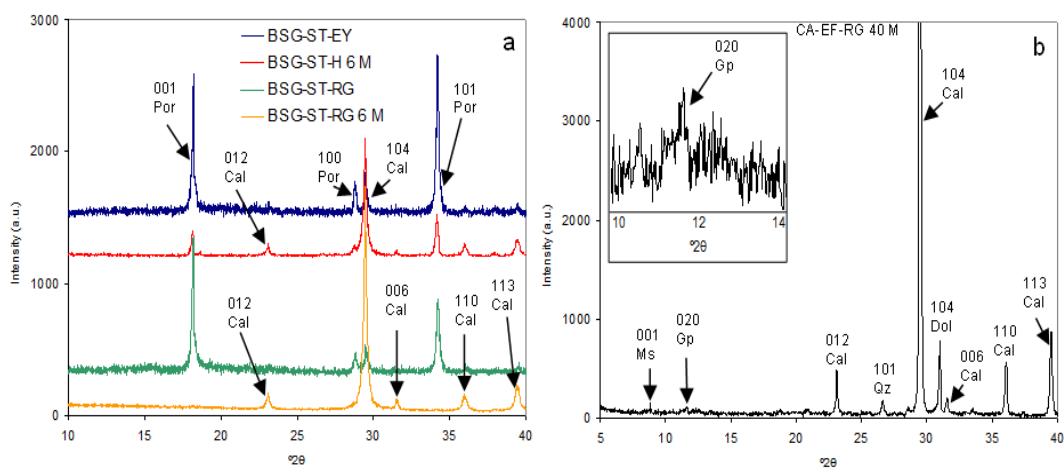


Fig.1. XRD patterns of outdoor-exposed paints; a) BSG-ST-RG dosimeter before and after 6-month exposure; b) CA-EF-RG paint exposed for 40 months. Inset shows detail of the 020 reflection of gypsum. Por = portlandite, Cal = calcite, Gp = gypsum, Ms = unspecified mica, and Qz = quartz. See Table 1 for acronyms.

Accelerated SO₂-aging test

Results of the accelerated SO₂-aging test evidenced the important role of the mineralogical composition of lime-based tempera paints on the susceptibility to sulfation (Table 3; Fig. 1, supplementary material Appendix III). Paints originally containing 85 wt% portlandite and 15 wt% calcite (i.e., BSG-ST- and BSG-C-based paints) suffered a more rapid sulfation as compared to paints only containing calcite (Table 3). Note that CaCO₃-RG paint followed the same trend as CA-EF-RG paint, and only data for the later sample are shown here as a representative example. During the first stage of sulfation only calcium sulfite hemihydrate (CaSO₃·0.5H₂O) was detected in all dosimeters. Note that calcium sulfite has long been recognized as an intermediate product during sulfation, eventually transforming into gypsum (Amoroso and Fassina, 1983). After 82 h of exposure, gypsum was indeed observed additional to calcium sulfite hydrate in BSG-based paints. In these paints only trace amounts of portlandite and calcite remained (Table 3). In both calcite-based paints, in contrast, only calcium sulfite hemihydrate was detected after 82 h. The relative broadness of the Bragg peaks of this phase suggests its low crystallinity (Fig. 1, supplementary material Appendix II), which is in agreement with FESEM observation showing its nanogranular morphology (see below). At the end of the test calcite-based paints still contained ~80 wt% calcite. This result is not surprising because portlandite is much more hygroscopic and soluble than calcite and, thus, reacts more readily with ambient SO₂ to form calcium sulfite/sulfate; a reaction which only occurs in the presence of water or sufficiently high relative humidity levels (Camuffo et al., 1984, Charola and Ware, 2002). Cultrone et al. (2008) already recognized the important role of portlandite in the fixation of SO₂ as sulfates. According to these authors, the high pH created by the dissolution of portlandite would facilitate SO₂ absorption and hydrolysis, leading to the formation of sulfite and subsequent oxidation to sulfate ions, which react with Ca²⁺ and, ultimately, precipitate as gypsum.

Experimental results also revealed the important influence of the organic binder on the susceptibility to sulfation. In the presence of rabbit glue, ~50 wt% of portlandite

transformed into 25 wt% calcium sulfite hemihydrate and 25 wt% calcite after 34 h SO₂-aging, in the case of the sample prepared with analytical grade Ca(OH)₂ (Table 3). In the absence of rabbit glue, in contrast, only 20 wt% of calcite remained and portlandite completely transformed into calcium sulfite hemihydrate. After 82 h, the sample Ca(OH)₂-H₂O contained ~10 wt% gypsum additional to 85 wt% calcium sulfite hemihydrate and 5 wt% calcite, whereas gypsum had not formed in the Ca(OH)₂-RG sample (Table 3). Note that the blank Ca(OH)₂-RG sample contained 85 wt% portlandite at the beginning of the accelerated SO₂-aging test and, based on its mineralogical composition, should have been more susceptible to sulfation than the corresponding sample mixed with water (Ca(OH)₂-H₂O), which contained 70 wt% calcite at the start of the ageing test. However, the organic binder acted as a barrier by creating a superficial film around pigment particles, which hindered the access of water and SO₂ to the calcite and/or portlandite surfaces. For sulfation to take place, water in direct contact with the calcite/portlandite surface is needed to induce the absorption and hydrolysis (and oxidation) of SO₂, and the dissolution of the substrate (i.e., source of Ca ions), in order to reach supersaturation with respect to calcium sulfite hemihydrate and/or gypsum. Over time, the rabbit glue suffered hydrolysis and dissolution as a result of the atmosphere's high RH and high SO₂ concentration, and was no longer effective as a barrier (Tsugita and Scheffler, 1982). Consequently, sulfation could progress at a faster rate (Table 3).

Effect of proteinaceous binder on pollution-induced sulfation

Table 3. Mineralogical evolution (wt%) based on semiquantitative XRD analysis of paint dosimeters during accelerated SO₂-aging (See Table 1 for acronyms).

Sample	Mineral phase and JCPDS* card number				
	Calcite (721652)	Portlandite (892779)	Dolomite (841208)	Calcium sulfite hemihydrate (840962)	Gypsum (741905)
BSG-ST-RG	15	85	-	-	-
BSG-ST-RG-34 h	20	60	-	20	-
BSG-ST-RG-82 h	Tr	Tr	-	40	60
BSG-C-RG	15	85	-	-	-
BSG-C-RG-34 h	35	50	-	15	-
BSG-C-RG-82 h	Tr	Tr	-	35	65
CA-EF-RG	90	-	10	-	-
CA-EF-RG-34 h	80	-	10	10	-
CA-EF-RG-82 h	80	-	5	15	-
Ca(OH) ₂ -RG	15	85	-	-	-
Ca(OH) ₂ -RG-34 h	25	50	-	25	-
Ca(OH) ₂ -RG-82 h	5	-	-	95	-
Ca(OH) ₂ -H ₂ O	70	30	-	-	-
Ca(OH) ₂ -H ₂ O-34 h	20	-	-	80	-
Ca(OH) ₂ -H ₂ O-82 h	5	-	-	85	10

JCPDS = Joint Committee on Powder Diffraction Standards

Tr = trace

5.3.2. Optical microscope study of blank and outdoor exposed dosimeters

Microscopic observations of blank dosimeters showed the influence of the pigment particle size on the surface roughness, coarser pigments leading to rougher, more irregular surfaces (Fig. 2). In paints prepared with the finest pigment (CA-EF) some large circular pockmarks were observed on the paint surface, which were relics of air bubbles (arrows in Fig. 2a and c). Generally, paints prepared with egg yolk had a more yellowish tint due to the strong yellow color of the binder.

On the surface of all outdoor-exposed dosimeters a large amount of dark brownish and yellowish particles was observed, which originated from deposited atmospheric particulate matter after 40 months of exposure. Elemental x-ray mapping allowed the identification of deposited particles as quartz, aluminosilicates, iron-bearing oxides/hydroxides, and dolomite (see below). The amount of deposited particles depended on the paint's surface roughness, a larger amount of deposited particles accumulating on rougher surfaces. Charola and Ware (2002) also recognized the relationship between surface roughness and amount of deposited pollutants (i.e., gases and particles). They further stated that deposition would be facilitated by a high surface moisture content. Actually, surface moisture will be higher in BSG-based paints, containing an important amount of portlandite, which is more hygroscopic than calcite (Beruto et al., 2005). Deposited particulate matter plays an important role in the acid-induced degradation of carbonate material such as limestone, lime mortar, and lime-based tempera paints. On the one hand, carbonaceous particles contribute to the dry deposition of SO₂ as a result of their high surface area (Charola and Ware, 2002). On the other hand, metallic particles (especially iron oxides/hydroxide) facilitate catalytic oxidation of SO₂ in the presence of humidity, resulting in the formation of sulfuric acid. The acid, in turn, will react with the calcium carbonate in the substrate and lead to the formation of calcium sulfates (Rodríguez-Navarro and Sebastian, 1996).

The paint sample prepared with CA-EF suffered severe material loss regardless of binder type due to the periodic impact of rain (Fig. 2b and d), whereas paints prepared with BSG pigments appeared intact (Fig. 2f, h, j, and l). It has been demonstrated previously (Elert et al. 2018), that in the case of tempera paints prepared with BSG pigments (i.e., pigments containing ~85 wt% portlandite), pigment-binder interactions during carbonation lead to the formation of an organic-inorganic hybrid material similar to biominerals with high weathering resistance. In calcite-based paints (CA-EF), in contrast, no such pigment-binder interactions occurred and the paint disintegrated upon dissolution and leaching of the organic binder impacted by rain. As a consequence, part of the deposited particulate

matter was also washed away and hardly any yellowish and brownish particles were observed (Fig. 2b and d).

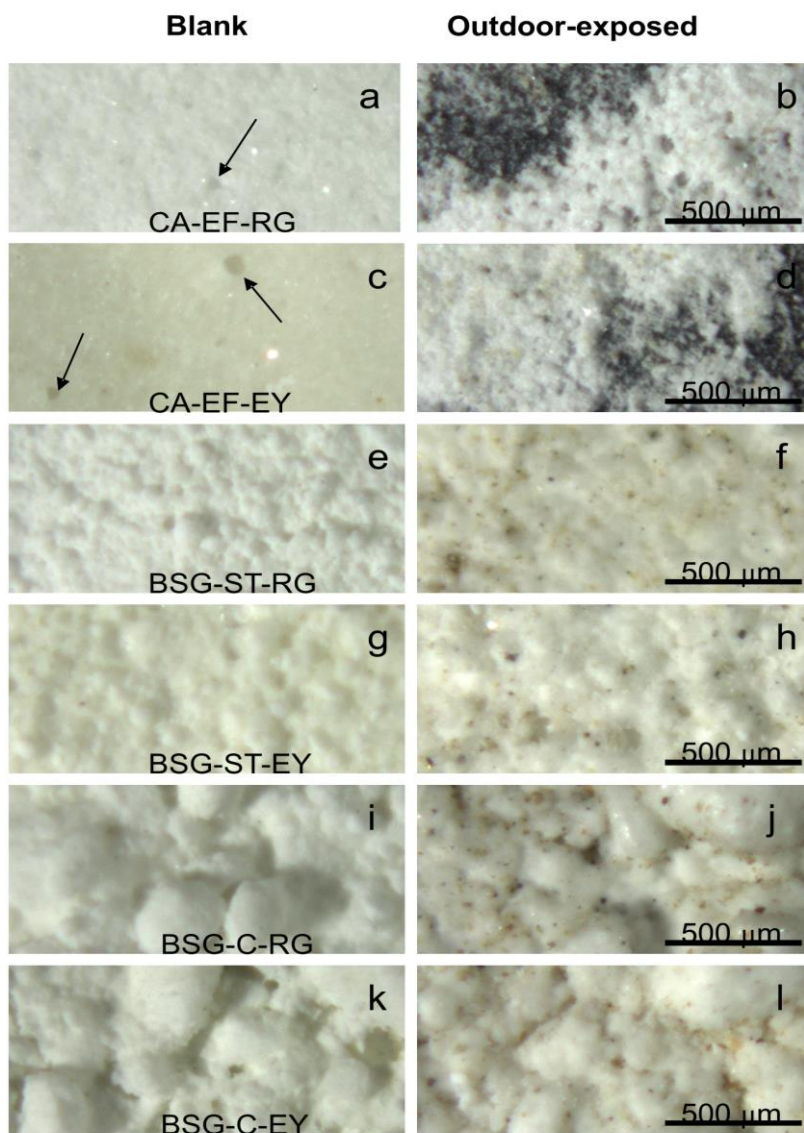


Fig.2. Optical microscopy images of blank dosimeters and dosimeters exposed outdoors during 40 months. Arrows indicate pockmarks, being relics of air bubbles. See Table 1 for acronyms.

5.3.3. Color measurements of blank and outdoor-exposed dosimeters

Spectrophotometry results revealed that L^* was lower in paints prepared with CA-EF as compared to BSG-based paints regardless of binder type (Table 4). This can be explained by the substantial amount of dolomite in this pigment; dolomite absorbing more light in the visible spectrum as compared to calcite (Gaffey, 1986). Color measurements were in agreement with optical microscopy observations, showing that paint prepared with egg yolk were more yellowish than rabbit glue-based paints as indicated by a higher b^* value. Remarkably, b^* values generally diminished upon outdoor exposure for up to 12 months, especially in the case of egg yolk-based paints (Fig. 3a). The reason for this decrease is twofold. On the one hand, it is known that egg yolk loses part of its yellow color upon exposure to light and/or heat (Kühn 1981, Mayer and Sheehan, 1991). On the other hand, partial binder loss, especially in the case of paints prepared with CA-EF, was responsible for the observed reduction in b^* . However, after 12 months of outdoor exposure b^* generally increased again and L^* decreased in dosimeters prepared with BSG, indicating a color change towards yellow, which might be attributed to the deposition of yellowish/brownish atmospheric dust particles. The amount of deposited particles increased over time, resulting in a reduction of L^* of up to 8 units at the end of the outdoor exposure (Fig. 3b). Additionally, sunlight-induced degradation of the organic binder, which turned more yellowish especially in the case of rabbit glue-based paints, also had an important contribution to the observed color change (Dilley, 1973, Elert et al., 2018).

Overall, paint dosimeters suffered important color changes (ΔE^*), which were generally well above the established limit for human perception after prolonged exposure (Fig. 3c) (Berns, 2000). The very small amount of gypsum (i.e., generally <5 wt%) detected with XRD, Raman spectroscopy and SEM in outdoor-exposed dosimeters (see below) is not thought to be sufficient to contribute to any color change.

Table 2. Color measurements of blank dosimeters. See Table 1 for acronyms.

Sample	L*	a*	b*
CA-EF-EY	88,74±0,07	-1,31±0,01	7,40±0,31
BSG-ST-EY	94,62±0,13	-1,68±0,04	8,70±0,22
BSG-C-EY	95,68±0,21	-1,05±0,07	6,52±0,66
CA-EF-RG	90,32±0,40	-0,41±0,10	3,51±0,10
BSG-ST-RG	96,08±0,09	-0,53±0,02	3,42±0,03
BSG-C-RG	93,48±0,38	-0,35±0,03	5,77±0,18

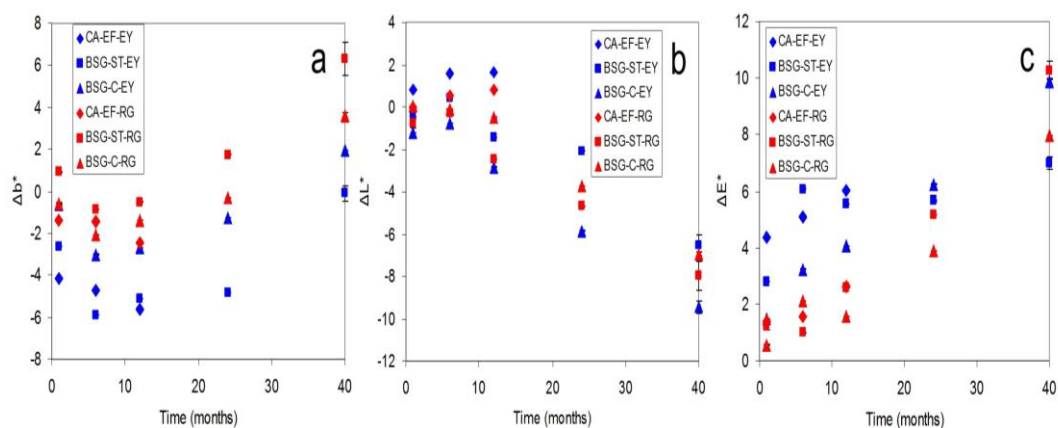


Fig.3. Color changes a) Δb^* , b) ΔL^* , and c) ΔE^* undergone by paint dosimeters during outdoor exposure for up to 40 months. Error bars are included. Note that errors were in most cases too small to be visualized in the graphs. See Table 1 for acronyms.

5.3.4. FESEM analysis of pigments and paint dosimeters before and after long-term outdoor exposure and accelerated SO₂-aging test

Pigments

FESEM images of lime-based pigments show that CA-EF had a very distinct morphology as compared to BSG-ST/C pigments (Fig. 4a and d). The former was comprised of blocky calcite crystals (10-100 μm) with irregular edges and a fractured appearance, typical for pigments obtained by grinding of bigger lumps. These large crystals were accompanied by smaller crystals, $\leq 1 \mu\text{m}$ in size (Fig. 4a). Images of BSG pigments, in contrast, revealed the presence of aggregates formed by nano-sized portlandite/calcite crystals. The morphological differences have an important influence on the paints' susceptibility to pollution-induced deterioration; BSG pigments offering a much larger surface area (i.e., specific surface area of BSG-ST and BSG-C being 12.6 m^2/g and 11.7 m^2/g , respectively) for reaction with atmospheric contaminants as compared with the CA-EF pigment (i.e., specific surface area being 1.6 m^2/g).

Outdoor exposure

After 40-month outdoor exposure only minor changes in the calcite crystal morphology could be detected in CA-EF-based paints regardless of binder type (Fig. 4b and c). The edges of larger crystals seemed slightly rounded, possibly due to dissolution processes. Occasionally, calcite crystals showed fractures, likely being induced by severe diurnal T changes (Fig. 4c, dashed line). Rodriguez-Navarro et al. (2004) demonstrated that thermally-induced physical weathering of calcite is related to the mineral's anisotropic thermal expansion. Note that fracturing was no artifact of sample preparation because samples were not ground prior to FESEM analysis. BSG-based paints underwent important changes due to the dissolution and carbonation of portlandite (Fig. 4e and f). Samples mixed with rabbit glue showed nanogranular structures and rhombohedral calcite crystals, presenting in some cases rounded edges (Fig. 4e, arrows). These morphological features have typically been observed upon calcite crystallization in the presence of organics

(Rodriguez-Navarro et al. 2016, Elert et al. 2018). Furthermore, spherical or semispherical structures typical for vaterite were detected in BSG-based paints prepared with egg yolk (Fig. 4f). The presence of vaterite was confirmed by Raman spectroscopy (see below). Vaterite is a metastable phase and normally transforms readily into calcite under most ambient conditions (Rodriguez et al., 2007). However, it has been demonstrated that the presence of organics may result in a kinetic stabilization of vaterite and prevent or delay its transformation into calcite (Manoli et al., 2002; Xie et al., 2005; Rodriguez-Navarro et al., 2013). Note that vaterite was detected with XRD and SEM in identical samples exposed to very similar environmental conditions (Elert et al. 2018).

The comparison of elemental x-ray maps of blank and outdoor-exposed dosimeters revealed the appearance of isolated areas of high sulfur concentration upon prolonged exposure (Fig. 4g and h). All outdoor-exposed dosimeters showed these sulphur-rich areas but only the elemental map of CA-EF-EY is included here as a representative example. The observed sulphur signal in the blank CA-EF-EY dosimeter corresponded to background noise and no sulphur-rich impurities can be detected in this sample (Fig. 4g). Note that elemental mapping also disclosed the presence of Al, Si, Fe, K, and Mg on outdoor-exposed dosimeters, all elements likely being related with deposited atmospheric particulate matter such as quartz, aluminosilicates, iron-bearing oxides/hydroxides, and dolomite. FESEM imaging (Fig. 4i) in combination with microanalysis allowed the unambiguous identification of the sulphur-rich areas as gypsum aggregates, showing similar morphological features as those of authigenic gypsum (i.e., tabular-shaped crystals either isolated or forming small clusters), formed in tempera paint samples subjected to accelerated SO₂-aging (Fig. 5). However, solely based on FESEM results it was impossible to unambiguously determine the origin of gypsum crystals (i.e., deposited gypsum particles or sulfated calcite particles) because the very early stages of calcite/portlandite sulfation could not be detected. In many cases, gypsum crystals seemed to be deposited on the surface and a calcite/gypsum intergrowth was not observed. Even though direct evidence for sulfation was not detected in outdoor-exposed tempera paints, the presence of gypsum

particles is of importance because they can act as templates for gypsum crystallization via self-epitaxy (Rodríguez Navarro and Sebastian, 1996).

The lack of any clear sign of sulfation was unexpected. Especially, considering the relatively high SO₂ and particulate matter concentrations in Granada's urban air (Table 2). Moreover, Urosevic et al. (2012) found relatively rapid gypsum formation on limestone samples exposed for 1 year to urban air in Granada's historic city center. Most likely, the organic binder in tempera paints hindered gypsum formation over the course of the 40-month outdoor exposure. First of all, the organic binder acted as a barrier by creating a film around the pigment particles as observed in the case of dosimeters exposed to accelerated SO₂-aging (Table 3; Fig. 1, supplementary material Appendix III). However, the thickness of the organic film will gradually be reduced during the outdoor exposure by the periodic impact of rain and photo-induced degradation. As a result, the film will no longer be effective as a protective barrier. In the case of BSG-based paints, portlandite almost completely carbonated in the presence of the organic binder during the first 6 months of the outdoor exposure (Fig. 1a). Subsequently, an organic-inorganic hybrid material formed, where part of the organic binder is incorporated in the organic-inorganic calcite structure and cannot easily be leached out (Elert et al., 2018). Recent studies demonstrated that these hybrid materials not only have higher mechanical resistance, but also show improved chemical weathering resistance, which would explain the lack of any clear sign of sulfation in this type of paints (Jroundi et al., 2017). Obviously, in the case of calcite-based paints, the organic binder is not incorporated into the calcite structure and organic-inorganic hybrid materials do not form. Actually, optical microscopy observations revealed the lower weathering resistance of this type of paints, suffering severe material loss (Fig. 2b and d). Considering the relatively high solubility of gypsum (solubility = 2.4 g/L at 20°C) as compared to calcite (solubility = 0.013 g/L at 25°C), it is possible that most of the sulfate weathering products together with part of the calcite-based paint have been washed away by the periodic impact of rain. In fact, gypsum formation is generally not detected on surfaces which are "washed" by the direct impact of rain (Camuffo, 1984; Urosevic et al., 2012).

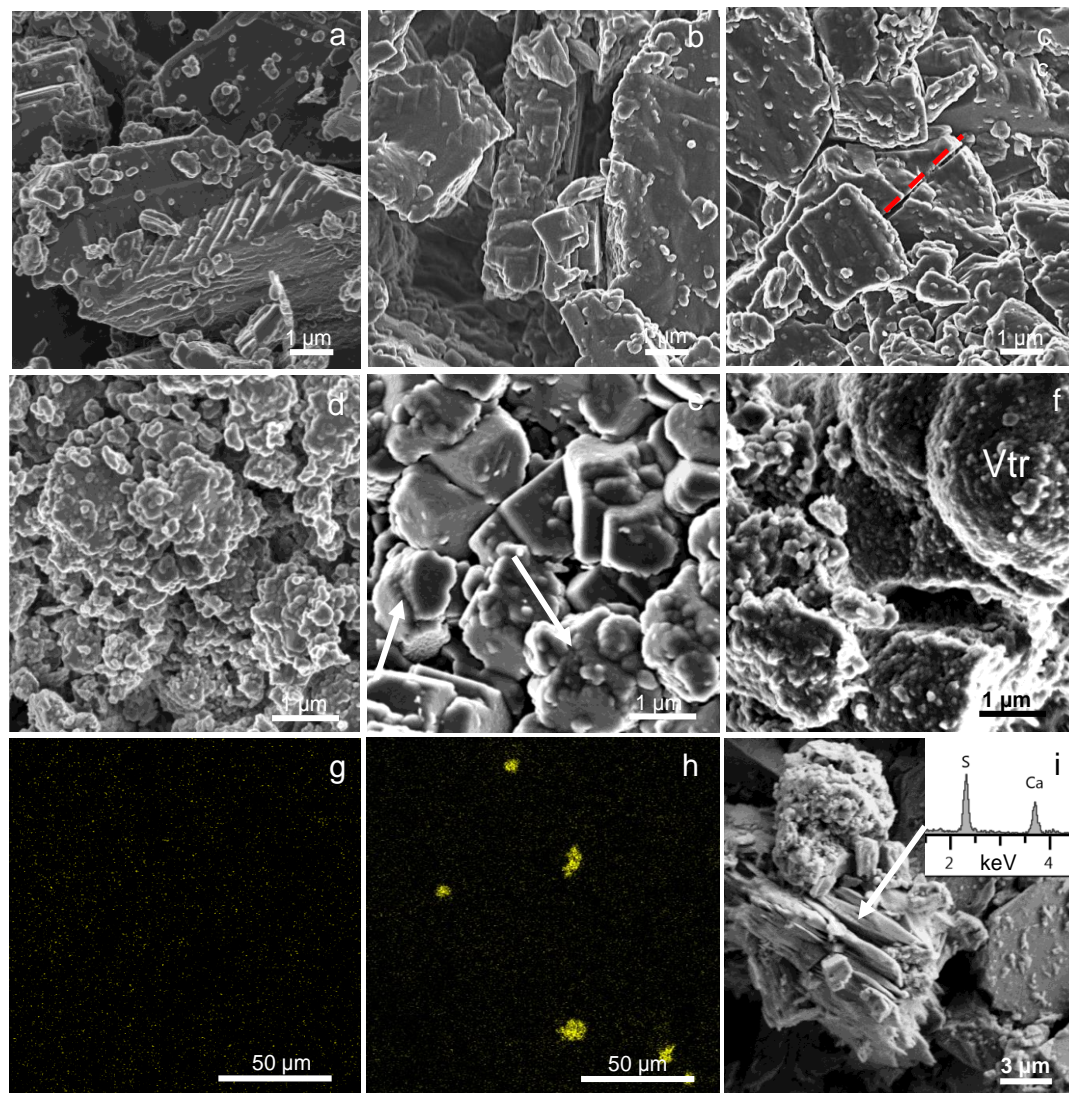


Fig.4. FESEM images of a) CA-EF pigment; b) CA-EF-RG outdoor-exposed for 40 months; c) CA-EF-EY outdoor-exposed for 40 months; d) BSG-ST pigment; e) BSG-ST-RG outdoor-exposed for 40 months (arrows indicate nanogranular structures and calcite crystals with rounded edges); f) BSG-ST-EY outdoor-exposed for 40 months, Vtr = vaterite; g) Sulfur x-ray map of CA-EF-EY blank; h) Sulfur x-ray map of CA-EF-EY dosimeter outdoor-exposed for 40 months; and i) gypsum detected on CA-EF-EY dosimeter outdoor-exposed for 40 months (microanalysis in inset). See Table 1 for acronyms

Accelerated SO₂-aging test

The extreme conditions during the SO₂-aging test provoked significant morphological changes in lime-based tempera paints. Paint samples prepared by mixing reagent grade Ca(OH)₂ with water, which contained ~70 wt% calcite according to XRD analysis, originally showed calcite crystal bundles with the typical scalenohedral morphology of carbonated Ca(OH)₂ pastes (Cizer et al., 2012) (Fig. 5a). After 82 h of SO₂ exposure, scalenohedral calcite crystals suffered severe dissolution and blocky gypsum crystals formed (Fig. 5b). However, it was not possible to unambiguously identify calcium sulfite hemihydrate in this sample based on morphological characteristics.

In the case of CA-EF-RG paint, the originally smooth surface of calcite crystals (Fig. 5c) was almost completely covered with a film of nanogranular calcium sulfite hemihydrate after 82 h (Fig. 5d). The observed nanostructural features of the newly formed phases are in agreement with XRD results, which hinted a low crystallinity of calcium sulfite hemihydrate. The FESEM image shows that no crystallographic continuity exists between the dissolving calcite (Fig. 5d, arrow indicates dissolution-induced macro steps) and the newly formed sulfite product layer (which is separated from the calcite substrate by a gap). Although the produced sulfite grossly preserves the overall rhombohedral shape of calcite crystals (Fig. 2, supplementary material Appendix III), thereby pointing to a possible pseudomorphic replacement, there is no epitaxy between parent and product phases (Fig. 5d, dashed arrow). This implies that no passivation layer will form and the reaction would continue under adequate environmental conditions until all calcite is transformed (Ruiz-Agudo et al., 2016).

BSG-based paints revealed a structure formed by aggregated nano-sized particles (Fig. 5e). After 82 h of SO₂ exposure, a massive formation of tabular-shaped gypsum clusters was observed, completely replacing portlandite and ~90 wt% of the original calcite according to XRD data. Furthermore, spherical morphologies typical for vaterite were detected. Note that the corresponding blank dosimeters did not contain any vaterite and it can be ascertained that this phase formed during the SO₂ exposure. Actually, Fernández-Díaz et

al. (2010) were able to demonstrate that vaterite was stabilized in the presence of SO_4 over a relative long period of time (i.e., >250 h). The presence of the metastable vaterite will add to the destabilization of tempera paints exposed to SO_2 -aging. On the one hand, phase transition is accompanied by volume changes (i.e., transformation of portlandite into gypsum or vaterite, and calcite transformation into gypsum) (Table 5). Furthermore, vaterite will eventually transform into calcite, which again will result in a volume change. On the other hand, the spherical vaterite will have inferior mechanical strength as compared to scalenohedral calcite crystals, which forms an interlocked structure with higher cementing capacity (Cizer et al., 2012).

Table 5. Molar volume ($\text{cm}^3 \text{mol}^{-1}$) of minerals and calculated volume change (%) upon phase transition.

Mineral	Molar volume ($\text{cm}^3 \text{mol}^{-1}$)	Volume change (%)
Por	33.2	19 (Por→Vtr) 11 (Por→Cal) 123 (Por→Gp)
Vtr	39.4	-6 (Vtr→Cal)
Cal	36.9	111 (Cal→Gp)
Gp	74.1	

Por = portlandite, Vtr = vaterite, Cal = calcite, Gp = gypsum.

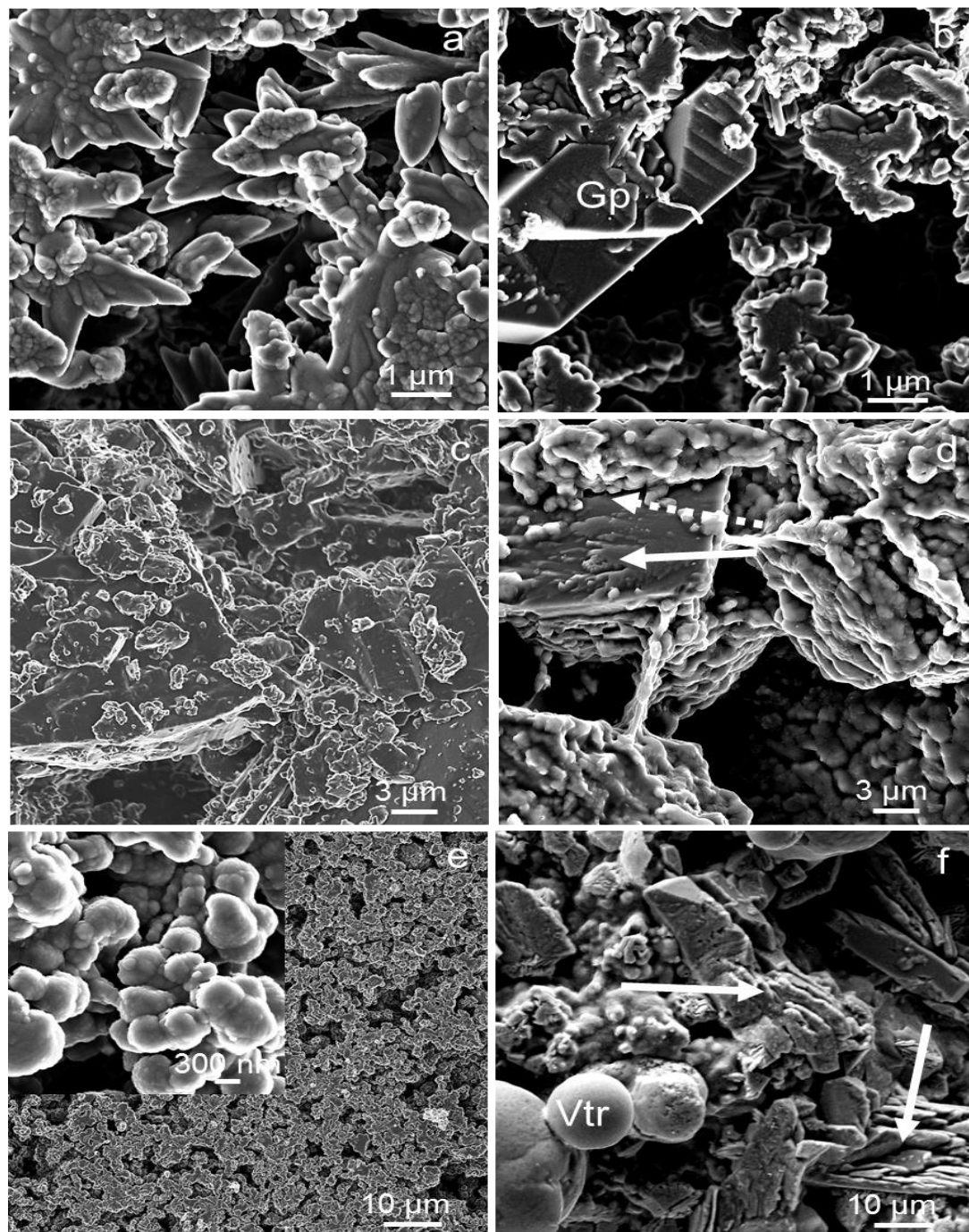


Fig.5. FESEM images of a) $\text{Ca(OH)}_2\text{-H}_2\text{O}$ blank; b) $\text{Ca(OH)}_2\text{-H}_2\text{O}$ after 82 h SO_2 -aging test, Gp = gypsum c) CA-EF-RG blank; d) CA-EF-RG after 82 h SO_2 -aging test; e) BSG-C-RG blank (high magnification image in inset); and f) BSG-C-RG after 82 h SO_2 -aging test (arrows indicate gypsum crystals). See Table 1 for acronyms.

5.4. Raman analysis

Outdoor exposure

Raman spectroscopy confirmed XRD and SEM data (see below), revealing the presence of gypsum in outdoor-exposed paint dosimeters, indicated by low intensity gypsum bands at 415 and 1013 cm^{-1} (Fig. 6a). Note that only spectra of the BSG-ST-EY sample are included here as representative examples. Raman spectra also showed a decrease in portlandite content over time in BSG-based paints as a result of the reaction with atmospheric CO_2 (Fig. 6a), and allowed the detection of vaterite, which was not present in a sufficiently high concentration to be detected by XRD. In samples exposed to accelerated SO_2 -aging, abundant amounts of gypsum and calcium sulfite hemihydrate were observed, the spectrum of the later being almost identical to hannebachite ($2\text{CaSO}_3 \cdot (\text{H}_2\text{O})$) (Fig. 6b, Frost and Keeffe, 2009). Note that the presence of vaterite in SO_2 -aged samples could not be confirmed unambiguously with this technique.

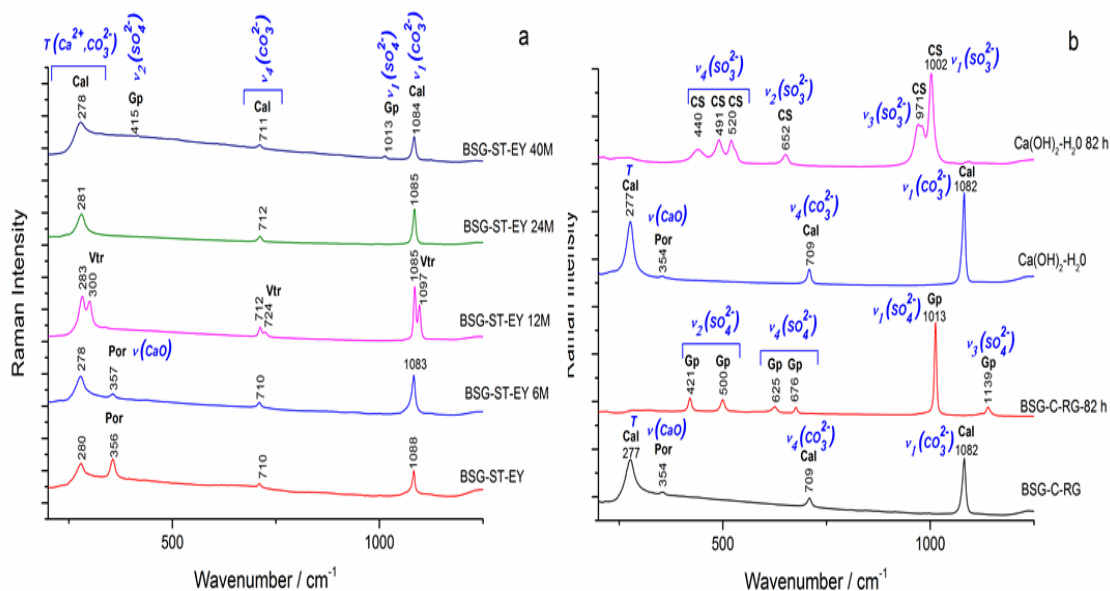


Fig.6. Raman spectra a) BSG-ST-EY paint before and during outdoor exposure; b) BSG-C-C and $\text{Ca}(\text{OH})_2 \cdot \text{H}_2\text{O}$ before and after accelerated SO_2 -aging for 82 h. T = torsion, Gp = gypsum, Vtr = vaterite, Por = portlandite, Cal = calcite, Gp = gypsum, and CS = calcium sulfite hemihydrate. See Table 1 for acronyms.

5.5. Conclusions

Analytical results revealed the important influence of the pigment's mineralogical composition and specific surface area on the susceptibility towards sulfation; pigments containing portlandite showing faster sulfation than pigments containing only calcite. Furthermore, the organic binder delayed the reaction between lime-based paints and atmospheric SO₂. However, the presence of organic binder also slows down carbonation in the case of BSG-based paints and thus the formation of organic-inorganic hybrid materials. Future studies should be performed to determine the optimal binder content which would effectively delay sulfation without impeding a fast carbonation. Resulting organic-inorganic hybrid materials formed in BSG-based paints can be expected to have high chemical weathering resistance.

Regardless of pigment composition, calcium sulfite hemihydrate was always detected as an intermediate phase on samples exposed to SO₂, forming a nanogranular film on the pigment particle's surface. Direct transformation of calcite into gypsum was not detected and the lack of crystallographic continuity of calcium sulfite hemihydrate with the underlying calcite implies that the sulfation process will not cease until complete sulfation is achieved. However, the sulfation reaction requires water and might halt under dry conditions (i.e., low RH and little or no precipitation) but resume as water becomes available.

Remarkably, no clear evidence for sulfation was detected in lime-based tempera paints after 40-month outdoor exposure to polluted urban air. Several reasons might explain this result. On the one hand, carbonation of portlandite in the presence of organics (i.e., rabbit glue or egg yolk binder) might have promoted the formation of organic-inorganic hybrid materials with high resistance towards chemical weathering in the case of BSG-based paints. On the other hand, periodic impact of rain might have washed off calcium sulfite/sulfate phases, especially in the case of calcite-based paints, which showed severe material loss after prolonged outdoor exposure.

The selection of lime-based paints for conservation interventions in polluted environments should be made considering the prevailing climate conditions. In dry climates where a severe delay in the carbonation reaction can be expected, the use of calcite-based paints might be advisable. In humid climates or under direct impact of rain, in contrast, BSG-based paints are preferable, forming organic-inorganic hybrid materials with high resistance towards physical and chemical weathering. The use of organic additives such as rabbit glue might also be beneficial to improve the chemical weathering resistance of lime mortars and plasters. However, as pointed out before, the optimal organic content has to be established to allow for sufficiently fast carbonation.

Acknowledgements

Financial support was provided by the Spanish Government and the Junta de Andalucía (research projects AERIMPACT, CGL2012-30729 and EXPOAIR, P12-FQM-1889), the European Regional Development Fund (ERDF) and the Andalusian Research Groups RNM-179. Analyses were performed at the Scientific Instrumentation Center (CIC) of the University of Granada (Spain). J.A. Herrera Rubia is funded by a Spanish grant from the AERIMPACT Project (ref.BES-2013-065507). J.S. Pozo-Antonio was supported by a postdoctoral contract with the University of Vigo within the framework of the 2011–2015 Galician Plan for Research, Innovation and Growth (Plan I2C) for 2014. K. Elert is a post-doctoral fellow in the EXPOAIR Project. We thank C. Rodriguez-Navarro for comments and suggestions.

References

- AENOR, Natural Stone Test Methods. Determination of Resistance to Ageing by SO₂ Action in the Presence of Humidity (UNE-EN 13919:2003, Madrid), 2003.
- Amoroso, G., Fassina, V., 1983. Stone Decay and conservation: atmospheric pollution, cleaning, consolidation and protection. Elsevier, Amsterdam.
- Beruto, D.T., Barberis, F., Botter, R., 2005. Calcium carbonate binding mechanisms in the setting of calcium and calcium-magnesium putty limes. *J. Cult. Herit.* 6, 253-260.
- Berns, R.S., 2000. *Principles of Color Technology*, 3rd ed. Wiley-Blackwell, Hoboken.
- Brunauer, S., Emmett, P.H., Teller, E., 1938. Adsorption of gases in multimolecular layers. *J. Am. Chem. Soc.* 60, 309–319.
- Camuffo, D., 1984. The influence of run-off on weathering of monuments. *Atmos. Environ.* 18, 2273–2275.
- Camuffo, D., Del Monte, M., Sabbioni, C., 1983. Origin and growth of the sulfated crusts on urban limestone. *Water, Air, Soil Pollut.* 19, 351-359.
- Capitán-Vallvey, L. F., Manzano, E., & Flórez, V. M., 1993. Estudio de materiales de las pinturas murales de la Torre de las Damas (Granada) y estado de conservación. *Al-Qantara.* 14, 177-203.
- Cardell, C., Herrera, A., Guerra, I., Navas, N., Simón, L. R., Elert, K., 2017. Pigment-size effect on the physico-chemical behavior of azurite-tempera dosimeters upon natural and accelerated photo aging. *Dyes Pigm.* 141, 53-65.
- Cennini C., 1988. *El libro del Arte*. AKAL S.L., Madrid (Spain).
- Charola, A. E., Ware, R., 2002. Acid depostion and the deterioration of stone: a brief review of a broad topic. in: Siegesmund, S., Weiss, T., Vollbrecht, A. (EDS.), *Natural Stone, Weathering Phenomena, Conservation Strategies and Case Studies.*, Geological Society Special Publication No.205, London, pp.393-406.
- CIE S014-4/E:2007, 2007. *Colorimetry Part 4: CIE 1976 L*A*b* Colour Space.*. Commission Internationale de l'eclairage. CIE Central Bureau, Vienna
- Cizer, Ö., Rodriguez-Navarro, C., Ruiz-Agudo, E., Elsen, J., Van Gemert, D., Van Balen, K., 2012. Phase and morphology evolution of calcium carbonate precipitation by carbonation of hydrated lime. *J. Mater. Sci.* 47, 6151-6165.

Cultrone, G., Arizzi, A., Sebastián, E., & Rodríguez-Navarro, C., 2008. Sulfation of calcitic and dolomitic lime mortars in the presence of diesel particulate matter. *Environ. Geol.* 56, 741-752.

Dilley, K.J., 1973. Loss of tryptophan associated with photo-polymerization and yellowing of proteins exposed to light over 300 nm. *Biochem. J.* 133, 821-826.

Ecologistas en acción, 2015. Informe - La calidad del aire en el Estado español durante 2014, pp.104.

Ecologistas en acción, 2016. Informe - La calidad del aire en el Estado español durante 2015, pp.110.

Ecologistas en acción, 2017. Informe - La calidad del aire en el Estado español durante 2016, pp.119.

Elert, K., Herrera, A., Cardell, C., 2018. Pigment-binder interactions in calcium-based tempera paints. *Dyes Pigm.* 148, 236-248.

European Environment Agency, 2013a. Air pollution fact sheet 2013 – Spain, European Environment Agency, Copenhagen.

European Environment Agency, 2013b. <http://www.eea.europa.eu/themes/air/interactive/so2> (accessed 5 January 2017).

Fernández-Díaz, L., Fernández-González, Á., Prieto, M., 2010. The role of sulfate groups in controlling CaCO₃ polymorphism. *Geochim. Cosmochim. Acta* 74, 6064-607

Frost, R.L., Keeffe, E. C., 2009. Raman spectroscopic study of the sulfite-bearing minerals scotlandite, hannebachite and orschallite: implications for the desulfation of soils. *J. Raman Spectrosc.* 40, 244-248.

Gaffey, S.J., 1986. Spectral reflectance of carbonate minerals in the visible and near infrared (0.35-2.55 microns): calcite, aragonite, and dolomite, *J. Raman Spectrosc.* 71, 151-162.

Herrera, A., Navas, N., Cardell, C., 2016. An evaluation of the impact of urban air pollution on paint dosimeters by tracking changes in the lipid MALDI-TOF mass spectra profile. *Talanta* 155, 53-61.

Horemans, B., Cardell, C., Bencs, L., Kontozova-Deutsch, V., De Wael, K., Van Grieken, R., 2011. Evaluation of airborne particles at the Alhambra monument in Granada, Spain. *Microchem. J.* 99, 429-438.

Jroundi F, Schiro M, Ruiz-Agudo E, Elert K, Martin-Sanchez I, Gonzalez-Munoz MT, Rodríguez-Navarro C., 2017. Protection and consolidation of stone heritage by self-inoculation with indigenous carbonatogenic bacterial communities. *Nat. Commun.* 8, 279.

Kontozova-Deutsch, V., Cardell, C., Urosevic, M., Ruiz-Agudo, E., Deutsch, F., Van Grieken, R., 2011. Characterization of indoor and outdoor atmospheric pollutants impacting architectural monuments: the case of San Jerónimo Monastery (Granada, Spain). *Environ. Earth Sci.* 63, 1433-1445.

Kühn, H., 1981. *Erhaltung und Pflege von Kunstwerken und Antiquitäten 1*. Keyserische Verlagsbuchhandlung, München.

Manoli, F., Kanakis, J., Malkaj, P., Dalas, E., 2002. The effect of aminoacids on the crystal growth of calcium carbonate. *J. Cryst. Growth* 236, 363-370.

Manzano, E., García Bueno, A., González-Casado, A., Del Olmo, M., 1999. Mortars, pigments and binding media of wall paintings in the 'Carrera del Darro' in Granada, Spain. *J. Cult. Herit.* 1, 19–28.

Maravelaki-Kalaitzaki, P., 2005. Black crusts and patinas on Pentelic marble from the Parthenon and Erechtheum (Acropolis, Athens): characterization and origin. *Analyt. Chim. Acta* 532, 187-198.

Martín-Ramos, J.D., 2004. *Using X Powder: A Software Package for Powder X-Ray Diffraction Analysis*, (GR 1001/04. ISBN 84-609-1497-6).

Matteini, M., 1992. In Review: An Assessment of Florentine Methods of Wall Painting Conservation Based. *The Conservation of Wall Paintings*. The Getty Conservation Institute, Los Angeles, pp. 137-148.

Mayer, R., Sheehan, S., 1991. *The artist's handbook of materials and techniques*. The Viking., New York.

Pacheco, F., 1990. *El arte de la pintura*. Cátedra, Madrid.

Patrón, D., Lyamani, H., Titos, G., Casquero-Vera, J. A., Cardell, C., Močnik, G., Alados-Arboledas L., Olmo, F. J., 2017. Monumental heritage exposure to urban black carbon pollution. *Atmos. Environ.* 170, 22-32.

Rodríguez-Navarro, C., Jimenez-Lopez, C., Rodríguez-Navarro, A., Gonzalez-Munoz, M.T., Rodríguez-Gallego, M., 2007. Bacterially mediated mineralization of vaterite. *Geochim. Cosmochim. Acta* 71,1197-1213.

Rodríguez-Navarro, C., Rodríguez-Navarro, A., Elert, K., Sebastian, E., 2004. Role of marble microstructure in near-infrared laser-induced damage during laser cleaning. *J. Appl. Phys.* 95, 3350-3357.

Rodríguez-Navarro, C., Ruiz-Agudo, E., Harris, J., Wolf, S. E., 2016. Nonclassical crystallization in vivo et in vitro (II): nanogranular features in biomimetic minerals disclose a general colloid-mediated crystal growth mechanism. *J. Struct. Biol.* 196, 260-287.

Rodríguez-Navarro, C., Sebastian, E., 1996. Role of particulate matter from vehicle

exhaust on porous building stones (limestone) sulfation. *Sci. Total Environ.* 187, 79–91.

Rodríguez-Navarro, C., Suzuki, A., Ruiz-Agudo, E., 2013. Alcohol dispersions of calcium hydroxide nanoparticles for stone conservation. *Langmuir* 29, 11457-11470.

Ruiz-Agudo, E., Álvarez-Lloret, P., Ibañez-Velasco, A., & Ortega-Huertas, M., 2016. Crystallographic control in the replacement of calcite by calcium sulfates. *Crystal Growth & Design* 16, 4950-4959.

Sayre, E. V., Majewski, L. J., 1963. II. Technical investigation of the deterioration of the paintings. *Stud. Conser.* 8, 42-54.

Schaffer, R.J., 1932. *The Weathering of Natural Building Stones*, DSIR, Building Research Special Report 18, Stationary Office, London, 34 pp.

Smith, B. J., Gomez-Heras, M., & McCabe, S., 2008. Understanding the decay of stone-built cultural heritage. *Prog. Phys. Geogr.* 32, 439-461.

Török, Á., 2008. Black crusts on travertine: factors controlling development and stability. *Environ. Geol.* 56, 583-594.

Tsugita, A., Scheffler, J. J., 1982. A rapid method for acid hydrolysis of protein with a mixture of trifluoroacetic acid and hydrochloric acid. *Eur. J. Biochem.* 124, 585-588.

Urosevic, M., Yebra-Rodríguez, A., Sebastián-Pardo, E., Cardell, C., 2012. Black soiling of an architectural limestone during two-year term exposure to urban air in the city of Granada (S Spain). *Sci. Total Environ.* 414, 564-575.

Velilla, N., 2017. Estación meteorológica Granada-Albayzín (España)

(www.ugr.es/~velilla/meteo-albayzin/resumen.htm, accessed 07/10/2016).

Xie, A.J., Shen, Y.H., Zhang, C.Y., Yuan, Z.W., Zhu, X.M., Yang, Y.M. 2005. Crystal growth of calcium carbonate with various morphologies in different amino acid systems. *J. Cryst. Growth* 285, 436-443.

Zehnder, K., 1996. Gypsum efflorescences in the zone of rising damp. Monitoring of slow decay processes caused by crystallizing salts on wall paintings. in: Riederer, J. (ed.), *Proc. 8th Inter. Congress on Deterioration and Conservation of Stone*. Möller Druck, Berlin, pp 1669–1678.

Conclusiones

***"Todo lo que alguna vez
has deseado, está al otro
lado del miedo"***

George Addair



Leonardo Da Vinci-*Ultima
cena*

I. General conclusions

The main conclusions of this Doctoral Thesis relate to the chemical (of the binder and pigments), physical (color and texture) and mechanical (resistance to chemical and physical attack) decay suffered by paint dosimeters (mock-ups of artists' paints) exposed to the elements in (semi-)open monuments in the city of Granada, in different urban atmospheric pollution scenarios. In our research we focused among other aspects on the interaction between the pigment and the binder, a subject often overlooked in the bibliography due to the difficulties involved in its analysis and interpretation. We also analysed the influence of various factors in the processes of interaction between the components of the paint. These factors included urban atmospheric pollution and the impact of solar radiation, the nature of the pigment and its grain size, and the nature and concentration of the protein binder used in the paint.

The results we obtained from the natural aging tests conducted on paint dosimeters by exposure to different urban air scenarios in the city of Granada were compared with those obtained in accelerated aging tests in the laboratory in which the dosimeters were exposed to an atmosphere rich in SO₂ and UV radiation in order to define differences and similarities, and thus to improve knowledge of the weathering mechanisms of paintings exposed to urban atmosphere.

The application of chemometric tests to the color data obtained from the naturally aged paint dosimeters enabled us to identify the parameters that cause them to decay in different ways, so allowing us to predict color change tendencies in the paints over longer periods of time. The results of the different studies that we conducted and the optimization of the analytical techniques lead us to propose the application of new analytical methodologies for the characterization of artists' paints and for studying the decay they undergo when exposed to urban air pollution. Likewise, it is convenient to perform a multi-

Conclusiones

analytical study of the weathering processes that affect the paint dosimeters in order to avoid mistakes in the interpretation of the results and assure correct conclusions.

In our research we used pigments manufactured according to traditional recipes used by mediaeval artists. Our results revealed that the actual composition and grain size of these pigments do not always coincide with the manufacturer's specifications. It is therefore essential to characterize the paint materials before carrying out scientific studies or restoration work on cultural heritage of this kind. This process must include analyses of the mineralogical composition (so as to ensure the quality of the pigment and identify any impurities) and the grain size of the pigment and of the amount of organic binder that may have been added during the manufacture of the pigment, as these can significantly alter the chemical, physical and optical characteristics of the pigments and therefore the interaction between the pigment and the binder, and ultimately the aging processes in the paints.

The studies conducted during the course of this Doctoral Thesis also enable us to make recommendations regarding the restoration and conservation of paintings, in terms of the pigments and binders that can be used, in that when selecting the most suitable pigments the prevailing climate and atmospheric pollution conditions must be taken into account.

II. Specific conclusions

Physical-chemical and/or mineralogical decay in paint dosimeters due to natural and artificial aging

In this Ph.D. thesis we conducted the first exhaustive study of the role played by pigment grain size in the pigment-binder interaction in paint. Our results have demonstrated that this morphological characteristic of the pigment is crucial in the mechanisms that cause the paint to decay in that the grain size controls the quantity and the distribution of the organic binder (in general more likely to suffer decay than the mineral-based pigments) required to obtain paint with the right consistency. Our research was conducted on paint dosimeters made with azurite (different grain sizes) and rabbit glue, aged under artificial (accelerated photo decay with UV radiation) and natural (exposure to different atmospheric urban pollution scenarios) conditions.

This research revealed that the paint dosimeter made with standard azurite (with a smaller average grain size than the other azurites) has very different chromatic characteristics from the other paint dosimeters, due to the fact that it has a greater binder content, part of which was added during the manufacture of standard azurite (Michel Price method, used by *Kremer Pigments GmbH & Co. KG*). The organic binders are more susceptible to aging than the inorganic pigments and therefore play a crucial role in the color changes that take place in the paints, in particular if the paints contain pigments with a fine grain size, as more binder is normally required.

In general, the changes in color in the aged paint dosimeters made with azurite and rabbit glue were caused by the decay of the binder. Although in all the dosimeters there were chromatic changes visible to the human eye, those aged by exposure to the open air underwent less change than those aged in the laboratory, a finding attributable to the loss of rabbit glue in the paint. This left unaltered azurite crystals exposed and reduced the adhesion between the azurite particles and their adhesion to the substrate. These results

Conclusiones

therefore call into question the suitability of rabbit glue as a binder in paints exposed to the open air and suggest that their use in conservation work should be limited. Another interesting observation was that the initial stage of transformation of azurite (blue) into malachite (green) was only identified in the dosimeters aged in the open air. This suggests that the color of these paints tends naturally to change to greenish tones over time.

The accelerated aging via UV radiation of the paint dosimeters made with the largest grain azurites produced severe cracking in the rabbit glue. As a result, we concluded that the best way to prevent crack formation would be through a combination of large grain and fine grain (in small amounts) azurite. The fine grains would fill the spaces between the large grains, so avoiding having to use large amounts of binder and reducing changes in volume due to variations in humidity and/or temperature. The amount of binder must be kept to a minimum, so as to preserve the color properties of the paint and limit the binder-pigment interaction.

The FTIR-ATR analysis of the paint dosimeters made with azurite and rabbit glue confirmed that the pigment-binder interactions are stronger in the presence of fine grain azurites, causing conformational structure changes in the rabbit glue, specifically in the amides. The changes in the structure of the binder are probably responsible for the change in the color of the aged paints towards yellow and/or green. The color change becomes more accentuated as the pigment grain size falls. This is because more binder must be added to the paint.

In the research conducted during this Doctoral Thesis, we analyzed modern reproductions of the pigments used by mediaeval artists. Our research revealed the key role played by the mineralogical composition of the pigments made with a calcite base, and their specific area, in the susceptibility to sulfation of the paints made with tempera. The result is that the sulfation process is quicker if the pigment contains both calcite and portlandite. We also confirmed that the protein binder present in the lime-based paints delays the reaction between the paints and atmospheric SO₂. However, this binder also slows down

carbonatation in the paints made with the commercial pigment known as *Bianco di San Giovanni* (which contains portlandite), and therefore in the formation of organic-inorganic hybrid compounds. Future studies must therefore be conducted to determine the optimum binder content, which would effectively delay the sulfation of this kind of paint without impeding its rapid carbonation. We would also expect that the organic-inorganic hybrid compounds that form in the paints that contain portlandite would increase the chemical resistance of the paints to the elements.

Regardless of the composition of the calcite-based pigment, *calcium sulfite hemihydrate* is always detected as an intermediate phase in the process of sulfation of paints exposed to SO_2 , forming a nanogranular film on the surface of the pigment. The direct transformation of calcite into gypsum was not detected during sulfation, and the lack of crystallographic continuity of the calcium sulfite hemihydrate with the underlying calcite would suggest that this process will continue until complete sulfation is achieved. However, the sulfation process requires water and may therefore stop in dry conditions (i.e. conditions of low relative humidity or of no rain) and will start again when water becomes available.

We were surprised to discover that there was no clear evidence of sulfation in the paint dosimeters made with calcite and exposed to the open air in the city of Granada for 40 months. This could be for various reasons. Firstly, in the dosimeters made with *Bianco di San Giovanni*, pigment, the carbonation of the portlandite in the presence of organic substances (e.g. rabbit glue or egg yolk) could have encouraged the formation of organic-inorganic hybrid materials that are highly resistant to chemical alteration. Furthermore, the periodic impact of the rain may have washed away the phases of calcium sulfite and/or sulfate from the paint, especially in the dosimeters made with calcite, which experienced severe loss of material after long-term exposure to the elements.

As a result, the selection of lime-based paints for conservation work in polluted atmospheric environments must take into account the prevailing climatic conditions. In dry climates a severe delay in the carbonation process is likely making the use of calcite-based

Conclusiones

paints advisable. In humid climates however or those exposed to the direct impact of rain it would be better to use paints containing portlandite (e.g. the pigment *Bianco di San Giovanni*), which form organic-inorganic hybrid materials that are highly resistant in both physical and chemical terms to exposure to the elements. The results of our research could also be extrapolated to other materials used in historic buildings in that the use of organic additives such as rabbit glue can help to improve the resistance of lime and gypsum mortars to the elements. However, as mentioned earlier, the optimum organic content must be determined so as to ensure that carbonation occurs quickly.

The lipids (contained in the binder) in the paint dosimeters made with egg yolk tempera aged due to exposure to the elements in a polluted urban atmosphere have a unique “lipid fingerprint” when analyzed with MALDI-TOF/MS. However, we propose that the decay mechanisms for the lipids in all the paint dosimeters we studied are similar (i.e. β -oxidation breakdowns and breaks in the chain), as a reduction in the m/z signals can be observed within a very similar mass spectrum range in all of them. By contrast, there is an increase in the mass signals in the aged paint dosimeter made with lead white. This may be because oxidation takes place more slowly in the lead white pigment than in the other pigments we studied and that these reactions occur in almost all the double bonds in unsaturated fatty assets. This phenomenon is probably related with the capacity of lead white to form soaps.

Optimization, new analytical methodology and interpretation in historic paints

In our MALDI-TOF/MS analysis of the lipids from the paint dosimeters made with egg yolk binder, we applied one of the most commonly used procedures for the extraction of proteins and lipids, the Bligh-Dyer method (BD). During the optimization of this method it became clear that we needed to include an intermediate washing stage that was capable of eliminating most of the adducts that had formed. This step, which had not been considered in previous research, is crucial for the subsequent analysis of the lipid fraction using MALDI-TOF/MS.

In the mass spectral region situated between 500-700 m/z for the lipids analyzed with MALDI-TOF/MS, we discovered the products of the transesterification process. This process is due to the organic solvent (methanol) used in the lipid fraction extraction stage. This means that erroneous results may be obtained if this reaction is not taken into account. We therefore propose that the signals detected in the 500-700 m/z mass range are the result of transesterification reactions between reactive agents, lipids and pigments.

The mass spectrum range for interpreting the changes that took place in the lipid fraction of the paint dosimeters made with an egg-yolk binder is 700-1000 m/z . This region is therefore selected as the “lipid fingerprint” which allows us to evaluate the changes that have taken place in the lipid fraction of the paint samples made with egg-yolk binder after they were exposed to the elements in a polluted urban atmosphere. In this “lipid fingerprint” the products of the transesterification reactions with methanol are eliminated.

The “lipid fingerprints” from different types of eggs are spectrally very similar. We therefore propose that the differences in the paint dosimeters are mainly due to the nature of the pigment, as each paint dosimeter is characterized by a different “lipid fingerprint”. We therefore concluded that the pigment-binder interactions depend on the particular pigment used in each paint, each of which interacts with the egg-yolk binder in its own unique way.

The following 5 m/z signals were detected in all the paint dosimeters, both blank and aged, except for the lead white dosimeter: 719.52 m/z , 725.15 m/z , 913.78 m/z , 948.58 m/z and 954.90 m/z . We propose that these m/z signals be used as markers to identify the presence of egg-yolk in tempera-based paints with this binder, as these signals are always present, in spite of the differences between the “lipid fingerprints” of the blank dosimeters and those aged by exposure to polluted urban air.

Finally, our results suggest the presence in the egg-yolk paint dosimeters of various compounds (plasmalogens, ceramides and sphingomyelin) which had never been detected before in paint samples in the cultural heritage field.

Conclusiones

Benefits of the application of chemometrics

In this Doctoral Thesis, Principal Component Analysis (PCA) was applied to a new field of study, using discrete data about color obtained from paint dosimeters exposed to different urban air pollution scenarios. In general, we concluded that the paint dosimeters made with azurite underwent the most important changes over time, regardless of the quality of the urban air, while the dosimeters painted with malachite and lapis lazuli were the least affected. This new analytical approach to color change in paint mockups exposed to urban atmospheres can be extrapolated to historic artworks painted on the façades of buildings or otherwise exposed to the elements, providing very useful, highly valuable information when it comes to preparing preventive strategies for their conservation.

The information obtained by applying this innovative PCA-based approach to discrete color parameters has enabled us to visualize and interpret more easily the color change tendencies in paint dosimeters exposed long-term to the urban atmosphere. PCA allowed us to distinguish between paint dosimeters on the basis of the composition of the protein binder (egg-yolk or rabbit glue), the type of pigment and the different pigment grain sizes (in the azurite dosimeters). This pioneering approach offers a fast, efficient and inexpensive exploratory procedure for obtaining important information about paint composition and texture that is not always obvious to the naked eye.

In general, as regards the binders and their color change process over time due to exposure to the urban atmosphere, we confirmed the tendency of the dosimeters made with rabbit glue to become brighter and more luminous compared to the tendency of the egg-yolk dosimeters to turn yellow. This happens regardless of type of pigment used in the dosimeter. The multi-analytical study of paint dosimeters conducted in this Doctoral Thesis has confirmed that this tendency to change color is due to the loss of rabbit glue binder as a result of exposure to the elements, a subject referred to earlier in the dosimeters made with azurite and rabbit glue, given that the loss of binder leaves the intact crystals of the pigment exposed. By contrast, the egg-yolk binder showed greater physical-chemical

resistance when exposed to the elements. There was no loss of this binder, although it did undergo color changes due to, for example, oxidation processes. As a result, both the lapis lazuli and azurite dosimeters tend to turn slightly greener when prepared with an egg yolk binder.

The data exploration strategy we employed has enabled us to establish that the color of the paint dosimeter also depends on the pigment grain size, something we discovered in the paints made with different pigment grain size (i.e. azurite). In particular, we propose that the dosimeters that contain azurite pigment with small grain size have a higher chance of green tones over time. Both of these findings are probably due to the high binder content of the paint dosimeters made with small grain azurite, given that in general the higher the amount of binder the more likely the paint is to go yellow.

III. Conclusiones generales

En esta Tesis Doctoral las principales conclusiones están relacionadas con la degradación química (del aglutinante y pigmentos), física (color y textura) y mecánica (resistencia a ataque químico-físico) de dosímetros pictóricos (pinturas artísticas modelo) expuestos a la intemperie en monumentos (semi-)abiertos de la ciudad de Granada, ubicados en diversos escenarios de contaminación atmosférica urbana. En las investigaciones realizadas se ha tenido en consideración la interacción pigmento-aglutinante, obviada con frecuencia en la literatura por la problemática que entraña su análisis e interpretación. Además se aborda la influencia que en los procesos de interacción entre materiales pictóricos tienen: la polución atmosférica urbana y el impacto de la radiación solar, la naturaleza y el tamaño de grano del pigmento, y la naturaleza y concentración de aglutinante proteico en la pintura artística.

Los resultados obtenidos del ensayo de envejecimiento natural de dosímetros pictóricos por exposición a la intemperie se han comparado con los resultados de dos ensayos de envejecimiento acelerado en laboratorio por exposición a atmósfera enriquecida en SO₂ y radiación UV, con el fin de definir similitudes y discrepancias, y así profundizar en el conocimiento de los mecanismos de degradación de pinturas situadas en el exterior urbano.

La aplicación de técnicas quimiométricas a los datos de color obtenidos en las pinturas modelo envejecidas de forma natural, ha permitido precisar los parámetros (tipo de aglutinante, pigmento y textura pintura) que condicionan su diferente degradación, posibilitando predecir la tendencia en la variación cromática de las pinturas a lo largo del tiempo. Los resultados de los diversos estudios realizados, y la optimización de las técnicas analíticas usadas, han llevado a proponer la aplicación de nuevas metodologías analíticas para el estudio de la caracterización y degradación de pinturas artísticas. Además se pone de manifiesto la necesidad de realizar un estudio multianalítico del proceso de deterioro

Conclusiones

de las pinturas modelo, para evitar errores en la interpretación de los resultados, permitiendo establecer las conclusiones correctas.

Asimismo, los resultados obtenidos han revelado que la composición y tamaño de grano de los pigmentos históricos difieren de las especificaciones suministradas por el vendedor. En consecuencia, es imprescindible realizar una caracterización de los materiales pictóricos adquiridos antes de realizar estudios científicos o intervenciones en el patrimonio cultural. Los análisis realizados deben incluir la composición mineralógica (para asegurar la calidad del pigmento e identificar impurezas), el tamaño de partícula, y la cantidad de aglutinante orgánico posiblemente añadido durante la fabricación del pigmento, puesto que pueden afectar significativamente a las características químicas, físicas y ópticas de los pigmentos, y por tanto en la interacción pigmento-aglutinante, y en última instancia en los procesos de envejecimiento de las pinturas.

Por otra parte, los estudios realizados en esta Tesis Doctoral permiten sugerir recomendaciones a la hora de realizar intervenciones de conservación-restauración de obras pictóricas, respecto a los pigmentos y aglutinantes que pueden emplearse, pues su selección ha de realizarse considerando las condiciones climáticas y de contaminación atmosférica predominantes.

IV. Conclusiones específicas

Degradación físico-química y/o mineralógica en dosímetros pictóricos debido al envejecimiento natural y artificial

El primer estudio exhaustivo sobre el papel desempeñado por el tamaño de grano del pigmento en la interacción pigmento-aglutinante, realizado en esta Tesis Doctoral, ha demostrado que esta característica morfológica del pigmento es determinante en los mecanismos de degradación de las pinturas, ya que el tamaño de grano controla la cantidad y la distribución del aglutinante orgánico (en general más propenso a sufrir degradación que los pigmentos minerales) para obtener una pintura de consistencia adecuada. La investigación se realizó en dosímetros pictóricos elaborados con azurita (distinto tamaño de grano) y cola de conejo, envejecidos por foto-degradación acelerada (radiación UV) y natural (exposición a distintos escenarios de contaminación atmosférica).

Esta investigación reveló que el dosímetro pictórico a base de azurita estándar (con menor tamaño medio de grano que el resto de azuritas) posee características cromáticas muy diferentes a las demás pinturas modelo, debido a su mayor contenido en aglutinante, parte del cual fue añadido durante la elaboración de la azurita estándar (método Michel Price, adoptado por *Kremer Pigments GmbH & Co. KG*). Siendo los aglutinantes orgánicos más susceptibles a envejecer que los pigmentos inorgánicos, su papel es, por tanto, clave en los cambios cromáticos ocurridos en las pinturas, en particular si éstas contienen pigmentos de tamaño de grano fino, pues la demanda de aglutinante suele ser mayor.

En general, los cambios de color de los dosímetros pictóricos envejecidos de azurita-cola de conejo se relacionan con la degradación del aglutinante. Aunque en todos ellos se constatan variaciones cromáticas perceptibles al ojo humano, los cambios fueron menores en los dosímetros expuestos a la intemperie en comparación con los envejecidos en laboratorio, atribuible a la pérdida de cola de conejo de la pintura que deja expuestos los cristales de azurita inalterados. Más aún, esto reduce la adhesión entre las partículas de azurita y su fijación al sustrato. Por lo tanto, estos resultados cuestionan la idoneidad de la

Conclusiones

cola de conejo como aglutinante a ser usado en pinturas expuestas al exterior, y limitan su uso en intervenciones de conservación. Por otra parte, únicamente en los dosímetros envejecidos al aire urbano se identificó el estadio inicial de transformación de azurita (azul) a malaquita (verde), siendo por tanto la tendencia natural de estas pinturas a virar hacia tonalidades verdosas con el tiempo.

Los resultados de este estudio mostraron que el envejecimiento con radiación UV de los dosímetros pictóricos elaborados con las azuritas más gruesas originó un agrietamiento severo en la cola de conejo. En consecuencia se concluye que la mezcla de pigmentos de gran tamaño con una pequeña cantidad de azurita de grano fino sería beneficiosa para evitar la formación de grietas. Los granos más finos llenarían los espacios entre los granos gruesos evitando usar gran cantidad de aglutinante y, por lo tanto, reduciendo los cambios de volumen que sufre por variaciones de humedad y/o temperatura. Sin embargo, la cantidad añadida de aglutinante debe mantenerse al mínimo para preservar las propiedades de color de la pintura y limitar la interacción aglutinante-pigmento.

Los análisis realizados con FTIR-ATR en los dosímetros de azurita con cola de conejo, confirman que las interacciones pigmento-aglutinante son más fuertes en presencia de azuritas de grano fino, originando cambios estructurales conformacionales de la cola de conejo, concretamente en las amidas. Los cambios en la estructura del aglutinante son probablemente responsables de la variación del color hacia el amarillo y/o verde de las pinturas envejecidas, siendo el cambio cromático más acentuado a medida que disminuye el tamaño de grano del pigmento, pues la cantidad de aglutinante añadido a la pintura aumenta.

La investigación realizada en esta Tesis Doctoral también ha revelado el papel clave que juega la composición mineralógica de pigmentos históricos comerciales elaborados a base de calcita, y su superficie específica, en la susceptibilidad a la sulfatación de pinturas elaboradas al temple, tal que el proceso de sulfatación es más rápido si el pigmento, además de calcita, contiene portlandita. Igualmente se confirma que el aglutinante proteico presente en las pinturas a base de cal retrasa la reacción que se produce entre

éstas y el SO_2 atmosférico. Sin embargo, este aglutinante también ralentiza la carbonatación en el caso de que la pintura esté elaborada con el pigmento comercial *Bianco di San Giovanni* (en cuya composición interviene la portlandita), y, por consiguiente, en la formación de compuestos híbridos orgánico-inorgánicos. En consecuencia, se deberían realizar estudios futuros para determinar el contenido óptimo de aglutinante que retrasaría efectivamente la sulfatación de este tipo de pinturas sin impedir una carbonatación rápida. Por otra parte, es de esperar que los compuestos híbridos orgánico-inorgánicos formados en pinturas que contienen portlandita aumenten la resistencia química de las mismas a la intemperie.

Independientemente de la composición del pigmento histórico comercial elaborado a base de calcita, el sulfito de calcio hemihidrato siempre se detecta como una fase intermedia en el proceso de sulfatación de pinturas expuestas al SO_2 , formando una película nanogranular en la superficie del pigmento. Durante la sulfatación la transformación directa de calcita en yeso no se detecta, y la falta de continuidad cristalográfica del sulfito de calcio hemihidrato con la calcita subyacente implica que este proceso no cesará hasta que se logre la sulfatación completa. Sin embargo, el proceso de sulfatación requiere agua, por lo que puede detenerse en condiciones de sequedad (es decir, condiciones de baja humedad relativa y poca o ninguna precipitación) pero se reanuda a medida que el agua vuelve a estar disponible.

Sorprendentemente, en los dosímetros pictóricos elaborados a base de calcita expuestos 40 meses al aire urbano de Granada capital, no se detectaron pruebas claras de sulfatación. Varias razones pueden explicar este resultado. Por un lado, en los dosímetros con pigmento *Bianco di San Giovanni*, la carbonatación de la portlandita en presencia de sustancias orgánicas (e.g. cola de conejo o yema de huevo) podría haber promovido la formación de materiales híbridos orgánico-inorgánicos con alta resistencia a la alteración química. Por otro lado, el impacto periódico de la lluvia podría haber lavado las fases de sulfito y/o sulfato de calcio de las pinturas modelo, especialmente en los dosímetros elaborados con

Conclusiones

calcita, que muestran una pérdida importante de material tras su exposición prolongada a la intemperie.

Por consiguiente, la selección de pinturas a base de cal para las intervenciones de conservación en ambientes atmosféricos contaminados debe hacerse teniendo en cuenta las condiciones climáticas imperantes. Así, en climas secos se puede esperar un retraso severo en el proceso de carbonatación, por lo tanto, el uso de pinturas a base de calcita podría ser aconsejable. En cambio, en climas húmedos o bajo el impacto directo de la lluvia se aconseja el uso de pinturas que contengan portlandita (e.g. pigmento *Bianco di San Giovanni*), que forman materiales híbridos orgánico-inorgánicos con alta resistencia física y química a la intemperie. Por otra parte, los resultados de esta investigación podrían extrapolarse a otros materiales usados en patrimonio arquitectónico, pues el uso de aditivos orgánicos como la cola de conejo también podría ser beneficioso para mejorar la resistencia a la intemperie de morteros de cal y yeso. Sin embargo, como se señaló anteriormente, debe establecerse el contenido orgánico óptimo para permitir una carbonatación suficientemente rápida.

Los lípidos (contenidos en el aglutinante) de los dosímetros pictóricos elaborados al temple con yema de huevo envejecidos por exposición a la intemperie en una atmósfera urbana tienen una “huella dactilar lipídica” única cuando son analizados con MALDI-TOF-MS. Sin embargo, se propone que los mecanismos de degradación de los lípidos en todos los dosímetros pictóricos estudiados son similares (i.e. rupturas β -oxidativas y cortes de cadena), ya que se observa una disminución en las señales m/z en un rango del espectro de masa muy similar en todos ellos. En cambio, el dosímetro pictórico envejecido elaborado con blanco de plomo muestra un aumento en las señales de masa. Se sugiere que esto se debe a que la oxidación en el pigmento blanco de plomo es más lenta respecto a los otros pigmentos estudiados, y que estas reacciones ocurren en casi todos los dobles enlaces de ácidos grasos insaturados. Probablemente este fenómeno esté relacionado con la capacidad del blanco de plomo de formar jabones.

Optimización, nueva metodología analítica e interpretación en pinturas históricas

En el análisis mediante MALDI-TOF/MS de los lípidos de los dosímetros pictóricos a base de yema de huevo, se ha aplicado uno de los procesos más utilizados para la extracción de proteínas y lípidos, concretamente el método Bligh-Dyer (BD). Durante la optimización del método se puso de manifiesto la necesidad de incluir una etapa intermedia de lavado, capaz de eliminar la mayor parte de los aductos formados. Este paso, no considerado en estudios anteriores, es crucial para el posterior análisis de la fracción lipídica mediante MALDI-TOF/MS.

En la región entre 500-700 m/z del espectro de masas de los lípidos (obtenido mediante MALDI-TOF/MS), se encuentran los productos del proceso de transesterificación. Este proceso es debido al disolvente orgánico (metanol) utilizado en el paso de extracción de la fracción lipídica. Por consiguiente, los resultados pueden ser erróneos si no se tiene en cuenta esta reacción. Por tanto se propone que las señales detectadas en el intervalo de masas 500-700 m/z proceden de reacciones de transesterificación entre reactivos, lípidos y pigmentos.

La zona del espectro de masas informativa para interpretar los cambios producidos en la fracción lipídica de los dosímetros pictóricos de yema de huevo es la comprendida entre 700-1000 m/z . Así, se selecciona esta región como la “huella dactilar lipídica” que permite evaluar los cambios producidos en la fracción lipídica de muestras pictóricas elaboradas con aglutinante yema de huevo tras ser expuestas a la intemperie en atmosférica urbana. En esta “huella dactilar lipídica” quedan eliminados los productos de las reacciones de transesterificación con metanol.

Las “huellas dactilares lipídicas” de distintos tipos de huevos poseen un alto grado de similitud espectral. Por tanto se propone que las diferencias en los perfiles espectrales de los dosímetros pictóricos patrón se deben principalmente a la naturaleza del pigmento, ya que cada dosímetro pictórico está caracterizado por una “huella dactilar lipídica” diferente. Por consiguiente se concluye que las interacciones pigmento-aglutinante dependen del

Conclusiones

pigmento particular presente en cada pintura, el cual promueve una interacción única con el aglutinante yema de huevo.

En todos los dosímetros pictóricos, tanto patrón como envejecidos, excepto en el dosímetro a base de blanco de plomo, se detectaron las cinco señales m/z siguientes: 719.52 m/z , 725.15 m/z , 913.78 m/z , 948.58 m/z y 954.90 m/z . Se propone que estas señales de m/z sean marcadores para identificar la presencia de yema de huevo en pinturas al temple elaboradas con este aglutinante, pues son señales siempre presentes, a pesar de las diferencias en las “huellas dactilares lipídicas” de los dosímetros patrón o envejecidos por exposición a la contaminación atmosférica urbana.

Por último, se sugiere la presencia de varios compuestos en los dosímetros pictóricos de yema de huevo que hasta ahora no se han detectado en muestras de pintura en el ámbito del patrimonio cultural, estos son los plasmalógenos, las ceramidas y la esfingomiolina.

Beneficios de la aplicación de la quimiometría

En esta Tesis Doctoral se ha aplicado el análisis mediante PCA a un nuevo contexto de estudio, esto es, empleando datos discretos de color obtenidos en dosímetros pictóricos expuestos en distintos escenarios de contaminación atmosférica urbana. De forma global se concluye que los dosímetros pictóricos elaborados con azurita experimentan los cambios de color más importantes con el tiempo, independientemente de la calidad del aire urbano, mientras que los dosímetros de malaquita y lapislázuli son los menos afectados. Este nuevo enfoque de análisis de la evolución cromática de muestras pictóricas modelo expuestas a atmósferas urbanas es extrapolable a obras pictóricas artísticas, proporcionando una información muy útil y de gran valor para proponer estrategias preventivas de conservación de tales obras pictóricas cuando están expuestas a la intemperie.

La información obtenida al aplicar este innovador enfoque basado en PCA de parámetros de color discretos ha permitido visualizar e interpretar más fácilmente las tendencias de

cambio cromático en el tiempo de los dosímetros pictóricos expuestos a largo plazo a la atmósfera urbana. El PCA permitió discriminar dosímetros pictóricos en función de la composición del aglutinante proteico (yema de huevo o cola de conejo), de la naturaleza del pigmento, y del diferente tamaño de grano de este último (en los dosímetros de azurita). Por lo tanto, este enfoque novedoso ofrece un procedimiento exploratorio eficiente, rápido y no costoso para obtener información importante sobre la composición y textura de las pinturas, no apreciable a simple vista.

De forma general, en cuanto a los aglutinantes y su evolución cromática en el tiempo por exposición a la atmósfera urbana, se confirma la tendencia que poseen los dosímetros elaborados con cola de conejo a volverse más brillantes y luminosos respecto a la tendencia a amarillear que tienen los dosímetros de yema de huevo. Este fenómeno es independiente de la naturaleza del pigmento presente en el dosímetro. El estudio multianalítico de los dosímetros pictóricos realizado en esta Tesis Doctoral ha confirmado que tal tendencia cromática se justificaría por la pérdida de cola de conejo que sufren las pinturas exhibidas a la intemperie, cuestión antes mencionada en la investigación realizada en dosímetros de azurita y cola de conejo, puesto que la pérdida de aglutinante deja expuestos los cristales intactos del pigmento. En cambio, el aglutinante de yema de huevo muestra mayor resistencia físico-química a la intemperie, permaneciendo en la pintura, aunque sufre cambios de color debido a, por ejemplo, procesos de oxidación. Así, tanto los dosímetros de lapislázuli como los de azurita tienden a un tono ligeramente más verde cuando el aglutinante con el que están mezclados es yema de huevo.

Esta estrategia de exploración de datos ha permitido establecer que el color del dosímetro pictórico depende también del tamaño de grano del pigmento, hecho constatado en las pinturas elaboradas con diferente tamaño de grano (i.e. azurita). En particular se propone que los dosímetros que contienen azurita de grano más pequeño tienen mayor tendencia a tonos verdosos con el tiempo. Este hecho se justificaría, al igual que en el punto anterior, por el alto contenido en aglutinante que poseen los dosímetros pictóricos elaborados con

Conclusiones

azurita de menor tamaño de grano, puesto que, en general, a mayor cantidad de aglutinante mayor será su contribución a amarillar la pintura.

Appendix I

Supplementary Material

An evaluation of the impact of urban air pollution on paint dosimeters by tracking changes in the lipid MALDI-TOF mass spectra profile

Appendix I

Supplementary Table 1. Attribution of the main ions observed in the spectra of all paint dosimeters in the mass range 524-700 m/z.

m/z	Attribution	Egg yolk	Lapislazuli	Hematite	Malachite	Azurite	Minium	Calcite	Gypsum	Cinnabar	White lead
524,73	LPC(18:0/0:0)	X	X	X	X	X	X	X	X	X	X
529,74	***	X	X	X	X	X	X	X	X	X	X
556,12	LPC(18:3(6Z,9Z,12Z)/0:0)K+	X		X	X	X			X		X
560,15	Cer(d18:1/16:0)Na+	X			X		X	X	X	X	X
	LPC(18:1(9Z)/0:0)K+										
566,47	LPC(20:4(5Z,8Z,11Z,14Z)/0:0)Na+	X	X	X	X	X	X	X	X	X	X
573,09	HCCA[3M+Na-H2O]+	X	X	X	X	X	X	X	X	X	X
579,94	***	X									
581,34	DG(O-16:0/18:1(9Z) [radical])	X	X	X	X		X			X	
586,57	Cer(d18:1/18:1(9Z) (Na adduct))	X									
588,73	Cer(d18:0/18:1(9Z) (Na adduct))	X	X	X	X		X			X	
592,45 6	DG(16:0/18:2(9Z,12Z)/0:0 [radical])	X				X					
598,51	Cer(d18:1/18:12(9Z,12Z)K+		X				X				
602,4	Cer(d18:1/18:1(9Z)K+	X						X		X	
604,26	Cer(d18:0/18:1(9Z)K+		X								
607,25	DG(16:0/16:0/0:0) [radical])	X	X								
608,66	***	X		X	X	X	X		X	X	X
614,1	DG(16:1(9Z)/20:4(5Z,8Z,11Z,14Z)[radical])		X								
	DG(18:2(9Z,12Z)/18:3(9Z,12Z,15Z)[radical])										
620,1	DG(18:0/18:3(9Z,12Z,15Z)		X								
	DG(18:1(9Z)/18:2(9Z,12Z)										
624,35	DG(18:0/18:0/0:0)[radical])	X	X	X	X	X	X	X	X	X	
629,58	DG(16:0/18:3(9Z,12Z,15Z))K+[radical])	X	X			X	X				
632,74	Cer(d16:1/22:0)K+	X		X	X		X				
640,61	DG(16:0/22:6(4Z,7Z,10Z,13Z,16Z,19Z)[radical])	X									
	DG(18:2(9Z,12Z)/20:4(5Z,8Z,11Z,14Z)[radical])										
644,59	PA(16:1(9Z)/16:1(9Z))[radical])	X	X	X	X	X	X	X		X	X

	PA(14:0/18:2(9Z,12Z))[radical]										
	DG(18:0/20:4(5Z,8Z,11Z,14Z))[radical]										
	DG 18:0/20:4(5Z,8Z,11Z,14Z)[radical]										
650,48	PE O-16:0/14:0		X				X				
656,66	PA P-16:0/18:2(9Z,12Z)		X				X				
660,54	PA P-18:0/16:0	X		X	X		X	X		X	
662,51	DG 18:3(9Z,12Z,15Z)/22:6(4Z,7Z,10Z,13Z,16Z, 19Z)					X					
666,52	DG 18:1(9Z)/22:6(4Z,7Z,10Z,13Z,16Z,19Z)	X	X			X	X	X			X
672,46	PE(O-16:0/14:0)Na+		X				X	X			
677,33	SM(d18:0/14:0)	X		X	X				X	X	X
682,5	PA P-18:0/18:3(6Z,9Z,12Z)[radical]	X	X	X	X	X	X	X	X	X	X
	PA O-16:0/20:4(5Z,8Z,11Z,14Z)[radical]										
687,45	PA P-18:0/18:1(9Z)	X	X				X	X		X	
	PA O-18:0/18:2(9Z,12Z)										
693,85	PA 14:0/22:6(4Z,7Z,10Z,13Z,16Z,19Z)	X	X	X			X			X	
	PA 18:3(9Z,12Z,15Z)/18:3(9Z,12Z,15Z)										
698,73	***	X		X							

Appendix I

Supplementary Table 2. Attribution of the main ions observed in the spectra of all paint dosimeters in the mass range 700-850 m/z.

m/z	attribution	Egg yolk	Lapislazuli	Hematite	Malachite	Azurite	Minium	Calcite	Gypsum	Cinnabar	White lead
700,11	SM(d18:2/16:0)				X	X	X			X	X
702,9	SM(d18:1/16:0)										
704,29	SM(d18:0/16:0)					X					
705,94	PE(16:0/14:0)	X	X	X							X
709,85	PA(16:0/18:3(9Z,12Z,15Z)K ⁺)	X		X						X	
716,02	PE(16:1(9Z)/18:1(9Z))	X		X	X	X	X	X	X	X	X
719,52	PE(16:1(9Z)/18:0)		X								
	PE(16:0/18:1(9Z))										
721,51	***		X			X	X				X
728,08	PE(O-18:0/18:3(6Z,9Z,12Z))		X								
	PE(P-18:0/18:2(9Z,12Z))										
732,05	PE(O-18:0/18:1(9Z))	X		X	X		X	X	X	X	
738,26	PE 16:1(9Z)/20:4(5Z,8Z,11Z,14Z)		X								
740,03	SM d16:1/18:0 K ⁺			X	X		X				X
748,11	PE P- 16:0/22:6(4Z,7Z,10Z,13Z,16Z, 19Z)	X								X	
	PC O-16:0/18:0										
754,38	PC 18:3(6Z,9Z,12Z)/16:1(9Z)	X	X	X	X	X		X			X
756,46	PC 18:3(6Z,9Z,12Z)/16:0										
760,18	PE 16:1(9Z)/20:4(5Z,8Z,11Z,14Z) Na ⁺	X	X								
	PE 18:3(9Z,12Z,15Z)/18:2(9Z,12Z)										
780,54	PE 18:3(9Z,12Z,15Z)/18:0 K ⁺	X				X					
	PC 16:1(9Z)/20:4(5Z,8Z,11Z,14Z))										
783,97	PE 22:6(4Z,7Z,10Z,13Z,16Z,19Z)/ 16:1(9Z)Na ⁺	X	X								
	PI 16:0/14:0										
793,91	PC 18:3(9Z,12Z,15Z)/16:0 K ⁺						X				

	PC 18:2(9Z,12Z)/16:1(9Z)K ⁺										
798,92	PC 16:0/18:1(9Z)										
	PE P- 18:0/22:6(4Z,7Z,10Z,13Z,16Z, 19Z)Na ⁺		X								X
802	PC 20:4(5Z,8Z,11Z,14Z)/16:1(9Z) Na ⁺	X	X								
808,64	PC 20:4(5Z,8Z,11Z,14Z)/18:1(9Z)										
	PE 22:6(4Z,7Z,10Z,13Z,16Z,19Z)/ 18:3(6Z,9Z,12Z)Na ⁺		X								
	PC(18:1(9Z)/18:1(9Z)Na ⁺										
812,2	PE 20:4(5Z,8Z,11Z,14Z)/22:6(4Z, 7Z,10Z,13Z,16Z,19Z)	X									
837,69	PI 16:0/18:1(9Z)	X						X			

Appendix I

Supplementary Table 3. Attribution of the main ions observed in the spectra of all paint dosimeters in the mass range 850-1000 m/z.

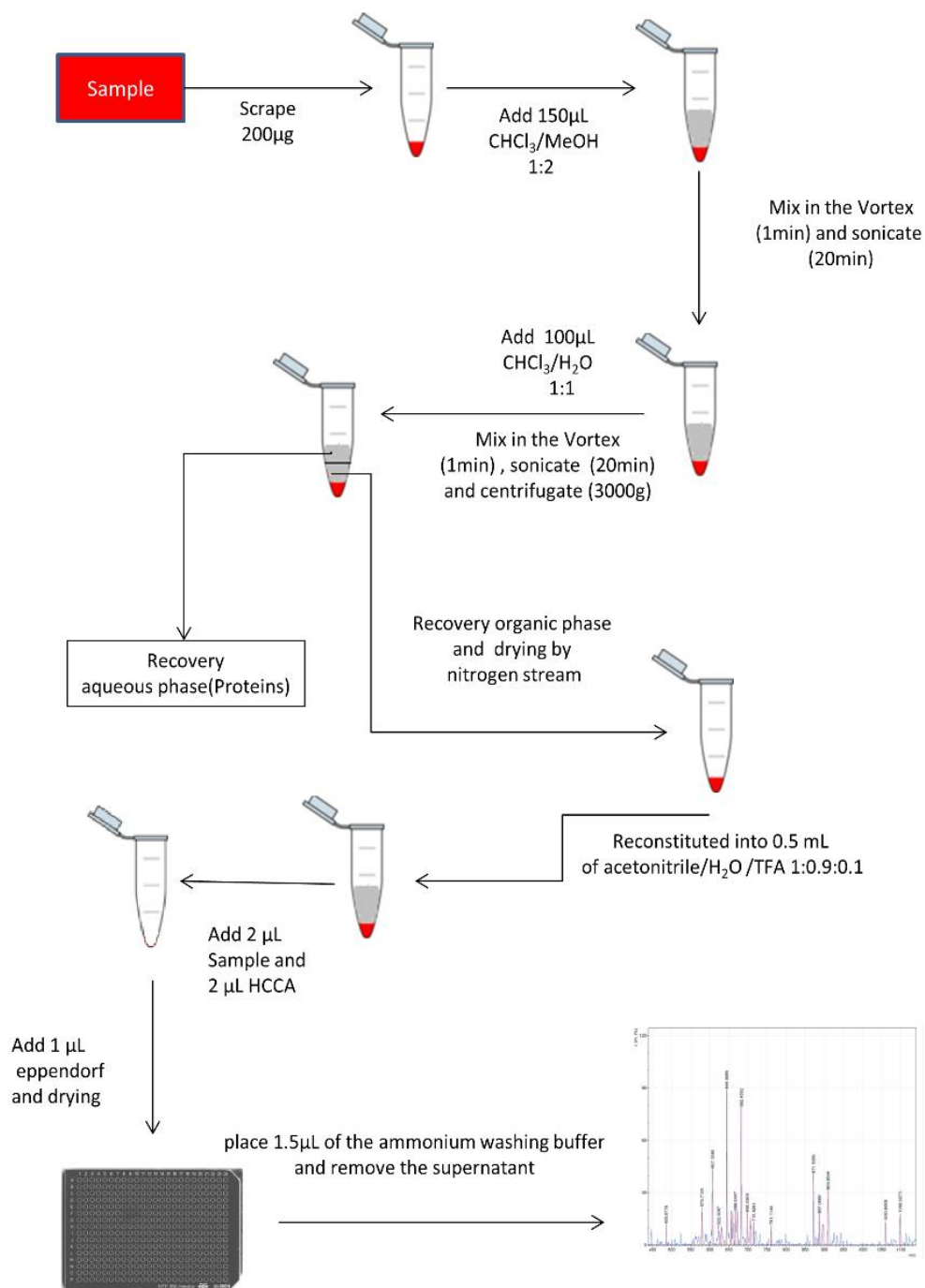
m/z	Atribution	Egg yolk	Lapislazuli	Hematite	Malachite	Azurite	Minium	Calcite	Gypsum	Cinnabar	White lead
851, 9	TG 16:0/16:0/18:3(9Z,12Z,15Z)Na+	X								X	
	TG 16:0/16:1(9Z)/18:2(9Z,12Z)Na+										
861, 83	TG 16:0/18:0/18:1(9Z)		X				X	X			
868, 12	TG 16:1(9Z)/16:1(9Z)/18:1(9Z)K+	X									
871, 69	TG 14:0/16:1(9Z)/22:6(4Z,7Z,10Z,13Z,16Z,19Z)Na+	X	X	X	X	X	X	X	X	X	X
	TG 16:1(9Z)/18:0/18:0 K+										
877, 73	TG 16:0/18:3(9Z,12Z,15Z)/20:4(5Z,8Z,11Z,14Z)		X				X	X			
	TG 16:0/18:1(9Z)/18:3(9Z,12Z,15Z)Na+										
887, 53	TG 18:0/18:0/18:2(9Z,12Z)	X		X	X		X			X	
	PI 18:0/18:1(9Z)Na+										
894, 73	***	X	X			X	X	X			X
905, 79	TG(16:1(9Z)/18:0/22:6(4Z,7Z,10Z,13Z,16Z,19Z)	X		X	X	X	X	X	X	X	X
	PI 22:6(4Z,7Z,10Z,13Z,16Z,19Z)/18:3(9Z,12Z,15Z)										
909, 63	TG 18:0/18:0/18:1(9Z)Na+	X	X		X	X					X
	PI 18:1(9Z)/22:6(4Z,7Z,10Z,13Z,16Z,19Z)										
911, 36	TG 18:0/18:0/18:0 Na+						X				
921, 97	PI(20:4(5Z,8Z,11Z,14Z)/18:2(9Z,12Z)K+)	X									
	TG 16:1(9Z)/18:3(9Z,12Z,15Z)/22:6(4Z,7Z,10Z,13Z,16Z,19Z)Na+										
	TG 18:3(9Z,12Z,15Z)/18:3(9Z,12Z,15Z)/20:4(5Z,8Z,11Z,14Z)Na+			X	X				X		X
	TG(18:0/18:1(9Z)/18:3(9Z,12Z,15Z)K)										
	TG 18:2(9Z,12Z)/18:2(9Z,12Z)/18:0 K+										
926, 52	TG 18:1(9Z)/18:3(9Z,12Z,15Z)/22:6(4Z,7Z,10Z,13Z,16Z,19Z))	X				X					
933, 36	(TG(18:0/18:1(9Z)/22:6(4Z,7Z,10Z,13Z,16Z,19Z))										X
936, 54	TG(18:0/18:3(9Z,12Z,15Z)/22:6(4Z,7Z,10Z,13Z,16Z,19Z))						X				X

938, 13	TG 18:3(9Z,12Z,15Z)/18:3(9Z,12Z,15Z)/20:4(5Z,8Z,11Z,14Z)K+	X									X	
944, 16	TG 16:0/18:1(9Z)/22:6(4Z,7Z,10Z,13Z,16Z,19Z)K+	X		X	X		X	X	X	X	X	X
	TG 16:1(9Z)/18:0/22:6(4Z,7Z,10Z,13Z,16Z,19Z)K+											
950, 25	TG 18:0/18:0/20:4(5Z,8Z,11Z,14Z)K+											
960, 1	***	X		X	X						X	
971, 28	TG 18:3(9Z,12Z,15Z)/20:4(5Z,8Z,11Z,14Z)/22:6(4Z,7Z,10Z,13Z,16Z,19Z)Na+											X
	TG 18:0/18:1(9Z)/22:6(4Z,7Z,10Z,13Z,16Z,19Z)K+											
976, 05	TG 20:4(5Z,8Z,11Z,14Z)/20:4(5Z,8Z,11Z,14Z)/22:6(4Z,7Z,10Z,13Z,16Z,19Z)	X	X								X	
	TG 18:1(9Z)/20:4(5Z,8Z,11Z,14Z)/22:6(4Z,7Z,10Z,13Z,16Z,19Z)Na+											
982, 47	***											X

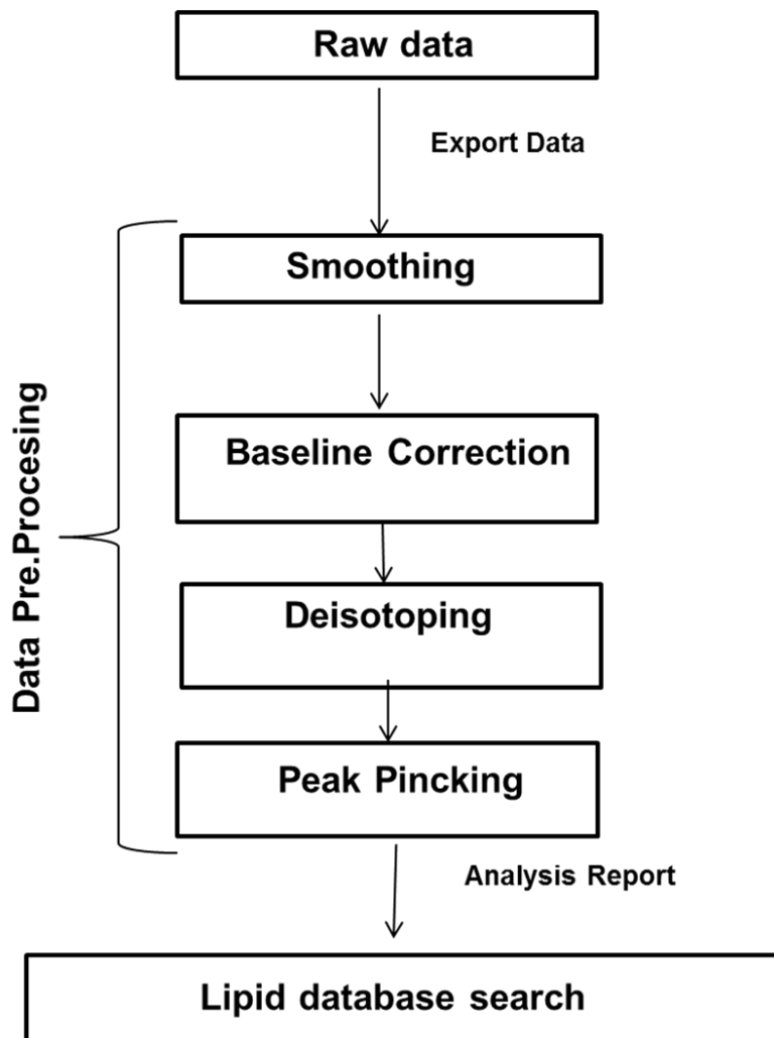
Appendix I

Supplementary Table 4. *Egg yolk lipids.*

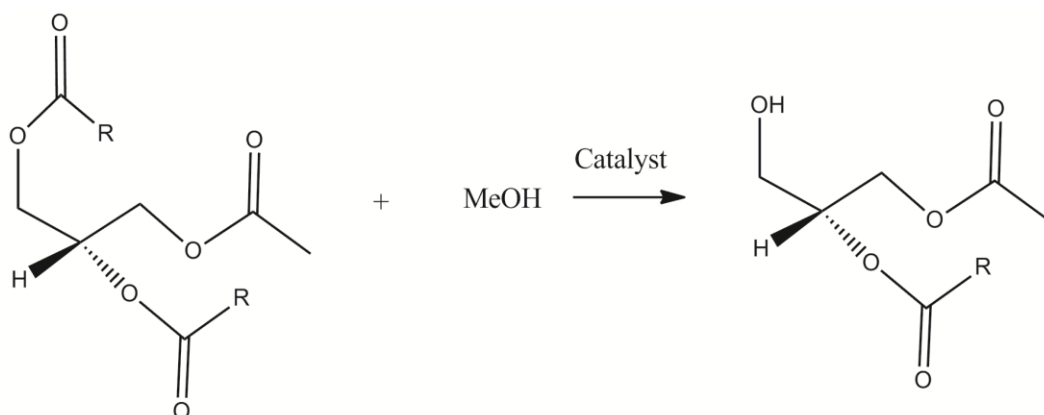
Fraction	Total lipid (%)	Phospholipid fraction (%)
Triglycerides (TAG)	66	
Phospholipid (PL):	28	
Phosphatidylcholine (PC)		73
Phosphatidylethanolamine (PE)		15,5
Lysophosphatidylcholine(LPC)		5,8
Sphingomyelin (SM)		2,5
Lysophosphatidylethanolamine (LPE)		2,1
Plasmalogens		0,9
Phosphatidylinositol (PI)		0,6
Cholesterol,ceramides, cholesterol esters and other	0.6	



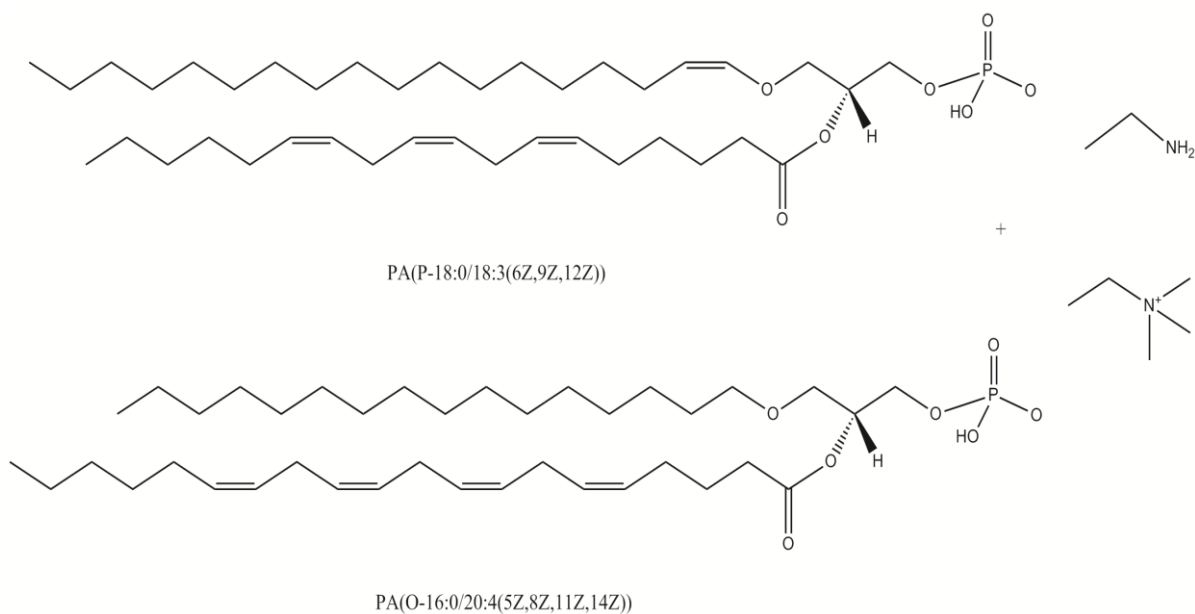
Supplementary Figure 1: Final protocol for lipid analysis in paint (egg-yolk) binding media.



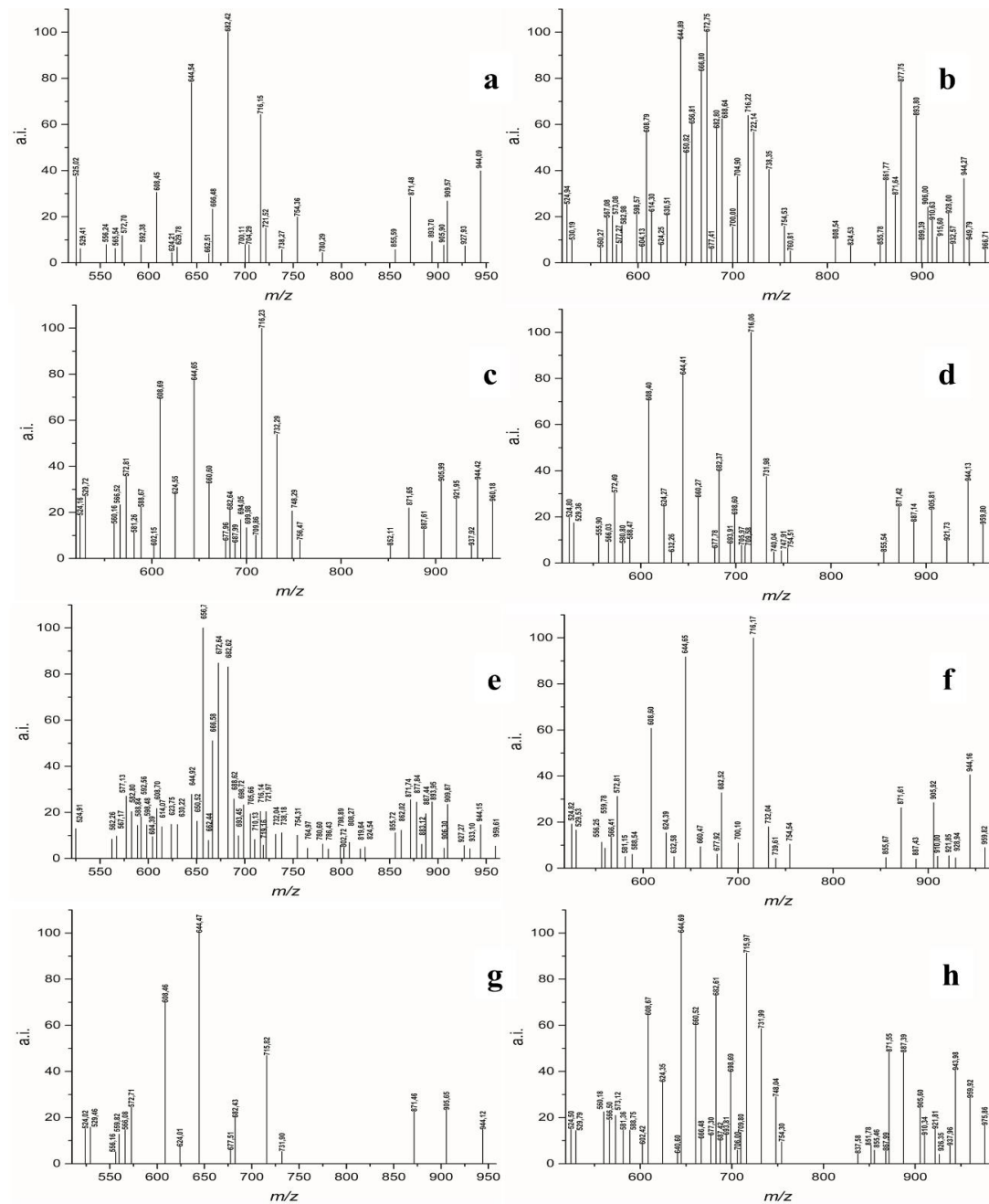
Supplementary Figure 2: *Lipidomic data processing work-flow.*



Supplementary Figure 3: *Transesterification or alcoholysis mechanisms of lipids.*



Supplementary Figure 4: *Structure plasmalogens.*

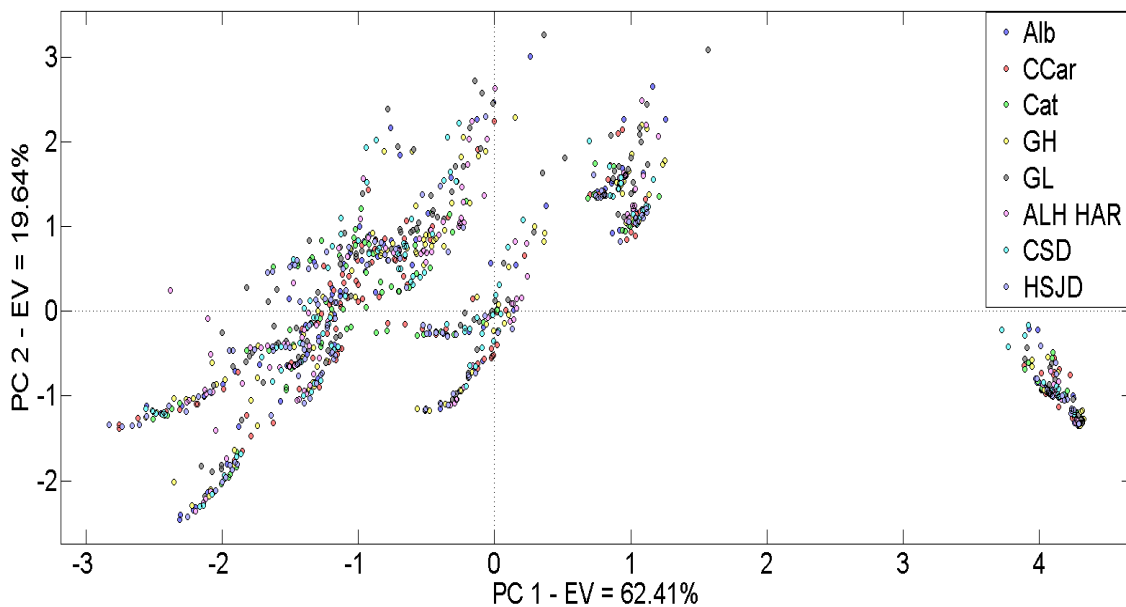


Supplementary Figure 5: MALDI-TOF mass spectra of the lipid fractions in the paint dosimeters, (a) Azurite-based paint dosimeters, (b) Calcite-based paint dosimeters and (c) Cinnabar-based paint dosimeters (d) Hematite-based paint dosimeter (e) Lapis lazuli-based paint dosimeter (f) Malachite-based paint dosimeter (g) Gypsum based-paint dosimeter (h) Egg yolk-based paint dosimeter

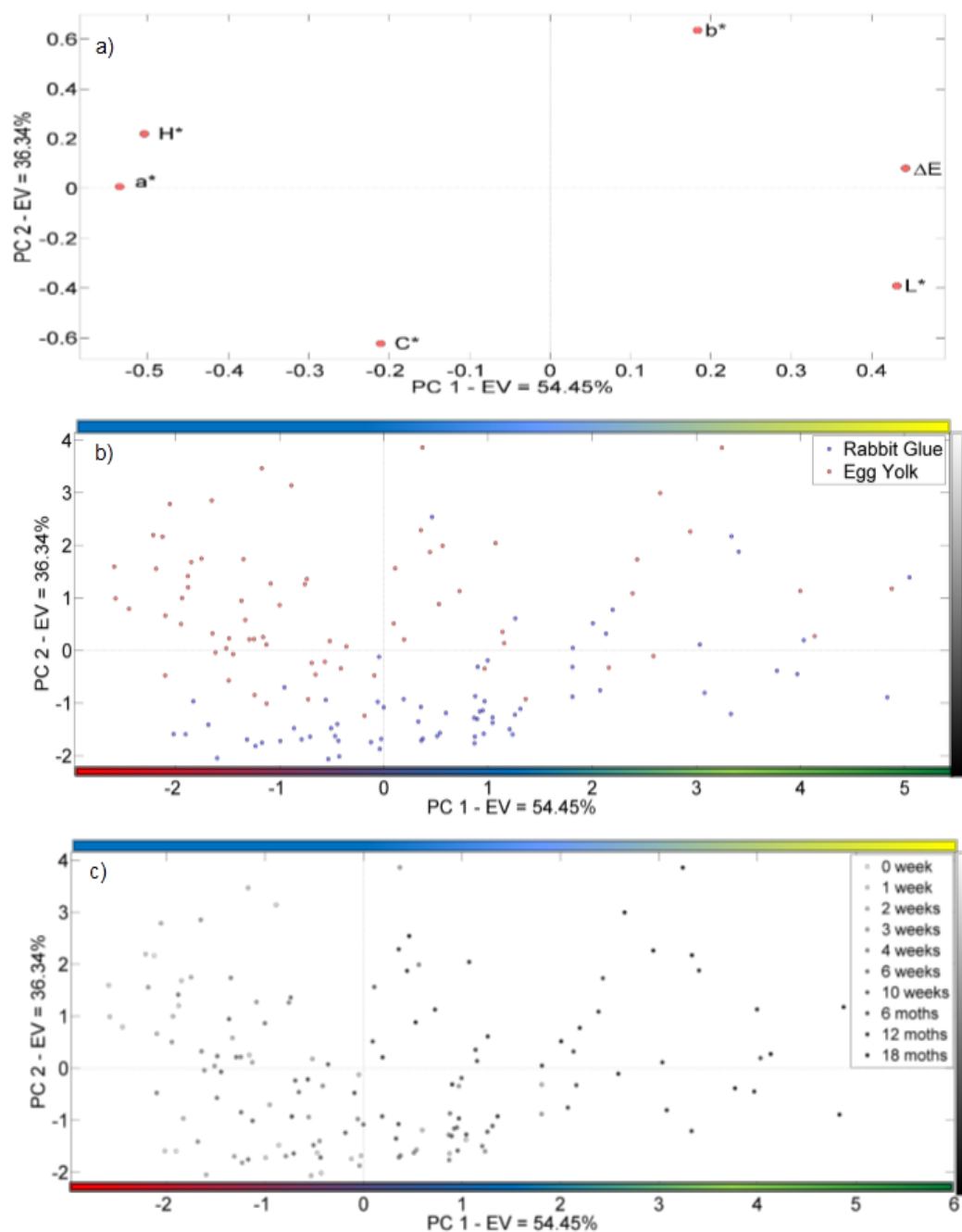
Appendix II

Supplementary Materials

Principal Component Analysis to interpret changes in chromatic parameters on paint dosimeters exposed long-term to urban air



Supplementary Figure 1. Sample scores colored according to location of the paint dosimeters in selected open-air monuments in Granada (South Spain) represented in PC1 and PC2. Alb: Albayzín; CCar: Corral del Carbón; Cat: Cathedral; GH: Generalife High; GL: Generalife Low; ALH HAR: Alhambra (Harem); CSD: Church of Santo Domingo; HSJD: Hospital San Juan de Dios



Supplementary Figure 2. PCA results for lapis lazuli-laden dosimeters: (a) loading plot PC1 vs PC2; (b) score plot PC1 vs PC2 (scores colored according to the kind of binder); (c) score plot PC1 vs PC2 (scores colored according to exposure times).

Supplementary Table 1. PCA statistical parameters. Data from all paint dosimeters.

Component	Eigenvalue	Explained variance %
PC1	3.744	62.4
PC2	1.178	19.6
PC3	0.967	16.1
PC4	0.061	1.0
PC5	0.035	0.6

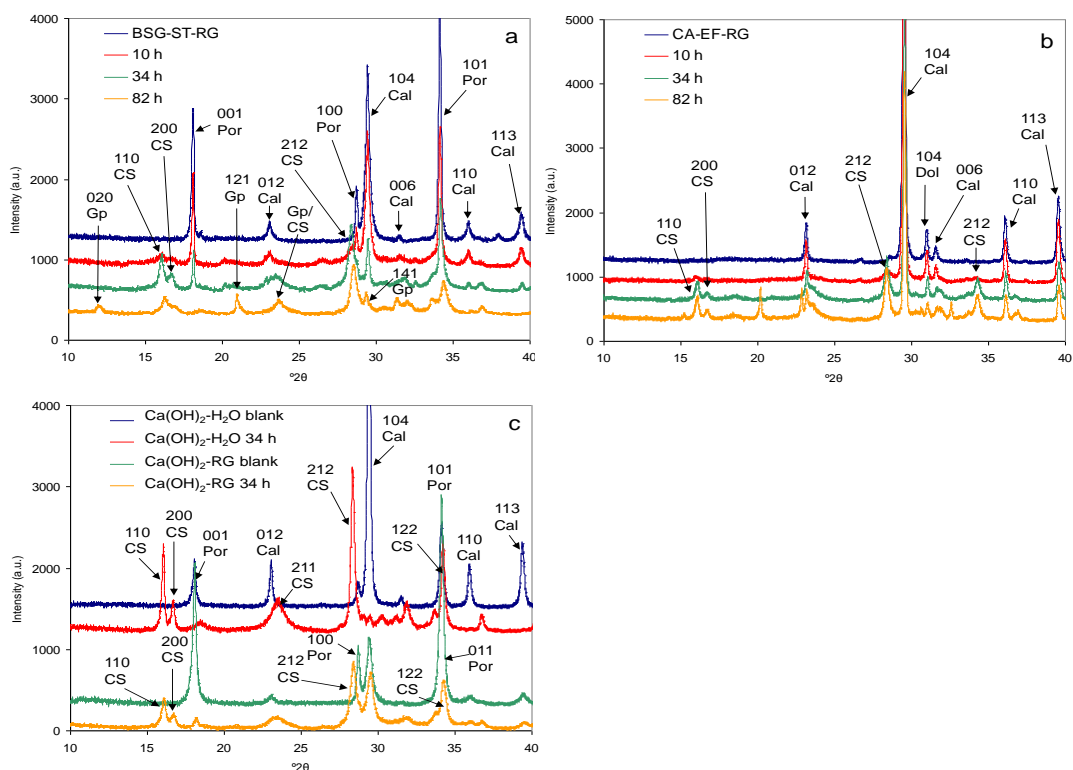
Supplementary Table 2. PCA statistical parameters for malachite, azurite and lapis lazuli laden dosimeters.

	Component	Eigenvalue	Explained variance %
Malachite	PC1	2.964	49.4
	PC2	2.439	40.7
	PC3	0.350	5.8
	PC4	0.237	3.9
	PC5	0.008	0.1
Azurite	PC1	3.269	54.5
	PC2	1.323	22.0
	PC3	1.043	17.4
	PC4	0.233	3.9
	PC5	0.130	2.2
Lapis lazuli	PC1	3.267	54.4
	PC2	2.180	36.3
	PC3	0.453	7.6
	PC4	0.089	1.5
	PC5	0.009	0.2

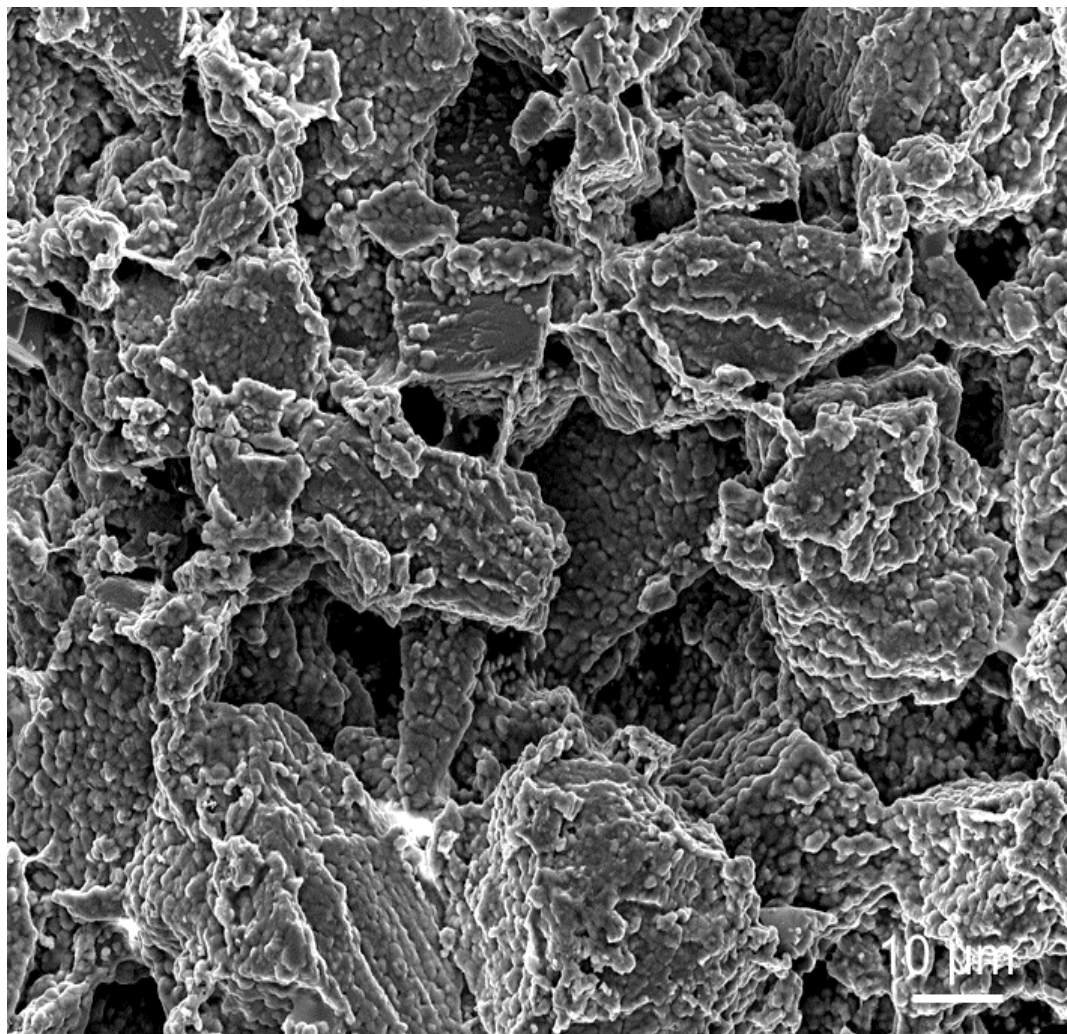
Appendix III

Supplementary Materials

**Effect of proteinaceous binder on pollution-induced sulfation of
lime-based tempera paints**



Supplementary Figure 1. XRD patterns of lime-based paints exposed to accelerated SO_2 aging; a) BSG-ST-RG paint, b) CA-EF-RG paint, c) paint prepared with analytical grade $\text{Ca}(\text{OH})_2$ and either water or rabbit glue. Gp = gypsum, CS = calcium sulfite hemihydrate, Cal = calcite, Por = portlandite. See Table 1 for acronyms.



Supplementary Figure 2. FESEM images of CA-EF-RG after 82 h SO_2 -aging. Pigments particles are covered with nanogranular calcium sulfite hemihydrate, which grossly preserves the overall shape of the rhombohedral calcite crystals.